Structural and functional relations in cobamide-containing reductive dehalogenases from anaerobic bacteria

Dissertation

To fulfill the requirements for the Degree of

„doctor rerum naturalium"

(Dr. rer. nat.)

Submitted to the Council of the Faculty of Biology and Pharmacy

of the Friedrich Schiller University Jena

by Cindy Kunze, M.Sc.

born on June 17, 1989 in Zwickau

Reviewers:

Dissertation:

Prof. Dr. Gabriele Diekert, Friedrich Schiller University Jena, Germany

Prof. Dr. Matthias Boll, Albert Ludwig University of Freiburg, Germany

Prof. David Leys PhD, University of Manchester, United Kingdom

Disputation:

Prof. Dr. Christine Römermann, Friedrich Schiller University Jena, Germany

Prof. Dr. Gabriele Diekert, Friedrich Schiller University Jena, Germany

Prof. Dr. Erika Kothe, Friedrich Schiller University Jena, Germany

PD Dr. Kerstin Voigt, Friedrich Schiller University Jena, Germany

Date of public disputation: 7th June 2018

Contents

Glossary

AMP /ATP	Adenosinmonophosphate / Adenosintriphosphate
Amp^R	Ampicillin resistance
ASU	Asymmetric unit
ATR	Adenosyltransferase
BhbA	Bromoxynil reductive dehalogenase
BP /CP /IP	Bromo- / Chloro- / Iodophenol
BvcA	Vinyl chloride RDase of *Dehalococcoides mccartyi* BAV1
Bza	Benzimidazole
Cba	Cobamide
CfrA	Chloroform reductive dehalogenase
$[Co^{I-III}]$	Cobamide cofactor in the respective oxidation states of the cobalt ion
CoA	Coenzyme A
CobC	Adenosylcobalamin/alpha-ribazole phosphatase
CobT	Nicotinate-nucleotide dimethylbenzimidazole phosphoribosyltransferase
CODH	Carbon monoxide dehydrogenase
CprA	3-chloro-4-hydroxyphenylacetate reductive dehalogenase
CtrA	Trichloroethane reductive dehalogenase
CV	Column volume
DBA /DCA /DFA	Dibromo- /dichloro- /difluoroethane (ethylene di*halide*)
DBE /DCE	Dibromo- / Dichloroethene
DBP /DCP /DFP	Dibromo- / Dichloro- / Difluorophenol
DcaA	Dichloroethane reductive dehalogenase
DcaT	Trigger-factor like chaperone for DcaA
DcpA	Dichloropropane reductive dehalogenase
DFG	German Research Foundation
DMB	5,6-Dimethylbenzimidazole
DNA	Deoxyribonucleic acid
DNO_2Bza	5,6-Dinitrobenzimidazole
DOMeBza	5,6-Dimethoxybenzimidazole
DSMZ	German Collection of Microorganisms and Cell Cultures
DTPA	Diethylene triamine pentaacetic acid
DTT	Dithiothreitol

EDTA	Ethylene diamine tetraacetic acid
EPR	Electron paramagnetic resonance
ESI-HMRS	Electrospray ionization high-resolution mass spectrometry
FMN	Flavin mononucleotide
FOR1530	Research Unit: Anaerobic biological dehalogenation
GC(-MS)	Gas chromatography (- mass spectrometry)
GSH/GS^-	Glutathione / glutathione thiolate
GST	Glutathione-S-transferase
Isc	Iron-sulfur-cluster formation
ITO	indium tin oxide
Kan^R	Kanamycin resistance
k_{cat}	Catalytic activity
K_m	Michaelis constant
MCA	Monochloroethane
MMACHC	Methylmalonic aciduria *cblC* type with homocysteinuria
MeBza	Methylbenzimidazole
NAD(P)	Nicotinamide adenine dinucleotide (phosphate)
nc	No conversion
ND / n.d.	Not determined
NCba	Norcobamide (*i.e.,* the cobamide is lacking a methyl group at C176)
NMR	Nuclear magnetic resonance
NpRdhA	*Ortho*-dibromophenol RDase of *Nitratireductor pacificus*
OD	Optical density
$OH\text{-}B_{12}$	Hydroxycobalamin
OHBza	Hydroxybenzimidazole
OMeBza	Methoxybenzimidazole
PCE	Tetrachloroethene / perchloroethylene
PceA	Tetrachloroethene reductive dehalogenase
PceT	Trigger-factor like chaperone for PceA
PCR	Polymerase chain reaction
PDB	Protein Data Bank
PEG	Polyethylene glycol
PGE	Pyrolytic graphite edge
pKa	Logarithmic acid dissociation constant

prePceA	Precursor of PceA
QueG	Epoxyqueuosine reductase
RDase /RdhA	Reductive dehalogenase
RdhB	Putative membrane anchor of RDases
RdhT	Putative trigger-factor like chaperone for RDases
RSQ	Residue-specific quality
RT	Room temperature
SDS-PAGE	Sodium dodecyl sulfate – polyacrylamide gel electrophoresis
SHE	Standard hydrogen electrode
S_N2	Bimolecular nucleophilic substitution
SSC	Saline sodium citrate
Suf	Sulfur mobilization
Tat	Twin arginine translocation peptide
TBE /TCE	Tribromo- / Trichloroethene
TBP /TCP /TFP	Tribromo- / Trichloro- / Trifluorophenol
TCA	Trichloroethane
TcbA	Tetrachlorobenzene reductive dehalogenase
TCEP	Tris(2-carboxylethyl)phosphine
TCHQ	Tetrachlorohydroquinone
TeCA	Tetrachloroethane
Tet^R	Tetracycline resistance
TmrA	Trichloromethane reductive dehalogenase
TOF	Turnover frequency
TON	Turnover number
tRNA	Transfer ribonucleic acid
(U)HPLC	(Ultra) high performance liquid chromatography
UV(-vis)	Ultraviolet (-visible)
VB /VC	Vinyl bromide /Vinyl chloride
VcrA	Vinyl chloride reductive dehalogenase
V_{max}	Maximal velocity
WT	Wild type strain
X-ray	X-radiation (roentgen radiation)

Summary

Biological degradation of persistent natural and synthetic halogenated hydrocarbons (organohalides) in anoxic environments is a vital part of the global halogen cycle. Cobamide-containing reductive dehalogenases (RDases) from organohalide-respiring bacteria play a key role in this process, since they utilize these compounds as terminal electron acceptors in a respiratory chain. So far, our knowledge about RDases was mainly limited to substrate ranges determined for several representatives and in some cases identification of cofactors and their redox states. In this study, the biochemical characterization of RDases was expanded towards structure and function analysis.

The structure of a tetrachloroethene-converting RDase (PceA) was elucidated by X-ray crystallography. Its comparison with the crystal structure of a non-respiratory *ortho*-dibromophenol RDase revealed two highly conserved elements, the topology of the intramolecular electron transfer chain and a Tyr-Arg/Lys pair in the active site involved in proton transfer to the substrate during halogen substitution reactions. The catalytically active cobamide cofactor was shown to be non-covalently bound in a permanent 'base-off' conformation with a weak water/hydroxyl group as upper axial ligand, thus facilitating the effective reduction of the cobalt ion in the course of the reaction. A variability in the utilization of different cobamide cofactors without the loss of dehalogenating ativity in PceA was observed based on guided biosynthesis towards different cobamide derivatives in the host organism. The distant positioning of the substrates in the active site of PceA crystals and the absence of an intimate cobalt-substrate interaction tracked with electron paramagnetic resonance spectroscopy suggested a dissociative long-range electron transfer mechanism for this enzyme. The catalytic cycle of dihaloeliminating RDases, a distinct mode of reductive dehalogenation, could be clearly distinguished from the halogen substitution mechanism by the need of proton transfer steps when heterologously produced RDase representatives for each reaction where applied to comparable site-directed mutagenesis. An extensive influence of the active site architecture on the substrate range of the enzyme and its reaction mechanism was discussed.

RDases could be unambiguously differentiated from other cobamide-containing biological catalysts like adenosycobalamin-dependent enzymes and methyltransferases. A reaction mechanism based on a dissociative long-range electron transfer directly from the cobalt in the center of the enzyme's cofactor to the substrate represents an unprecedented way of utilizing a cobamide in the multifarious chemistry of cobamide-containing enzymes.

Zusammenfassung

Der biologische Abbau von langlebigen, natürlichen und synthetischen, halogenierten Kohlenwasserstoffen (Organohaliden) in sauerstofffreien Umgebungen ist ein wichtiger Bestandteil des globalen Halogenkreislaufs. Cobamid-enthaltende reduktive Dehalogenasen (RDasen) aus Organohalid-respirierenden Bakterien spielen eine zentrale Rolle in diesem Prozess, da sie diese Verbindungen als terminale Elektronenakzeptoren in einer Atmungskette verwenden. Bislang ist unser Wissen über RDasen hauptsächlich auf die Substratvielfalt einiger Vertreter und in bestimmten Fällen auf die Identifizierung von Kofaktoren und deren Redoxzustände begrenzt. In dieser Studie wurde die biochemische Charakterisierung von RDasen auf Struktur- und Funktionsanalyse erweitert.

Die Struktur einer Tetrachlorethen-umsetzenden RDase (PceA) wurde mittels Röntgenkristallographie aufgeklärt. Der Vergleich mit der Kristallstruktur einer nicht-respirierenden *ortho*-Dibromphenol RDase offenbarte zwei hoch konservierte Elemente, die Anordnung der intramolekularen Elektronentransferkette und ein Tyr-Arg/Lys Paar im aktiven Zentrum, welches während der Halogensubstitutionsreaktion am Protonentransfer zum Substrat beteiligt ist. Es konnte gezeigt werden, dass der katalytisch-aktive Cobamid-Kofaktor nicht-kovalent in einer stabil bleibenden „base-off“ Konformation mit einem schwachen Wassermolekül/ einer schwachen Hydroxylgruppe als oberem Liganden gebunden wird, und somit die effektive Reduktion des Cobaltions im Verlauf der Reaktion erleichtert. Basierend auf einer gesteuerten Biosynthese von verschiedener Cobamid-Drivaten im Wirtsorganismus, konnte eine Variabilität in der Nutzung von unterschiedlichen Cobamid-Kofaktoren ohne Verlust in der Dehalgenierungsaktivität in PceA beobachtet werden. Eine distanzierte Positionierung von Substraten im aktiven Zentrum der PceA-Kristalle und das Fernbleiben von engeren Cobalt-Substrat-Interaktionen während Elektronenparamagnetischer Resonanz-spektroskopie weißen auf einen dissoziativen weitreichenden Elektronentransfermechanismus hin. Der katalytische Zyklus von dihaloeliminierenden RDasen, eine andere Art der reduktiven Dehalogenierung, konnte über die Notwendigkeit von Protontransferschritten deutlich vom Halogensubstitutionsmechanismus unterschieden werden, als heterolog produzierte RDase-Vertreter von jeder Reaktionsart mittels ortsgerichteter Mutagenese verglichen wurden. Ein extensiver Einfluss der Architekur des aktiven Zentrums auf das Substratspektrum des Enzyms und dessen Reaktionsmechanismus wurde erörtert.

RDases konnten eindeutig von anderen Cobamid-enthaltenden biologischen Katalysa-

toren wie Adenosylcobalamin-abhängigen Enzymen und Methyltransferasen abgegrenzt werden. Ein Reaktionsmechanismus basierend auf einem dissoziativen weitreichenden Elektronentransfer direkt vom Cobaltion im Zentrum des Proteinkofaktors zum Substrat stellt eine beispiellose Möglichkeit der Nutzung von Cobamiden in der vielfältigen Chemie von Cobamid-enthaltenden Enzymen dar.

1 Introduction

1.1 Organohalides in a global perspective

Organohalides are hydrocarbons containing at least one carbon-halogen (chlorine, bromine, iodine or fluorine) bond. Until the early 1970s, it was believed that organohalides are exclusively of anthropogenic origin and that the formation of carbon-halogen bonds in living organisms occurs only rarely. Halogenated compounds are used as solvents and industrial chemicals, as preservative agents for leather, vegetable fibres or dyes, as desinfectants or also as pesticides, fungicides or insecticides. Today we know, this actually represents only a small percentage of the total organohalide production. Halogenated alkyl and aryl halides occur ubiquitously in nature. So far, more than 5000 natural halogenated hydrocarbons have been identified (Gribble, 2003; Gribble, 2012). They derive from natural abiogenic sources such as volcanoes, rock disruption, biomass fires, or also from the decomposition of soil organic matter and processes of soil humus formation (Gribble, 2003; Jordan *et al.*, 2000; Leri *et al.*, 2007). Most of them are even produced by living organisms (Gribble, 2003; Gribble, 2012; Cabrita *et al.*, 2010; Field and Wijnberg, 2003). Basidiomycete fungi involved in the decomposition of forest litter and lignin, bacteria, marine sponges, algae species, lichen as well as terrestrial plants produce large quantities of chlorinated and brominated phenols, biphenyls, benzoates, methyl ethers, dioxins, terpenes or halogenated alkanes and alkenes (Abrahamson *et al.*, 1995; Swarts *et al.*, 1996; de Jong and Field, 1997; McConnell and Fenical, 1977; Swarts *et al.* 1998; Giese *et al.*, 1999; Harper and Hamilton, 2003; Gribble, 2003; Gribble, 2004; Paul and Pohnert, 2011; Walker and Chang, 2014). Even animals like grasshoppers, cockroaches, ticks or termites produce chlorinated phenols or chloroform as sex hormones, pheromones or repellents (Gribble, 1992; Gribble, 2003) and mammals synthesize tetra- and triiodothyronine known as thyroid hormones (Rokita *et al.*, 2010). Due to the physicochemical properties of the halogen substituents organohalides are mostly toxic and hazardous. An increasing number of halogen substituents led to decreased water solubility and conversely increased lipophilicity. Thus, organohalides adsorb on the surface of organic hydrocarbons and accumulate in soil, oceans, surface and ground water and even in food chains. In addition, halogenated methanes and

ethenes are highly volatile and detectable in high concentrations in the atmosphere. Today, organohalides are listed among the most frequently monitored and prioritized contaminants in groundwater (ATSDR 2013, 2015). The physical size and shape of a halogen substituent may also affect reactivity, due to steric constraints in the course of the reaction or hampered uptake into the cells. The carbon-fluorine bond belongs to the strongest single bonds in chemistry (Blanksby and Ellison, 2003) and makes organofluorines particularly recalcitrant. With increasing molecular weight of the halogen and decreasing electronegativity in the order fluorine - chlorine - bromine - iodine, these compounds get more reactive, which has consequences for the different approaches leading to their degradation. Under reductive conditions organohalides can be abiotically dehalogenated by zero-valent metals like iron, zinc and magnesium, or by bimetallic systems consisting of iron, copper, silver, palladium and nickel (Totten and Assaf-Anid, 2003; Tobiszewski and Namiesnik, 2012). Ultraviolet irradiation or ozone in the atmosphere allow for an oxidative dehalogenation of volatile compounds (Castro, 1998). However, these abiotic processes are very slow and polyhalogenated hydrocarbons appear persistent. Much more significance is assigned to microbial biodegradation. Dehalogenation reactions occur in aerobic, facultative and anaerobic organisms within the kingdoms of bacteria, archaea and eukaryotes. In aerobic environments as well as under denitrifying conditions less-substituted halogenated benzoates and lesser halogenated alkyls were found to be either degraded as sole carbon source or dehalogenated cometabolically by members of the α-, β- or γ-Proteobacteria and of Gram-positive bacteria with high G+C content (Fetzner and Lingens, 1994; Löffler *et al.*, 2003; Kiel and Engesser, 2015; Song *et al.*, 2000; Dijk *et al.*, 2003; Chen *et al.*, 2013). The acetogenic bacteria *Dehalobacterium formicoaceticum* and *Acetobacterium dehalogenans*, as well as *Dehalobacter* sp. and *Candidatus Dichloromethanomonas elyunquensis* ferment dichloromethane and chloromethane as sole source of carbon and energy (Mägli *et al.*, 1996; Traunecker *et al.*, 1991; Justicia-Leon *et al.*, 2012; Kleindienst *et al.*, 2017). Furthermore, cometabolical dehalogenation reactions of aliphatic organohalides were observed in facultative and strictly anaerobic bacteria like several methanogens, homoacetogens, clostridia and bacilli, or also in the iron-reducing *Shewanella putrefaciens* (Holliger *et al.*, 2003; Picardal *et al.*, 1993). Next to these, a special group of bacteria evolved in oxygen-depleted environments. These phylogenetically diverse microbes are able to couple the dehalogenation of organohalides to energy conservation in an anaerobic respiratory process and are called organohalide-respiring bacteria (Adrian and Löffler, 2016). In general, organohalides possess positive standard redox potentials in the range

of +250 mV to +600 mV (Dolfing and Janssen, 1994, Dolfing and Novak, 2015), which makes them suitable electron acceptors. Organohalide-respiring bacteria show highly diverse substrate ranges including less- and polyhalogenated methanes, ethanes, ethenes or propenes as well as less- and polyhalogenated benzenes, phenols or even biphenyls and dioxins (Adrian and Löffler, 2016). Representatives among δ- and ε-Proteobacteria and Firmicutes like *Desulfomonile* spp., *Sulfurospirillum* spp. or *Desulfitobacterium* spp. show a versatile metabolism and can use many different non-halogenated electron acceptors next to organohalides. In contrast, species belonging to the genera *Dehalobacter* (Firmicutes) or *Dehalococcoides* and *Dehalogenimonas* (Chloroflexi) are exclusively restricted to organohalide respiration using organohalides as the sole electron acceptors for growth (Maphosa *et al.*, 2010; Atashgahi *et al*., 2016). In general, these bacteria remove the halogen substituents and thus reduce the recalcitrance and toxicity of halogenated compounds and recover the organic carbon backbone as putative substrate for further organisms, which drives the global halogen cycle.

1.2 Enzymatic dehalogenation reactions

Several different strategies for the biodegradation of organohalides have evolved, depending on the redox potential of the environment (e.g. aerobic vs. anaerobic) or the availability of electron donors or acceptors. The critical step is the cleavage of the carbon-halogen bond that is mediated by a variety of different dehalogenating enzyme systems (i.e. dehalogenases).
Under aerobic conditions three main mechanisms were found, namely a hydrolytic, a thiolytic and an oxygenolytic dehalogenation reaction (Fig. 1.1). Hydrolytic dehalogenases replace the halide substituent with a hydroxyl group derived from a water molecule. Their structure and reaction mechanism was elucidated for the haloalkane dehalogenase from the 1,2-dichloroethane-degrading bacterium *Xanthobacter autotrophicus* GJ10 and the 4-chlorobenzoyl-CoA dehalogenase from the 4-chlorobenzoate-degrading *Pseudomonas* sp. strain CBS3 (Verschueren *et al.*, 1993; Pries *et al.*, 1994; Kennes *et al.*, 1995; Müller *et al.*, 1984; Benning *et al.*, 1998; Crooks *et al.*, 1995; Yang *et al.*, 1994). In both enzymes a nucleophilic attack (S_N2) of a conserved aspartate located in the active site cavity leads to the release of the substrate's halide and the formation of a substrate-enzyme complex (Fig. 1.1 A). The intermediate is hydrolyzed by the attack of an activated solvent water molecule on the carbonyl carbon of the aspartate. Thus the product is released and the free enzyme regenerated.

A thiolytic dehalogenation mechanism was described for dichloromethane-utilizing methylotrophic bacteria. Here, inducible θ-class glutathione *S*-transferases (GSTs) catalyze the formation of formaldehyde and chloride in the presence of glutathione (GSH) as cofactor (Fig. 1.1 B; Kohler-Staub and Leisinger, 1985; Kohler-Staub *et al.*, 1986; Leisinger *et al.*, 1994; Meyer *et al.*, 1991). The thiolate anion of the cofactor initiates a nucleophilic substitution (S_N2) reaction and an unstable *S*-chloromethyl GSH intermediate is formed, whereby one chloride is released (Gälli *et al.*, 1982; Wackett, 1992). It is likely, that the intermediate is than rapidly hydrolyzed by a solvent water molecule resulting in formaldehyde and the free cofactor.

In the presence of oxygen, several halogenated hydrocarbons can also be non-specifically cooxidized as analogs of the corresponding unsubstituted substrates by non-heme diiron-containing mono- and dioxygenases, which are known for their broad substrate ranges. A well-known example is the oxygenolytic degradation of trichloroethene by the methane-monooxygenase of *Methylosinus trichosporium* OB3b (Fig. 1.1 C; Fox *et al.*, 1990). The enzyme uses oxygen and $NADH+H^+$ to form epoxide-intermediates, which decompose spontaneously and fortuitously in water and thus release the halide.

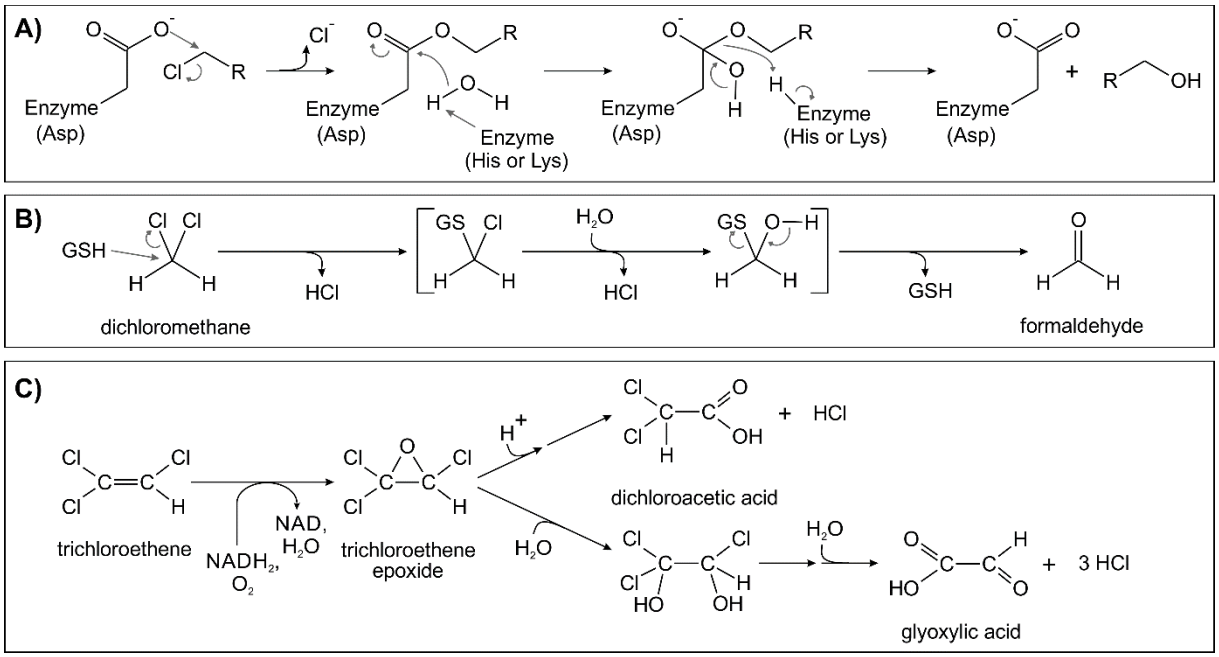

Figure 1.1: Enzymatic dehalogenation reactions under aerobic conditions. A) Hydrolytic dehalogenation involves nucleophilic attack of an aspartate before halide replacement by a hydrogen. B) Thiolytic mechanism for dichloromethane dehalogenation involves nucleophilic attack of glutathione (GSH). C) Unspecific oxygenolytic reaction by the methane monooxygenase of *Methylosinus trichosporium* OB3b initiate spontaneous decomposition.

Similar cometabolic dehalogenation reactions based on the formation of labile intermediates can be observed in methane, ammonia, propane, phenyl and benzoate mono- or dioxygenases (Ensley, 1991; Fetzner and Lingens, 1994).

All mechanisms described above favor hydrocarbons with only a limited number of halide substituents, whereas most of the polyhalogenated compounds such as hexachlorobenzene, tetrachloroethene or trichloromethane are inaccessible to these mechanisms. However, these compounds were found to be frequently degraded via reductive dehalogenation mechanisms that typically result in the replacement of the halogen substituent by a hydrogen atom. While this type of reaction is rather uncommon under oxic conditions, it clearly dominates in oxygen-depleted environments. In some aerobic and facultative anaerobic organisms reductive dehalogenation was shown to be involved in carbon metabolism. A well-known example is the degradation of pentachlorophenol by *Sphingomonas chlorophenolicum* (Orser *et al.*, 1993; Orser and Lange, 1994). The tetrachlorohydroquinone (TCHQ) intermediate is stepwise dechlorinated to tri- and dichlorohydroquinone by a TCHQ dehalogenase, a member of the ζ-class glutathione *S*-transferase family (Xun *et al.*, 1992; Board *et al.*, 1997). In contrast to the thiolytic GSTs, here two molecules of glutathione provide the reducing equivalents, and are thereby oxidized to glutathione disulfide (Fig. 1.2 A; Xun *et al.*, 1992). The reaction is initiated by the ketonization of the aromatic ring of THCQ followed by 1,4-elimination of HCl. During reduction of the electrophilic trichlorobenzoquinone intermediate a nucleophilic attack by a first glutathione thiolate (GS^-) leads to the formation of a glutathione-substrate intermediate (McCarthy *et al.*, 1997; Kiefer *et al.*, 2002). In a subsequent step, a highly conserved cysteine in the active site attacks the sulfur of the glutathionyl substituent resulting in the reduced product and a mixed disulfide between the cysteine and glutathione (McCarthy *et al.*, 1997). The free enzyme finally has to be regenerated by a second glutathione that replaces the cysteine in the mixed disulfide and forms glutathione disulfide. Another aerobic reductive dehalogenation mechanism was found in the iodotyrosine deiodinase, which is involved in the biosynthesis of the thyroid hormone in mammals (Rokita *et al.*, 2010; Phatarphekar *et al.*, 2014). The enzyme belongs to the nitro-FMN reductase superfamily and employs a flavin mononucleotide (FMN) as cofactor (Thomas *et al.*, 2009; Phatarphekar *et al.*, 2014). The substrates mono- and diiodotyrosine are proposed to be dehalogenated via an initial protonation and two subsequent dissociative electron-transfer steps from reduced FMN (Fig. 1.2 B; Bobyk *et al.*, 2015; Hu *et al.*, 2015;). Protonation of the halogen-binding carbon atom leads to a delocalization of the electrons within the substrate and thus to the formation of a nonaromatic

intermediate. For the elimination of the halide a first electron is transferred, whereby an electron-depleted tyrosyl radical is generated, which has to be reduced by a second electron to form tyrosine as end product.

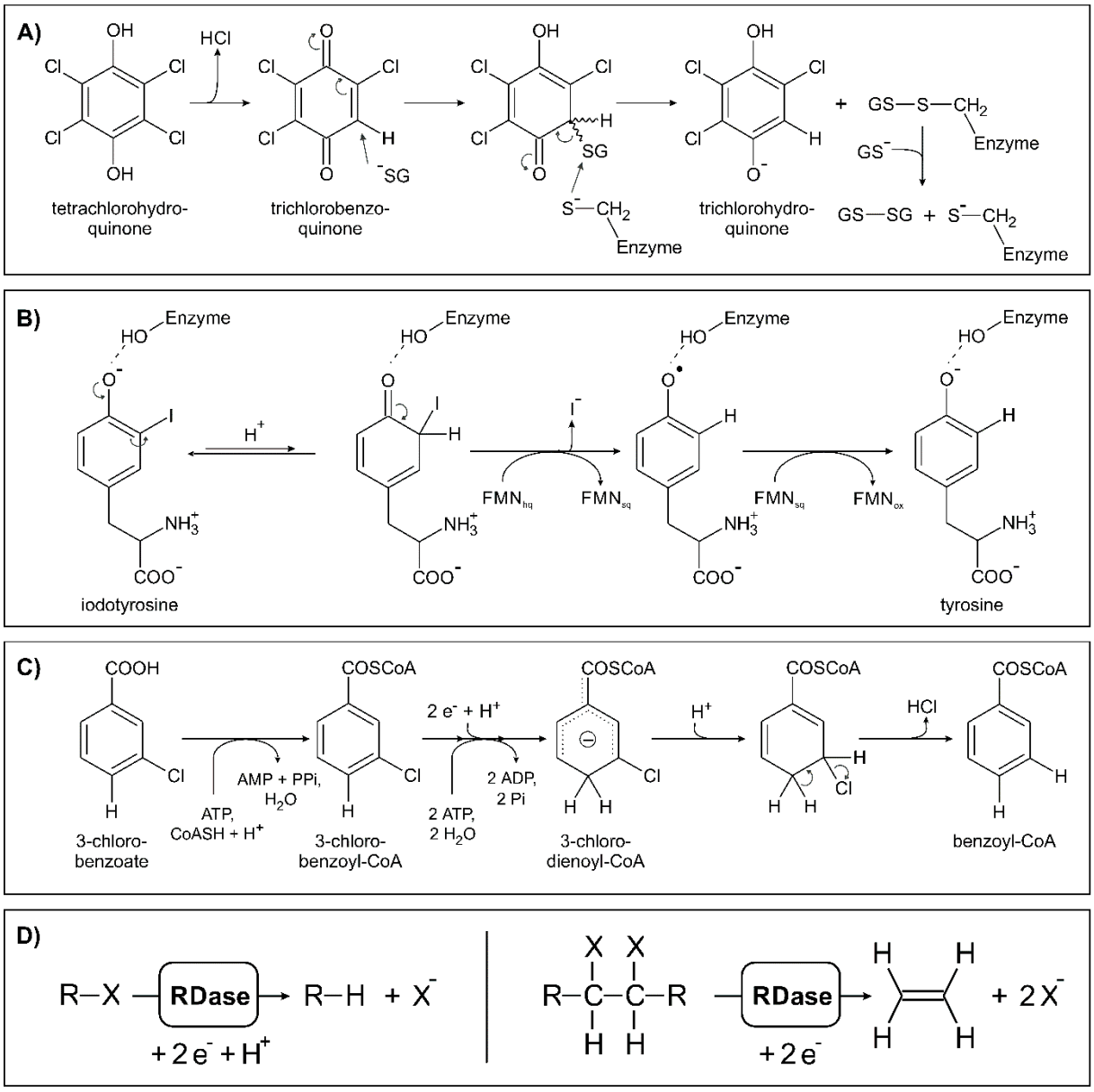

Figure 1.2: Enzymatic reductive dehalogenation reactions. A) Proposed mechanism for the tetrachlorohydroquinone dehalogenase from *S. chlorophenolicum* involves nucleophilic attack of glutathione (GSH). B) Dehalogenation of halogenated tyrosine via dissociative electron transfer from reduced flavin mononucleotide (FMN) in the iodotyrosine deiodinase. C) ATP-dependent class I benzoyl-CoA reductases catalyze an ATP-driven Birch-like mechanism leading to the elimination of HCl. D) Reductive dehalogenation in cobamide-containing reductive dehalogenases (RDases) either involves the substitution of one halide (X) by a proton (left) or the elimination of two vicinal halides leading to double bond formation (right).

In anaerobic bacteria reductive dehalogenation reactions play a more versatile role and were found to be involved in carbon metabolism and cometabolic processes as well as in energy conservation pathways. The denitrifying *Thauera chlorobenzoica* 3CB-1 relies on 3-chlorobenzoate as carbon source (Häggblom and Jung, 1999; Song *et al.*, 2000). To allow for its conversion the substrate has to be activated by a specific halobenzoate ligase in the first step (Kuntze *et al.*, 2011). The activated 3-chlorobenzoyl-CoA ester is then proposed to be reduced in a Birch-like mechanism by the ATP-driven transfer of two single solvated electrons to the non-aromatic chlorinated dienoyl-CoA, a reaction catalyzed by the iron-sulfur containing class I benzoyl-CoA reductase (Fig. 1.2 C; Kuntze *et al.*, 2011; Tiedt *et al.*, 2016). A subsequent protonation at the halogen-binding carbon initiates an either enzyme-mediated or spontaneous E2-elimination of HCl. Thus benzoyl-CoA is formed, which can be further converted in the benzoyl-CoA degradation pathway (Fuchs, 2008). However, the reductive dehalogenation reaction rather seems to be an intrinsic activity of all class I benzoyl-CoA reductases and only the activation of 3-chlorobenzoate requires halobenzoate-specialized enzymes (Schühle *et al.*, 2003; Kuntze *et al.*, 2011). More common in anaerobic bacteria is the use of transition-metal containing porphyrins for dehalogenation. Reduced iron-, cobalt- and nickel-containing porphyrins (hemes, cobamides and coenzyme F430) were shown to mediate the abiotic reductive dehalogenation of a variety of alkyl halides (Krone *et al.*, 1989a; Krone *et al.*, 1989b; Gantzer and Wackett, 1991; Schanke and Wackett, 1992). This intrinsic ability is exploited in several enzyme systems involved in cometabolic alkyl reductive dehalogenation reactions (reviewed in Mohn and Tiedje, 1992; Fetzner and Lingens, 1994; Holliger *et al.*, 2003). Particular attention is paid to cobamide-containing reductive dehalogenases (RDases), which use organohalides as terminal electron acceptor in a membrane-associated respiratory chain and are thus involved in energy conservation via electron transport phosphorylation (Hug *et al.*, 2013; Judger *et al.*, 2015; Schubert and Diekert, 2016; Judger *et al.*, 2016; Fincker and Spormann, 2017). RDase-mediated dehalogenation reactions can occur via the net transfer of two electrons leading to the removal of either one or two adjacent halogen atoms (Fig. 1.2 D). In the former, a single halogen substituent is replaced by a hydrogen in a halogen substitution / hydrogenolysis reaction. In contrast, the removal of two adjacent halogen substituents results in the formation of a double bond between the two carbon atoms initially bonding the halides, a process called dihaloelimination / vicinal reduction.

1.3 Cobamide-containing reductive dehalogenases

Cobamide-containing reductive dehalogenases (RDases) represent the largest family of dehalogenating enzyme systems. Up to date, about 300 putative RDase genes were found in bacteria that are able to respire a broad spectrum of structurally diverse organohalides ranging from monohalogenated alkenes and alkanes to more complex polyhalogenated benzenes, biphenyls and dioxins (Hug *et al.*, 2013). However, the presence of up to 36 RDase genes in a single organism, of which several may be even expressed under the same conditions, often hinders unambiguous assignment of substrate conversion to a specific RDase (Hug *et al.*, 2013; Judger *et al.*, 2015). In addition, slow growth rates and low biomass yields of most organohalide-respiring bacteria, especially of those strictly restricted to the use of organohalides (e.g. *Dehalococcoides mccartyi* (Löffler *et al.*, 2013)), hampered the isolation of the corresponding RDase proteins. In the last three years different strategies for heterologous production of RDases in either non-dehalogenating cobamide-producing organisms like *Shimwellia blattae* (formerly *Escherichia blattae*) and *Bacillus megaterium* (Mac Nelly *et al.*, 2014; Payne *et al.*, 2015a) or in *E. coli* (Parthasarathy *et al.*, 2015) were established, which might allow for the characterization of further so far not accessible RDases in future.

Up to date, only a limited number of RDases has been investigated in some detail, and their biochemical characterization was still limited to the elucidation of their substrate ranges and in a few cases to cofactor determination (see Tab. 1.1). The first RDase purified was the 3-chlorobenzoate utilizing reductive dehalogenase of *Desulfomonile tiedjei* (Ni *et al.*, 1995). Absorbance spectroscopy suggested the presence of a heme as redox center for the dehalogenation reaction. However, it soon became clear that this enzyme is rather an exception. All other characterized RDases employ cobamide derivatives (‘complete’ corrinoids) as cofactor (Tab. 1.1), which makes them unique among terminal reductases. Electron paramagnetic resonance (EPR) spectroscopy of the isolated proteins of the tetrachloroethene RDase (PceA) of *Dehalobacter restrictus* PER-K23 and the *ortho*-chlorophenol RDase (CprA) of *Desulfitobacterium dehalogenans* showed spectra that resembled a ‘base-off’ cobamide in the [Co^{II}] oxidation state (Schumacher *et al.*, 1997; van de Pas *et al.*, 1999). Later the presence of a cobamide cofactor was unambiguously proven, when the PceA of *Sulfurospirillum multivorans* (formerly *Dehalospirillum multivorans*) was isolated and the cofactor extracted and identified as norpseudo-B_{12} in the ‘base-off’ conformation (Kräutler *et al.*, 2003; see Fig. 1.3).

Table 1.1: Identified and biochemically characterized respiratory reductive dehalogenases (RDases).

RDase	Organism	Substrate	Product	Cofactors	Reference
3-Chlorobenzoate RDase	*Desulfomonile tiedjei*	3-chlorobenzoate	benzoate	heme	Ni *et al.*, 1995
Tetrachloroethene RDase (PceA)	*Sulfurospirillum multivorans*	PCE; TCE TBE; DBE *trans*-1,3-DCPr 2,3-DCPr 1,1,3-TCPr	*cis*-1,2-DCE VB *cis*-/*trans*-1,CPr, 3-CPr 2-CPr 1,1-DCPr	1 norpseudo-B_{12}, 8 Fe, 8 $S^{\#}$	Neumann *et al.*, 1996; Kräutler *et al.*, 2003; Neumann *et al.*, 2002; Ye *et al.*, 2010
Tetrachloroethene RDase (PceA)	*Desulfitobacterium hafniense* PCE-S	PCE; TCE TBE; DBE; VB	*cis*-1,2-DCE ethene	1 cobamide, 8 Fe, 10 $S^{\#}$	Miller *er al.*, 1998; Ye *et al.*, 2010
3-Chloro-4-hydroxy-phenylacetate RDase (CprA)	*Desulfitobacterium hafniense* DCB-2	3-Cl-4-OHPA	4-OHPA	1 cobamide, 12 Fe, 13 $S^{\#}$	Christiansen *et al.*, 1998
Tetrachloroethene RDase (PceA)	*Dehalococcoides mccartyi* 195	PCE 2,3-DCP	TCE 3-CP	cobamide*	Magnuson *et al.*, 1998; Fung *et al.*, 2007
Trichloroethene RDase (TceA)	*Dehalococcoides mccartyi* 195	TCE; DCE TBE; DBE; VB 1,2-DCA 1,2-DBA	VC ethene	cobamide*	Magnuson *et al.*, 1998; Magnuson *et al.*, 2000; Maymo-Gatell *et al.*, 1999
ortho-Chlorophenol RDase (CprA)	*Desulfitobacterium dehalogenans*	3-Cl-4-OHPA PCP 2,3-DCP; 2,4-DCP; 2,6-DCP; 2CP; 2-Br-4-ClP	4-OHPA 2,3,4,5-TeCP 3-CP; 4-CP; phenol	1 cobamide, 1 [4Fe-4S], 1 [3Fe-4S]	van de Pas *et al.*, 1999

(continued)

Table 1.1: continued

RDase	Organism	Substrate	Product	Cofactors	Reference
Tetrachloroethene RDase (PceA)	*Dehalobacter restrictus* PER-K23	PCE; TCE	*cis*-1,2-DCE	1 cobalamin, 2 [4Fe-4S]	Schumacher *et al.*, 1997; Maillard *et al.*, 2003
Tetrachloroethene RDase (PceA)	*Desulfitobacterium hafniense* PCE1	PCE; TCE	*cis*-1,2-DCE	cobamide*	van de Pas *et al.*, 2001
Chlorophenol RDase (CprA)	*Desulfitobacterium hafniense* PCE1	3-Cl-4-OHPA 2,3-DCP; 2,4-DCP; 2-6-DCP; 2-CP PCE	4-OHPA 3-CP; 4-CP TCE	cobamide*	van de Pas *et al.*, 2001; Gerritse *et al.*, 1996
Tetrachloroethene RDase (PceA)	*Desulfitobacterium hafniense* TCE1	PCE; TCE	*cis*-1,2-DCE	cobamide*	van de Pas *et al.*, 2001
3-Chloro-4-hydroxy-benzoate RDase (CprA)	*Desulfitobacterium chlororespirans*	3,5-Cl-4-OHB; 3-Cl-4-OHB 3-Cl-4-OHPA 2,3-DCP; 2,6-DCP; 2,4,6-TCP	4-OHB 4-OHPA 3-CP; 2-CP 2,4-DCP	1 cobamide, 8 Fe, 8 $S^{\#}$	Krasotkina *et al.*, 2001
Tetrachloroethene RDase (PceA)	*Desulfitobacterium hafniense* Y51	PCE; TCE HCA; PCA; 1,1,2,2-TeCA; 1,1,1,2-TeCA	*cis*-1,2-DCE 1,1-DCE	cobamide*	Suyama *et al.*, 2002; Suyama *et al.*, 2001
2,4,6-Trichlorophenol RDase (CrdA)	*Desulfitobacterium hafniense* PCP-1	PCP; 2,3,4,5-TeCP; 3,4,5-TCP; 2,3,5-TCP; 2,3,4-TCP; 2,3,6-TCP; 2,4,6-TCP; 2,4-DCP; 2,3-DCP	3,5-DCP; 3,4-DCP; 2,5-DCP; 4-CP; 3-CP	cobamide*	Boyer *et al.*, 2003

(continued)

Table 1.1: (continued)

RDase	Organism	Substrate	Product	Cofactors	Reference
3,5-Dichlorophenol RDase (CprA5)	*Desulfitobacterium hafniense* PCP-1	2,3,4,5-TeCP; 2,3,5-TCP; 2,4,5-TCP; 2,3,6-TCP; 2,3-DCP; 3,5-DCP	2,5-DCP; 3,4-DCP; 2,6-DCP; 2-CP; 3-CP	cobamide*	Thibodeau *et al.*, 2004
Vinyl chloride RDase (VcrA)	*Dehalococcoides mccartyi* VS	DCE; VC 1,2-DCA	ethene	cobalamin, 2 [4Fe-4S]	Müller *et al.*, 2004; Parthasarathy *et al.*, 2015
Chlorobenzene RDase[a] (CbrA)	*Dehalococcoides mccartyi* CBDB1	1,2,3,4-TeCB; 1,2,3-TCB	1,2,4-TCB 1,3-DCB	n.d.	Adrian *et al.*, 2007
Pentachlorophenol RDase (CprA3)	*Desulfitobacterium hafniense* PCP-1	PCP; 2,3,4,5-TeCP; 2,3,5,6-TeCP; 2,4,6-TCP; 2,3,6-TCP; 2,3,4-TCP	2,3,5-TCP; 3,4,5-TCP; 2,4-DCP; 2,3-DCP; 3,4-DCP	cobamide*	Bisaillon *et al.*, 2010
Vinyl chloride RDase[a] (BvcA)	*Dehalococcoides mccartyi* BAV1	TCE; DCE; VC 1,2-DCA	ethene	n.d.	Tang *et al.*, 2012
Chloroform RDase[a] (CfrA)	*Dehalobacter* sp. CF	TCM 1,1,1-TCA	DCM 1,1-DCA	n.d.	Tang and Edwards, 2013
Dichloroethane RDase[a] (DcrA)	*Dehalobacter* sp. DCA	1,1-DCA	CA	n.d.	Tang and Edwards, 2013
Dichloropropane RDase[a] (DcpA)	*Dehalogenimonas lykanthroporepellens* BL-DC-9	1,2-DCPa	propene	n.d.	Padilla-Crespo *et al.*, 2014

(continued)

Table 1.1: (continued)

RDase	Organism	Substrate	Product	Cofactors	Reference
RdhA3 (CprA)	*Desulfitobacterium hafniense* DCB-2	2,4,5-TCP; 2,4,6-TCP; 2,3-DCP; 2,4-DCP; 3,5-DCP PCE	3,4-DCP; 2-CP; 4-CP; 3-CP TCE	cobamide	Mac Nelly *et al.*, 2014; Kim *et al.*, 2012
Trichloroethane RDase[a] (CtrA)	*Desulfitobacterium* sp. strain PR	TCM; DCM 1,1,1-TCA; 1,1,2-TCA; 1,2-DCA	MCM CA	n.d.	Zhao *et al.*, 2015; Ding *et al.*, 2014
trans-Dichloroethene RDase[a] (TdrA)	*Dehalogenimonas* sp. WBC-2	DCE	VC	n.d.	Molenda *et al.*, 2016
Trichloromethane RDase[a] (TmrA)	*Dehalobacter* sp. UNSWDHB	TCM 1,1,1-TCA; 1,1-DCA 1,1,2-TCA	DCM CA VC; 1,2-DCA	(cobamide, FeS cluster)	Wong *et al.*, 2016; Judger *et al.*, 2017
Tetrachlorobenzene RDase[a] (TcbA)	*Dehalobacter* sp. strain TeCB1	1,2,4,5-TeCB; 1,2,4-TCB	1,3-DCB; 1,4-DCB	n.d.	Alfán-Guzmán *et al.*, 2017

BrClP: 2-bromo-4-chlorophenol; CA: chloroethane; ClOHB: 3,5-dichloro-4-hydroxybenzoate; ClOHPA: 3-chloro-4-hydroxyphenylacetate; CP: chlorophenol; CPr: chloropropene; DBA: dibromoethane; DBE: dibromoethene; DCA: dichloroethane; DCB: dichlorobenzene; DCE: dichloroethene; DCM: dichloromethane; DCP: dichlorophenol; DCPa: dichloropropane; DCPr: dichloropropene; HCA: hexachloroethane; OHB: hydroxybenzoate; MCM: monochloromethane; OHPA: hydroxyphenylacetate; PCA: pentachloroethane; PCE: tetrachloroethene (perchloroethylene); PCP: pentachlorophenol; TBE: tribromoethene; TCA: trichloroethane; TCB: trichlorobenzene; TCE: trichloroethene; TCM: trichloromethane; TCP: trichlorophenol; TCPr: trichloropropene; TeCA: tetrachloroethane; TeCB: tetrachlorobenzene; TeCP; tetra-chlorophenol; VB: vinyl bromide; VC: vinyl chloride; n.d.: not determined

[a] Identification and partial characterization of the enzyme via blue native polyacrylamide gel electrophoresis of cell extract coupled to RDase activity measurement in gel slices and identification of proteins involved using liquid chromatography tandem mass spectrometry.

* Light-sensitive inhibition of RDase activity by propyl iodide indicates cobamide involvement.

[#] Determination of iron and acid-labile sulfide as components of Fe-S cluster.

Norpseudo-B_{12} represents a novel type of natural cobamide only found in *Sulfurospirillum* spp. and is characterized by an adenine as lower ligand base and an unusual linker moiety lacking a methyl group at C176 (Kräutler *et al.*, 2003; Goris *et al.*, 2017). The natural upper ligand was not known, since it is replaced by cyanide in the course of the cobamide extraction (Stupperich *et al.*, 1986). The finding that the reductive dehalogenation reaction in PceA of *S. multivorans* was light-reversibly inhibited by the addition of propyl iodide (1-iodopropane) has been attributed to the alkylation of the superreduced [Co^{I}]-state of the cofactor in the dark (Neumann *et al.*, 1995; Neumann *et al.*, 1996), an effect also described for other cobamide-dependent enzymes (Weissbach *et al.*, 1965; Brot and Weissbach, 1965). This inhibition experiment became a standard test for the involvement of cobamides in other RDases (see references in Tab. 1.1). However, the structure of the natural cobamide cofactors in other RDases was not elucidated so far. The contracted tetrapyrrol ring system of the cobamide structure harboring a cobalt ion in its center is conserved among all natural cobamides, but the upper and lower axial ligands coordinated to the cobalt ion can vary (Renz, 1999; Banerjee and Ragsdale, 2003; Gruber *et al.*, 2011; Bridwell-Rabb and Drennan, 2017a). The adenine-containing cobamide cofactor in *Sulfurospirillum* spp. is synthesized *de novo*, however, other organohalide-respiring organisms like *D. restrictus* or *Dehalococcoides* spp. are corrinoid-auxotrophic and depend on cobamide salvaging and modification from their environment (Holliger *et al.*, 1998; Rupakula *et al.*, 2013; Löffler *et al.*, 2013; Moore and Escalante-Semerena, 2016). In this way, the dechlorinating activity in *Dehalococcoides* spp. was shown to depend on specific cobamides binding benzimidazole derivatives as lower ligand that were expected to be incorporated into the RDase proteins (Yan *et al.*, 2012; Yi *et al.*, 2012; Yan *et al.*, 2013; Yan *et al.*, 2016). A known consensus sequence for cobamide binding (DxHxxG), as it was shown for a subset of other cobamide-dependent enzymes (Ludwig and Matthews, 1997), is thereby not encoded in the RDase amino acid sequences, except in the dichloropropane RDase from *Dehalogenimonas lykanthroporepellens* BL-DC-9 (Padilla-Crespo *et al.*, 2014). This led to the assumption of a non-covalently binding of the cofactor to the enzyme. On the other hand, two binding motifs for iron-sulfur clusters are highly conserved in the C-terminal part of all RDase protein sequences (Hug *et al.*, 2013; Judger *et al.*, 2015). They can bind either two [4Fe-4S] cluster as shown for PceA of *D. restrictus* or VcrA of *Dehalococcoides mccartyi* (Schumacher *et al.*, 1997; Parthasarathy *et al.*,2015), or alternatively one [4Fe-4S] and one [3Fe-4S] cluster like in CprA of *D. dehalogenans* (van de Pas *et al.*, 1999). Determination of iron and acid-labil sulfide contents in further RDases rather points towards two [4Fe-4S] cluster as the common cofactors

(see Tab. 1.1). With low midpoint redox potentials of approximately -480 mV at pH 8 (Schumacher *et al.*, 1997) the cubane iron-sulfur clusters are proposed to be involved in the intramolecular electron transfer to the cobamide cofactor in the active site. The apparent molecular masses of the protein monomers ranging from 35 to 65 kDa.

The mature respiratory RDases are associated to the exoplasmic site of the cytoplasmic membrane (Nijenhuis and Zinder, 2005; John *et al.*, 2006; Reinhold *et al.*, 2012) most probably using a small hydrophobic, membrane integral RdhB as membrane anchor, a protein that is encoded in gene clusters together with the RDase genes (Futagami *et al.*, 2008; Judger *et al.*, 2015). A precursor protein bearing an N-terminal Tat (twin arginine translocation) signal peptide is produced inside the cell and equipped with all cofactors before export through the cytoplasmic membrane by the twin arginine translocation pathway (Palmer and Berks, 2012). A model of the PceA maturation in *S. multivorans* is depicted in Figure 1.3. The biosynthesis of the two iron-sulfur cluster might be mediated by the *isc*- and *suf*-systems (*isc*: iron-sulfur-cluster formation, *suf*: sulfur mobilization; reviewed in Fontecave and Ollagnier-de-Choudens (2008) before incorporation into the PceA apoprotein (Goris *et al.*, 2014). *De novo* biosynthesis of the norpseudo-B_{12} cofactor follows the complex, multi-step 'anaerobic pathway' described by Warren *et al.* (2002) and Moore *et al.* (2013). All genes for cobamide biosynthesis are encoded in one cluster located close to the *pceA* gene in the so-called organohalide respiration gene region (Goris *et al.*, 2014). The incorporation of variable lower ligand bases via the nucleotide loop assembly pathway is thereby the last step in the cobamide biosynthesis (Warren *et al.*, 2002). Prior to incorporation the nucleotide bases have to be activated by the addition of a phosphoribosyl moiety, a reaction mediated by the nicotinate-nucleotide dimethylbenz-imidazole phosphoribosyltransferase (CobT) (Trzebiatowski and Escalante-Semerena, 1997; Claas *et al.*, 2010; Hazra *et al.*, 2013; Chan *et al.*, 2014). Some RDase gene cluster additionally encode for putative trigger-factor like chaperones RdhT, which are expected to ensure accurate folding of the RDase (Morita *et al.*, 2009; Maillard *et al.*, 2011; Mac Nelly *et al.*, 2014). Such an RdhT homolog was not found in *S. multivorans*, but its function might be taken over by general molecular chaperones like Trigger Factor, DnaK or GroEL (Kim *et al.*, 2013; Castanié-Cornet *et al.*, 2014).

Only recently, two non-respiratory RDases functionally linked to NAD(P)H-dependent oxidoreductases were identified in the facultative aerobic *Comamonas* sp. 7D-2 and *Nitratireductor pacificus* that are lacking the Tat signal peptide and remain soluble in the cytoplasm (Chen *et al.*, 2013; Payne *et al.*, 2015a).

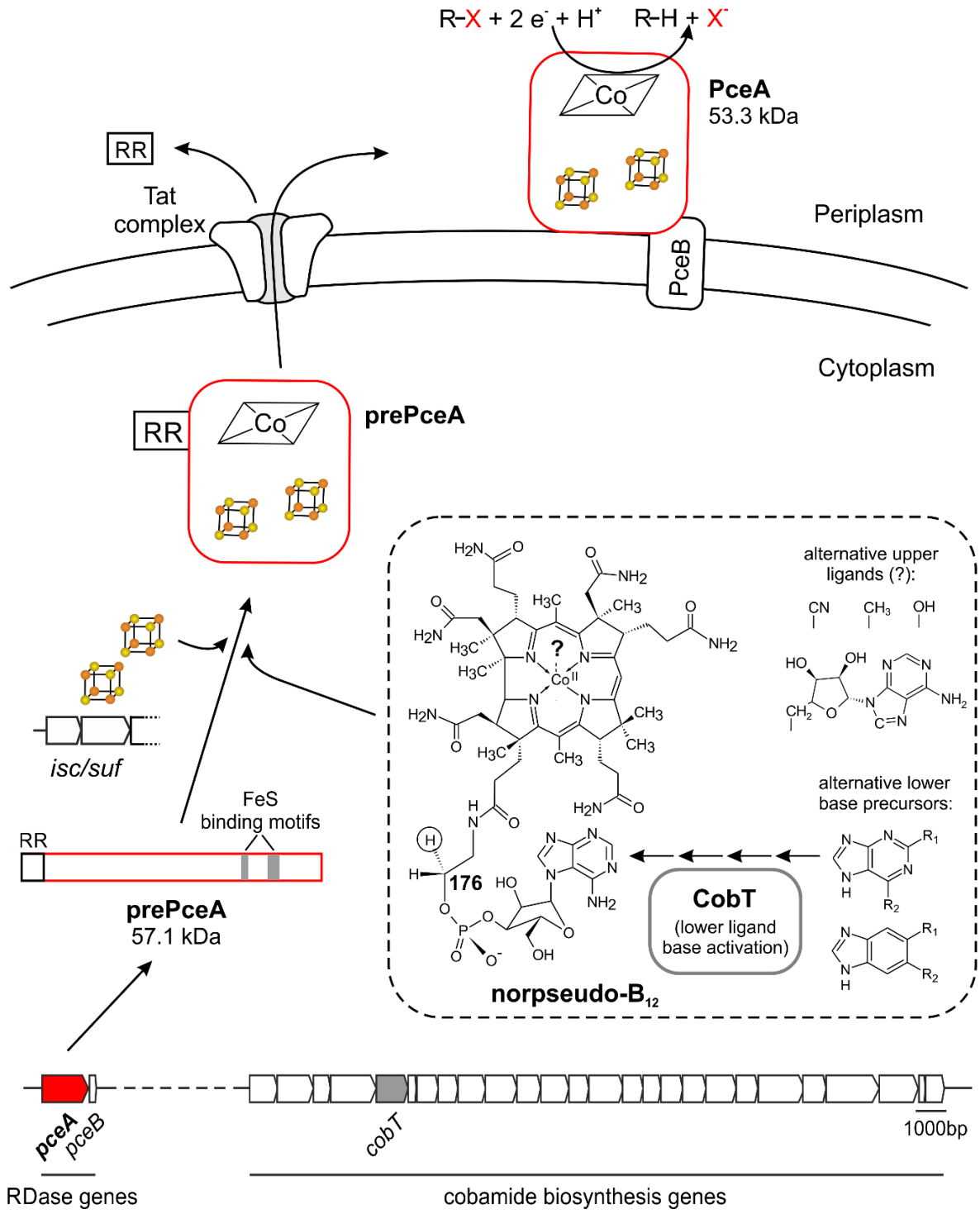

Figure 1.3: Model of the PceA maturation in *S. multivorans*. The structure of the norpseudo-B_{12} cofactor is highlighted in the box. Putative upper and lower axial ligands, known to be incorporated into cobamides in general, are listed. (pre)PceA: (precursor of) tetrachloroethene reductive dehalogenase; CobT: nicotinate-nucleotide dimethylbenzimidazole phosphoribosyl-transferase; PceB: membrane achor for PceA; *isc/suf*: iron-sulfur cluster biosynthesis genes; RR: twin arginine translocation (Tat) signal peptide for the Tat system; R: carbon backbone; X: halide.

These enzymes are not involved in energy conservation, but rather remove the halogen substituents and thus prepare organohalides for subsequent degradation of the carbon backbone. All respiratory RDases characterized so far, except the 3-chlorobenzoate RDase of *D. tiedjei*, are oxygen sensitive with half-life times in air of about one hour two several hours (see references Tab 1.1). How the non-respiratory enzymes prevent oxidative damage in an aerobic environment is not known.

In general, all RDases listed in Tab. 1.1 can be devided into three groups converting preferably either alkyl halides such as halogenated alkenes, or halogenated alkanes or aryl halides, all of them in a halogen substitution reaction. The conversion of aliphatic and aromatic organohalides by a single enzyme has rarely been described, but cannot be excluded (van de Pas *et al.*, 2001; Mac Nelly *et al.*, 2014). Next to these RDases, organohalide-respiring bacteria were found that catalyze a different type of dehalogenation reaction, namely the dihaloelimination of vicinal halogenated alkanes that results in the formation of a double bond. Growth of *Desulfitobacterium dichloroeliminans* strain DCA1 was described to be restricted to dihaloelimination reactions, and not being able to utilize any substrates via halogen substitution (De Wildemann *et al.*, 2003). Only one RDase gene, the dichloroethane (DCA) reductive dehalogenase (DcaA) gene, was found in the organism (Marzorati *et al.*, 2007). While the involvement of a cobamide cofactor was deduced from propyl iodide inhibition studies (De Wildemann *et al.*, 2003), further biochemical analysis of the corresponding DcaA protein is still missing. Further putative dihaloeliminating RDase genes were detected in *Dehalobacter* sp., *D. lykanthroporepellens* BL-DC-9 as well as in several 1,2-DCA dehalogenating enrichment cultures (Grostern and Edwards, 2009; Padilla-Crespo *et al.*, 2014; Marzorati *et al.*, 2010; Merlino *et al.*, 2015). So far, it is not clear what is different in these dihaloeliminating enzymes.

1.4 Cobamide-dependent enzymes and their mechanisms

RDases are classified within the subfamily of cobamide-containing iron-sulfur proteins apart from the well-characterized adenosylcobalamin-dependent enzymes and methyltransferases (Matthews, 2001; Banerjee and Ragsdale, 2003; Gruber *et al.*, 2011; Ding *et al.*, 2016; Bridwell-Rabb and Drennan, 2017a). Adenosylcobalamin-dependent (coenzyme-B_{12} dependent) enzymes are widely spread among carbon skeleton and amino mutases, isomerases and eliminases (Gruber *et al.*, 2011; Bridwell-Rabb and Drennan, 2017a). Here, a 5'-

deoxyadenosyl group is bound as upper ligand to the cobalt ion in the cobamide cofactor. These enzymes generate 5'-deoxyadenosyl radicals via homolytic cleavage of the [Co^{III}]-carbon bond, leaving the cobalt ion in the [Co^{II}]-state. The radicals then act as nucleophiles during catalysis of a variety of rearrangement reactions. In cobamide-dependent methyltransferases the [Co^{III}]-carbon bond in the methylcobalamin cofactor is cleaved either heterolytically in a nucleophilic S_N2 reaction releasing a methyl ion or homolytically releasing a methyl radical (Matthews, 2001; Ragsdale, 2008; Ding *et al.*, 2016). For regeneration of the methylcobalamin the highly nucleophilic superreduced [Co^{I}]-state of the cobamide cofactor directly attacks the methyl group donor substrates in an S_N2 reaction. Methyltransferases are involved in key steps of several metabolic pathways, like the fixation of CO_2 via the acetyl-CoA pathway, in methanogenesis or in methionine synthesis (Thauer, 1998; Matthews, 2001; Ragsdale, 2006). Both enzyme classes bind the cobamide cofactor mostly in a 'base-off/His-on' conformation, which means the coordination of the lower ligand towards the cobalt ion is replaced by a histidine of the protein backbone (Gruber *et al.*, 2011). RDase protein sequences do not encode for such a cobamide binding motif. The only proteins found, which share sequence similarities to RDases, are the cobamide-dependent epoxyqueuosine reductases (QueG) responsible for the formation of queuosine during tRNA modification (Miles *et al.*, 2011; Frey *et al.*, 1988). Structural and spectroscopic analysis of QueG from *Streptococcus thermophilus* (Payne *et al.*, 2015b) and *Bacillus subtilis* (Miles *et al.*, 2015; Dowling *et al.*, 2016) showed the cobamide cofactor bound in the 'base-off' conformation, e.g. the cobalt ion does not bind any lower ligand. The catalytic cycle was proposed to be based on a nucleophilic attack of the [Co^{I}]-state of the cobamide cofactor leading to cobalt-carbon bond formation with the substrate (alkylation). The alkyl substituent is than released by a heterolytic cleavage of the cobalt-carbon bond. However, function predictions for RDases should be drawn cautiously. In early studies the abiotic cobamide-dependent reductive dehalogenation of alkyl halides was shown to proceed via nucleophilic attack of the [Co^{I}]-state on the carbon backbone of the substrate leading to the alkylation of the cobalt (Schrauzer and Deutsch, 1969; Krone *et al.*, 1989a), similar to what was described for QueGs. Later, however, an initial dissociative single electron-transfer mechanism was proposed for the abiotic conversion of tetra- and trichloroethene (Glod *et al.*, 1997) as well as for the enzymatic reductive dehalogenation of chloropropenes and bromoethenes in PceA of *S. multivorans* (Schmitz *et al.*, 2007; Ye *et al.*, 2010). Also here, the superreduced [Co^{I}]-state was assumed to be the catalytically active form. In the latter case, only low potential electron donors (≤ -360 mV), which are potentially strong enough to reduce the

[Co^{II}]/[Co^{I}] redox pairs with midpoint potentials of -350 to -380 mV at pH 7.5-8 in PceA of *S. multivorans* and *D. restrictus* and in CprA of *D. dehalogenans* (Schumacher *et al.*, 1997; van de Pas *et al.*, 1999; Kräutler *et al.*, 2003), allow for substrate conversion (Miller *et al.*, 1997). However, so far all function predictions for RDases are only based on indications from product formation. Further detailed mechanistic studies will be necessary to elucidate the catalytic cycle of RDases.

1.5 Aims of the study

In this work, the in-depth structural and functional characterization of RDase enzymes should be intensified. Diekert and colleagues showed that PceA of *S. multivorans*, known for its ability to dehalogenate tetrachloroethene (PCE) to trichloroethene (TCE) and subsequently *cis*-1,2-dichloroethene (DCE) via halogen substitution reactions, could be isolated in higher concentrations allowing for cofactor extraction and identification (Neumann *et al.*, 1996; Kräutler *et al.*, 2003). The enzyme was therefore also chosen for the elucidation of the three-dimensional structure of an RDase by X-ray crystallography. Earlier studies suggest that the cobamide cofactor might vary between different RDases. The structural variability in the lower ligand base of the cobamide and its influence on substrate conversion should be studied in PceA by guiding the *de novo* cobamide biosynthesis in *S. multivorans* towards different cobamide derivatives. Building on the three-dimensional structure of PceA further insights into the reaction mechanism of RDases were expected from PceA crystals in complex with substrates and products as well as analogs of them. Putative protein-substrate interactions should be furthermore investigated during substrate turnover using EPR spectroscopy. In addition, important structural elements involved in the halogen substitution mechanism and the active site arrangement of RDases should be studied by site-directed mutagenesis in a heterologously produced PceA protein, and directly compared with the architecture of a dihaloeliminating RDase, the DcaA of *D. dichloroeliminans* DCA1 not biochemically characterized so far (De Wildemann *et al.*, 2003; Marzorati *et al.*, 2007).

Finally, the application of PceA from *S. multivorans* as a representative for other respiratory RDases should be discussed. And to open the way for a future use of RDases in bioremediation attemps on organohalide-contaminated sites the functionality of PceA in electrochemical reactors was tested.

2 Manuscripts

2.1 Structural basis for organohalide respiration

Bommer M, Kunze C, Fesseler J, Schubert T, Diekert G, Dobbek H (2014) *Science* 346, 455-458.

2.2 Selective utilization of benzimidazolyl-norcobamides as cofactors by the tetrachloroethene reductive dehalogenase of *Sulfurospirillum multivorans*

Keller S, Kunze C, Bommer M, Paetz C, Menezes RC, Svatoš A, Dobbek H, Schubert T; in preparation for submission in *J Bacteriol*.

2.3 Cobamide-mediated enzymatic reductive dehalogenation via long-range electron transfer

Kunze C, Bommer M, Hagen WR, Uksa M, Dobbek H, Schubert T, Diekert G (2017) *Nat Commun* 8, 15858.

2.4 Subtle changes in the active site architecture untangled overlapping substrate ranges and mechanistic differences of two reductive dehalogenases

Kunze C, Diekert G, Schubert T (2017) accepted in *FEBS J*, August 30, doi: 10.1111/febs.14258.

2.5 Selective light-driven enzymatic dehalogenations of organic compounds

Siritanaratkul B, Islam STA, Schubert T, Kunze C, Goris T, Diekert G, Armstrong FA (2016) *RSC Adv* 6, 84882-84886.

2.1 Structural basis for organohalide respiration

Bommer M*, Kunze C*, Fesseler J, Schubert T, Diekert G, Dobbek H (2014) *Science* 346, 455-458.

* These authors contributed equally to this work.

The first three-dimensional structure of a respiratory RDase was elucidated using PceA isolated from *S. multivorans*. The norpseudo-B_{12} cofactor was found to be non-covalently bound in its 'base-off' state in the center of the protein with the two [4Fe-4S] cluster in distances allowing for electron transfer from an external electron donor to the cobamide. Based on the architecture of the active site and the positioning of substrate and product analogues inside, a reaction mechanism for halgen substitution reactions was proposed involving a highly conserved tyrosine-arginine/lysine pair in proton transfer.

My own contribution to this publication covers about 40%.
I conducted all cultivations of *S. multivorans*, as well as purifications and enzyme activity assays of PceA. During two day stays at the Humboldt University to Berlin I prepared the crystallization samples with isolated PceA in various buffer solutions and screened them for crystals formed, a task that was otherwise performed by Martin Bommer. All Coauthors participated in the evaluation and interpretation of the crystallization data, and in writing the manuscript.
I contributed to the generation of the *S. multivorans* mutant strain in the course of my master thesis. Also size determination of PceA using gel filtration/ size exclusion chromatography was part of my master thesis.

For supplementary information see appendix, pp. i - xvii.

22. B. S. Fowler, P. J. Mikochik, S. J. Miller, *J. Am. Chem. Soc.* **132**, 2870–2871 (2010).
23. D.-W. Gao, Q. Gu, S.-L. You, *ACS Catal.* **4**, 2741–2745 (2014).
24. M. Tokunaga, J. F. Larrow, F. Kakiuchi, E. N. Jacobsen, *Science* **277**, 936–938 (1997).
25. D. R. Jensen, J. S. Pugsley, M. S. Sigman, *J. Am. Chem. Soc.* **123**, 7475–7476 (2001).
26. E. M. Ferreira, B. M. Stoltz, *J. Am. Chem. Soc.* **123**, 7725–7726 (2001).
27. J. Song, Y. Wang, L. Deng, *J. Am. Chem. Soc.* **128**, 6048–6049 (2006).
28. A. Berkessel, F. Cleemann, S. Mukherjee, *Angew. Chem. Int. Ed.* **44**, 7466–7469 (2005).
29. V. D. Bumbu, V. B. Birman, *J. Am. Chem. Soc.* **133**, 13902–13905 (2011).
30. S. Zhou *et al.*, *Angew. Chem. Int. Ed.* **53**, 7883–7886 (2014).

ACKNOWLEDGMENTS

We gratefully acknowledge The Scripps Research Institute and NIH (National Institute of General Medical Sciences, 2R01GM084019) for financial support. J.-Q. Y. and L.C. conceived the concept. L.C. developed the enantioselective C–H iodination. L.C. and K.-J.X. synthesized the amine substrates. J.-Q.Y. directed the project. We thank J. Spangler for constructive suggestions. Metrical parameters for the structures of **3l** are available free of charge from the Cambridge Crystallographic Data Centre under reference number CCDC-1021096.

SUPPLEMENTARY MATERIALS

www.sciencemag.org/content/346/6208/451/suppl/DC1
Materials and Methods
Supplementary Text
Tables S1 and S2
References (*31*–*35*)

9 July 2014; accepted 5 September 2014
10.1126/science.1258538

METALLOPROTEINS

Structural basis for organohalide respiration

Martin Bommer,[1]* Cindy Kunze,[2]* Jochen Fesseler,[1] Torsten Schubert,[2] Gabriele Diekert,[2]† Holger Dobbek[1]†

Organohalide-respiring microorganisms can use a variety of persistent pollutants, including trichloroethene (TCE), as terminal electron acceptors. The final two-electron transfer step in organohalide respiration is catalyzed by reductive dehalogenases. Here we report the x-ray crystal structure of PceA, an archetypal dehalogenase from *Sulfurospirillum multivorans*, as well as structures of PceA in complex with TCE and product analogs. The active site harbors a deeply buried norpseudo-B_{12} cofactor within a nitroreductase fold, also found in a mammalian B_{12} chaperone. The structures of PceA reveal how a cobalamin supports a reductive haloelimination exploiting a conserved B_{12}-binding scaffold capped by a highly variable substrate-capturing region.

Anaerobic microorganisms use alternative terminal electron acceptors during respiration, such as nitrate, sulfate, iron(III), or even organohalides. The accumulation of polluting organohalides such as perchloroethylene (PCE, also tetrachloroethene) and trichloroethene (TCE) in the environment, which have been heavily used for dry cleaning and degreasing, is problematic because of their toxicity; however, microbial organohalide respiration can transform these compounds into less toxic forms. Organohalide respiration requires reductive dehalogenases (RDases) for the central reduction step (*1*). In contrast to terminal reductases that contain prosthetic heme groups, molybdopterin, or flavins as cofactors, RDases harbor a corrinoid cofactor and two Fe/S clusters (*2*). RDases are able to convert some of the most noxious environmental pollutants, including halogenated phenols, dioxins, biphenyls, and aliphatic hydrocarbons. RDase genes were identified in distantly related bacterial genera belonging to the chloroflexi; firmicutes; gamma-, delta-, and epsilonproteobacteria; and even archaea (*3*).

[1]Institut für Biologie, Strukturbiologie/Biochemie, Humboldt-Universität zu Berlin, Unter den Linden 6, 10099 Berlin, Germany. [2]Institut für Mikrobiologie, Friedrich-Schiller-Universität Jena, Lehrstuhl für Angewandte und Ökologische Mikrobiologie, Philosophenweg 12, 07743 Jena, Germany.
*These authors contributed equally to this work. **†Corresponding author. E-mail: holger.dobbek@biologie.hu-berlin.de (H.D.); gabriele.diekert@uni-jena.de (G.D.)**

Several hundred RDase gene sequences deposited in databases await testing for functionality and determination of the substrate spectrum. Low growth yields and the oxygen sensitivity of the RDases have hindered large-scale purification and biochemical characterization of RDases (*1*). Genetic manipulation of the bacterial isolates has thus far been difficult, and only recently was functional heterologous production of RDases reported, but it remains challenging (*4*). Structural data will help to resolve how RDases evolved, function, and specifically select the many different substrates, some of which have been present in the biosphere for less than a century.

Here we report the crystal structure of a reductive dehalogenase, PceA (*5*), of the microaerophilic epsilonproteobacterium *Sulfurospirillum multivorans* (formerly *Dehalospirillum multivorans*) (*6*) (i) in an empty state; (ii) in the presence of TCE; (iii) in the presence of the *cis*-dichloroethene (*cis*-DCE) (product) analog *cis*-dibromoethene (*cis*-DBE); and (iv) in the presence of iodide, a substitute for the leaving chloride, at a maximum resolution of 1.6 Å (*7*). *S. multivorans* was isolated in the mid-1990s from activated sludge and possesses a flexible catabolism integrating numerous terminal reductases encoded in its genome (*8*). *S. multivorans* is able to couple the reductive dechlorination of PCE, TCE, or dibromoethene (DBE) to growth (*9*, *10*) through its prototypical RDase PceA.

The 464 amino acids of PceA are structured in a compact α/β fold domain (Fig. 1A). The structure can be divided into an N-terminal unit (residues 1 to 138), a norpseudo-B_{12} binding core (residues 139 to 163 and 216 to 323), an insertion unit (residues 164 to 215), an iron-sulfur cluster binding unit (residues 324 to 394) and a C-terminal unit (residues 395 to 464) (fig. S1). Two protomers in the $P4_1$ asymmetric unit interact tightly to form a dimer with a twofold noncrystallographic symmetry. Two α helices of the norpseudo-B_{12} binding core and one α helix of the N-terminal unit form a helical bundle with their symmetry mates. Along with extensive loop regions in the N- and C-terminal units, these bundles create the dimer interface. The interface covers 20% of the accessible surface area of the protomer, supporting a compact and stable dimeric arrangement. Using gel filtration, an apparent molecular mass of 89 kD (fig. S2) was determined for PceA purified from the membrane fraction, which agrees with a dimeric rather than a monomeric structure as reported previously for the soluble wild-type enzyme (*5*).

RDases lack obvious sequence similarities to other enzyme families, and the fold of PceA is unlike that of known corrinoid-dependent methyltransferases (*11*) or mutases (*12*). The most similar protein with clear homology found was methylmalonic aciduria *cblC* type with homocysteinuria (MMACHC) (*13*) (fig. S3). MMACHC is a B_{12}-trafficking chaperone essential for the formation of adenosyl- or methylcobalamin in humans by catalyzing the reductive removal of the upper axial ligands from cyanocobalamin and alkylcobalamins. Structural homology is limited to the B_{12}/norpseudo-B_{12}–binding core, which resembles the nitroreductase family fold (*14*) (fig. S3). Consequently, RDases and MMACHC most likely evolved from a common ancestral B_{12}-binding protein.

In addition to the norpseudo-B_{12} cofactor, PceA also harbors two [4Fe-4S] clusters. Short distances between the two [4Fe-4S] clusters and the proximal [4Fe-4S] cluster and the Co bound to the corrin ring are expected to allow for a rapid electron transfer within a protein monomer (*15*) (Fig. 1B). The proximal [4Fe-4S] cluster is in van der Waals (vdW) contact distance to the C83 carboxamide side chain and C8 of the corrin ring [for atom numbering, see (*2*)], with the carboxamide N84 being in hydrogen bond distance to a μ3-sulfido ligand of the [4Fe-4S] cluster. The two active sites of the PceA dimer are at a Co-Co distance of 42 Å without cofactors between them, indicating two independent catalytic units per dimer (Fig. 1A).

Both [4Fe-4S] clusters are within 6 Å of the enzyme surface, whereas norpseudo-B_{12} is deeply buried in the structure. Most interactions between the cobalamin cofactor's ring system and the protein matrix are due to hydrogen bonds between the cofactor and the norpseudo-B_{12}–binding core of PceA (Fig. 2). Binding of the phosphate and parts of the adenine group of norpseudo-B_{12} is mediated by a loop in the iron-sulfur cluster binding unit. Co is not coordinated by adenine (base off), and the conformation of the linker is curled rather than extended as is typical for base-off B_{12} (*14*, *16*). Compared to the base-on conformation of isolated norpseudovitamin B_{12} (*2*), several conformational changes, including a 90° rotation around the bond between phosphate and the C3′ of ribose and flip of the ribose, are needed to convert the base-on conformation into the base-off conformation found in PceA (Fig. 2). In comparison to the dimethylbenzimidazole moiety of B_{12}, the adenine moiety of norpseudo-B_{12} has several hydrogen-bond acceptor and donor functions, which in addition to anchoring the cofactor allows solvent accessibility (Fig. 2, inset). C176 of the nucleotide loop packs closely against the adjacent β sheet, and the methyl group found in B_{12} at this position would force the loop to adopt a different conformation, which might explain the preference for norpseudo-B_{12}.

PceA contains Co^{II} in the as-isolated state (*2*), for which an axial ligand is typically observed. Additional density is found above the β face of Co, with a Co-X distance of 2.5 Å. The density has been tentatively assigned to a water molecule. Reduction to the catalytically relevant super-reduced Co^{I} is probably facilitated by the weak axial ligation, making Co effectively tetracoordinated in the protein, and agrees with the elevated midpoint potential of the Co^{II}/Co^{I} transition of –380 mV (pH 7.5, versus a standard hydrogen electrode) (*2*).

Substrate access to the active site is restricted by a selection filter with the shape of a 3 × 5.5 Å "letterbox," a gap made up of side chains from

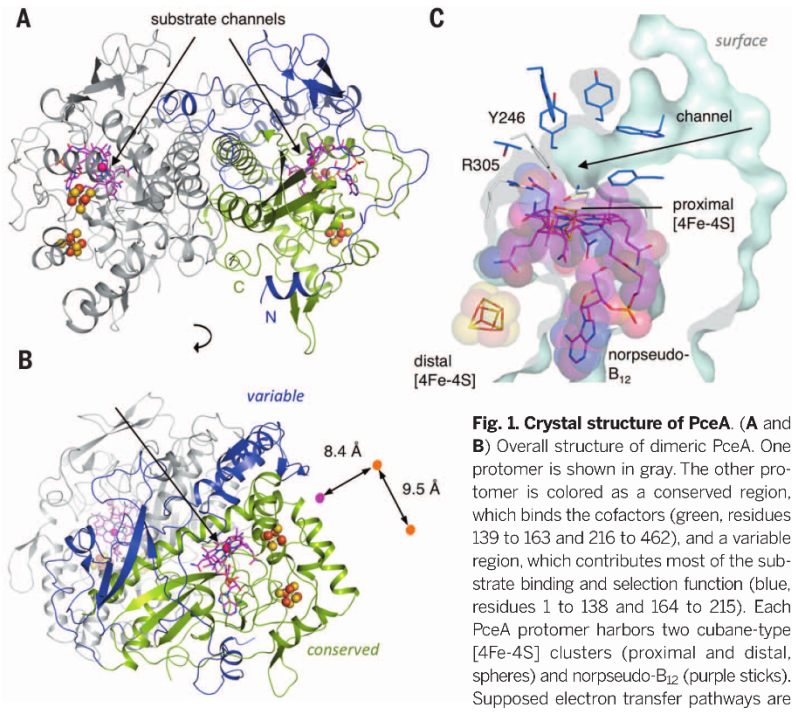

Fig. 1. Crystal structure of PceA. (**A** and **B**) Overall structure of dimeric PceA. One protomer is shown in gray. The other protomer is colored as a conserved region, which binds the cofactors (green, residues 139 to 163 and 216 to 462), and a variable region, which contributes most of the substrate binding and selection function (blue, residues 1 to 138 and 164 to 215). Each PceA protomer harbors two cubane-type [4Fe-4S] clusters (proximal and distal, spheres) and norpseudo-B_{12} (purple sticks). Supposed electron transfer pathways are indicated in (B), along with distances between the closest Fe atoms of the [4Fe-4S] clusters and Co of norpseudo-B_{12}. (**C**) Active-site cavity of PceA. Conserved polar residues in proximity to the axial position of Co are depicted as white sticks, hydrophobic residues of the second ligand sphere as blue sticks. A 12 Å–long channel was identified as the substrate entry site to the active-site dome.

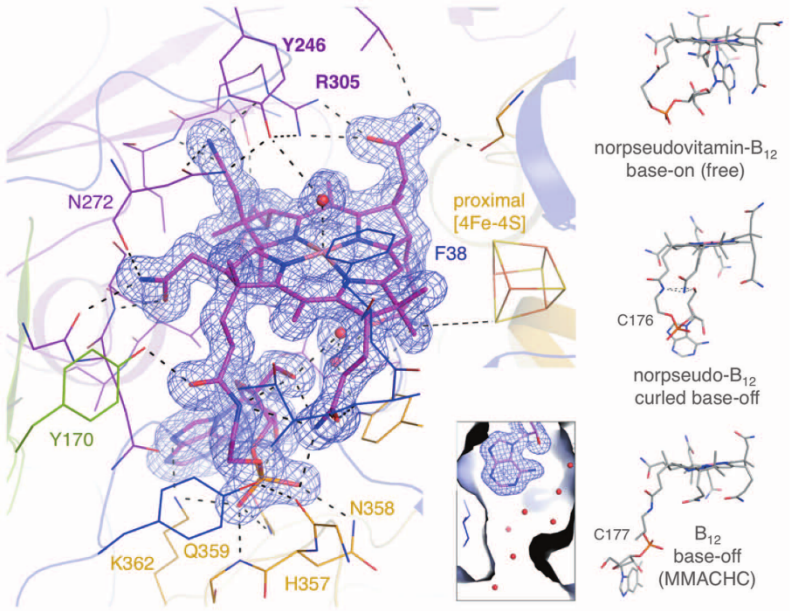

Fig. 2. Norpseudo-B_{12} binding. Potential hydrogen-bonding residues are colored according to their position within PceA: blue, N-terminal (residues 1 to 138); purple, norpseudo-B_{12}–binding core (residues 139 to 163 and 216 to 323); green, insertion unit (residues 164 to 215); yellow, [4Fe-4S]-cluster coordinating loop (residues 324 to 394). The 1σ 2_mFo-$_DFc$ electron density map for norpseudo-B_{12} and water molecules is shown as mesh. The inset shows the solvent-accessible adenine moiety. A comparison of corrinoid linker geometries is shown on the right: free norpseudovitamin B_{12} (*2*), base on (Cambridge Crystallographic Data Centre: 217274, top), norpseudo-B_{12} bound to PceA (middle), and base-off B_{12} in MMACHC (*14*) (Protein Data Bank: 3SOM, bottom). The β ligand is omitted for clarity.

the N-terminal and insertion units (fig. S4). After the filter, PCE and TCE have to pass through a 12 Å–long hydrophobic channel isolating the active site inside the core of the protein (Fig. 1C, arrow). The channel then expands to create the amphiphilic active site pocket at the β face of the corrin ring, where access to the cofactor itself is further restricted by a ring fence of side chains (fig. S4A). The cavity is predominantly lined by tryptophan and tyrosine residues, which define its shape and volume. Three adjacent polar residues, namely Tyr^{246}, Arg^{305}, and Asn^{272} from the B_{12}-binding core, are highly conserved (Figs. 2 and 3C). Of these Tyr^{246} is invariant, whereas some RDases have functionally conserved replacements with a lysine residue in place of Arg^{305} (fig. S5). Asn^{272} is conserved in a subset of RDases. The residues are close to the corrin ring and point with their side chains into the active site pocket, positioning the phenolic hydroxyl group of Tyr^{246} in hydrogen-bonding distance to the guanidinium group of Arg^{305} (Fig. 3C).

To further analyze how substrate specificity and regioselectivity are determined by the protein structure, we analyzed the structure of PceA with its substrate TCE and the tribromoethene dehalogenation product *cis*-DBE. After soaking with TCE, additional density matching the shape of TCE was found in the active site pocket above the corrin ring (Fig. 3), concomitant with a reduction in the occupancy of the close-by water ligand. TCE binds with the dichlorinated carbon (C1) facing the corrin ring. Judged by the shape of the electron density, TCE bound in two orientations with the lone chloride in cis and trans to the Co-facing chloride (Fig. 3A). The PCE/TCE binding pocket is restricted by vdW contacts to the surrounding aromatic side chains (fig. S4). Tyr^{246} is within hydrogen-bonding distance to the Cl substituent of TCE nearest to Co.

Reductive dehalogenation of TCE produces *cis*-DCE, whose binding site and orientation we revealed using *cis*-DBE. *cis*-DBE was used because the stronger anomalous scattering of Br as compared to Cl allowed identification of *cis*-DBE also at low occupancy. Two strong patches of density were observed in the same place as two Cl atoms in the minor orientation of TCE, marking the position of *cis*-DBE. The chloride atom of TCE nearest to Co and Tyr^{246} is unoccupied in the product complex (Fig. 3B and fig. S6).

The side chains in the substrate-binding pocket are tightly packed with little conformational freedom and probably disfavor the binding of molecules significantly larger than PCE or TCE by steric exclusion. Thus, the binding pocket provides a second gate for substrate selection. In contrast to the variable residues forming the channel entrance, aromatic residues within the pocket are partially conserved between different RDases but are dispersed in sequence (fig. S5). Two layers of control over substrate selection (the "letterbox" and the active site) could achieve the necessary selectivity within the wide range of organohalides converted by distinct RDases, which often exist within the same organism (*3*).

PceA is attached to the periplasmic side of the cytoplasmic membrane in *S. multivorans* cells (*17*). For both PceA monomers to function independently, the twofold noncrystallographic symmetry axis of the dimer should be perpendicular to the membrane plane in the PceA-PceB complex. This would agree with two principal orientations of our PceA structure on the membrane. Amino acid residues 411 to 431 (Fig. 4, red ribbon) show high flexibility in all crystals and could only be modeled in one out of six protomers in an alternative ($P2_1$) crystal form, where α-helix 15 (fig. S1) is stabilized by a crystal contact. The disordered helices in both monomers are on the same face of the structure, and we speculate that this is the site of interaction with the PceB membrane anchor that is destabilized after complex dissociation in the purification process. Our proposed arrangement would locate the two electron entrance ports close to the membrane and the substrate channel pointing toward the periplasmic space (Fig. 4).

RDase catalysis involves a transfer of two electrons and a proton, while accommodating the dissociation of a chloride ion from the substrate. The initial step in dechlorination of PCE probably involves a dissociative electron transfer from Co^{I} to PCE, resulting in the formation of a trichlorovinyl radical (*18*, *19*) by chloride elimination, while the cofactor is returned to the Co^{II} state (*18*, *20*, *21*). The distance for this electron transfer between Co and Cl of TCE is 5.8 Å in our structure (Fig. 4).

The intermittent water (Fig. 3A) is depopulated in the TCE-bound active site only, suggesting that the β-ligand water, 2.2 Å from the proximal chloride, is displaced by TCE. The same position was identified as a weak halide-binding site by a strong anomalous signal for iodide at 0.5 M concentration (fig. S6D) but the absence of such a signal at lower chloride concentrations. This would qualify the proximal chloride at C1 over the tightly enclosed distal chloride as the leaving group, ultimately yielding *cis*-DCE from the minor orientation of TCE displayed in Fig. 3A, consistent with the data obtained with the *cis*-DBE product analog.

Recombination of the trichlorovinyl radical with Co^{II}, forming an organometallic intermediate as proposed for free B_{12} (*22*), is an attractive next step but would be disfavored in PceA because of

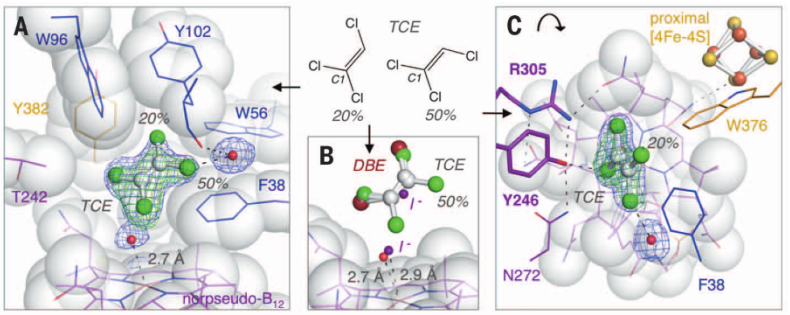

Fig. 3. Substrate/product–analog binding. (**A** and **C**) TCE, overlayed in a high- and low-occupancy (50 and 20% as modeled in the structure) orientation, as indicated in the chemical sketch. Electron density maps are shown for TCE, the β ligand, and water: $1\sigma\ 2_mFo\text{-}_DFc$ (blue) and $4\sigma\ _mFo\text{-}_DFc$ (green). (**B**) Overlay of the active site with TCE, *cis*-DBE, iodide, and the coordinated water (empty structure). Side chains forming the hydrophobic pocket are shown as sticks and are colored according to their position in PceA using the same scheme as in Fig. 2. Hydrogen bonding distances from Tyr^{246}: 2.8 Å (Asn^{272}), 2.9 Å (Arg^{305}), and 2.5 Å (TCE).

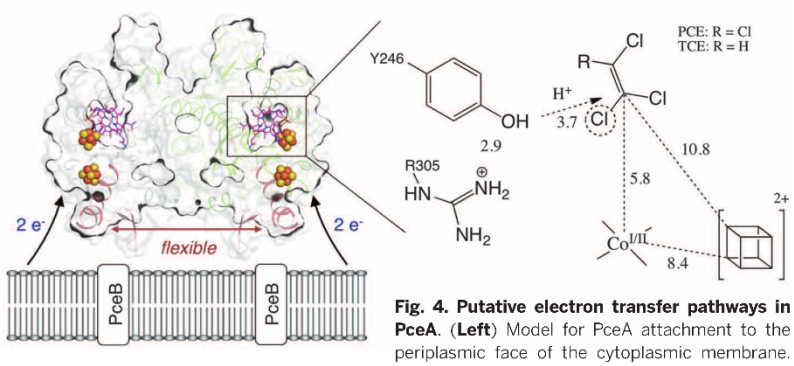

Fig. 4. Putative electron transfer pathways in PceA. (**Left**) Model for PceA attachment to the periplasmic face of the cytoplasmic membrane. The red helix/loop represents structure only observed (helix) or well defined (β sheet/loop) in the presence of a crystal contact in the $P2_1$ crystal form. (**Right**) Distances (in angstroms) for putative electron (dashed lines) and proton (arrow) transfers onto the substrate. The figure shows the geometry observed in the TCE bound crystal.

the dense packing above the β face of the corrin ring (fig. S4A). The same steric constraints would disable an initial nucleophilic attack of Co^{I} on PCE. Instead, the short substrate-cofactor distances would allow the second electron transfer to occur either directly from the proximal [4Fe-4S] cluster or via the Co ion (Fig. 4). The strictly conserved Tyr^{246} is pointing with its phenolic hydroxyl group toward C1 and could donate the required proton to neutralize the carbanion (*20*). Deprotonation of Tyr^{246} could be stabilized by the neighboring positive charge of Arg^{305}. Equally, a role of Tyr^{246} in a radical route (*18*) cannot be excluded.

REFERENCES AND NOTES

1. C. Holliger, G. Wohlfarth, G. Diekert, *FEMS Microbiol. Rev.* **22**, 383–398 (1998).
2. B. Kräutler *et al.*, *Helv. Chim. Acta* **86**, 3698–3716 (2003).
3. L. A. Hug *et al.*, *Philos. Trans. R. Soc. London Ser. B* **368**, 20120322 (2013).
4. A. Mac Nelly, M. Kai, A. Svatoš, G. Diekert, T. Schubert, *Appl. Environ. Microbiol.* **80**, 4313–4322 (2014).
5. A. Neumann, G. Wohlfarth, G. Diekert, *J. Biol. Chem.* **271**, 16515–16519 (1996).
6. H. Scholz-Muramatsu, A. Neumann, M. Messmer, E. Moore, G. Diekert, *Arch. Microbiol.* **163**, 48–56 (1995).
7. Materials and methods are available on *Science* Online
8. T. Goris *et al.*, *Environ. Microbiol.* 10.1111/1462-2920.12589 (2014).
9. E. Miller, G. Wohlfarth, G. Diekert, *Arch. Microbiol.* **166**, 379–387 (1996).
10. L. Ye, A. Schilhabel, S. Bartram, W. Boland, G. Diekert, *Environ. Microbiol.* **12**, 501–509 (2010).
11. C. L. Drennan, S. Huang, J. T. Drummond, R. G. Matthews, M. L. Ludwig, *Science* **266**, 1669–1674 (1994).
12. F. Mancia *et al.*, *Structure* **4**, 339–350 (1996).
13. J. Kim, C. Gherasim, R. Banerjee, *Proc. Natl. Acad. Sci. U.S.A.* **105**, 14551–14554 (2008).
14. D. S. Froese *et al.*, *Biochemistry* **51**, 5083–5090 (2012).
15. H. B. Gray, J. R. Winkler, *Proc. Natl. Acad. Sci. U.S.A.* **102**, 3534–3539 (2005).
16. T. Svetlitchnaia, V. Svetlitchnyi, O. Meyer, H. Dobbek, *Proc. Natl. Acad. Sci. U.S.A.* **103**, 14331–14336 (2006).
17. M. John, R. P. H. Schmitz, M. Westermann, W. Richter, G. Diekert, *Arch. Microbiol.* **186**, 99–106 (2006).
18. J. Shey, W. A. van der Donk, *J. Am. Chem. Soc.* **122**, 12403–12404 (2000).
19. R. P. H. Schmitz *et al.*, *Environ. Sci. Technol.* **41**, 7370–7375 (2007).
20. G. Glod, W. Angst, C. Holliger, R. P. Schwarzenbach, *Environ. Sci. Technol.* **31**, 253–260 (1997).
21. W. Schumacher, C. Holliger, A. J. Zehnder, W. R. Hagen, *FEBS Lett.* **409**, 421–425 (1997).
22. K. M. McCauley *et al.*, *J. Am. Chem. Soc.* **127**, 1126–1136 (2005).

ACKNOWLEDGMENTS

H.D. acknowledges support by the Cluster of Excellence "Unifying Concepts in Catalysis (UniCat)." G.D. and T.S. were supported by the Deutsche Forschungsgemeinschaft (DFG) (Research Unit FOR 1530). M.B. was funded by the DFG through grant SFB 1078-A5. We are grateful for the funding of C.K. by the Ernst Abbe Foundation; in addition, we thank the staff at the Helmholtz-Zentrum Berlin (HZB) MX beamlines and DESY PETRA III beamline P11 for their assistance. We acknowledge access to beamlines of the BESSY II storage ring (Berlin, Germany) via the Joint Berlin MX-Laboratory. The authors thank O. Einsle for critical reading of the manuscript. Structure factors and models have been deposited in the Protein Data Bank under accession numbers 4UQU (empty), 4UR0 (TCE bound), 4UR1 (*cis*-DBE bound), 4UR2 (iodide bound), and 4UR3 ($P2_1$ crystal form).

SUPPLEMENTARY MATERIALS

www.sciencemag.org/content/346/6208/455/suppl/DC1
Materials and Methods
Figs. S1 to S6
Table S1
References (*23*–*35*)

30 June 2014; accepted 18 September 2014
Published online 2 October 2014;
10.1126/science.1258118

WORKING MEMORY

Medial prefrontal activity during delay period contributes to learning of a working memory task

Ding Liu,[1,2]* Xiaowei Gu,[1,2]* Jia Zhu,[1,2]* Xiaoxing Zhang,[1] Zhe Han,[1,2] Wenjun Yan,[1,2] Qi Cheng,[1,2] Jiang Hao,[1]† Hongmei Fan,[1] Ruiqing Hou,[1] Zhaoqin Chen,[1] Yulei Chen,[1] Chengyu T. Li[1]‡

Cognitive processes require working memory (WM) that involves a brief period of memory retention known as the delay period. Elevated delay-period activity in the medial prefrontal cortex (mPFC) has been observed, but its functional role in WM tasks remains unclear. We optogenetically suppressed or enhanced activity of pyramidal neurons in mouse mPFC during the delay period. Behavioral performance was impaired during the learning phase but not after the mice were well trained. Delay-period mPFC activity appeared to be more important in memory retention than in inhibitory control, decision-making, or motor selection. Furthermore, endogenous delay-period mPFC activity showed more prominent modulation that correlated with memory retention and behavioral performance. Thus, properly regulated mPFC delay-period activity is critical for information retention during learning of a WM task.

Working memory (WM) is essential for cognition by allowing active retention of behaviorally relevant information over a short duration known as the delay period (*1*–*3*). Previous studies have shown that the prefrontal cortex (PFC) is crucial for WM, because perturbation of PFC activity impaired WM (*3*) and WM-related activity was observed during the delay period in neurons of dorsal-lateral PFC (DL-PFC) in primates and medial PFC (mPFC) in rodents (*3*–*10*). Nevertheless, the functional role of PFC delay-period activity in WM remains unclear. Memory retention and attentional control are leading candidates (*2*, *3*, *11*). However, PFC is also critical for other brain functions (*3*, *12*, *13*) and has been suggested to be important for inhibitory control (*14*), decision-making (*15*), or motor selection (*16*). These roles cannot be distinguished by a delayed-response task, in which decision-making precedes the delay period (*3*, *12*). In addition, traditional methods for perturbing neural activity (*3*), including transcranial magnetic stimulation (*17*) and electrical stimulation (*18*), do not provide the temporal resolution and cell-type specificity required for delineating the functional role of PFC delay-period activity in WM. We addressed these issues by using a WM task with a delay period designed to temporally separate memory retention from other functions (*5*, *6*, *19*, *20*) and optogenetic approaches (*21*) to bidirectionally manipulate mPFC activity of excitatory and inhibitory neurons during the delay period.

Head-fixed mice were trained to perform an olfactory delayed nonmatch to sample (DNMS) task (Fig. 1, A and B; fig. S1; and movie S1), a modified version of the behavioral paradigms previously used in rats (*19*, *20*). For each trial, an olfactory stimulus (ethyl acetate, EA, or 2-pentanone, 2P) was presented as the sample, followed by a delay period (4 to 5 s) and then a testing olfactory stimulus, either matched or non-matched to the sample. Water-restricted mice were rewarded with water if they licked within a response time window in the nonmatch but not match trials (Fig. 1B and fig. S2). During the delay period, mice need to retain the information associated with the odor sample. The performance correct rate (referred to hereafter as performance), correct rejection rate, discriminability (d'), and lick efficiency steadily increased throughout the training, but there was a ceiling effect for the hit rate (Fig. 1, C and D, and fig. S3). The potential involvement of visual, auditory, or somatosensory cues was excluded (fig. S4A). The performance decreased with increasing duration of the delay period (fig. S4B), a typical hallmark of WM paradigms (*1*, *3*). For a genuine WM task, subjects should be able to perform beyond two cues (*19*, *20*), which was indeed observed (fig. S4C). We next expressed hM4Di, a designer receptor exclusively activated by designer drug (DREADD) (*22*), in mPFC with adeno-associated virus (AAV). Suppression of neural activity (fig. S5) by intraperitoneal injection of clozapine-N-oxide (CNO) significantly impaired the performance of the mice during the learning phase (days 1 to 5, Fig. 1E; statistics shown in table S1).

It is essential that mice were using WM instead of residual odor during the delay period to perform the task. Photoionization detector (PID)

[1]Institute of Neuroscience and Key Laboratory of Primate Neurobiology, Shanghai Institutes for Biological Sciences, Chinese Academy of Sciences, Shanghai 200031, China. [2]University of Chinese Academy of Sciences, Beijing 100049, China.
*These authors contributed equally to this work. †Present address: Friedrich Miescher Institute for Biomedical Research, Maulbeerstrasse 66, 4058 Basel, Switzerland. ‡Corresponding author.
E-mail: tonylicy@ion.ac.cn

2.2 Selective utilization of benzimidazolyl-norcobamides as cofactors by the tetrachloroethene reductive dehalogenase of *Sulfurospirillum multivorans*

Keller S, Kunze C, Bommer M, Paetz C, Menezes RC, Svatoš A, Dobbek H, Schubert T; in preparation for submission in *J Bacteriol*

The variability in the utilization of different cobamide cofactors distinguished by their lower ligand bases, and its influence on substrate conversion was studied in PceA of *S. multivorans*. While the maturation of PceA was shown to be retarded in the presence of norcobalamin instead of the de novo produced norpseudo-B_{12} (Keller *et al.*, 2014), single substituted benzimidazolyl-norcobamides were found that can replace the purinyl-norcobamide cofactor and still allow for correct folding and activity of the enzyme. Structural analysis of PceA equipped with various cobamide cofactors revealed a conserved binding of the nucleotide loop of the different cobamides without steric constraints, which raises the question of an incompatibility specifically for methylated benzimidazolyl-norcobamides that are known to be suitable cobamide cofactors in other RDases.

My own contribution to this publication covers about 15%.
This includes the cultivation of *S. multivorans* in the presence of different lower ligand bases (5-MeBza, 5-OHBza, 5-OMeBza) and the purification of the PceA protein from the respective cells. I performed enzyme activity assays using the purified PceA variants and analyzed and quantified their cobamide cofactors. Furthermore, I prepared the PceA samples for crystallization, and I participated in the revision of the manuscript.

For supplementary information see appendix, pp. xviii - xxxiv.

Selective utilization of benzimidazolyl-norcobamides as cofactors by the tetrachloroethene reductive dehalogenase of *Sulfurospirillum multivorans*

Sebastian Keller[1], Cindy Kunze[1], Martin Bommer[2,§], Christian Paetz[3], Riya C. Menezes[4], Aleš Svatoš[4], Holger Dobbek[2], and Torsten Schubert[1#]

[1]Department of Applied and Ecological Microbiology, Institute of Microbiology, Friedrich Schiller University, Philosophenweg 12, D-07743 Jena, Germany

[2]Structural Biology / Biochemistry, Department of Biology, Humboldt-Universität zu Berlin, Philippstrasse 13, D-10115 Berlin, Germany

[3]Research Group Biosynthesis / NMR and [4]Research Group Mass Spectrometry, Max Planck Institute for Chemical Ecology, Hans-Knöll-Strasse 8, D-07745 Jena, Germany

[§]Present address: Max Delbrück Center for Molecular Medicine, Robert-Roessle-Str. 10, D-13092 Berlin, Germany

[#]Corresponding author: Dr. Torsten Schubert
Friedrich Schiller University, Institute of Microbiology, Philosophenweg 12, D-07743 Jena, Germany
Tel.: +49 (0) 3641-949349; Fax: +49 (0) 3641-949302
e-mail: torsten.schubert@uni-jena.de

SUMMARY

The organohalide-respiring bacterium *Sulfurospirillum multivorans* produces a unique cobamide, namely norpseudo-B_{12}, which serves as cofactor of the tetrachloroethene reductive dehalogenase (PceA). As previously reported, an exchange of the adeninyl-moiety, the lower base of the cofactor, by exogenously applied 5,6-dimethylbenzimidazole led to inactive PceA. In this study, the susceptibility of the organism for guided biosynthesis of various singly substituted benzimidazolyl-norcobamides was investigated and their use as cofactor by PceA was analyzed. Exogenously applied 5-methylbenzimidazole (5-MeBza), 5-hydroxybenzimidazole (5-OHBza), and 5-methoxybenzimidazole (5-OMeBza) were found to be efficiently incorporated as lower bases into norcobamides (NCbas) replacing the endogenous lower base, adenine. Structural analysis of the NCbas by nuclear magnetic resonance spectroscopy uncovered a regioselectivity in the utilization of these precursors for NCba biosynthesis. When 5-MeBza was added to cultures a mixture of 5-MeBza-norcobamide and 6-MeBza-norcobamide was formed and the PceA enzyme activity was affected. In the presence of 5-OHBza, almost exclusively 6-OHBza-norcobamide was produced, while in the presence of 5-OMeBza, predominantly 5-OMeBza-norcobamide was detected. Both NCbas were incorporated into PceA and no negative effect on the PceA activity was observed. In crystal structures of PceA, both NCbas were bound in the 'base-off' mode with the 6-OHBza and 5-OMeBza lower bases accommodated by the same solvent-exposed hydrophilic pocket that harbors the adenine as lower base. This study shows a selective *in vivo* production of different cobamide isomers containing singly substituted benzimidazoles as lower bases and provides unique structural insights into the utilization of different cobamides as cofactors by a cobamide-containing enzyme.

IMPORTANCE

Exogenous singly substituted benzimidazoles efficiently replaced adenine as base of the natural norcobamide produced by the organohalide-respiring epsilonproteobacterium *Sulfurospirillum multivorans*. An unprecedented specificity in the formation of norcobamide isomers containing singly hydroxylated or methoxylated benzimidazoles was observed that implicated a strict regioselectivity of the norcobamide biosynthetic machinery in the organism. In contrast to 5,6-dimethylbenzimidazolyl-norcobamide, the incorporation of singly substituted benzimidazolyl-

norcobamides as cofactor into the tetrachloroethene reductive dehalogenase (PceA) was not impaired. PceA was found to be functional with different norcobamide isomers and structural analysis of the enzyme visualized the various cofactors bound at the same position inside the enzyme. This report provides novel insights into a cobamide-containing enzyme binding both, purinyl- and benzimidazolyl-norcobamide cofactors for function.

INTRODUCTION

Prokaryotes produce structurally different cobamides (Cbas; analogs of vitamin B_{12}), but little is known about their selective or non-selective utilization as cofactors in cobamide-dependent enzymes, such as the reductive dehalogenases (RDases) (1-3). Cobamides are composed of a contracted tetrapyrrole ring system harboring a cobalt ion as central atom (4). In addition to the four nitrogens of the pyrrole ring system in cobamides, the cobalt is bound by two axial ligands ('upper' and 'lower' ligand). Cbas vary in their structure by harboring different lower bases, either purines or benzimidazoles, which can be replaced by phenols (5). Purines or benzimidazoles serve as lower ligand to the cobalt, while phenols cannot. A 5'-deoxyadenosyl-moiety, a methyl group, a hydroxyl group or a water molecule were described as natural upper ligands of Cbas (1-3).

Cobamide-containing RDases function as terminal reductases in the membrane-bound electron transport chain of different anaerobic bacteria, which conserve energy via organohalide respiration (6-8). The need for Cbas as RDase cofactors in the so-called organohalide-respiring bacteria is covered either by *de novo* biosynthesis or by salvaging of Cbas from the surroundings (summarized in 9). The norpseudo-B_{12} of the tetrachloroethene (PCE)-respiring bacterium *Sulfurospirillum multivorans* is synthesized *de novo*, whereby the norcobamide (NCba) biosynthesis is induced in the presence of PCE (10-12). In comparison to the structure of vitamin B_{12}, the norpseudovitamin B_{12} lacks the methyl group at C176 in the linker moiety of the Cba (the prefix 'nor-' refers to this fact) and contains an adenine moiety as lower base (13). So far, a final proof for the binding and function of a standard-type cobamide such as pseudo-B_{12} in the PCE reductive dehalogenase (PceA) has not been provided. Although a clash within the protein structure was expected (14), a previous study indicated that the PceA structure might be flexible to some extent in incorporating NCbas or Cbas. The presence of mainly Cba instead of NCba (*i.e.*, addition of a methyl group at C176 of the linker moiety) did

not completely diminish PceA activity in cell free extracts (15). Hence, a specific need for the production of NCbas by *Sulfurospirillum* spp. (13, 16) has not been proven yet.

When 5,6-dimethylbenzimidazole (DMB), which serves as lower base in vitamin B_{12}, was added to cultures of *S. multivorans*, the DMB efficiently replaced the adenine in the norcobamide produced by the organism (10). *S. multivorans* does not possess genes for benzimidazole production (11) neither for the direct formation of DMB from flavin in an oxygen-dependent reaction (17) nor for the anoxic formation of DMB via 5-OHBza, 5-OMeBza, and 5-methoxy-6-methylbenzimidazole from 5-aminoimidazole ribotide (18), an intermediate of the purine biosynthesis. However, exogenously provided DMB can be used for cobamide guided biosynthesis (5). Prior to their incorporation into Cbas, the various benzimidazoles are activated by the nicotinate-nucleotide dimethylbenzimidazole phosphoribosyltransferase (CobT), which adds a phosphoribosyl moiety and forms α-ribotides (19). The relaxed specificity of some CobTs thereby allowed for the formation of uncommon 6-substituted benzimidazolyl-ribotides from singly substituted benzimidazoles such as 5-hydrozybenzimidazole (5-OHBza) or 5-methoxybenzimidazole (5-OMeBza), which can lead to the formation of unusual Cba isomers (20).

The PCE-dependent growth of *S. multivorans*, the PceA enzyme activity, and the PceA maturation was impaired in the presence of DMB (10). A plausible explanation for this inhibitory effects might be an incompatibility of a specific lower base in a Cba cofactor with the Cba binding site of a particular RDase. Negative effects on enzymatic reductive dehalogenation caused by the modification of the Cba structure have also been reported for *Dehalococcoides mccartyi* strains (21-24). The obligate organohalide-respiring *D. mccartyi* is a Cba auxotroph (25). The dechlorination of TCE by *D. mccartyi* strain 195 was dependent on the availability of Cbas with either DMB, 5-methylbenzimidazole (5-MeBza), or 5-OMeBza as lower base. Cbas with alternative lower bases such as 5-OHBza or benzimidazole (Bza) did not sustain TCE-dependent growth of the organism.

The lower ligand base, which is part of the Cba's nucleotide loop and thereby covalently bound to the cofactor, can be displaced from the cobalt (‘base-off’) in the protein-bound state. Here, an alternative lower ligand such as a histidine residue (‘base-off/His-on’) often fulfills this function (26, 27). For Cba cofactors bound to RDases a lower ligand of the cobalt was not detected by structural analysis (14, 28). The two RDases analyzed so far harbors the Cba cofactor deeply buried inside the protein bound by a network of hydrogen bonds. In the RDase-bound state the lower base of the Cba is not placed in proximity to the cobalt, it is completely

moved out of the position it obtains in the protein-free state of the cofactor. In the case of the two known RDase structures, binding of an alternative ligand is prevented by the protein structure. These observations were confirmed by spectroscopic analyses of different RDases using electron paramagnetic resonance spectroscopy, which also detected the Cba cofactor in the 'base-off' state (28-30).

In order to shed light on the functionality of a single RDase with different Cba cofactors, we investigated the utilization of various benzimidazolyl-NCbas by PceA of *S. multivorans* and analyzed the similarities or variations in binding a Cba harboring either a purine or a benzimidazole as lower base on the structural level. Thereby, we identified PceA of *S. multivorans* as a Cba-containing protein functioning with both, purinyl- and benzimidazolyl-NCbas, but limited in recruiting methylated benzimidazolyl-NCbas. Furthermore, we found evidence for an unusually strict regioselectivity of the *S. multivorans* norcobamide biosynthetic machinery that is controlled by the type of substituent present in singly substituted benzimidazoles.

RESULTS

Guided biosynthesis of benzimidazolyl-NCbas. In order to test the utilization of various exogenous benzimidazoles as lower bases for the production of NCbas (Fig. 1A), *S. multivorans* was cultivated in the presence of DMB, 5-MeBza, Bza, 5-OMeBza, and 5-OHBza and the produced NCbas were extracted. The incorporation efficiency of all benzimidazoles was tested by analyzing the NCba fractions from cells cultivated in the presence of different concentrations of the lower base precursors (Fig. 1B). The total amount of Cba extracted from cells cultivated in the presence of benzimidazoles was not altered in comparison to untreated cells. The absolute yield was about 1 µmol norcobamide per gram protein used for the extraction in every case. A strong divergence among the various benzimidazoles with respect to their appearance as lower bases in the NCba fraction was not observed, which indicates an efficient benzimidazole influx into the cells and enzymatic activation in all cases. Whether the benzimidazoles are actively taken up by the cells is not known. The extracted NCbas were applied to high performance liquid chromatography (HPLC) coupled to photometric detection (Fig. 1C).

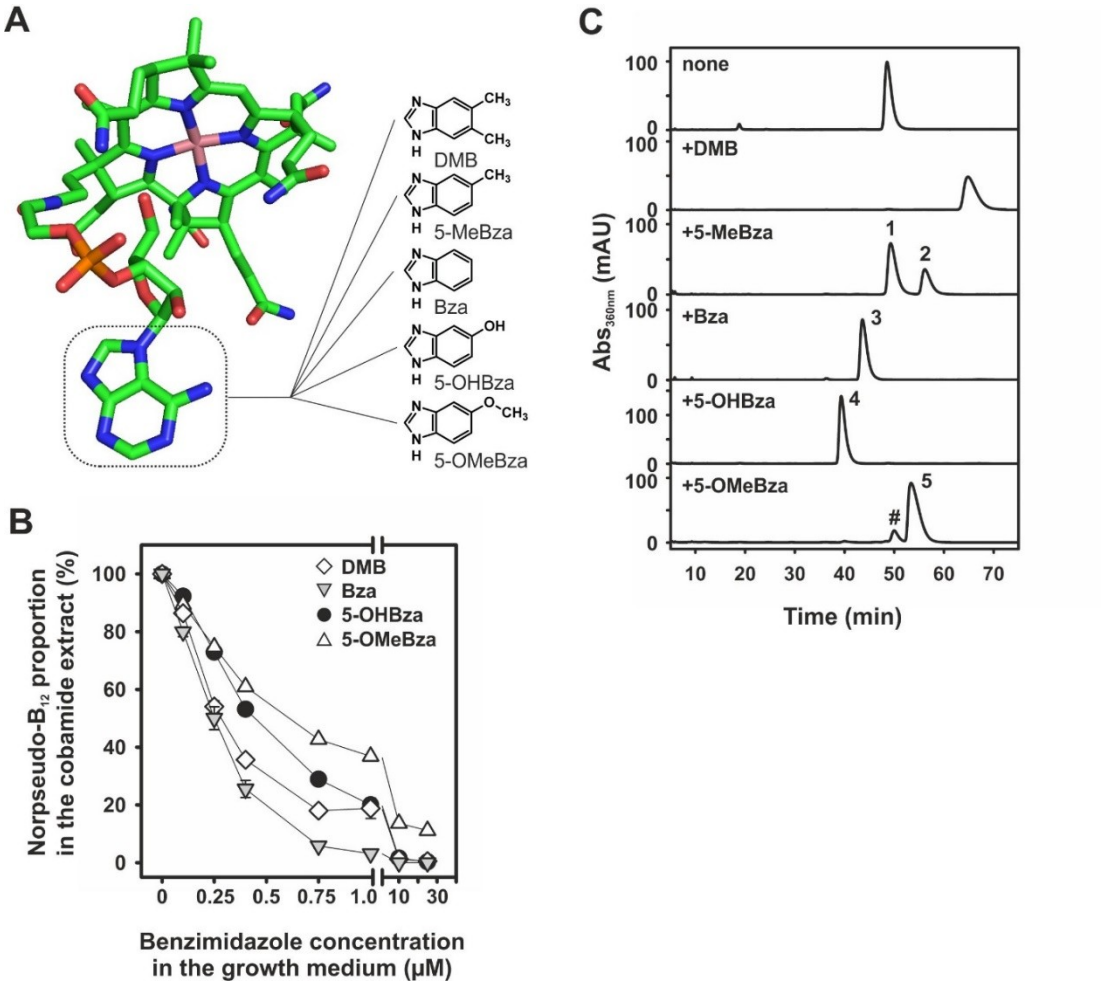

Fig. 1: Guided-NCba biosynthesis in *S. multivorans*. A) Norpseudo-B_{12} cofactor in its conformation obtained in the PceA crystal structure (14). A frame marks the adeninyl-moiety in the nucleotide loop. The structures of the exogenous benzimidazoles, which were tested in the study, are depicted. B) Ratio between norpseudo-B_{12} and various benzimidazolyl-NCbas formed in the presence of different concentrations of exogenous benzimidazoles. 5-MeBza was excluded from the analysis of the incorporation efficiency, since the norpseudo-B_{12} still present in cells exposed to lower concentrations of exogenous 5-MeBza, has not been efficiently separated from the MeBza-NCba (signal 1 in Fig. 1C) by HPLC. This circumstance made a direct quantification of the portion of MeBza-NCba impossible. The data presented in part B were obtained from two independent experiments. The maximal deviation is given. C) HPLC-analysis and mass determination of NCbas extracted from *S. multivorans* cells cultivated in the presence of different benzimidazoles (25 µM, respectively). The hash marks the norpseudo-B_{12} in the Cba extract from cells treated with 5-OMeBza. Singly and doubly protonated ions were detected which were assigned to the respective NCbas using UHPLC-ESI-HRMS: *m/z* 1327.5443 $[M+H]^+$ (calculated for $C_{61}H_{85}O_{14}N_{14}CoP$, 1327.5439, 0.745 ppm) and *m/z* 664.2763 $[M+2H]^{2+}$ (calculated for $C_{61}H_{86}O_{14}N_{14}CoP$, 664.2753, 1.492 ppm) for peak 1 and *m/z* 1327.5446 $[M+H]^+$ (calculated for $C_{61}H_{85}O_{14}N_{14}CoP$, 1327.5439, 0.873 ppm) and *m/z* 664.2762 $[M+2H]^{2+}$ (calculated for $C_{61}H_{86}O_{14}N_{14}CoP$, 664.2753, 1.266 ppm) for peak 2 of the sample derived from the 5-MeBza-treated cells, *m/z* 1313.5232 $[M+H]^+$ (calculated for

$C_{60}H_{83}O_{14}N_{14}CoP$, 1313.5238, -3.465 ppm) and *m/z* 657.2647 $[M+2H]^{2+}$ (calculated for $C_{60}H_{84}O_{14}N_{14}CoP$, 657.2675, -4.2 ppm) for the Bza-NCba, *m/z* 1329.5215 $[M+H]^{+}$ (calculated for $C_{60}H_{83}O_{15}N_{14}CoP$, 1329.5232, -0.899 ppm) and *m/z* 665.2640 $[M+2H]^{2+}$ (calculated for $C_{60}H_{84}O_{15}N_{14}CoP$, 665.2650, -1.430 ppm) for the OHBza-NCba and *m/z* 1343.5381 $[M+H]^{+}$ (calculated for $C_{61}H_{85}O_{15}N_{14}CoP$, 1343.5389, -0.168 ppm) and *m/z* 672.2722 $[M+2H]^{2+}$ (calculated for $C_{61}H_{86}O_{15}N_{14}CoP$, 672.2728, -0.887 ppm) for the OMeBza-NCba. In the latter sample, ions for the residual norpseudo-B_{12} were also detected at *m/z* 1330.5283 $[M+H]^{+}$ (calculated for $C_{58}H_{82}O_{14}N_{17}CoP$, 1330.5291, -0.607 ppm).

The addition of DMB to the growth medium resulted in the formation of nor-B_{12} as it has been reported previously (10). The presence of all other benzimidazoles gave rise to the production of new compounds, which showed characteristic Cba absorbance spectra (data not shown) and different retention times compared to norpseudo-B_{12} and nor-B_{12}. After three subsequent cultivations in the presence of 25 µM exogenously applied benzimidazoles, the amount of norpseudo-B_{12} in the cells was reduced to a non-detectable level (Fig. 1C). Exclusively in the case of 5-OMeBza, a residual amount (about 10%) of norpseudo-B_{12} was observed. In order to identify the unknown Cbas, all samples were analyzed using ultra high performance liquid chromatography coupled with electrospray ionization high-resolution mass spectrometry (UHPLC-ESI-HRMS). By applying this technique, the efficient incorporation of all benzimidazoles as lower bases into the nucleotide loop of the NCbas produced by *S. multivorans* was confirmed, since the results are in agreement with the predicted masses. In the case of the NCba extract obtained from cells cultivated in the presence of 5-MeBza, two NCba compounds were detected in a ratio of 2:1. Both NCbas showed an identical mass which was attributed to MeBza-NCba. The difference in the retention time of the two isomers might be caused by a difference in the position of the methyl group of the MeBza moiety in the NCba structure.

The purified NCbas formed in cells cultivated in the presence of the singly substituted benzimidazoles 5-MeBza, 5-OHBza, and 5-OMeBza were identified by nuclear magnetic resonance (NMR) spectroscopy. Thus, the assumption on the incorporation of the different benzimidazoles into the NCba structure was confirmed (Fig. 2 and Fig. S1-26). In theory, singly 5-substituted benzimidazoles can be incorporated in two different orientations into the cobamide structure, which can give rise to 5- or 6-substituted benzimidazolyl-Cbas. The determined chemical shifts in the NMR analysis obtained for the sample prepared from 5-OHBza-treated cells allowed for the identification of 6-OHBza-NCba (Fig. 2A), whereas in the

case of the sample from 5-OMeBza-treated cells the formation of 5-OMeBza-NCba was proven (Fig. 2B). The NMR data were in accordance with previously published results by Taga and coworkers (19). Furthermore, the position of the substituent within the lower base structure was determined in both NCbas obtained from 5-MeBza-treated cells and the occurrence of two orientations of MeBza in the nucleotide loop was approved (Fig. 2 C, D).

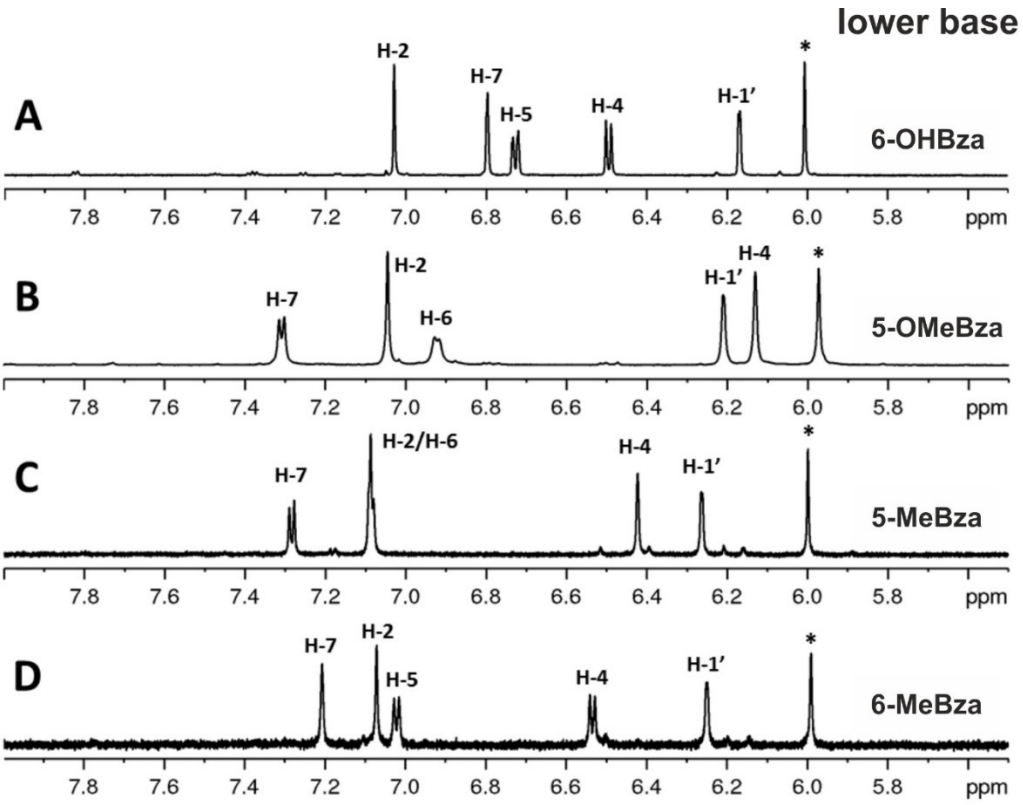

Fig. 2: Low field range of ^{1}H-NMR spectra of the isolated NCbas. (A) 6-OHBza-NCba, (B) 5-OMeBza-NCba, (C) 5-MeBza-NCba (peak 1 in Fig. 1C), and (D) 6-MeBza-NCba (peak 2 in Fig. 1C). The depicted sections show the signals for the respective benzimidazolyl moieties and the signal for the anomeric position of the α-ribosyl unit. The signal marked with an asterisk belongs to position 10 of the corrin scaffold.

Effect of singly substituted benzimidazoles on PceA production. The exchange of the adeninyl moiety in the norpseudo-B_{12} cofactor by DMB caused a negative effect on the PCE-dependent growth and the biosynthesis of catalytically active PceA in *S. multivorans* (10). Up to date, no other benzimidazoles were tested in this respect. Thus, 5-MeBza, Bza, 5-OHBza, or 5-OMeBza (25 µM, respectively) was added to cultures of *S. multivorans* that contained pyruvate and PCE as substrates. None of the benzimidazoles affected the PCE-dependent

growth of the organism such as DMB (Fig. S27 shows the results for DMB, 5-MeBza, and Bza). In order to evaluate their impact on PceA function, the enzyme activity was tested in crude extracts of the various cell types (Fig. 3). Cultures of *S. multivorans* grown on PCE in the presence of the different benzimidazoles were harvested in the late exponential growth phase, *i.e.*, the protein concentration was 70-80 µg/mL, which was reached after approx. 16 hours of cultivation. In the case of the DMB-containing cultures, the same growth phase was reached after approximately 80-90 hours of cultivation. Crude extracts were prepared and the specific PceA activity was measured in a photometric assay using reduced methyl viologen as artificial electron donor. The activity determined in cells treated with either Bza, 5-OHBza, or 5-OMeBza was similar to the PceA activity monitored in the non-treated *S. multivorans* cells (Fig. 3A).

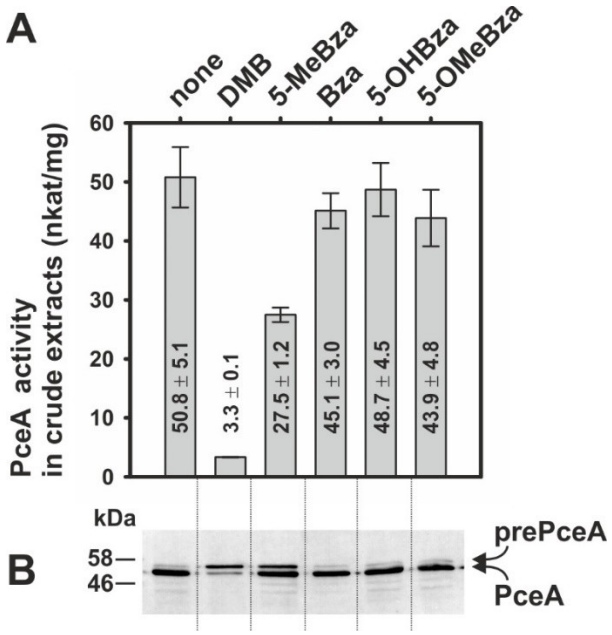

Fig. 3: PceA activity (A) and protein level (B) in crude extracts derived from cells grown with PCE in the presence of different benzimidazoles (25 µM). For the immunological analysis 5 µg of protein was applied to each lane. The immunoblot was developed with an antiserum containing polyclonal antibodies against PceA. The data for the PceA activity were obtained from three different cultures. The standard deviation is given. prePceA: precursor with the N-terminal Tat signal peptide, PceA: processed form without the Tat signal peptide.

In contrast, the presence of 5-MeBza caused a substantial reduction in the enzyme activity (about 50%). This reduction was not as high as in DMB-treated cells (about 90%) and appeared to be still sufficient for unaffected growth with PCE. The absence of a severe growth defect in

case of 5-MeBza-treated cells might indicate a surplus of PceA present in *S. multivorans* that exceeds the amount of enzyme needed for energy conservation via organohalide respiration. It was observed before that the growth rate of *S. multivorans* with PCE was not severely reduced when the PceA activity in such cells was lowered by about 50% (15).

The reduction in PceA activity in cells cultivated in the presence of 5-MeBza might be accompanied by a retardation in maturation and processing of the PceA precursor (prePceA) as it was observed for DMB before (10). Thus, the presence of both forms of the enzyme was analyzed in crude extracts separated on an SDS-PAGE and applied to an immunoblot developed with PceA-specific antibodies (Fig. 3B). In comparison to the crude extract of non-treated cells, which displayed an intense band for the mature PceA enzyme (predicted molecular mass: 53.3 kDa) and only a thin band for the Tat (twin arginine translocation) signal peptide-containing prePceA (predicted molecular mass: 57.1 kDa), the amount of prePceA was increased in 5-MeBza-treated cells. In cells cultivated in the presence of Bza, 5-OHBza, and 5-OMeBza, the total amount of the enzyme and its processing was apparently not affected.

Incorporation of benzimidazolyl-NCbas into PceA. The quantification of the incorporation efficiency of the DMB-NCba into PceA was hindered in a previous study, since a sufficient amount of pure PceA enzyme was not obtained from such DMB-treated cells (10). These difficulties and the negative effect on the maturation of the PceA precursor under these conditions indicated an incompatibility between the DMB-NCba, containing the doubly substituted lower base, and the enzyme. Alternative doubly substituted benzimidazoles such as 5,6-dinitrobenzimidazole (DNO_2Bza) or 5,6-dimethoxybenzimidazole (DOMeBza) were tested in this study. In the case of DNO_2Bza (25 µM in the growth medium) a reduction of about 80% in PceA activity in crude extracts was observed, comparable to what was found before with DMB. While in DNO_2Bza-treated cells the norpseudo-B_{12} cofactor was nearly completely replaced, in cells cultivated in the presence of DOMeBza (25 µM) almost no production of the DOMeBza-NCba was detected, which hindered the evaluation of its effect on PceA function. Also the use of DNO_2Bza did not lead to conclusive results. Most probably due to chemical transformations of the two NO_2-groups several norcobamides were extracted from DNO_2Bza-treated cells (data not shown). As revealed by mass determination a DNO_2Bza-NCba was not included, which hindered further evaluation of the effect of this doubly substituted benzimidazole.

In contrast to the effects observed with DMB, the analysis of the PceA activity in cells treated

with 5-OHBza or 5-OMeBza showed no negative effect (Fig. 3). This result indicated an efficient utilization of both NCbas, the 6-OHBza-NCba and the 5-OMeBza-NCba, as cofactors of the PceA enzyme. Indeed, extraction of the norcobamides from PceA isolated from the respective type of cells uncovered a 100% saturation of the enzyme (1 mol cofactor per 1 mol PceA) in both cases, as well as in enzyme extracted from 5-MeBza-treated cells, and the elution profiles of the extracted cofactors obtained via HPLC separation (Fig. S28) mirrored the patterns observed earlier for the NCbas extracted from whole cells (Fig. 1C). For unravelling similarities or differences in the binding mode of these cofactors and for obtaining indications for the exclusion of the DMB-NCba, the different PceA enzymes were crystallized and subjected to structural analysis. However, crystals of PceA suitable for X-ray scattering and structural analysis were only gained for the enzyme purified from cells treated with 5-OHBza or 5-OMeBza. The inability of the PceA-sample equipped with the mixture of both MeBza-NCba isomers to form suitable crystals might indicate an inhomogeneity of the sample and the presence of misfolded PceA. This assumption was supported by the fact that the specific activity of PceA purified from cells cultivated in the presence of 5-MeBza was about 50% lower compared to the PceA purified from cells treated with 5-OHBza or 5-OMeBza (687 nkat/mg PceA versus 1280 nkat/mg PceA).

In both known RDase structures (14, 28), the Cba cofactor is deeply buried within the protein. Access to the upper, the *β*-face of the corrin ring within the substrate binding pocket of PceA is limited by the protein structure. The nucleotide loop of the adeninyl-NCba (norpseudo-B_{12}) in PceA is positioned in the 'base-off' conformation (Fig. 4A). The unusual curled conformation of the tail is stabilized by intramolecular interactions - hydrogen bonds between O5 of the ribosyl moiety (for numbering of the atoms in norpseudo-B_{12} see reference 13), the linker amide, and the carboxamide side chain connected to ring C of the corrin core (Fig. 4B) (14). These stabilizing interactions are conserved in both, the PceA equipped either with the 6-OHBza-NCba or the 5-OMeBza-NCba. Another intramolecular hydrogen bond connects the amino group of the adenine and O2 of the ribosyl moiety only in the adeninyl-NCba. (Fig. 4B). The tight binding of the phosphate and sugar moieties in all PceA structures restricts the movement of the base to a rotation of the bond connecting base and sugar. The same rotation in turn is restricted by the protein surroundings. The base is placed in between the Cba-binding core of PceA (purple in figure 4) and a loop from the region binding the iron-sulfur clusters (14). Lys362 from this loop is within hydrogen-bonding distance of both the base and the phosphate. Gln364 reaches across the base and hydrogen bonds to O2 of the sugar.

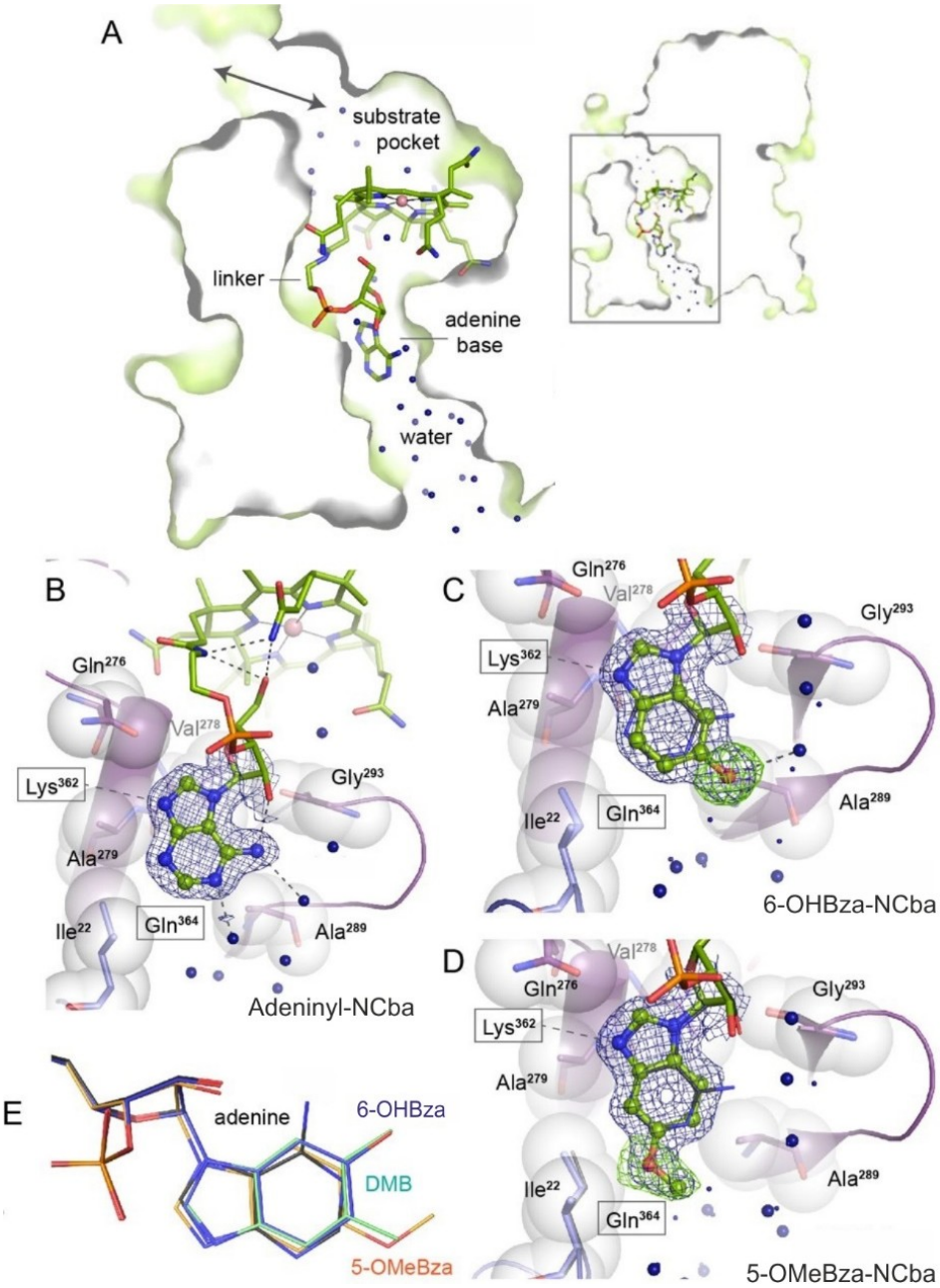

Fig. 4: NCba cofactor-binding in PceA. A+B) Slice through a monomer of PceA showing the norpseudo-B_{12} cofactor. The adenine base (ball and stick in B) is sandwiched between the B_{12}-binding core (residues 139-163 and 216-323, behind the view, purple) and a loop from the iron-sulfur cluster binding unit (residues 324-394, in front of the view and thus not shown, but Lys362 and Gln364 are indicated as boxes). Lys362 is within hydrogen bonding distance of the imidazole moiety in all three bases (dashed lines). C) When 6-OHBza is substituted for adenine, only the base is shifted slightly (thin blue lines represent the position of adenine). Greater change was observed for the water structure shown in blue balls (small dots denote water positions in norpseudo-B_{12} bound PceA). Electron density maps are shown for the base only (blue 1 σ 2Fo-Fc and green 2.5 σ Fo-Fc difference maps when the benzimidazole substituents were omitted). D) The same as described in C is shown for the 5-OMeBza-NCba. E) Overlay of the bases in B-D and a hypothetical positioning of DMB, which was overlaid to 6-OHBza.

Thus, intramolecular and protein interactions effectively lock the position of the base and this is reflected by the conserved position observed for both benzimidazole-containing NCbas (Fig. 4C, D). In PceA, but not in the structure of the non-respiratory RDase NpRdhA from *Nitratireductor pacificus* (28), a solvent channel reaches from the protein surface to the far end of the base and the amino group and N1 of the adeninyl base are in hydrogen-bonding distances to water molecules (Fig. 4B). The three different substituents on the various bases, namely the amino group of the adeninyl moiety (Fig. 4B), the hydroxyl group of the 6-OHBza moiety (Fig. 4C), and the methoxy group of the 5-OMeBza moiety (Fig. 4D) are accommodated by a change in the water structure rather than a change in the position of the base or a reorientation of surrounding side chains.

The closest interactions between the new substituents were seen between Ala289 and the 6-OHBza moiety (3 Å) and Ile22 of the N-terminal loop region and the 5-OMeBza moiety (3.5 Å). A substitution at a position other than C5 or C6 may not be possible without a change in the protein scaffold. Given the positioning of the 6-OHBza- and the 5-OMeBza-moieties in PceA, no clash with the protein would be expected with a hypothetical MeBza or DMB as lower base (Fig. 4E). Hence, the static, folded structure cannot fully explain the apparent lack of functionality of the MeBza-NCba and the DMB-NCba. The unique feature of PceA is the solvent accessible and water-bound base. Such solvation might play a role in cofactor acquisition and correct functional folding of both PceA enzyme and cofactor.

DISCUSSION

An important function of the cobamide's nucleotide loop in enzymes harboring a ‘base-off’ cobamide is the binding of the cofactor to the protein and thus stabilizing the correct position of the cobamide in the enzyme. The nucleotide loop of Cbas is variable in structure and this diversity might interfere with the incorporation and correct positioning of the cofactor in Cba-dependent enzymes. This assumption is expected to be especially relevant for the RDase enzyme family, since these biological catalysts bind the cofactor with a network of hydrogen bonds deeply inside the protein (14, 28). The PceA enzyme of *S. multivorans* equipped with either the norpseudo-B_{12} or singly substituted benzimidazole-containing NCbas, *i.e.*, the 6-OHBza-NCba and the 5-OMeBza-NCba, revealed no difference in binding of the cofactor in general and the lower base in particular. Actually, the positioning of the lower base was found to be nearly identical. Also in the case of MeBza-NCbas, incorporation at all did not appear to

be hindered, since both NCba isomers, the 5-MeBza- and the 6-MeBza-containing variant, were detected in the enzyme and the cofactor incorporation efficiency was >98%. However, the enzyme activity of the pool of PceA molecules was reduced and the difficulties observed in crystallization of purified PceA indicated an inhomogeneity of the sample. Crystallization of 5- and 6-MeBza NCba-containing PceA resulted in a different crystal packing in which the base could not be fully resolved, thus, its detailed structure remains unknown. Since 5-OHBza or 5-OMeBza incorporated as lower bases in 6-OHBza-NCba or 5-OMeBza-NCba were functional in the enzyme, it is hard to conclude on the specific isomer of MeBza-NCba that causes PceA malfunction. In the case of DMB, the respective NCba was most probably even excluded from the incorporation into PceA (see also 10). However, also the incompatibility of DMB as lower base might not be due to steric hindrance inside the binding pocket. No structural clash between the substituents at the benzimidazole moiety and the protein environment were identified in the structure. Hence, it has to be assumed that the lower base substitution pattern might interfere with the folding process rather than with the dimensions of the binding pocket present in the fully-folded enzyme.

Whether the cofactor has to attain a specific conformation prior to the incorporation into the enzyme and whether this might be differentially affected in the various benzimidazolyl-NCbas tested here remains elusive. Here, the hydrophobic methyl groups in DMB-NCba and MeBza-NCbas could interfere with the incorporation process. The lower base of the NCba cofactor in PceA is placed in a solvent-flooded cavity, which might be incompatible with the hydrophobic character of the methylated benzimidazoles. The DMB of the Cba cofactor in NpRdhA is protected from solvent (28), which could result in a different preference for alternative Cba cofactors.

It was observed earlier that the structure of the lower base influences the ratio between the ‘base-off’ and the ‘base-on’ form of Cbas in solution. This might influence the incorporation efficiency especially when the Cba cofactor has to obtain its ‘base-off’ conformation prior to the assembly with the RDase apoprotein. Kräutler and coworkers showed the adenine-containing pseudocoenzyme B_{12} having a higher tendency to occur in the ‘base-off’ form in solution when compared to the DMB-containing coenzyme B_{12} (31). Even between structural isomers, the tendency to obtain the ‘base-off’ conformation differs. Taga and coworkers reported a lower pK_a value for 5-OMeBza-Cba in comparison to 6-OMeBza-Cba (20). However, a systematic analysis of the impact of all potential lower bases on the constitution of the cofactor under physiological conditions is not available, yet. A cooperative process

including PceA folding and structural adaptation of the NCba cofactor that lead to the final constitution of the enzyme-cofactor complex cannot be excluded. Reconstitution experiments with apoprotein of PceA, which would help to analyze the compatibility of the unfolded protein with different NCba/Cba cofactors, were not successful or have not been tried yet with Cbas containing lower bases different from DMB. These efforts are going to be intensified in future studies.

The role of chaperones in the Cba cofactor incorporation was not investigated so far. Specific chaperones, such as RdhT homologoues (32, 33) are not found in *S. multivorans* and have not been identified in *D. mccartyi*. Banerjee and coworkers reported the transfer of the Cba cofactor to the methylmalonyl-CoA mutase to be mediated by the adenosyltransferase (ATR) (34). An ATR homologue is not present in *S. multivorans*. Since the NCba cofactor of PceA is catalytically active without the adenosyl-moiety, this gene function is dispensable in the organism.

Not all RDases seem to bind the Cba cofactor in the 'base-off' mode. As recently reported for the reconstituted VcrA of *D. mccartyi* strain VS, the DMB-containing Cba cofactor showed the lower ligand bound to the cobalt also in the enzyme-bound state (35). In addition, other RDases show different preferences in the type of the lower base in the Cba cofactor (21-24), which implies that a general rule for the cofactor compatibility of RDases does not exist or cannot be derived from the data available at the moment.

The specificity in the formation of 6-OHBza-NCba out of 5-OHBza and 5-OMeBza-NCba out of 5-OMeBza was an unexpected finding and adds a new facet to the unusual nucleotide loop assembly pathway in *S. multivorans* (36). Earlier, Friedrich and Bernhauer (37) reported the extraction and identification of 5-MeBza-Cba and 6-MeBza-Cba produced by *Propionibacterium shermanii* in the presence of 5-MeBza, albeit in a ratio of 96:4, which showed a clear preference for the formation of 5-MeBza-Cba in this organism. In *Methanobacterium thermoautotrophicum*, which has been shown to produce OHBza-Cba, approximately 10% of 6-OHBza-Cba was detected (38). And only recently, Taga and coworkers found a mixture of Cba isomers in *Sinorhizobium meliloti* and *Veillonella parvula*, both cultivated in the presence of 5-OMeBza or 5-OHBza (20, 39). However, the exclusive biosynthesis of benzimidazolyl-Cbas with a single substituent in position 6 of the benzimidazolyl-moiety as shown here for *S. multivorans* has not been described so far. Cbas are channeled into the Cba biosynthetic pathway by the activity of the phosphoribosyltransferase CobT. It is currently under investigation in our laboratory whether

the regioselectivity of CobT from *S. multivorans* lays the foundation for the observed structural diversity in the NCbas containing OMeBza or OHBza in the organism.

MATERIALS AND METHODS

Cultivation of bacteria. *Sulfurospirillum multivorans* (DSMZ 12446) was cultivated as described previously in Keller *et al.* (10). Anoxic and sterile stock solutions of the different benzimidazoles (up to 4 mM) were prepared in ultrapure water and used for the amendment of the media prior to the inoculation. All benzimidazole derivatives were purchased from Sigma-Aldrich (Munich, Germany), except for 5-OHBza that was delivered by Combi-Blocks, Inc. (San Diego, CA, USA) and DNO_2Bza that was purchased from Santa Cruz Biotechnology (Dallas, TX, USA). Cells of *S. multivorans* were adapted to the different cultivation conditions in two subsequent pre-cultures prior to the cultivation of cells for growth monitoring, PceA activity measurements, or cobamide extraction. The inoculum was 10%. The cells were transferred when the culture without the amendment of benzimidazoles reached the maximal OD. In every case, the first pre-culture was inoculated from a pyruvate/PCE-grown culture of *S. multivorans* routinely prepared for strain maintenance.

Measurement of PceA activity, immunoblot, cobamide extraction and HPLC analysis. The production of cell free extracts and the determination of the PceA enzyme activity in crude extracts from *S. multivorans* cells was performed as described previously (10). This also applies to immunological detection of PceA in cell free extracts. The cobamide extraction and analysis was conducted in accordance to the protocol published earlier (10). The cells were cultivated in 1 L pyruvate/fumarate-containing medium and harvested when the optical density (OD_{578}) reached 0.55. The mobile phases used for separation of the cobamides via high-performance liquid chromatography (HPLC) were 12% methanol/0.2% acetic acid (solvent A) and 99.8% methanol/0.2 % acetic acid (solvent B). The flow rate was 0.5 mL/min and the separation was performed isocratically at 30°C. The 6-OHBza norcobamide was purified additionally via solid phase extraction on a CHROMABOND® HR-X column (3 mL, 200 mg; Macherey-Nagel, Düren, Germany) according to the manufacturer's instructions.

UHPLC-ESI-HRMS. For UHPLC, an Ultimate 3000 series RSLC (Dionex, Sunnyvale, CA, USA) was used, applying an Acclaim C18 column (150 × 2.1 mm, 2.2 µm particles with 120

Å pore diameter, Dionex, Sunnyvale, CA, USA) with a flow rate of 300 µL min^{-1} in a binary solvent system of water (Solvent A) and acetonitrile (hypergrade for LC MS, Merck, Darmstadt Germany) (Solvent B), both containing 0.1% (v/v) formic acid (eluent additive for LC-MS, Sigma Aldrich, Munich, Germany). Sample volumes were loaded onto the column and eluted by using a gradient as follows: linear increase from 0% B to 100% B within 15 min - 100% B constant for 5 min – equilibration time at 0% B for 5 min. This system was coupled to a LTQ-Orbitrap XL mass spectrometer (Thermo Fisher Scientific, Bremen, Germany). Ionization was accomplished using Electrospray Ionization (ESI). ESI source parameters were set to 4 kV for spray voltage, 35 V for transfer capillary voltage at a capillary temperature 275 °C. The samples were measured in positive ion mode in the mass range of m/z 100 to 2000 using 30,000 m/Δm resolving power in the Orbitrap mass analyzer. Data was evaluated and interpreted using XCALIBUR software (Thermo Fisher Scientific, Waltham, MA, USA).

NMR measurements. NMR spectra (^{1}H NMR, ^{1}H-^{1}H COSY, ^{1}H-^{1}H ROESY, ^{1}H-^{13}C HSQC and ^{1}H-^{13}C HMBC) were recorded on a Bruker Avance III HD 700 spectrometer, equipped with a cryoplatform and a 1.7 mm TCI microcryoprobe (Bruker Biospin GmbH, Rheinstetten, Germany). NMR tubes of 1.7 mm outer diameter were used for all measurements. All NMR spectra were recorded using D_2O as a solvent. Accurate tuning of the spectrometer frequencies (700.45 MHz for ^{1}H and 176.14 MHz for ^{13}C) was accomplished prior to the experiments. Chemical shifts were left uncorrected. Data acquisition and processing were accomplished using TopSpin ver3.2. (Bruker Biospin). Standard pulse programs as implemented in TopSpin were used for data acquisition.

Crystallization of PceA and structural analysis. For the purification of PceA the *S. multivorans* mutant strain GD21 was cultivated as reported before (14, 40) in the presence of different benzimidazoles (see also above). The purification of PceA was performed as described in previous reports (14, 40). Crystallization and flash cooling of crystals were performed under anoxic conditions in a glove box (model B; COY Laboratory Products, Grass Lake, MI, USA) under an atmosphere of 95% N_2/5% H_2 and less than 10 ppm oxygen. Crystals were grown by the sitting drop vapor diffusion method at room temperature. 1 µL of 5-15 mg mL^{-1} PceA in 30 mM Tris-HCl, pH 7.5, 5 mM TCEP was mixed with 1 µL of crystallization solution containing 12-17% (w/v) PEG 3350 and 0.2 M sodium malonate, 2% benzamidine-HCl and 50 mM Tris-HCl, pH 7.5. Crystals were flash cooled in liquid nitrogen after protection in the crystallization

solution supplemented with 20% (v/v) glycerol and 25% (final w/v) PEG 3350. Once plunged into liquid N_2, crystals were removed from the anoxic atmosphere, from thereon stored, and handled under liquid N_2.

Diffraction data for PceA equipped with 5-OMeBza norcobamide were collected on BL14.1 operated by the Helmholtz-Zentrum Berlin (HZB, Germany) at the BESSY II electron storage ring (Berlin-Adlershof, Germany) (41). Data for PceA equipped with 6-OHBza norcobamide were collected at beamline P11 at PETRA-III (DESY, Hamburg, Germany) (42, 43). Data were indexed and integrated with the XDS package (44) and XDSAPP (45). Restraints for the base were generated by the Grade Server v1.001 and used to modify the vitamin B_{12} restraint file posted by Oliver Smart (Global Phasing Ltd., Cambridge, UK). Models were fitted in COOT (46), refined with phenix.refine (47) and validated with Molprobity (48). Data collection and refinement statistics are summarized in the Table S1. Model coordinates and structure factors for PceA equipped with different norcobamides have been deposited at the protein data bank (PDB) under accessions numbers 5OBP (PceA with 6-OHBza norcobamide cofactor) and 5OBI (PceA with 5-OMeBza norcobamide cofactor).

ACKNOWLEDGEMENTS

This work was financially supported by the German Research Foundation (DFG; grant SCHU 2605/1-1). The efforts of Cindy Kunze were funded by the DFG Research Unit FOR1530 and the Ernst Abbe Foundation. The efforts of Martin Bommer were financed by the SFB1078 (Protonation Dynamics in Protein Function). We acknowledge access to beamlines of the BESSY II storage ring (Berlin, Germany) via the Joint Berlin MX-Laboratory sponsored by the Helmholtz-Zentrum Berlin für Materialien und Energie (HZB), the Freie Universität Berlin, the Humboldt-Universität zu Berlin, the Max-Delbrück-Centrum, and the Leibniz-Institut für Molekulare Pharmakologie. Parts of this research were carried out at PETRA-III at DESY, a member of the Helmholtz Association (HGF). We would like to thank Olga Lorbeer and Anja Burkhardt for assistance in using beamline P11. The authors are grateful to Gabriele Diekert for helpful discussions and acknowledged the excellent technical assistance of Peggy Brand-Schön.

REFERENCES

1. Banerjee R, Ragsdale, SW. 2003. The many faces of vitamin B_{12}: catalysis by cobalamin-dependent enzymes. Annu Rev Biochem. 72:209-247.
2. Gruber K, Puffer B, Kräutler B. 2003. Vitamin B_{12}-derivatives-enzyme cofactors and ligands of proteins and nucleic acids. Chem Soc Rev. 40:4346-4363.
3. Bridwell-Rabb J, Drennan, CL. 2017. Vitamin B_{12} in the spotlight again. Curr Opin Chem Biol. 37:63-70.
4. Lenhert PG, Hodgkin DC. 1961. Structure of the 5,6-dimethyl-benzimidazolylcobamide coenzyme. Nature. 192:937-938.
5. Renz P. 1999. Biosynthesis of the 5,6-dimethylbenzimidazole moiety of cobalamin and of the other bases found in natural corrinoids, p 557-576. *In* Banerjee R (ed), Chemistry and biochemistry of B_{12}, John Wiley & Sons Inc., New York.
6. Holliger C, Wohlfarth G, Diekert G. 1999. Reductive dechlorination in the energy metabolism of anaerobic bacteria. FEMS Microbiol Rev. 22:383-398.
7. Jugder BE, Ertan H, Bohl S, Lee M, Marquis CP, Manefield M. 2016. Organohalide Respiring Bacteria and Reductive Dehalogenases: Key Tools in Organohalide Bioremediation. Front Microbiol. 7:249.
8. Fincker M, Spormann AM. 2017. Biochemistry of Catabolic Reductive Dehalogenation. Annu Rev Biochem. 86:357-386.
9. Moore TC, Escalante-Semerena JC. 2016. Corrinoid Metabolism in Dehalogenating Pure Cultures and Microbial Communities, p 455-484. *In* Adrian L, Löffler FE (ed), Organohalide-Respiring Bacteria, Springer-Verlag, Berlin/Heidelberg.
10. Keller S, Ruetz M, Kunze C, Kräutler B, Diekert G, and Schubert T. 2014. Exogenous 5,6-dimethylbenzimidazole caused production of a non-functional tetrachloroethene reductive dehalogenase in *Sulfurospirillum multivorans*. Environ Microbiol. 16:3361-3369.
11. Goris T, Schubert T, Gadkari J, Wubet T, Tarkka M, Buscot F, Adrian L, Diekert G. 2014. Insights into organohalide respiration and the versatile catabolism of *Sulfurospirillum multivorans* gained from comparative genomics and physiological studies. Environ Microbiol. 16:3562-3580.
12. Goris T, Schiffmann CL, Gadkari J, Schubert T, Seifert J, Jehmlich N, von Bergen M, Diekert G. 2015. Proteomics of the organohalide-respiring Epsilonproteobacterium *Sulfurospirillum multivorans* adapted to tetrachloroethene and other energy substrates. Sci Rep. 5:13794.
13. Kräutler B, Fieber W, Ostermann S, Fasching M, Ongania KH, Gruber K, Kratky C, Mikl C, Siebert A, Diekert G. 2003. The Cofactor of Tetrachloroethene Reductive Dehalogenase of *Dehalospirillum multivorans* Is Norpseudo-B_{12}, a New Type of a Natural Corrinoid. Helv Chim Acta. 86:3698-3716.
14. Bommer M, Kunze C, Fesseler J, Schubert T, Diekert G, Dobbek H. 2014. Structural basis for organohalide respiration. Science. 346:455-458.
15. Keller S, Treder A, von Reuss SH, Escalante-Semerena JC, and Schubert T. 2016. The SMUL_1544 Gene Product Governs Norcobamide Biosynthesis in the Tetrachloroethene-Respiring Bacterium *Sulfurospirillum multivorans*. J Bacteriol. 198:2236-2243.
16. Goris T, Schenz B, Zimmermann J, Lemos M, Hackermüller J, Schubert T, Diekert G. 2017. The complete genome of the tetrachloroethene-respiring Epsilonproteobacterium *Sulfurospirillum halorespirans*. J Biotechnol. 255:33-36.

17. Taga ME, Larsen NA, Howard-Jones AR, Walsh CT, Walker GC. 2007. BluB cannibalizes flavin to form the lower ligand of vitamin B_{12}. Nature. 446:449-453.
18. Hazra AB, Han AW, Mehta AP, Mok KC, Osadchiy V, Begley TP, Taga ME. 2015. Anaerobic biosynthesis of the lower ligand of vitamin B_{12}. Proc Natl Acad Sci USA 112:10792-10797.
19. Trzebiatowski JR, Escalante-Semerena JC. 1997. Purification and characterization of CobT, the nicotinate-mononucleotide:5,6-dimethylbenzimidazole phosphoribosyl-transferase enzyme from *Salmonella typhimurium* LT2. J Biol Chem. 272:17662-17667.
20. Crofts TS, Hazra AB, Tran JL, Sokolovskaya OM, Osadchiy V, Ad O, Pelton J, Bauer S, Taga ME. 2014. Regiospecific formation of cobamide isomers is directed by CobT. Biochemistry 53:7805-7815.
21. Yi S, Seth EC, Men YJ, Stabler SP, Allen RH, Alvarez-Cohen L, Taga ME. 2012. Versatility in corrinoid salvaging and remodeling pathways supports corrinoid-dependent metabolism in *Dehalococcoides mccartyi*. Appl Environ Microbiol 78:7745-7752.
22. Yan J, Im J, Yang Y, Löffler FE. 2013. Guided cobalamin biosynthesis supports *Dehalococcoides mccartyi* reductive dechlorination activity. Philos Trans R Soc Lond B Biol Sci. 368:20120320.
23. Yan J, Ritalahti KM, Wagner DD, Löffler FE. 2012. Unexpected specificity of interspecies cobamide transfer from *Geobacter* spp. to organohalide-respiring *Dehalococcoides mccartyi* strains. Appl Environ Microbiol. 78:6630-6636.
24. Yan J, Şimşir B, Farmer AT, Bi M, Yang Y, Campagna SR, Löffler FE. 2016. The corrinoid cofactor of reductive dehalogenases affects dechlorination rates and extents in organohalide-respiring *Dehalococcoides mccartyi* ISME J 10:1092-1101.
25. Löffler FE, Yan J, Ritalahti KM, Adrian L, Edwards EA, Konstantinidis KT, Müller JA, Fullerton H, Zinder SH, Spormann AM. 2013. *Dehalococcoides mccartyi* gen. nov., sp. nov., obligately organohalide-respiring anaerobic bacteria relevant to halogen cycling and bioremediation, belong to a novel bacterial class, *Dehalococcoidia* classis nov., order *Dehalococcoidales* ord. nov. and family *Dehalococcoidaceae* fam. nov., within the phylum *Chloroflexi*. Int J Syst Evol Microbiol. 63:625-635.
26. Ludwig ML, Matthews RG. 1997. Structure-based perspectives on B_{12}-dependent enzymes. Annu Rev Biochem. 66:269-313.
27. Buckel W, Golding BT. 2008. Chemistry of B_{12}-Dependent Enzyme Reactions. Wiley Encyclopedia of Chemical Biology. 1-9.
28. Payne KA, Quezada CP, Fisher K, Dunstan MS, Collins FA, Sjuts H, Levy C, Hay S, Rigby SE, Leys D. 2015. Reductive dehalogenase structure suggests a mechanism for B_{12}-dependent dehalogenation. Nature. 517:513-516.
29. Schumacher W, Holliger C, Zehnder AJ, Hagen WR. 1997. Redox chemistry of cobalamin and iron-sulfur cofactors in the tetrachloroethene reductase of *Dehalobacter restrictus*. FEBS Lett 409:421-425.
30. van de Pas BA, Smidt H, Hagen WR, van der Oost J, Schraa G, Stams AJ, de Vos WM. 1999. Purification and molecular characterization of ortho-chlorophenol reductive dehalogenase, a key enzyme of halorespiration in *Desulfitobacterium dehalogenans*. J Biol Chem 274:20287-20292.
31. Fieber W, Hoffmann B, Schmidt W, Stupperich E, Konrat R, Kräutler B. 2002. Pseudocoenzyme B_{12} and Adenosyl-Factor A: Electrochemical Synthesis and Spectroscopic Analysis of Two Natural B_{12} Coenzymes with Predominantly 'Base-off' Constitution. Helv Chim Acta 85:927-944.

32. Morita Y, Futagami T, Goto M, Furukawa K. 2009. Functional characterization of the trigger factor protein PceT of tetrachloroethene-dechlorinating *Desulfitobacterium hafniense* Y51. Appl Microbiol Biotechnol 83:775-781.
33. Maillard J, Genevaux P, Holliger C (2011) Redundancy and specificity of multiple trigger factor chaperones in *Desulfitobacteria*. Microbiology. 157:2410-2421.
34. Padovani D, Labunska T, Palfey BA, Ballou DP, Banerjee R. 2008. Adenosyltransferase tailors and delivers coenzyme B_{12}. Nat Chem Biol 4:194-196.
35. Parthasarathy A, Stich TA, Lohner ST, Lesnefsky A, Britt RD, Spormann AM. 2016. Biochemical and EPR-spectroscopic investigation into heterologously expressed vinyl chloride reductive dehalogenase (VcrA) from *Dehalococcoides mccartyi* strain VS. J Am Chem Soc. 137:3525-3532.
36. Schubert T. 2017. The organohalide-respiring bacterium *Sulfurospirillum multivorans*: a natural source for unusual cobamides. World J Microbiol Biotechnol 33:93.
37. Friedrich W, Bernhauer K. 1958. Zur Chemie und Biochemie der „Cobalamine", VIII. Über die 5- und 6-Methyl-benzimidazol-cobalamin-Analoga. Chemische Berichte 91:1665-1670.
38. Kräutler B, Moll J, Thauer RK. 1987. The corrinoid from *Methanobacterium thermoautotrophicum* (Marburg strain). Spectroscopic structure analysis and identification as Co□-cyano-5'-hydroxybenzimidazolyl-cobamide (factor III). Eur J Biochem. 162:275-278.
39. Crofts TS, Seth EC, Hazra AB, Taga ME. 2013. Cobamide structure depends on both lower ligand availability and CobT substrate specificity. Chem Biol. 20:1265-1274.
40. Kunze C, Bommer M, Hagen WR, Uksa M, Dobbek H, Schubert T, Diekert G. 2017. Cobamide-mediated enzymatic reductive dehalogenation via long-range electron transfer. Nat Commun 8:15858.
41. Mueller U, Darowski N, Fuchs MR, Förster R, Hellmi M, Paithankar KS, Pühringer S, Steffien M, Zocher G, Weiss MS. 2012. Facilities for macromolecular crystallography at the Helmholtz-Zentrum Berlin. J Synchrotron Radiat 19:442-449.
42. Meents A, Reime B, Stübe N, Fischer P, Warmer M, Göries D, Röver J, Meyer J, Fischer J, Burkhardt A, Vartiainen I, Karvinen P, David C. 2013. Development of an in-vacuum x-ray microscope with cryogenic sample cooling for beamline P11 at PETRA III. Proceedings of SPIE 8851, X-Ray Nanoimaging: Instruments and Methods, 88510K.
43. Burkhardt A, Pakendorf T, Reime B, Meyer J, Fischer P, Stübe N, Panneerselvam S, Lorbeer O, Stachnik K, Warmer M, Rödig P, Göries D, Meents A. 2016. Status of the crystallography beamlines at PETRA III. Eur Phys J Plus. 131:56.
44. Kabsch W. 2010. *XDS*. Acta Crystallogr D Biol Crystallogr. 66:125-132.
45. Krug M, Weiss MS, Heinemann U, Mueller U. 2012. *XDSAPP*: a graphical user interface for the convenient processing of diffraction data using *XDS*. J Appl Cryst. 45:568-572.
46. Emsley P, Lohkamp B, Scott WG, Cowtan K. 2010. Features and development of Coot. Acta Crystallogr D Biol Crystallogr. 66:486-501.
47. Afonine PV, Grosse-Kunstleve RW, Echols N, Headd JJ, Moriarty NW, Mustyakimov M, Terwilliger TC, Urzhumtsev A, Zwart PH, Adams PD. 2012. Towards automated crystallographic structure refinement with *phenix.refine*. Acta Crystallogr D Biol Crystallogr 68:352-367.
48. Chen VB, Arendall WB 3rd, Headd JJ, Keedy DA, Immormino RM, Kapral GJ, Murray LW, Richardson JS, Richardson DC. 2010. MolProbity: all-atom structure validation for macromolecular crystallography. Acta Crystallogr D Biol Crystallogr. 66:12-21.

2.3 Cobamide-mediated enzymatic reductive dehalogenation via long-range electron transfer

Kunze C*, Bommer M*, Hagen WR, Uksa M, Dobbek H, Schubert T, Diekert G (2017) *Nat Commun* 8, 15858.

* These authors contributed equally to this work.

The reductive dehalogenation of alkyl and aryl halides by a single RDase enzyme is found only rarely. In this study, the PCE-dechlorinating PceA of *S. multivorans* was shown to efficiently convert also brominated phenols, thus allowing for structure and function analysis of an RDase able to dehalogenate both substrate classes. An unambiguous positioning of halogenated phenols at some distance from the cobamide in the active site of PceA, combined with the absence of an intimate cobalt-substrate interaction in EPR spectroscopy suggest a new reaction mechanism for cobamide cofactors involving a dissociative long-range electron transfer from the cobalt to the substrate. Thus, the catalytic cycle of RDases can be clearly distinguished from other B_{12}-containing enzymes like adenosylcobalamin-dependent enzymes and methyltransferases.

My own contribution to this publication covers about 40%.
I conducted the cultivation of *S. multivorans* GD21, the purification of PceA and enzyme activity assays with the isolated protein. During a day stay at the Bessy II electron storage ring I performed soaking experiments with PceA crystals and generated diffraction patterns of the crystals, a task that was otherwise performed by Martin Bommer. All coauthors participated in the interpretation of the results. I have written the original manuscript and revised it including comments from all coauthors.
The characterization of the mutant strain *S. multivorans* GD21, the optimization of the PceA purification and maturation and the determination of the redox states of the cofactors of PceA using EPR (performed during a research stay at WR Hagen's lab) was the subject of my master thesis.

For supplementary information see appendix, pp. xxxv - lvi.

nature COMMUNICATIONS

ARTICLE

Received 3 Mar 2017 | Accepted 3 May 2017 | Published 3 Jul 2017

DOI: 10.1038/ncomms15858 OPEN

Cobamide-mediated enzymatic reductive dehalogenation via long-range electron transfer

Cindy Kunze[1,*], Martin Bommer[2,*,†], Wilfred R. Hagen[3], Marie Uksa[1,†], Holger Dobbek[2], Torsten Schubert[1] & Gabriele Diekert[1]

The capacity of metal-containing porphyrinoids to mediate reductive dehalogenation is implemented in cobamide-containing reductive dehalogenases (RDases), which serve as terminal reductases in organohalide-respiring microbes. RDases allow for the exploitation of halogenated compounds as electron acceptors. Their reaction mechanism is under debate. Here we report on substrate–enzyme interactions in a tetrachloroethene RDase (PceA) that also converts aryl halides. The shape of PceA's highly apolar active site directs binding of bromophenols at some distance from the cobalt and with the hydroxyl substituent towards the metal. A close cobalt–substrate interaction is not observed by electron paramagnetic resonance spectroscopy. Nonetheless, a halogen substituent *para* to the hydroxyl group is reductively eliminated and the path of the leaving halide is traced in the structure. Based on these findings, an enzymatic mechanism relying on a long-range electron transfer is concluded, which is without parallel in vitamin B_{12}-dependent biochemistry and represents an effective mode of RDase catalysis.

[1] Department of Applied and Ecological Microbiology, Institute of Microbiology, Friedrich Schiller University, Philosophenweg 12, Jena D-07743, Germany. [2] Structural Biology/Biochemistry, Institute of Biology, Humboldt Universität zu Berlin, Philippstrasse 13, Berlin D-10115, Germany. [3] Department of Biotechnology, Faculty of Applied Sciences, Delft University of Technology, van der Maasweg 9, Delft 2629HZ, The Netherlands. * These authors contributed equally to this work. † Present address(es): Max-Delbrück-Centrum for Molecular Medicine, Robert-Roessle-Str. 10, Berlin D-13092, Germany (M.B.); Institute of Soil Science and Land Evaluation, University of Hohenheim, Emil-Wolff-Strasse 27, Stuttgart D-70593, Germany (M.U.). Correspondence and requests for materials should be addressed to T.S. (email: torsten.schubert@uni-jena.de) or to G.D. (email: gabriele.diekert@uni-jena.de).

Several anaerobic bacteria use organohalides as terminal electron acceptors in their respiratory metabolism. These often toxic, hazardous and usually highly persistent compounds, which originate from industrial, biotic or geochemical sources, are reductively dehalogenated by these microbes. This biological process mobilizes the halogens and counteracts the accumulation of organohalides in oxygen-depleted environments. Hence, organohalide respiration contributes significantly to the global halogen cycle. Reductive dehalogenase (RDase) enzymes are membrane-bound terminal reductases in organohalide respiration and harbour two Fe–S clusters and a cobamide cofactor (reviewed in ref. 1). The utilization of a cobamide cofactor makes RDases unique among terminal reductases. With almost 300 RDase genes identified so far, organohalide respiration is present in different bacterial phyla, including Chloroflexi, Firmicutes and Proteobacteria[2]. However, only a dozen of the corresponding gene products were biochemically characterized including the tetrachloroethene RDase (PceA) of the epsilonproteobacterium *Sulfurospirillum multivorans*[3]. PceA was described to mediate the reductive dehalogenation of chlorinated and brominated ethenes or propenes[4,5] (Supplementary Fig. 1). The cobamide cofactor of PceA was identified as norpseudo-B_{12}, a derivative of vitamin B_{12}, which is characterized by a unique nucleotide loop composition[6]. The crystal structure of PceA showed the norpseudo-B_{12} non-covalently bound in its 'base-off' conformation deeply inside the protein[7]. The two [4Fe–4S] clusters of PceA connect the surface and cobamide cofactor at distances short enough to allow intramolecular electron transfer to the active site and potentially also from the proximal Fe–S cluster to the substrate. An identical arrangement of the metal cofactors was detected in the *ortho*-dibromophenol RDase (NpRdhA) of the marine alphaproteobacterium *Nitratireductor pacificus* pH-3B[8], a non-respiratory RDase with 28% amino acid sequence identity to PceA.

Apart from methyltransferases, adenosylcobalamin-dependent enzymes (for example, eliminases, mutases and ribonucleotide reductase) and *S*-adenosylmethionine radical enzymes[9–11], RDases form a distinct subfamily of cobamide-dependent enzymes together with the epoxyqueuosine reductase[12]. Cobamide-dependent methyltransferases heterolytically cleave the cobalt–carbon bond in methylcobalamin and transfer a methyl ion. Adenosylcobalamin-dependent enzymes generate a 5′-deoxyadenosyl radical via homolytic cleavage of the Co–C bond. The adenosyl radical then serves as reactive species during catalysis. Different from these extensively investigated modes of cobamide cofactor function, recently alternative mechanisms have been proposed for the cobamide-dependent *S*-adenosylmethionine radical enzymes catalysing either methylations or substrate rearrangements[13,14].

Little is known about the catalytic mechanism of RDases that harbour derivatives of hydroxocobalamin or aquocobalamin rather than adenosylcobalamin or methylcobalamin as cofactors. The super-reduced [Co^{I}]-state was proposed to initially attack the substrates[7,8]. However, different reaction mechanisms for cobamide-dependent reductive dehalogenation have been proposed (Fig. 1). The formation of a cobalt–carbon bond[15] after alkylation of the cobalt by a nucleophilic attack of [Co^{I}] on the carbon backbone of the organohalide, the formation of a cobalt–halogen bond after direct [Co^{I}] attack on the halogen substituent[8] or a long-range electron transfer from [Co^{I}] leading to substrate radical formation followed by the formation of a carbanion after elimination of the halogen substituent[5,7,16] were considered. As revealed by the structural analysis of PceA and NpRdhA, an alkylation of the cobalt during substrate conversion is unlikely due to spatial restraints caused by the amino acid arrangement at the active site[7,8]. For NpRdhA, spectroscopic analysis and substrate modelling pointed towards the formation

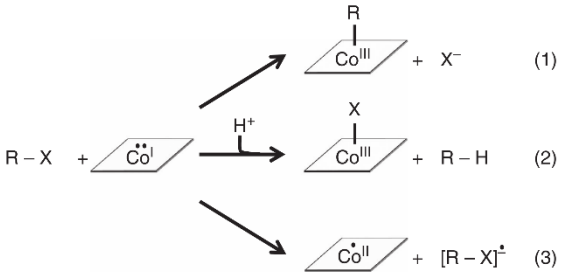

Figure 1 | Proposed initial steps in the catalytic mechanism of RDases. (1) Alkylation of the cobalt by a nucleophilic attack of [Co^{I}] on the carbon backbone of the organohalide. (2) Formation of a cobalt–halogen bond after [Co^{I}] attack directly at the halogen substituent followed by heterolytic cleavage of the carbon–halogen bond. (3) Long-range electron transfer from [Co^{I}] leading to substrate radical formation and finally to the formation of a carbanion after elimination of the halogen substituent (the elimination is not shown). [Co^{I-III}]: oxidation states of the cobalt ion in the cobamide cofactor; R: hydrocarbon backbone; X: halogen substituent.

of a cobalt–halogen bond during the conversion of brominated aromatic substrates[8]. The structure of PceA occupied by trichloroethene (TCE) showed cofactor distances of 5.8 Å to the cobalt, 10.8 Å to the proximal [4Fe–4S] cluster and 3.7 Å to a potential proton donor, a highly conserved tyrosine[7]. However, the small size of the ligand, two different orientations and the lack of a defined binding site did not allow for an unambiguous deduction of the course of the reaction. A reorientation of the substrate in the reduced enzyme and a direct interaction of the substrate with the cobalt would have been feasible, even though this was not observed in the crystal structure. So far, there is no direct evidence for a long-range electron transfer in RDases, but there are indications for an undirected electron transfer mechanism in PceA during reductive dehalogenation of tribromoethene (TBE) to all isomers of dibromoethene (DBE)[5] and of *trans*-1,3-dichloropropene to a mixture of *cis*-1-, *trans*-1- and 3-chloropropene[4] (Supplementary Fig. 1). In addition, adduct formation with radical traps or chloropropenyl radicals was observed during the conversion of chloropropenes and interpreted as indicative for the generation of substrate radicals[16].

In this study, the binding and conversion of brominated and chlorinated phenols by PceA of *S. multivorans* is investigated in detail. These organohalides are chosen for three reasons: (i) The active site cavity of PceA allows for the binding of larger halogenated phenols, which might overcome the ambiguity in substrate orientation. (ii) Specific halogenated phenols could be selected, whose substitution pattern presumably would allow probing of potential substrate–cobalt interactions. (iii) Halogenated phenols are applied for a direct comparison with RDases specialized in converting aromatic organohalides. Here we show that PceA is also able to convert brominated phenols. Structural analysis of PceA–substrate complexes displays the hydroxyl substituent positioned above the cobalt at a distance of 4.7 Å. From the absence of a direct cobalt–substrate coupling during substrate turnover, which is verified by electron paramagnetic resonance (EPR) spectroscopy, an attack via a long-range electron transfer is concluded as initial step. The reductive dehalogenation at the active site initiated by the dissociative electron transfer is visualized in the PceA crystal.

Results

Dehalogenation of bromophenols (BPs) by PceA. Structural analysis showed the active site of PceA located at the centre of the enzyme[7]. The narrow, triangular-shaped substrate-binding

NATURE COMMUNICATIONS | DOI: 10.1038/ncomms15858 ARTICLE

Table 1 | Conversion of halogenated substrates by purified Strep-tagged PceA isolated from *S. multivorans* GD21 and the effect of ammonium on the reaction.

Substrate	Product	Without NH_4^+			With NH_4^+		Fold increase in activity with NH_4^+
		V_{max} (nkat mg^{-1} PceA)	k_{cat} (s^{-1})	k_{cat}/K_m ($mM^{-1}s^{-1}$)	V_{max} (nkat mg^{-1} PceA)	k_{cat} (s^{-1})	
PCE	TCE	1,008 ± 24	54	270	3,363 ± 47	180	3.4
TCE	*cis*-1,2-DCE	890 ± 4	48	200	3,613 ± 278	193	4.1
2-BP	phenol	38,108 ± 1,660	2,035	ND	39,934 ± 14	2,132	1
3-BP	phenol	9,204 ± 256	492	ND	8,475 ± 1,534	453	0.9
4-BP	phenol	15,143 ± 332	809	8,172	15,332 ± 27	819	1
2,4-DBP	4-BP	4,653 ± 229	252	2,655	5,975 ± 50	319	1.2
2,5-DBP	3-BP, 2-BP	40,704 ± 12,183	2,173	ND	40,420 ± 5,256	1,898	0.9
2,6-DBP	2-BP	14,176 ± 0	757	ND	15,871 ± 2,059	848	1.1
3,5-DBP	3-BP	152 ± 0.3	8	ND	167 ± 30	9	1.1
2,4,6-TBP	2,4-DBP	107 ± 46	8	53	102 ± 21	5	0.65
2,3-DCP	3-CP	43 ± 0	2	ND	35 ± 0	2	0.8
2,5-DCP	3-CP	6 ± 1	0.3	ND	5 ± 0.5	0.3	1

ND, Km was not determined.
k_{cat} of dibromophenols comprised the formation of the corresponding bromophenol as well as further reduction to phenol, whereby all turnovers were included in its calculation. S.d. is given. No dehalogenating activity was measured with 2-, 3- or 4-CP, 2,4-DCP, 2,6-DCP, 3,4-DCP, 3,5-DCP, 2,3,4-TCP, 2,4,5-TCP, 2,4,6-TCP and 3,4,5-TCP, with the larger halogenated aromatics 3-chlorobenzoate, 3-chloro-4-hydroxyphenyl-acetate or with *cis*-1,2-dichloroethene (*cis*-1,2-DCE). The variety of bromophenols tested here was limited to commercially available compounds. The detection limit of phenolic compounds was 5 µM. K_m for PCE is 0.2 mM and for TCE 0.24 mM[3].

pocket with its base above the corrin ring and its maximal height above the cobalt ion, both dimensions about 10 Å in length, easily allows access for chlorinated and brominated ethenes and propenes, which are the known substrates of PceA[3–5]. In order to investigate structural restrictions in the active site that are responsible for substrate selectivity and substrate positioning, the substrate range of PceA was revisited and broadened towards bulkier electron acceptors. Enzyme activity measurements revealed that besides aliphatic hydrocarbons brominated and chlorinated phenols are also converted by the enzyme (Table 1). The halogenated phenols are expected to be readily accessible for the reduction by the super-reduced [Co^I] of PceA (midpoint potential of the [Co^{II}]/[Co^I] couple: −380 mV at pH 7.5 (ref. 6)), because of their positive redox potentials ($E^{\circ\prime} = 300–500$ mV)[17]. All tested brominated phenols were completely reduced to phenol. BPs were converted with turnover numbers up to ~2,000 s^{-1}, thus 40-fold higher compared to the k_{cat} of 54 s^{-1} for tetrachloroethene (perchloroethylene (PCE)). While most of the brominated phenols were selectively dehalogenated, 2,5-dibromophenol (DBP) was debrominated to 3- and 2-BP. Conversion rates about 20–30 times lower than for PCE were measured for 3,5-DBP and 2,4,6-tribromophenol (TBP). In general, PceA preferentially removed the bromine substituent at the *ortho*-position followed by the halogen substituent at either the *meta*- or *para*-position. With the exception of the 3,5-dichlorophenol RDase[18] of *Desulfitobacterium hafniense* PCP-1, all biochemically characterized RDases favour the removal of the *ortho*-substituent of chlorinated phenols and preferentially convert polyhalogenated phenols[19–22]. In case of PceA, the conversion rate increased with a decrease in the number of halogen substituents, as shown for 2,4,6-TBP to 2,4-DBP and 4-BP, while the K_m values for all three substances were similar. The apparent K_m for 4-BP was 99 µM, for 2,4-DBP 95 µM and for 2,4,6-TBP 158 µM. Substrate concentrations >600 µM for 2,4-DBP to 1,000 µM for 2,4,6-TBP inhibited PceA. RDases have not been previously described to use both alkyl and aryl halides. For the chlorophenol RDases of *Desulfitobacterium dehalogenans* and *Desulfitobacterium hafniense* DCB-2, a dehalogenation of chlorinated ethenes was detected but at low rates[19,20]. PceA being an RDase that converts both types of substrates at similarly high rates, it allows for mechanistic studies on a single RDase reductively dehalogenating alkyl and aryl halides. The efficient dehalogenation of brominated phenols by the PceA enzyme sheds a new light on its role in nature that has been defined so far as an effective catalyst for the dehalogenation of alkyl halides such as PCE and TCE, both substrates of mainly anthropogenic origin. In contrast to brominated phenols, PceA did not dehalogenate most of their chlorinated analogues. A similar preference for brominated substrates rather than their chlorinated counterparts has been reported for NpRdhA[8]. PceA dechlorinated only 2,3- and 2,5-dichlorophenol (DCP) with a k_{cat} of 1.9 s^{-1} and 0.3 s^{-1}, respectively. Both substrates were exclusively dehalogenated at the *ortho*-position. The formation of phenol was not observed with either substrate.

PceA dehalogenated 4-iodophenol (4-IP) three times faster than 4-BP, while 4-chlorophenol (4-CP) was not converted. The dehalogenating activity increased with decreasing electronegativity and decreasing partial negative charge from the chlorine to the iodine substituent. Partial charge models and Gibbs free energy calculations for chlorinated and brominated organohalides provide a rationale for these observations[23,24]. Previous studies on PceA of *S. multivorans* revealed that the presence of ammonium ions stimulates the conversion of halogenated ethenes[3,5]. To test the effect of ammonium ions on the reduction of halogenated phenols, 4 mM $(NH_4)_2SO_4$ was added to the assay. Conversion of PCE was stimulated 3.3-fold, but no effect on the turnover of halogenated phenols was observed (Table 1). This difference was also described earlier for chlorinated propenes compared to chloroethenes[16]. However, the positive effect of ammonium ions on PCE conversion remains inexplicable. The different conversion rates depending on the redox potential of the artificial electron donor described earlier by Miller *et al.*[25] for PCE were confirmed here for 4-BP (Supplementary Table 1).

The conversion of substrates was strictly dependent on the intact enzyme, involving the super-reduced [Co^I]-state of the cobamide cofactor. No abiotic conversion of any substrates mediated by protein-free cobamides was detected, even when heat-inactivated PceA was applied in a 120- to 160-fold concentration compared to that of native PceA. However, the involvement of the enzyme-bound cobamide cofactor in the catalysis was corroborated by the complete inhibition of the PceA-mediated 4-BP dehalogenation by propyl iodide in the dark. Propyl iodide is an inhibitor that binds irreversibly to the

[Co^{I}]-state of cobamides in the absence of light[26,27]. Subsequent exposure to light reversed the inhibition of 4-BP conversion. The inhibition of the dehalogenating activity of cobamides by propyl iodide has been attributed to an alkylation of the [Co^{I}]-state, which implies the formation of a cobalt–carbon bond for the propyl iodide probe. However, this is not the case for phenolic substrates as will be shown below.

Binding of halogenated phenols in the active site cavity. The conversion of halogenated phenols by PceA raised the question of their positioning in the active site. With respect to their dimensions, monoaromatic substrates with several substituents should fit into the active site of PceA. However, due to the arrangement of the amino acid side chains, aryl halides are expected to be limited in their orientation. To test for the validity of this hypothesis, PceA crystals harbouring the five coordinated [Co^{II}]-state of the cobamide cofactor were soaked with halogenated phenols and the 3D structure of the enzyme–substrate complex was determined and analysed. Several monoaromatic halogenated compounds up to the size of 2,4,6-TBP were visualized in the active site pocket. Restricted by the protein environment, the phenol ring of 2,4,6-TBP is oriented at an angle of approximately 40° away from the surface normal vector of the corrin ring and enclosed by Trp96, Tyr382, Trp56, Trp376, Tyr102 and Tyr246 (Fig. 2a). The substrate enters the active site through an opening between Phe38, Trp376, Tyr102 and Asn272 at the bottom of the substrate channel. The binding pocket is thus lined with hydrophobic side chains, while the substrate is shielded from the polar protein backbone. At the far end of the hydrophobic-binding pocket, a gap of the size of a single halide atom between residues Tyr102, Trp56 and Tyr382 (arrows in Fig. 2a) allows access to a polar upper cavity containing the hydroxyl groups of Tyr102 and Tyr382, as well as Glu92, Lys64 and three water molecules. The hydroxyl group of 2,4,6-TBP is located 4.7 Å away from the cobalt and 2.4 Å from the Tyr246-OH. The bromine substituent at C2 is fully enclosed, while the bromine at C6 points towards the substrate channel and the bromine at C4 towards the upper cavity, where it is restrained in its position by Tyr102 and Tyr382. The hydrogen at C3 points at the Tyr382 phenyl group. The two rings interact in an edge-to-face geometry, precluding a bulky halogen substituent at this place. In addition, C_{beta} of Tyr102 is only 3.3 Å away from C5 of the aromatic substrate ring, leaving little space for an additional halogen substituent. Hence, binding of the planar, triangular 2,4,6-TBP to PceA with a bromine substituent towards Co is likely to be impossible (see Fig. 2 and Supplementary Fig. 2a,b) and would place the other bromine substituents in conflict with the aromatic ring of Tyr382 or into the substrate channel between Tyr102 and Phe38, a position too narrow to accommodate a bromine. While the latter may be resolved by not-yet-observed plasticity within the binding site, the short distance between the conserved Tyr246 and the substrate hydroxyl group (2.4 Å) in the observed position should be noted. This is likely to prevent the binding of the bulkier bromine substituent at the current hydroxyl position or closer in not only 2,4,6-TBP but also many other brominated phenols tested in this study. The low K_m value for 2,4,6-TBP supports the reliability of the analysed enzyme–substrate complex, since it indicates a high affinity for the substrate without any steric hindrance in substituent positioning.

Based on the position of the aromatic ring of 2,4,6-TBP, a tentative model for the probability of a halogen substitution at the different C-atoms in monoaromatic organohalides was drafted as working hypothesis (Fig. 2b). This model suggests that the substitution pattern governs the substrate orientation in the binding pocket and might thereby influence the reactivity. When

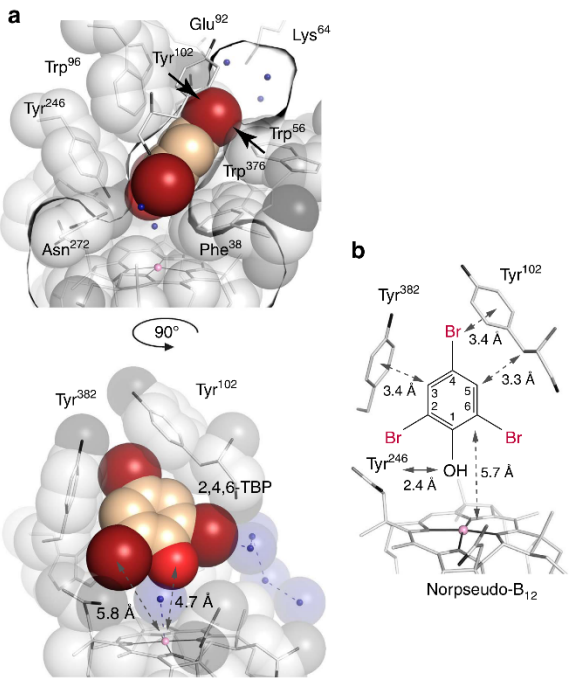

Figure 2 | The PceA substrate-binding pocket. (**a**) Positioning of 2,4,6-TBP in the active site as revealed by structural analysis. Shown is a cross-section through the binding pocket viewed from the substrate channel (Tyr102) (upper figure) or viewed from Tyr246 with the substrate channel on the right (lower figure). The Co-water/hydroxyl ligand and further water molecules are shown as blue spheres. (**b**) Distances between 2,4,6-TBP and Tyr102, Tyr246, Tyr382 and cobalt. A single hydrogen bond may be formed to the phenolic hydroxyl of Tyr246. Probability of a halogen substituent at different C-atoms provides a tentative model for the binding of other monoaromatic substrates. Besides the allowed substitution positions shown, the Tyr102-oriented position is possibly allowed after a small rotation of the substrate. A substituent at the Tyr382-oriented position is not possible due to bulky obstruction.

crystals were treated with 2 mM Ti(III) citrate or up to 5 mM Eu(II)EDTA/DTPA and 0.2 mM methyl viologen, the electron density for the upper ligand of the cobamide cofactor disappeared, which was attributed to the presence of the super-reduced [Co^{I}]-state of the cobalt ion. Since there were no further conformational changes visible upon reduction of the substrate-free enzyme, other than lacking the upper ligand, it is likely that the substrates will be positioned the same way in the [Co^{I}]-enzyme. Unfortunately, the destabilizing effect of reducing agents onto PceA crystals occupied with substrates did not allow for an analysis of enzyme–substrate complexes under these conditions. Furthermore, when incubated with substrate and reducing agent, PceA crystals apparently reverted to the [CoII] state as judged by their colour and the presence of the upper Co-ligand (Fig. 3a). In order to confirm the functionality of PceA in the crystals, activity assays were performed with crystallized PceA under the same buffer conditions used for crystal generation and storage. Reductive dehalogenation of 4-IP, 4-BP and TCE was observed upon reduction of the crystals with methyl viologen and Ti(III) citrate. Conversion of other substrates was not tested with crystals.

To verify our hypothesis on the binding mode of phenolic substrates presented in Fig. 2b and to understand the sequence and mechanism of organohalide reduction, PceA crystals in the

NATURE COMMUNICATIONS | DOI: 10.1038/ncomms15858 ARTICLE

[Co^{II}]-state were soaked with 2,4-DBP and 4-BP, the dehalogenation products of 2,4,6-TBP (Fig. 3a and Supplementary Fig. 3). Interestingly, 2,4-DBP and 4-BP, which were expected to freely rotate around the vertical and horizontal axis, occupied the same position as 2,4,6-TBP. While the substrate hydroxyl groups were nearest to the cobalt at a distance of 4.7 Å, a ring formed by Arg305, Trp376, Asn272, Phe38 and the carboxamide side chains of the cobamide cofactor restricts access of the substrate to the metal ion. The substrate hydroxyl group is close to Tyr246-OH (2.4 Å), which additionally limits its approach to Co, thus disfavouring a coupling of the cobalt with the hydroxyl group of the substrate. All in all, the binding mode of halogenated phenols confirmed the previous assumption that an alkylation of the cobalt during the course of the reaction is unlikely. Moreover, the orientations of 2,4,6-TBP, 2,4-DBP and 4-BP contradict the formation of a cobalt–halogen bond and rather indicate a long-range electron transfer during catalysis. According to the prediction of allowed halogen positions (Fig. 2b), *meta*-halogenated phenols might not fit into the active site with the hydroxyl group pointing towards the cobalt. In 3-BP soaked crystals, the hydroxyl group is turned by one position towards the substrate channel/Tyr102 and the bromine substituent is oriented towards the upper cavity (Fig. 3b). None of the substituents are orientated towards the cobalt ion, precluding a direct attack.

In the first step of the reaction, the electrons could be externally transferred to the bromine substituent or to the aromatic ring. For 2,4,6-TBP, the bromine substituents adjacent to the hydroxyl group seem to be preferentially removed and could accept electrons from the aromatic ring as well as from the cobalt ion itself, considering their distance of approximately 5.8 and 6.6 Å from the cobalt. However, the *para*-position of 4-BP and the *meta*-position of 3-BP are placed distantly away, towards the upper cavity of the substrate-binding pocket, and yet reductive dehalogenation was not impaired. In these cases, electrons from [Co^{I}] have to be transferred via the aromatic ring to the respective substituent. Crystals were also soaked with 2,4,6-trichlorophenol and 3-CP (Supplementary Fig. 4a,b). Both phenols were positioned in the same orientation as their brominated analogues in the substrate-binding pocket but were not dehalogenated. Activity measurements using 4-CP, 4-BP and 4-IP showed an enhanced reduction rate with decreasing electronegativity of the halogen substituent from chloride to iodide. The position and orientation of the analogues 4-CP, 4-BP and 4-IP in the active site of substrate–enzyme complexes is thereby identical, independent of the type of halogen (Fig. 3c). It has to be concluded that exclusively the differences in the energy of the various carbon–halogen bonds determine the displacement or continuance of the substituent.

It should be noted that the hydrophobic substrate-binding pocket of PceA did not form hydrogen bonds with its substrates. Hence, the position of the substrate and its halide substituents is not strictly fixed. A subset of substrates or substrate analogues was identified, which did not match with the orientation of 2,4,6-TBP in the active site pocket (Supplementary Fig. 4c).

Though the dimensions of the active site allow for the binding of monoaromatic organohalides, access to the pocket is restricted by a 5.5 × 3 Å 'letter box' entry of the substrate channel, which is embedded within a hydrophobic groove on the protein surface and lined by the side chains of Thr39, Phe44, Phe57, Leu186 and Glu189 (ref. 7). These side chains appear to be immobile and were found at the same position in crystal structures of oxidized, substrate-bound and reduced PceA. 4-IP and 2,6-DBP bind to the groove in multiple positions, as shown at Leu186 (Supplementary Fig. 2b,c). The position of all letter box side chains is severely restrained and Leu186 is the only side chain, which from observation of possible side-chain rotamers, may move

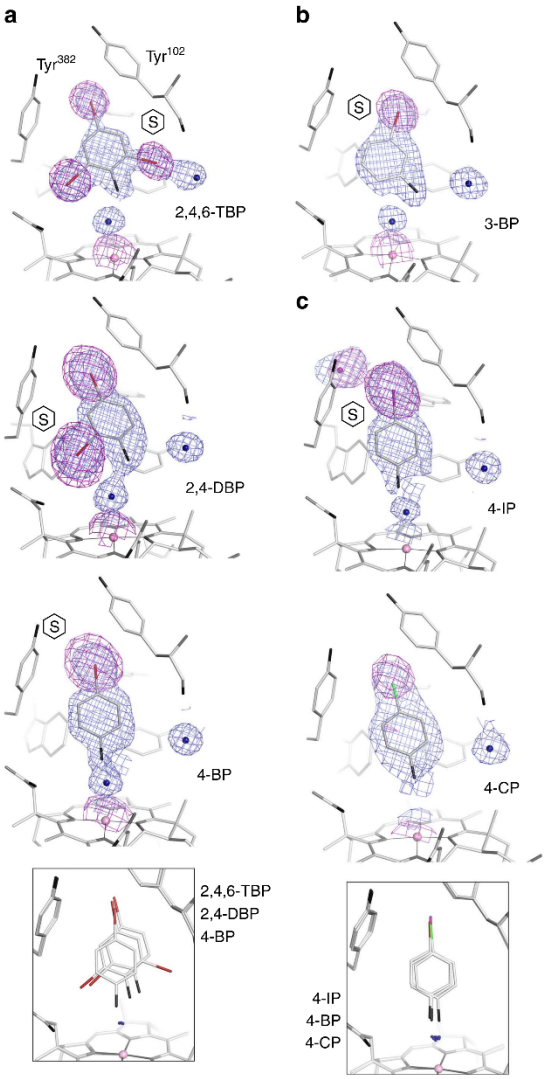

Figure 3 | Substrates and analogues bound to the PceA substrate-binding pocket. (**a**) Positioning of 2,4,6-TBP, 2,4-DBP and 4-BP. An overlay of the three substrates is depicted in the inset. Stereo representations are shown in Supplementary Fig. 3. (**b**) Positioning of the *meta*-halogenated 3-BP. (**c**) Influence of halogen type on positioning of *para*-halogenated phenols. In the direction shown, the binding site is flanked by Tyr382, Tyr102 and the corrin ring. For all substrates, 1 sigma $2F_o - F_c$ electron density (blue) for substrate, Co-ligand water/hydroxyl and the first water molecule in the substrate channel are shown. Anomalous difference density (indicative of a heavy atom) is shown around the substrate for bromine (5 sigma map, red stick), chlorine (3.5 sigma, green stick) or iodine (5 sigma, violet stick). The hydroxyl group is shown in black. (S) Indicates the leaving group of a substrate. Note that products were bound to PceA at high concentrations and represent substrate rather than product, except for a signal modelled as iodide ion which may have dissociated from 4-IP in the 1.9 Å wavelength X-ray beam. 2,4-DBP was incubated in a buffer containing 200 mM Cl^-; other incubations were performed in chloride-free buffer. 2,4-DBP and 4-BP were incubated in the presence of 2 mM Ti(III) citrate and 0.2 mM methyl viologen. No cobalt β-ligand was modelled for 4-CP because of the lower resolution (2.3 Å versus 1.6–1.9 Å for other structures).

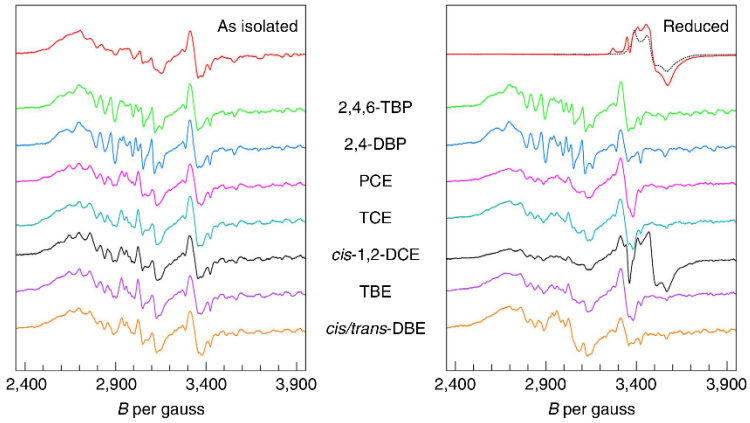

Figure 4 | Stack plot of substrate-induced and turnover-induced changes in the [Co^{II}]-EPR of PceA. The red trace in the left-hand panel is the spectrum of the as-isolated enzyme. Subsequent traces are for incubation of the as-isolated PceA with 2,4,6-TBP (green trace), 2,4-DBP (blue trace), PCE (magenta trace), TCE (cyan trace), *cis*-1,2-DCE (black trace), TBE (violet trace) and *cis/trans*-1,2-dibromoethene (*cis/trans*-DBE, gold trace). In the right-hand panel, the red trace is the spectrum of reduced PceA. Reduction of PceA (3 mg ml^{-1}) with 1 mM Ti(III) citrate and 20 μM methyl viologen for about 5 min led to a [4Fe-4S]$^{1+}$ spectrum accompanied by the spectra of Ti(III) citrate and a methyl viologen radical. The lack of a [Co^{II}]-signal indicated the reduction of the cobalt to the EPR silent [Co^{I}]-state. The black dotted line is the spectrum of Ti(III) citrate alone. The subsequent traces are the equivalents of the traces in the left-hand panel after turnover of substrates induced by reduction of PceA for about 5 min. Experimental EPR conditions were: microwave frequency, 9,338 MHz; microwave power, 12.7 mW; modulation frequency, 100 kHz; modulation amplitude, 8 Gauss; temperature, 22 K.

away from the opening. While such open conformation was not observed, Leu186 was poorly defined when crystals were incubated with 3-BP and a peak in the anomalous difference map suggests a partial occupation by a 3-BP bromine substituent (Supplementary Fig. 2d–f). Leu186 may thus shift to allow access of larger compounds such as 2,4,6-TBP to the active site.

EPR spectroscopic analysis of PceA–substrate interactions. To confirm the hypothesis of a long-range electron transfer mechanism during the reductive dehalogenation of halogenated phenols, enzyme–substrate complexes were studied by EPR spectroscopy. As-isolated PceA in solution showed the characteristic low-spin $S = 1/2$ spectrum of the [Co^{II}]-state of the cobamide cofactor (Fig. 4, left panel). The addition of 2,4,6-TBP and 2,4-DBP did not change the [Co^{II}]-signal significantly (Fig. 4, green and blue traces). An increase in resolution was observed that was accompanied by minor changes in the effective spin Hamiltonian parameters, which are estimated to be $<0.1\%$ in the *g*-value and a few gauss in the hyperfine splittings (see also Supplementary Fig. 5). This might be attributed to modest effects of substrate binding on the conformation of the active site and/or the global protein conformation. The lack of any superhyperfine splitting from bromine nuclei argues against a direct cobalt–halogen bond formation in the [Co^{II}]-state. Upon reduction of PceA with 1 mM Ti(III) citrate and 20 μM methyl viologen, the [Co^{II}]-signal disappeared, indicating the formation of the EPR silent [Co^{I}]-state (Fig. 4, right panel). At the same time, a characteristic [4Fe–4S]$^{1+}$-signal appeared, which was combined with the spectra of excess Ti(III) citrate and methyl viologen radicals. Reduction of PceA mixed with excess substrate and incubation for about 5 min led to re-oxidation of the cobamide due to substrate conversion. Since the resulting spectra resembled those of the as-isolated enzyme, the oxidation state of the cobalt appeared to be similar. Neither the substrates nor the products caused a change in the [Co^{II}]-spectrum. Both observations seemed to exclude a direct coupling and thus strongly supported the hypothesis of an alternative mechanism, such as long-range electron transfer.

While none of the brominated phenols trapped in the crystal pointed with a bromine substituent towards the cobalt, PceA crystals soaked with TCE showed two substrate orientations, both exposing a chlorine substituent towards the cobalt[7]. A direct binding of the substrate-bound chloride was not observed, but it was unclear if either the substrate or leaving halide ion may move to bind the cobalt ion during catalysis. From molecular simulations for PceA–PCE/TCE complexes, Liao *et al.*[28] suggested the formation of a cobalt–halogen bond after heterolytic cleavage of the substrate–chloride bond, comparable to what was previously described for NpRdhA. However, addition of PCE and TCE in EPR analyses did not change the EPR signal of the as-isolated PceA (Fig. 4, magenta and cyan traces). In addition, the spectrum of a turnover-induced re-oxidized enzyme has largely reverted to the spectrum of the as-isolated PceA, contradicting a direct cobalt–halogen interaction. PCE is selectively reduced via TCE to *cis*-1,2-dichloroethene (*cis*-1,2-DCE). The reduced PceA sample incubated with *cis*-1,2-DCE showed a residual Ti(III) citrate signal and a methyl viologen radical signal consistent with the lack of measurable dehalogenation activity for this substrate (Fig. 4, black traces). Though *cis*-1,2-DCE is not converted by PceA, a low [Co^{II}]-amplitude is present in the EPR measurement after reduction and *cis*-1,2-DCE addition. This suggests that a single electron might be transferred from [Co^{I}] onto *cis*-1,2-DCE, resulting in the oxidation to [Co^{II}]. However, the energy required for the formation of vinyl chloride was calculated to be 29.3 kJ mol^{-1} higher than for TCE reduction[28]. This energetic barrier is probably not broken by the *S. multivorans* PceA, so that the enzyme is not able to eliminate a chlorine substituent from *cis*-1,2-DCE. The energetic barriers for the formation of *trans*- and 1,1-DCE from TCE were calculated to be higher than that for *cis*-1,2-DCE formation, which may also prevent their formation[28]. An undirected formation of all isomers of DBE was described for the reduction of TBE, which are even further reduced to vinyl bromide by PceA[5] (Supplementary Fig. 1). The presence of bromine substituents rather than chlorine substituents might lower the energetic requirements as mentioned before. TBE and *cis*-/*trans*-DBE were tested in EPR measurements and led to the formation of the [Co^{II}]-state in the reduced sample, which is based on substrate conversion (Fig. 4,

NATURE COMMUNICATIONS | DOI: 10.1038/ncomms15858 ARTICLE

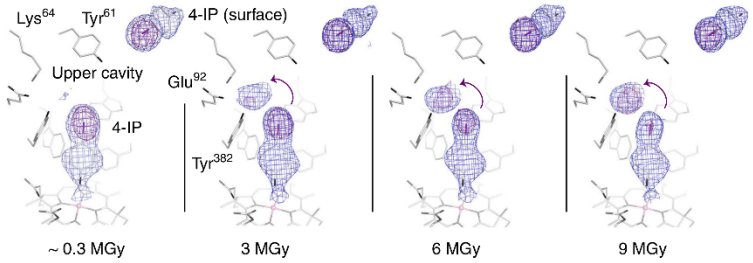

Figure 5 | X-ray photon-induced dehalogenation. Time-series of a crystal soaked in 4-iodophenol under non-reducing conditions, exposed to a 50 µm diameter synchrotron X-ray beam (approximately 10^{11} photons s^{-1}, $\lambda = 1.4$ Å) at 100 K. Both $2F_o$-F_c (blue, 1 σ) and iodine-anomalous difference (purple, 5 σ) electron density, shown for the substituent, successively shifted away from C4 into the cavity around Lys64, Glu92 and Tyr382.

violet and gold traces). Again, no direct cobalt–halogen interaction was detected.

Photon-induced dehalogenation in the PceA active site. During the measurement of diffraction data, crystals were exposed to X-rays with approximate X-ray doses of 10^6–10^7 Gy (Raddose-3D server[29]). Such radiation may induce photoreduction in metalloproteins (reviewed in ref. 30), whereby electrons radiolytically produced from the protein or solvent are trapped in the active site, potentially mimicking an electron transfer step[31]. Changes in the active site can precede global changes in the protein by orders of magnitude[32]. In crystals incubated with 4-IP, dissociation of the halide substituent was routinely visible in the electron density map (Fig. 5). When data were measured in a highly redundant manner, such that individual dose-dependent subsets of data could be used for structure solution, the iodine substituent clearly dissociated from 4-IP during data collection. Electron density of the substituent, weakened at the position of the leaving halide compared to the remainder of the substrate, and a nearby peak in the anomalous difference map, indicative of an appearing halide, were tracing a route for a leaving halide ion into the upper cavity and providing a model for the reductive halogen dissociation at C4. In contrast, a 4-IP bound to the surface of PceA did not show such photon-induced reduction (Fig. 5), which indicates that the active site architecture contributes to the observed dehalogenation reaction by trapping 4-IP in a state predestined to act as acceptor for free electrons within the protein. The source of such electrons differs and it is thus uncertain if the path taken by X-ray electrons follows that during catalysis. Although the possibility of X-ray-induced photoreduction of protein-bound cobamides from [Co^{III}] to [Co^{II}] has been reported before[33], the direct involvement of the super-reduced [Co^{I}] in the photon-induced dehalogenation of 4-IP remains elusive. A photon-induced dehalogenation of brominated or chlorinated phenols has not been observed as clearly as it was monitored for 4-IP.

Discussion

In the study presented here, the cobamide-containing and haloethene-converting PceA was shown to efficiently dehalogenate brominated phenols. Comparison of substrate–enzyme complexes allowed for conclusions on the initial attack by the cobamide cofactor. The distant positioning of the substrates with the hydroxyl group towards the cobalt and the absence of intimate cobalt–substrate interactions during conversion strongly suggested a long-range electron transfer mechanism in PceA. The super-reduced [Co^{I}] acts as reactive species, whereby electrons might be transferred to the phenol ring (Fig. 6a). Especially the halogen substituents in the *para*-position apparently must receive the electrons via the aromatic ring. The fate of the substrate is then largely decided by internal charge distribution and the substitution pattern. According to the theory of substituent effects, the phenolic hydroxyl group shows a more positive resonance effect increasing the electron density particularly at the *ortho*- and *para*-positions, while the halogen substituents have a stronger inductive effect. The bromine substituent with the most positive σ partial charge is predicted to be removed. The substrate 2,4,6-TBP is completely dehalogenated to phenol via 2,4-DBP and 4-BP. This observation is consistent with predictions derived from the natural bond orbital model based on the partial charges for each substituent[23]. The substrate radical formed upon the first electron transfer accompanied by the elimination of the halogen has to be neutralized by another electron transferred via [Co^{I}] or the proximal [4Fe–4S] cluster and a proton. The proton required to support substitution at the *para*-position C4 may be provided by a network of water molecules and ionizable side chains, including Tyr102 and Tyr382 in the upper cavity (Fig. 6b). A proton for neutralization at the *ortho*-positions C2 and C6 can be provided by Tyr246, pointing with its hydroxyl group towards the substrate at a distance of 4.3 Å from the bromine substituents or alternatively from solvent molecules in the substrate channel (Fig. 6c). In NpRdhA, mutation of the highly conserved Tyr246 equivalent inactivated the enzyme[8], which highlights its essential role. The leaving halide may move from C4 into the upper cavity and from C6 into the solvent channel. Movement of a bromide ion from C2 or C6 towards the cobalt or from C2 away from the substrate would require a concerted dissociation of the substrate from its position.

NpRdhA–substrate complex models using automatic docking or molecular dynamics simulations placed the substrate in orientations with either the bromine substituent *ortho* to the hydroxyl group above the cobalt or out of the axial position with the hydrogen in *meta*-position closest to the cobalt[8,34]. For the enzyme–substrate complex of NpRdhA with 3,5-dibromo-4-hydroxybenzoate, a direct interaction between substrate-bound bromine and cobalt was observed by EPR[8]. The 3,5-dibromo-4-hydroxybenzoate might be located closer to the cobalt in NpRdhA than 2,4,6-TBP in PceA, allowing a cobalt–halogen interaction in this enzyme. Recently, different mechanisms for the enzymatic reductive dehalogenation of chloroanilines were proposed for different organohalide-respiring bacteria[35]. Based on the variations in the range of products formed during substrate conversion combined with quantum chemical calculations, an initial attack on a halogen substituent or alternatively on a carbon-attached hydrogen atom was discussed. Hence, the mode of electron transfer from the cobalt to the substrate may vary between different RDases or even within one enzyme depending on the substrate. We show that in PceA phenolic substrates are excluded from direct interaction with [Co^{II}] and most likely [Co^{I}] by a tight packing of aromatic side chains that places the substrate at an angle of

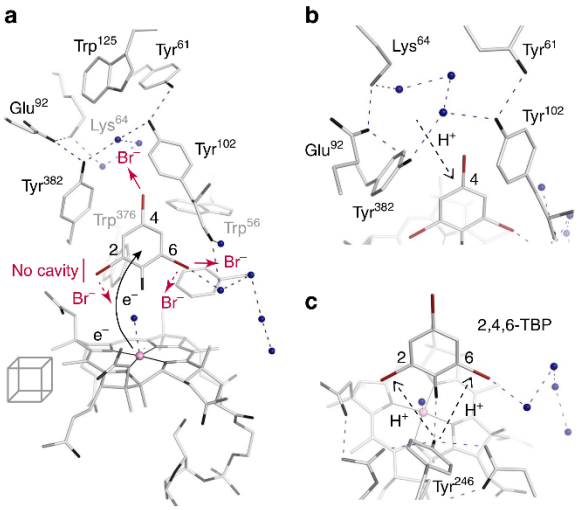

Figure 6 | Potential electron and proton movements during halide ion release. (**a**) Position of proximal iron–sulfur cluster, cobalt and 2,4,6-TBP substrate constrained by protein side chains. Within the constraints of the binding pocket, a leaving C2 substituent is not free to diffuse away from the substrate, a C4 halide may move to the upper cavity and a C6 halide may move to the substrate channel. It is not clear if the Co-water/hydroxyl ligand can be exchanged for a C2 or C6 halide with the substrate bound after reduction of PceA. (**b**) Exchangeable protons near C4 are present in the upper pocket in a network of ionizable side chains and water molecules. (**c**) Tyr246 may act as proton donor for C2 or C6. The view shows residues in front of panel **a**.

40° against the surface normal vector of the corrin ring, where it is kept at a distance of 4.7 Å from the cobalt. So far, only selected organohalides such as propyl iodide seem to overcome the structural barrier above the cobamide cofactor at the active site of PceA and directly interact with the cobalt. However, propyl iodide inhibited PceA function and slowed down substrate conversion as it has been shown for 4-BP or PCE[36]. Adduct formation in PceA was very recently proposed by Johannissen *et al.*[37], who reported on the probability of cobalt–halogen interaction between [Co^{I}] and TCE based on density functional theory calculations. The instability of PceA crystals harbouring [Co^{I}] and the substrate did not allow for approving this assumption for BPs and halogenated ethenes in the study presented here. However, the finding that none of the halogenated compounds showed a direct interaction between cobalt and substrate in EPR analyses rather points towards an alternative mechanism. This is furthermore supported by earlier reports about the formation of substrate radicals during the conversion of chlorinated propenes[4,16]. In addition, the appearance of [Co^{II}] after incubation of super-reduced PceA with *cis*-1,2-DCE suggests that a single electron is transferred, although no vinyl chloride is formed.

The PceA structure does not seem to reduce the energetic barrier of *cis*-1,2-DCE dechlorination sufficiently. However, other TCE RDases have been described that convert *cis*-1,2-DCE further to vinyl chloride and ethene[38]. The molecular basis for these differences needs further investigation. Overall, PceA displays an unforeseen way of utilizing a cobamide cofactor for enzymatic reductive dehalogenation, which clearly differs from classical cobamide-dependent biochemistry. In order to evaluate the distribution and utilization of the three possible modes of initializing cobamide-mediated enzymatic reductive dehalogenation, more information from RDase structural and spectroscopic analyses is required.

Methods

Cultivation of bacteria. *S. multivorans* (DSMZ 12446) and its mutant strain GD21 were cultivated anaerobically at 28 °C in a defined mineral medium[39] in the absence of exogenous cobamide and yeast extract (for generation of the mutant strain, see below). Pyruvate (40 mM) was used as an electron donor and PCE (10 mM nominal concentration) as an electron acceptor. PCE was added from a sterile and anoxic 0.5 M stock solution in hexadecane. The iron concentration in the medium was adjusted to 720 µM using an autoclaved and anoxic 144 mM $FeSO_4$ solution prepared in 50 mM H_2SO_4. For each experiment, two consecutive cultivations were performed, whereby the second culture served as inoculum (10%) for the main culture. Cells were harvested at an optical density of 0.26–0.28 (578 nm) by centrifugation (12,000*g*, 10 min, 10 °C) under aerobic conditions. The cell pellets were stored at − 20 °C.

Purification of PceA-Strep. The recombinant PceA–Strep was purified via affinity chromatography using Strep-Tactin Superflow column material (IBA, Göttingen, Germany). Since the membrane attachment of the enzyme is rather loose and PceA is sheared off during cell breakage, the enzyme was purified from the soluble and the membrane fraction. All steps were performed in an anaerobic glove box (CoyLab, Grass Lake, MI, USA). The cells of *S. multivorans* GD21 were resuspended in anoxic buffer A (100 mM Tris/HCl pH 8.0) (2 ml per 1 g wet cells) amended with protease inhibitor (cOmplete Mini EDTA-free Protease Inhibitor Cocktail; Roche Diagnostics, Mannheim, Germany). The cell lysate obtained after cell disruption in a French Press at 1,000 Psi (French Pressure Cell Press; Thermo Fisher Scientific, Germany) was subjected to ultracentrifugation (100,000*g*, 45 min, 4 °C; L8-M Ultracentrifuge, Rotor Ti70; Beckman Coulter, Krefeld, Germany). The supernatant, henceforth referred to as soluble extract, was transferred to a Strep-Tactin column (1 ml bed volume; IBA). PceA–Strep was eluted from the column using buffer A amended with 2.5 mM desthiobiotin (IBA). Tris(2-carboxyethyl)phosphine (TCEP) (Alfa Aesar, Karlsruhe, Germany) (5 mM) was added to protein samples applied to crystallization. Protein samples used for EPR spectroscopy contained 10% glycerol. PceA–Strep was concentrated via ultrafiltration in a Vivaspin 6 (30 K) centrifugal concentrator (Sartorius, Göttingen, Germany). The membrane pellet obtained from the ultracentrifugation (see above) was resuspended in buffer A (2 ml per 1 g pellet) and stirred overnight at 4 °C. Subsequently, the sample was again subjected to ultracentrifugation. The supernatant, henceforth referred to as membrane extract, was transferred to a Strep-Tactin column and PceA–Strep was purified and concentrated following the protocol described above. For crystallization, prePceA–Strep (bearing the twin-arginine translocation (Tat) signal peptide) and mature PceA–Strep (without the signal peptide) was separated using a Mono Q column (1 by 10 cm). The elution fractions were pooled and diluted 1:7 in basal buffer (50 mM Tris/HCl pH 7.5, 0.5 mM DTT amended with 5 mM TCEP) before application on the pre-equilibrated column. The mature enzyme eluted at 0.17 M NaCl in a stepwise gradient from 0 to 0.25 M in 5 column volumes (CV) and from 0.25 to 0.5 M NaCl in 2 CV. The elution buffer was replaced by the storage buffer (30 mM Tris-HCl, pH 7.5, 5 mM TCEP) by repeated concentration and resuspension of PceA. Structural analysis of PceA in complex with 3-BP was conducted with enzyme containing methoxybenzimidazolyl-norcobamide rather than norpseudo-B_{12} as cofactor. Pure PceA enzyme was stored at − 80 °C. In total, 4 mg of purified PceA–Strep were obtained from 3 g cell protein. The protein concentrations were measured with the Bradford assay[40] using the Roti-Nanoquant reagent (Roth, Karlsruhe, Germany). For the separation of proteins, SDS–polyacrylamide gel electrophoresis (12.5%) was applied. The immunological analysis was conducted in accordance with John *et al.*[41]. The Strep-tag antibody solution (IBA) was diluted 3,000-fold and the antibodies were detected via a secondary antibody coupled to alkaline phosphatase (Sigma-Aldrich, Munich, Germany). A representative SDS–polyacrylamide gel electrophoresis with all purification fractions is shown in Supplementary Fig. 6. Further details about determination of the cofactor contents are given in Supplementary Table 2.

Enzyme activity measurement. All substrates used in this study were purchased from Sigma-Aldrich GmbH and abcr GmbH (Karlsruhe, Germany) in the highest purity available. Activity measurements of the PceA enzyme were conducted in HPLC vials (volume 1.5 ml) sealed with butyl rubber stoppers and flushed with nitrogen. The assay was performed in 100 mM Tris-HCl pH 7.5 at 22 °C. The artificial electron donor methyl viologen (0.5 mM) was reduced by adding 1.4 mM Ti(III) citrate. Pure PceA–Strep was present in concentrations of 3–36 nM for activity measurements with PCE and brominated phenols and 300–450 nM for chlorinated phenols. The organohalides were added from stock solutions in ethanol (80–100 mM) to get a final concentration of 0.5 mM in the assay mixture. After an incubation time of 1 min the reaction was stopped by rapid cooling of the reaction vessel to − 20 °C. To test for the influence of ammonium ions on the dehalogenating activity, 4 mM $(NH_4)_2SO_4$ were added. K_m values were determined by fitting enzyme kinetic data to Michaelis-Menten kinetics. Activity assays with PceA crystals were performed in crystallization solution (100 mM Tris-HCl, pH 7.5, 200 mM sodium malonate, 2% (w/v) benzamidine, 25% (w/v) PEG 3350, 20% glycerol) amended with 0.5 mM methyl viologen and 1.4 mM Ti(III) citrate. Crystal fragments of a 1 mg ml^{-1} PceA stock were added to the buffer. All enzyme activity measurements were performed in at least two biological replicates. Chlorinated ethenes were detected with a flame ionization detector coupled to a Clarus 500 Gas

NATURE COMMUNICATIONS | DOI: 10.1038/ncomms15858 ARTICLE

Chromatograph (Perkin Elmer, Rodgau, Germany), which was equipped with a CP-PoraBOND Q FUSED SILICA 25 m × 0.32 mm column (Agilent Technologies, Böblingen, Germany). A headspace sample was taken from a 1 ml assay mixture incubated at 95 °C for 6 min. The chlorinated ethenes were separated under constant nitrogen flow in a temperature gradient from 4 min at 150 °C to 280 °C in 10 °C min^{-1} steps (detector at 300 °C). Nonane was used as an internal standard. Retention times were as follows: PCE 9.8 min; TCE 6.9 min; *cis*-1,2-DCE 4.3 min. Halogenated phenols were separated using a reversed-phase HPLC system (Merck-Hitachi, Darmstadt, Germany) equipped with an RP8 column (LiChrosphere 100, ID 4.6 × 100 nm, Merck, Darmstadt, Germany) and an ultraviolet/visible detector (210 nm). Also, 50% (v/v) methanol/0.3% (v/v) H_3PO_4 was used as a mobile phase with a flow rate of 0.4 ml min^{-1}. Retention times were as follows: 2,4,6-TBP 73.8 min; 2,4-DPB 34.9 min; 2,6-DPB 21.3 min; 2,5-DPB 31.8 min; 3,5-DPB 56.6 min; 2-BP 11.8 min; 3-BP 15.9 min; 4-BP 15.3 min; 4-IP 17.7 min; phenol 6.5 min; 2,3-DCP 22.2 min; 2,5-DCP 24 min; 3-CP 13.2 min; nd 4-CP 12.7 min. Non-enzymatic conversion of the substrates was tested with heat-inactivated PceA–Strep, which was incubated anoxically for 10 min at 95 °C before addition to the activity assay. The final concentration of heat-inactivated PceA–Strep was 526 nM, and the reaction mixture was incubated for 20 min. The inhibition of PceA–Strep (47 nM) converting 4-BP was tested by adding 100 µM propyl iodide before incubation of the assay mixture in the dark for 2 min.

Crystallization and structure determination. Crystallization, ligand incubation and flash cooling of crystals were performed under anoxic conditions in a glove box (model B; CoyLab) under an atmosphere of 95% N_2/5% H_2 and < 10 p.p.m. oxygen. Crystals were grown by the sitting drop vapour diffusion method at room temperature. In all, 1 µl of 12 mg ml^{-1} PceA in 30 mM Tris-HCl, pH 7.5, and 5 mM TCEP was mixed with 1 µl of crystallization solution containing 12–17% (w/v) PEG 3350 and 0.2 M sodium malonate, 2% benzamidine-HCl and 50 mM Tris-HCl, pH 7.5. Crystals were flash cooled in liquid nitrogen after protection in the crystallization solution supplemented with 20% (v/v) glycerol and 25% (final w/v) PEG 3350 (substrates 3-CP, 2,4-DBP, 2,6-DCP and 2,4,6-TCP). For all other substrates, a chloride-free cryo-incubation buffer was prepared from 50 mM Tris (free base), 2% benzamidine (free base), adjusted to pH 8 with malonic acid, followed by the addition of 25% PEG 3350 and 20% glycerol. Ten-fold concentrated substrate stock solutions were prepared in cryo-buffer at saturating concentrations and crystals were incubated with cryo-protectant/substrate-incubation buffer for 30–120 min. 4-BP and 2,4-DBP crystals were first reduced with 2 mM Ti(III)citrate and 0.2 mM methyl viologen. Once plunged into liquid N_2, crystals were removed from the anoxic atmosphere and from thereon stored and handled under liquid N_2.

Diffraction data were collected at 100 K on BL14.1 operated by the Helmholtz-Zentrum Berlin (HZB, Germany) at the BESSY II electron storage ring (Berlin-Adlershof, Germany)[42] at 1.9 Å X-ray wavelength for 3-CP, 4-CP, 2,6-DCP, 2,4,6-TCP and 2,4,5-TCP and at 0.91841 Å for all other substrates. Data were indexed and integrated with the XDS package[43] and XDSAPP[44]. Restraints for substrate ligands were prepared using eLBOW[45] (2,6-DCP, 2,4-DBP) and the Grade Server v1.001 (Global Phasing Ltd., Cambridge, UK). Models were fitted in COOT[46], refined with phenix.refine[47] and validated with Molprobity[48]. Nearly all of the residues (98%) were in the favoured region of the Ramachandran plot and no outliers were detected. Data collection and refinement statistics are summarized in Supplementary Table 3.

Electron paramagnetic resonance spectroscopy. EPR spectra were recorded on a Bruker ECS-106 X-band spectrometer equipped with home-built helium-cryogenics. Low-spin [Co^{II}] was typically detected at a temperature of circa 22–31 K and $[4Fe\text{–}4S]^{1+}$ clusters at circa 17 K. For substrate–cobalt interaction measurements, the enzyme (approximately 56 µM) was reduced by the addition of 1 mM Ti(III) citrate in combination with 20 µM methyl viologen as electron mediator. The substrates were added in a final concentration of 5 mM from stock solutions in ethanol. The maximal water solubility for 2,4,6-TBP, PCE and TBE is < 1 mM, thus the EPR samples were oversaturated with substrate. All additions of substrates and/or reductant/oxidant were done anaerobically. Samples taken directly from the liquid nitrogen storage were prepared for additions by connecting the EPR tube to a vacuum/argon manifold with subsequent 10 vacuum/argon cycles until the onset of thawing and with all subsequent handlings under Argon 5.0 (0.2 bar overpressure). Additions of substrates and the reductant Ti(III) citrate were performed with Hamilton syringes from anaerobic solutions through the rubber connecting the EPR tube with the manifold. For the determination of the oxidation states of the cofactors of PceA (see Supplementary Fig. 7), EPR absorption spectra were recorded using PceA or PceA–Strep as isolated. The sample preparation was performed in an anaerobic chamber. For this purpose, 200 µl of the purified enzyme, stored in Tris-HCl buffer (50 mM Tris-HCl (pH 7.5), 10% (v/v) glycerol) were transferred to an EPR tube and frozen in liquid nitrogen. In parallel, the species of the iron–sulfur clusters was determined in 200 µl samples of purified enzyme reduced by the addition of 10 mM sodium dithionite. Sodium dithionite was added as 200 mM solutions in anoxic Tris-HCl buffer (50 mM Tris-HCl (pH 7.5), 10% glycerol). For oxidation of the sample, 0.5 mM $K_3[Fe(CN)_6]$ was added to the 200 µl sample. After incubation for 5 min, the samples were frozen in liquid nitrogen and stored at − 80 °C until measurement. EPR spectra were recorded with modulation amplitude of 8 Gauss and a modulation frequency of 100 kHz. Spin quantification was done versus an external copper standard (10 mM $CuSO_4$, 10 mM HCl, 2 M $NaClO_4$) as described previously[49].

Plasmid construction. All enzymes used for DNA modification in this study were purchased from Fermentas (St Leon-Rot, Germany) or New England Biolabs (Ipswich MA, USA). All plasmids used in this study are summarized in Supplementary Table 4. The cloning steps were conducted according to standard techniques described in Sambrook *et al.*[50] using the *Escherichia coli* strain Dh5α. The plasmid pY179 (ref. 51) was used as the starting material. This plasmid is a derivative of pBluescript II SK + (Stratagene, La Jolla CA, US). Plasmids were extracted using the GeneJET Plasmid Miniprep Kit (Thermo Scientific, Darmstadt, Germany). The plasmid pY179 contains a 6-kb *Eco*RI DNA-fragment derived from *S. multivorans* genomic DNA. The DNA-fragment encloses the *pceAB* gene cluster. In order to reduce the size of the subcloned DNA fragment (3.2 kb) to almost only the *pceAB* gene cluster, the plasmid pY179 was cut with the restriction enzymes *Xho*I and *Bgl*II, treated with Klenow fragment and re-ligated. The resulting construct of this initial modification, plasmid pTOS024, was provided as template in an inverse PCR reaction conducted with the following primer pair T68/T69: 5′-TATGGCTAGCCATCACCATCACCATCACTCATGAAATTATTAAATATTT-TAAATTATAAAGCG-3′ and 5′-ATCGGCTAGCTGATTTTTTAACCCTA-TCCTTTC-3′. Using this method, a DNA sequence encoding a 6 × His-tag was fused to the 3′-end of the DNA sequence encoding the *pceA* gene. As a result of the inverse PCR reaction, a *Nhe*I-restriction site was generated at both ends of the PCR product. After the restriction with *Nhe*I, the PCR fragment was circularized and plasmid pTOS036 was formed. Subsequently, the DNA sequence encoding the 6 × His-tag was replaced by a DNA sequence encoding a Strep-tag II. For this purpose, a 250-bp PCR fragment was generated using plasmid pY179 as template and the oligonucleotides T110/AN38: 5′-TATGGCTAGCTGGAGCCAC-CCGCAGTTCGAAAAATCATGAAATTATTAAATATTTTAAATTA-TAAAGCG-3′ and 5′-GCGATCTAGCTCAAAAGAGAG-3′. The PCR fragment was cut with *Nhe*I and *Afl*II and ligated into the similarly cut pTOS036 yielding plasmid pTOS071.

For the transformation of *S. multivorans*, the plasmid pBR322 (ref. 52) was used as carrier. In order to generate a homologous DNA sequence within this plasmid, which would allow for recombination into the *pceAB* gene cluster in the *S. multivorans* genome, a 3.2-kb DNA-fragment was cut from plasmid pY179 with *Bgl*II and *Bam*HI and ligated into pBR322 cut with *Bam*HI, yielding plasmid pTOS001. The subcloned DNA fragment contained the complete *pceAB* gene cluster with the upstream and downstream intergenic regions, including the promoter and terminator sequences of *pceAB*. As a selective marker for proving successful homologous recombination, the kanamycin-resistance cassette from plasmid pUC4K[53] was used. For this purpose, plasmid pUC4K was cut with *Bam*HI. The resulting 1.3-kb DNA fragment was treated with Klenow fragment and ligated into plasmid pTOS001 cut with *Bst*XI and treated with Klenow fragment. In the resulting plasmid pTOS012, the kan^R cassette was located in the intergenic region downstream of the *pceAB* gene cluster and orientated against the *pceAB* genes. In order to transfer the modified DNA-sequence encoding the C-terminal Strep-tagged PceA from plasmid pTOS071 into plasmid pTOS012, pTOS071 was cut with *Pml*I and *Afl*II and the resulting 620-bp DNA fragment ligated into the similarly cut pTOS012. Finally, plasmid pTOS077 was generated.

Transformation of *S. multivorans*. The protocol for transformation of *S. multivorans* was adapted from the procedure described by Simon *et al.*[54] for the transformation of *W. succinogenes*. Cells of *S. multivorans* were cultivated in anoxic medium containing 40 mM pyruvate as an electron donor and 40 mM fumarate as an electron acceptor. The cells were harvested in the exponential growth phase and washed twice with a sucrose (0.5 M)/glycerol (10% v/v) solution; finally the cells were resuspended in this solution (approximately 10 g protein l^{-1}). The electroporation of the cells and all subsequent steps were conducted in an anaerobic chamber (CoyLab). An aliquot of *S. multivorans* cells (40 µl) was mixed with plasmid DNA (approximately 1 µg) and transferred into an electroporation cuvette (0.2 cm pathlength; Bio-Rad, Hercules, CA, USA). The plasmid DNA was purified by precipitation with ammonium acetate[55]. The electroporation was performed in a Gene Pulser XCell (Bio-Rad, Hercules, CA, USA) under the following conditions: 25 µF, 2.5 kV, 200 Ω. Immediately after application of the pulse, 1 ml anoxic pyruvate/fumarate-containing medium was added to the cell suspension. After an incubation period of at least 1 h at 28 °C, the cells were transferred to solid medium. The solid medium contained all the ingredients of the liquid medium described above plus 1% (w/v) washed agar (AppliChem, Darmstadt, Germany) and 0.2% yeast extract. It was amended with 100 µg ml^{-1} kanamycin. The plated cells were incubated for 1–2 weeks at 28 °C. Using plasmid pTOS077 for the electroporation, the mutant strain *S. multivorans* GD21 (PceA–Strep) was generated (Supplementary Fig. 8). The transformation efficiency was very low (a single transformant per 10 µg plasmid). The application of linear DNA in the transformation procedure did not have a positive effect on the transformation efficiency.

Southern hybridization. Genomic DNA of *S. multivorans* was isolated by phenol–chloroform isoamylalcohol extraction[56]. The DNA (30 µg) was cut with *Eco*RI, *Eco*RV and *Xmn*I. After inactivation of the restriction enzymes (65 °C, 20 min), the fragmented genomic DNA was loaded onto a 0.8% agarose gel prepared with 0.5-fold Tris-borate-EDTA buffer (44.5 mM Tris, 44.5 mM boric acid, 1 mM EDTA). For subsequent evaluation of the gel, a Digoxigenin-labelled DNA molecular weight marker (Roche Diagnostics) was applied. The gel was run for 3 h at 90 V. The separated DNA fragments were blotted onto a nylon membrane (Boehringer, Mannheim, Germany) using a semi-dry blot device (Bio-Rad Laboratories, Munich, Germany). The current applied was 3 mA cm^{-2} for 1 h. Subsequently, the membrane was washed for 5 min in twofold saline–sodium citrate (SSC) buffer (30 mM Na–citrate pH 7.0, 0.3 M NaCl). The membrane was transferred into the denaturing solution (0.4 M NaOH, 10 mM EDTA, 1.5 M NaCl). After 10 min incubation at room temperature, the membrane was rinsed with 2 × SSC and dried. The DNA fragments were crosslinked with the membrane by ultraviolet-light exposure. The membrane was incubated for 2 h at 60 °C in hybridization solution (5 × SSC containing 0.1% lauroylsarcosine and 0.02% SDS). The *pceA* and the *kan* DNA probes were diluted 1,000-fold in hybridization solution before their application to the membrane. The DNA probes were generated as follows: The primers 5′-AACCTTGGTTTTTATCAGCATATG-3′ and 5′-GGTCTTCTATCTAACCCTACTG-3′ were used to amplify the DNA fragment for the *pceA* probe and the oligonucleotides 5′-TGAGCCATATTC-AACGGG-3′ and 5′-GAATGCTGTTTTCCCGGG-3′ for synthesis of the *kan* probe via PCR. The DNA probes were labelled with Digoxigenin using the DIG DNA Labelling Kit (Roche, Mannheim, Germany) according to the manufacturer's instructions. The hybridization of the blotted DNA fragments with the DNA probes was conducted in a hybridization oven (HB-1,000 Hybridizer, UVP-Laboratory Products, Cambridge, UK) overnight at 65 °C. Subsequently, the membrane was washed twice for 5 min at room temperature (RT) in 2 × SSC, 0.1% SDS, followed by two washing steps for 15 min at RT and 42 °C, respectively, in 0.5 × SSC, 0.1% SDS. After incubation for 1 h in 1% blocking reagent (Roche Diagnostics), the membrane was washed three times for 10 min in MST-buffer (0.1 M maleic acid pH 7.5, 150 mM NaCl, 0.05% Tween 20). Subsequently, the membrane was incubated for 2 h in MST-buffer containing Anti-Digoxigenin-Alkaline Phosphatase, Fab-Fragments (Roche Diagnostics) that were diluted 5,000-fold. The membrane was washed twice with MST-buffer for 10 min. After a washing step in the developing buffer (0.1 M Tris/HCl pH 9.5, 0.1 M NaCl, 50 mM $MgCl_2$), the blot was stained in developing buffer containing 0.34 mg nitroblue tetrazolium and 0.175 mg 5-bromo-4-chloro-3-indolyl phosphate (Roth) per ml solution.

Data availability. Model coordinates and structure factors for ligand-bound PceA have been submitted to the protein data bank (PDB) under accessions numbers 5M2G (2,4,6-TBP), 5M8U (4-BP), 5M8W (4-CP), 5M8X (2,4,5-TCP), 5M8Y (3-CP), 5M8Z (2,3-DFP), 5M90 (3,4,5-TFP), 5M91 (2,6-DBP), 5M92 (2,4-DBP), 5MA2 (4-IP), 5MAA (3-BP), 5MA0 (2,6-DCP) and 5MA1 (2,4,6-TCP).

References

1. Holliger, C., Wohlfarth, G. & Diekert, G. Reductive dechlorination in the energy metabolism of anaerobic bacteria. *FEMS Microbiol. Rev.* **22,** 383–398 (1998).
2. Hug, L. A. *et al.* Overview of organohalide-respiring bacteria and a proposal for a classification system for reductive dehalogenases. *Philos. Trans. R. Soc. B* **368,** 20120322 (2013).
3. Neumann, A., Wohlfarth, G. & Diekert, G. Purification and characterization of tetrachloroethene reductive dehalogenase from *Dehalospirillum multivorans*. *J. Biol. Chem.* **271,** 16515–16519 (1996).
4. Neumann, A. *et al.* Tetrachloroethene reductive dehalogenase of *Dehalospirillum multivorans*: substrate specificity of the native enzyme and its corrinoid cofactor. *Arch. Microbiol.* **177,** 420–426 (2002).
5. Ye, L., Schilhabel, A., Bartram, S., Boland, W. & Diekert, G. Reductive dehalogenation of brominated ethenes by *Sulfurospirillum multivorans* and *Desulfitobacterium hafniense* PCE-S. *Environ. Microbiol.* **12,** 501–509 (2010).
6. Kräutler, B. *et al.* The cofactor of tetrachloroethene reductive dehalogenase of *Dehalospirillum multivorans* is norpseudo-B_{12}, a new type of a natural corrinoid. *Helv. Chim. Acta* **86,** 3698–3716 (2003).
7. Bommer, M. *et al.* Structural basis for organohalide respiration. *Science* **346,** 455–458 (2014).
8. Payne, K. A. P. *et al.* Reductive dehalogenase structure suggests a mechanism for B_{12}-dependent dehalogenation. *Nature* **517,** 513–516 (2015).
9. Banerjee, R. & Ragsdale, S. W. The many faces of vitamin B_{12}: catalysis by cobalamin-dependent enzymes. *Annu. Rev. Biochem.* **72,** 209–247 (2003).
10. Gruber, K., Puffer, B. & Kräutler, B. Vitamin B_{12}-derivatives enzyme cofactors and ligands of proteins and nucleic acids. *Chem. Soc. Rev.* **40,** 4346–4363 (2011).
11. Bridwell-Rabb, J. & Drennan, C. L. Vitamin B_{12} in the spotlight again. *Curr. Opin. Chem. Biol.* **37,** 63–70 (2017).
12. Miles, Z. D., McCarty, R. M., Molnar, G. & Bandarian, V. Discovery of epoxyqueuosine (oQ) reductase reveals parallels between halorespiration and tRNA modification. *Proc. Natl Acad. Sci. USA* **108,** 7368–7372 (2011).
13. Benjdia, A. *et al.* The thiostrepton A tryptophan methyltransferase TsrM catalyses a cob(II)alamin-dependent methyl transfer reaction. *Nat. Commun.* **6,** 8377 (2015).
14. Bridwell-Rabb, J., Zhong, A., Sun, H. G., Drennan, C. L. & Liu, H. W. A B_{12}-dependent radical SAM enzyme involved in oxetanocin A biosynthesis. *Nature* **544,** 322–326 (2017).
15. Schrauzer, G. N. & Deutsch, E. Reactions of cobalt(I) supernucleophiles. The alkylation of vitamin B_{12}s, cobaloximes(I), and related compounds. *J. Am. Chem. Soc.* **91,** 3341–3350 (1969).
16. Schmitz, R. P. H. *et al.* Evidence for a radical mechanism of the dechlorination of chlorinated propenes mediated by the tetrachloroethene reductive dehalogenase of *Sulfurospirillum multivorans*. *Environ. Sci. Technol.* **41,** 7370–7375 (2007).
17. Dolfing, J. & Novak, I. The Gibbs free energy of formation of halogenated benzenes, benzoates and phenols and their potential role as electron acceptors in anaerobic environments. *Biodegradation* **26,** 15–27 (2015).
18. Thibodeau, J. *et al.* Purification, cloning, and sequencing of a 3,5-dichlorophenol reductive dehalogenase from *Desulfitobacterium frappieri* PCP-1. *Appl. Environ. Microbiol.* **70,** 4532–4537 (2004).
19. van de Pas, B. A. *et al.* Purification and molecular characterization of ortho-chlorophenol reductive dehalogenase, a key enzyme of halorespiration in *Desulfitobacterium dehalogenans*. *J. Biol. Chem.* **274,** 20287–20292 (1999).
20. Mac Nelly, A., Kai, M., Svatos, A., Diekert, G. & Schubert, T. Functional heterologous production of reductive dehalogenases from *Desulfitobacterium hafniense* strains. *Appl. Environ. Microbiol.* **80,** 4313–4322 (2014).
21. van de Pas, B. A., Gerritse, J., de Vos, W. M., Schraa, G. & Stams, A. J. M. Two distinct enzyme systems are responsible for tetrachloroethene and chlorophenol reductive dehalogenation in *Desulfitobacterium* strain PCE1. *Arch. Microbiol.* **176,** 165–169 (2001).
22. Krasotkina, J., Walters, T., Maruya, K. A. & Ragsdale, S. W. Characterization of the B_{12}- and iron-sulfur-containing reductive dehalogenase from *Desulfitobacterium chlororespirans*. *J. Biol. Chem.* **276,** 40991–40997 (2001).
23. Cooper, M. *et al.* Anaerobic microbial transformation of halogenated aromatics and fate prediction using electron density modeling. *Environ. Sci. Technol.* **49,** 6018–6028 (2015).
24. Liao, R.-Z., Chen, S.-L. & Siegbahn, P. E. M. Which oxidation state initiates dehalogenation in the B_{12}-dependent enzyme NpRdhA, Co^{I}, Co^{II} or Co^{0}? *ACS Catal* **5,** 7350–7358 (2015).
25. Miller, E., Wohlfarth, G. & Diekert, G. Studies on tetrachloroethene respiration in *Dehalospirillum multivorans*. *Arch. Microbiol.* **166,** 379–387 (1997).
26. Weissbach, H., Redfield, B. G., Dickerman, H. & Brot, N. Studies on methionine biosynthesis: effect of alkylcobamide derivatives on the formation of holoenzyme. *J. Biol. Chem.* **240,** 856–862 (1965).
27. Brot, N. & Weissbach, H. Enzymatic synthesis of methionine: chemical alkylation of the enzyme-bound cobamide. *J. Biol. Chem.* **240,** 3064–3070 (1965).
28. Liao, R.-Z., Chen, S.-L. & Siegbahn, P. E. M. Unraveling the mechanism and regioselectivity of the B_{12}-dependent reductive dehalogenase PceA. *Chem. Eur. J.* **22,** 12391–12399 (2016).
29. Zeldin, O. B., Gerstel, M. & Garman, E. F. *RADDOSE-3D*: time- and space-resolved modelling of dose in macromolecular crystallography. *J. Appl. Crystallogr.* **46,** 1225–1230 (2013).
30. Holton, J. M. A beginner's guide to radiation damage. *J. Synchrotron Radiat.* **16,** 133–142 (2009).
31. Schlichting, I. *et al.* The catalytic pathway of cytochrome P450cam at atomic resolution. *Science* **287,** 1615–1622 (2000).
32. Berglund, G. I. *et al.* The catalytic pathway of horseradish peroxidase at high resolution. *Nature* **417,** 463–468 (2002).
33. Champloy, F., Gruber, K., Jogl, G. & Kratky, C. XAS spectroscopy reveals X-ray-induced photoreduction of free and protein-bound B_{12} cofactors. *J. Synchrotron Radiat.* **7,** 267–273 (2000).
34. Pietra, F. Uptake of organohalide pollutants, and release of partially dehalogenated products, by NpRdhA, a 'base-off' cob(II)alamin-dependent reductive dehalogenase from a deep sea bacterium. A molecular dynamics investigation. *Chem. Biodivers.* **12,** 1945–1953 (2015).
35. Zhang, S. *et al.* Anaerobic dehalogenation of chloroanilines by *Dehalococcoides mccartyi* strain CBDB1 and *Dehalobacter* strain 14DCB1 via different pathways as related to molecular electronic structure. *Environ. Sci. Technol.* **51,** 3714–3724 (2017).
36. Neumann, A., Wohlfahrt, G. & Diekert, G. Properties of tetrachloroethene and trichloroethene dehalogenase of *Dehalospirillum multivorans*. *Arch. Microbiol.* **163,** 276–281 (1995).
37. Johannissen, L. O., Leys, D. & Hay, S. A common mechanism for coenzyme cobalamin-dependent reductive dehalogenases. *Phys. Chem. Chem. Phys.* **19,** 6090–6094 (2017).

38. Magnuson, J. K., Romine, M. F., Burris, D. R. & Kingsley, M. T. Trichloroethene reductive dehalogenase from *Dehalococcoides ethenogenes*: sequence of *tceA* and substrate range characterization. *Appl. Environ. Microbiol.* **66,** 5141–5147 (2000).
39. Scholz-Muramatsu, H., Neumann, A., Messmer, M., Moore, E. & Diekert, G. Isolation and characterization of *Dehalospirillum multivorans* gen. nov., sp. nov., a tetrachloroethene-utilizing, strictly anaerobic bacterium. *Arch. Microbiol.* **163,** 48–56 (1995).
40. Bradford, M. M. A rapid and sensitive method for the quantification of microgram quantities of protein utilizing the principle of protein-dye binding. *Anal. Biochem.* **72,** 248–254 (1976).
41. John, M. *et al.* Retentive memory of bacteria: Long-term regulation of dehalorespiration in *Sulfurospirillum multivorans*. *J. Bacteriol.* **191,** 1650–1655 (2009).
42. Mueller, U. *et al.* Facilities for macromolecular crystallography at the Helmholtz-Zentrum Berlin. *J. Synchrotron Radiat.* **19,** 442–449 (2012).
43. Kabsch, W. XDS. *Acta Crystallogr. D Biol. Crystallogr.* **66,** 125–132 (2010).
44. Krug, M., Weiss, M. S., Heinemann, U. & Mueller, U. *XDSAPP*: a graphical user interface for the convenient processing of diffraction data using *XDS*. *J. Appl. Cryst.* **45,** 568–572 (2012).
45. Moriarty, N. W., Grosse-Kunstleve, R. W. & Adams, P. D. *electronic Ligand Builder and Optimization Workbench* (*eLBOW*): a tool for ligand coordinate and restraint generation. *Acta Crystallogr. D Biol. Crystallogr.* **65,** 1074–1080 (2009).
46. Emsley, P., Lohkamp, B., Scott, W. G. & Cowtan, K. Features and development of Coot. *Acta Crystallogr. D. Biol. Crystallogr* **66,** 486–501 (2010).
47. Afonine, P. V. *et al.* Towards automated crystallographic structure refinement with phenix.refine. *Acta Crystallogr. D Biol. Crystallogr.* **68,** 352–367 (2012).
48. Chen, V. B. *et al.* MolProbity: all-atom structure validation for macromolecular crystallography. *Acta Crystallogr. D Biol. Crystallogr.* **66,** 12–21 (2010).
49. Hagen, W. R. EPR spectroscopy as a probe of metal centres in biological systems. *Dalton. Trans.* **37,** 4415–4434 (2006).
50. Sambrook, J., Fritsch, E. F. & Maniatis, T. *Molecular Cloning: A Laboratory Manual* 2nd edn (Cold Spring Harbor Laboratory Press, 1989).
51. Neumann, A., Wohlfarth, G. & Diekert, G. Tetrachloroethene dehalogenase from *Dehalospirillum multivorans*: cloning, sequencing of the encoding genes, and expression of the *pceA* gene in *Escherichia coli*. *J. Bacteriol.* **180,** 4140–4145 (1998).
52. Bolivar, F. *et al.* Construction and characterization of new cloning vehicles. II. A multipurpose cloning system. *Gene* **2,** 95–113 (1977).
53. Vieira, J. & Messing, J. The pUC plasmids, an M13mp7-derived system for insertion mutagenesis and sequencing with synthetic universal primers. *Gene* **19,** 259–268 (1982).
54. Simon, J., Gross, R., Ringel, M., Schmidt, E. & Kröger, A. Deletion and site-directed mutagenesis of the *Wolinella succinogenes* fumarate reductase operon. *Eur. J. Biochem.* **251,** 418–426 (1998).
55. Saporito-Irwin, S. M., Geist, R. T. & Gutmann, D. H. Ammonium acetate protocol for the preparation of plasmid DNA suitable for mammalian cell transfections. *Biotechniques* **23,** 424–427 (1997).
56. Bollet, C., Gevaudan, M. J., de Lamballerie, X., Zandotti, C. & de Micco, P. A simple method for the isolation of chromosomal DNA from gram positive or acid-fast bacteria. *Nucleic Acids Res.* **19,** 1955 (1991).

Acknowledgements
This work was financially supported by the DFG Research Unit FOR1530 (grant DI 314/14-2), the Jena School for Microbial Communication (JSMC) and the Ernst Abbe Foundation. Peggy Brand-Schön is acknowledged for excellent technical assistance. Martin Bommer was financed by the DFG Collaborative Research Centre SFB 1078. We acknowledge access to beamlines of the BESSY II storage ring (Berlin, Germany) via the Joint Berlin MX-Laboratory sponsored by the Helmholtz Zentrum Berlin für Materialien und Energie, the Freie Universität Berlin, the Humboldt-Universität zu Berlin, the Max-Delbrück-Centrum and the Leibniz-Institut für Molekulare Pharmakologie.

Author contributions
G.D. and T.S. conceived and coordinated the study. C.K. performed purification, biochemical characterization and activity assays with PceA. M.B. performed in-crystal substrate-binding experiments and built the ligand-bound structures. W.R.H. performed metal-cofactor analysis and substrate–cobalt interaction studies using EPR. T.S., C.K. and M.U. were involved in the generation and characterization of the *S. multivorans* mutant strain GD21. All authors participated in data analysis, discussion and writing of the manuscript.

Additional information
Supplementary Information accompanies this paper at http://www.nature.com/naturecommunications

Competing interests: The authors declare no competing financial interests.

Reprints and permission information is available online at http://npg.nature.com/reprintsandpermissions/

How to cite this article: Kunze, C. *et al.* Cobamide-mediated enzymatic reductive dehalogenation via long-range electron transfer. *Nat. Commun.* **8,** 15858 doi: 10.1038/ncomms15858 (2017).

Publisher's note: Springer Nature remains neutral with regard to jurisdictional claims in published maps and institutional affiliations.

2.4 Subtle changes in the active site architecture untangled overlapping substrate ranges and mechanistic differences of two reductive dehalogenases

Kunze C, Diekert G, Schubert T (2017) accepted in *FEBS J,* August 30, doi: 10.1111/febs.14258.

Next to RDases catalyzing halogen substitution reactions, a distinct group of putative 1,2-dichloroethane (DCA)-RDases (DcaA) were found that convert their substrates in a dihaloelimination reaction. Comparable *in silico* structural analysis and functional investigation of a tetrachloroethene-converting and a dichloroethane-converting representative unraveld an extensive influence of the active site's architecture on the functionality and substrate spectrum of the enzymes. The two types of reductive dehalogenation reactions have been clearly delineated from each other with regard to the involvement of proton transfer steps.

My own contribution to this publication covers about 90%.
I conducted all experiments. I have written the original manuscript and revised it including comments from all coauthors.

For supplementary information see appendix, pp. lvii - lxiv.

The FEBS Journal

FEBS PRESS science publishing by scientists

Subtle changes in the active site architecture untangled overlapping substrate ranges and mechanistic differences of two reductive dehalogenases

Cindy Kunze, Gabriele Diekert and Torsten Schubert

Department of Applied and Ecological Microbiology, Institute of Microbiology, Friedrich Schiller University, Jena, Germany

Keywords
cobamide cofactor; hydrogenolysis; proton transfer; reductive dehalogenation; vicinal reduction

Correspondence
T. Schubert and G. Diekert, Department of Applied and Ecological Microbiology, Institute of Microbiology, Friedrich Schiller University, Philosophenweg 12, D-07743 Jena, Germany
Fax: +49 3641 949302
Tel: +49 3641 949349
E-mails: torsten.schubert@uni-jena.de (TS); gabriele.diekert@uni-jena.de (GD)

(Received 21 June 2017, revised 20 August 2017, accepted 30 August 2017)

doi:10.1111/febs.14258

Reductive dehalogenases (RDases) of organohalide-respiring bacteria are cobamide-containing iron–sulfur proteins that catalyze different reductive dehalogenation reactions. Here, we report a functional analysis of two recombinant RDases, the tetrachloroethene (PCE) reductive dehalogenase (PceA) of *Desulfitobacterium hafniense* Y51 and the 1,2-dichloroethane (1,2-DCA) reductive dehalogenase (DcaA) of *Desulfitobacterium dichloroeliminans* DCA1. Both enzymes share 88% protein sequence identity, but appeared to have divergent mechanisms. In this study, the heterologously produced DcaA converted 1,2-DCA and 1,1,2-trichloroethane (1,1,2-TCA) via dihaloelimination to ethene and vinyl chloride, respectively. In addition, halogen substitution at PCE, trichloroethene (TCE) and tribromoethene (TBE) was observed, but only at low rates. In contrast, recombinant PceA exclusively converted halogenated ethenes and showed no dihaloelimination activity. *In silico* structural analysis of both RDases revealed similar architectures of their active site cavities. Exchange of the highly conserved Tyr298 to Phe led to a complete loss of the PCE, TCE and TBE conversion by both RDases, strengthening the assumption that Tyr298 functions as proton donor in the course of halogen substitution. The exchange did not affect the ability of DcaA to convert 1,2-DCA and 1,1,2-TCA. This result makes the involvement of a proton transfer in the dihaloelimination reaction unlikely and allows for a clear differentiation between two mechanisms working in DcaA and PceA. The analysis of the role of the active site structure for RDase function was extended to the mutations W118F that had a negative effect on DcaA function and W432F or T294V that caused alterations in the substrate specificity of the enzyme.

Enzymes
Tetrachloroethene reductive dehalogenase (EC 1.21.99.5), DCA -RDase.

Abbreviations
DBA, dibromoethane; DBE, dibromoethene; DcaA, DCA reductive dehalogenase; DCA, dichloroethane; DcaT, trigger-factor-like chaperone of DcaA; DCE, dichloroethene; DFA, difluoroethane; DMB, dimethylbenzimidazole; MCA, monochloroethane; NpRdhA, *ortho*-dibromophenol reductive dehalogenase of *Nitratireductor pacificus* pH-3B; OH–B_{12}, hydroxocobalamin; OMeBza, methoxybenzimidazole; PceA, PCE reductive dehalogenase; $PceA_{Smul}$, PceA of *Sulfurospirillum multivorans*; PCE, tetrachloroethene (perchloroethylene); RDase, reductive dehalogenase; RSQ, residue-specific quality; TBE, tribromoethene; TCA, trichloroethane; TCE, trichloroethene; TeCA, tetrachloroethane; VC, vinyl chloride.

Introduction

Chlorinated ethenes and ethanes are listed among the most frequently detected and prioritized groundwater contaminants and are, therefore, in the focus of remediation attempts [1,2]. Biological degradation of halogenated contaminants at anoxic sites relies on microbial activity. Their utilization as electron acceptors by microbes is enabled by reductive dehalogenase (RDase) enzymes that function as terminal reductases in respiratory chains [3]. These enzymes transfer electrons onto chlorinated, brominated or iodinated substrates, which leads to their dehalogenation. On one hand the enzymatic process mobilizes halogens and on the other hand increases the availability of the carbon backbone as energy and carbon source for growth of other microbes. Essential cofactors of RDases are a cobamide at the active site and two iron–sulfur clusters [4,5]. The physiologically active form of RDases is attached to the exoplasmic face of the cytoplasmic membrane [6–8]. The cytoplasmic precursor bears an N-terminal twin arginine translocation (Tat) signal peptide [9] for membrane transport. Low growth yields of most organohalide-respiring bacteria and the presence of numerous RDase homologs in a single organism often hampered biochemical characterization of the enzymes [10,11]. Thus, only a few representatives were characterized with regard to substrate spectrum and function [11–15]. Recently, protocols for functional heterologous production of RDases or nonfunctional heterologous production and subsequent reconstitution of active enzyme have been reported [5,16,17]. These approaches were expected to allow for an analysis of RDase substrate range and reaction mechanism. Conclusions on substrate specificities of uncharacterized RDases drawn from amino acid sequence alignments should be considered with caution. A comparison of the tetrachloroethene (perchloroethylene, PCE) RDases characterized so far showed a wide range of amino acid sequence identities from 99% to 27% [18–24]. In contrast, the PCE reductive dehalogenase (PceA) of *Desulfitobacterium hafniense* Y51 [24] and the 1,2-dichloroethane (1,2-DCA) reductive dehalogenase (DcaA) of *Desulfitobacterium dichloroeliminans* DCA1 [25] share 88% identity, but show different substrate preferences and might even perform different types of reactions. *Desulfitobacterium dichloroeliminans* DCA1 has been shown to grow on halogenated alkanes such as 1,2-DCA, which was converted to ethene via dihaloelimination/vicinal reduction [26] (Fig. 1). H_2, formate or lactate served as electron donor. In the presence of H_2 or formate, acetate was added as carbon source.

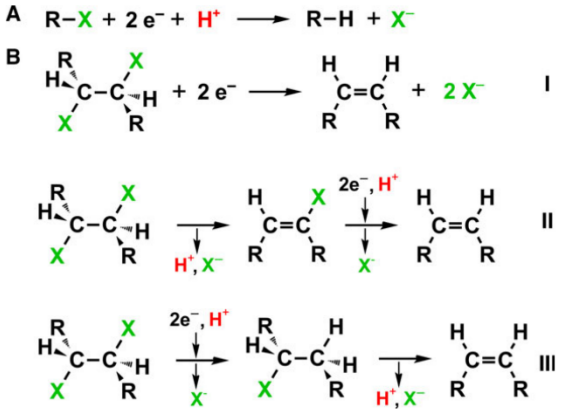

Fig. 1. Reductive dehalogenation reactions. (A) Halogen substitution: a halogen substituent is replaced by a proton and two electrons. (B) Putative dihaloelimination reactions: (I) β-elimination of two halogen substituents, (II) combination of a β-elimination of a halogen as a result of proton abstraction and a subsequent halogen substitution reaction, (III) combination of a halogen substitution step and a following β-elimination of a halogen and a proton. X: halogen substituent, R: carbon backbone or hydrogen atom.

1,1,2-trichloroethane (TCA) replaced 1,2-DCA as alternative electron acceptor during growth, while tetra-, penta- and hexachloroethanes or halogenated ethenes were not utilized. The *dcaA* gene was identified by Daffonchio *et al.* (2007) [25], but the DcaA protein was not purified and characterized. PceA of *D. hafniense* Y51 appeared to be specialized on chloroethenes [24]. PCE is converted via trichloroethene (TCE) to *cis*-1,2-dichloroethene (*cis*-1,2-DCE). Single chlorine substituents are replaced by hydrogen atoms in substitution reactions (Fig. 1). The vinyl chloride (VC) RDase of *Dehalococcoides mccartyi* VS performs both, halogen substitution and dihaloelimination [17]; 1,1-DCE and VC were dehalogenated via halogen substitution and 1,2-DCA via dihaloelimination. The structural determinants that decide upon the fate of the substrate are not known for any of these RDases.

In general, cobamide-dependent enzymatic reductive dehalogenation requires the superreduced [Co^{I}]-state for the initial attack onto the substrate [4,5,27,28]. The two cubane iron–sulfur clusters are proposed to be involved in the intramolecular electron transfer to the active site. Structural analysis of PceA from *Sulfurospirillum multivorans* ($PceA_{Smul}$) and the *ortho*-dibromophenol reductive dehalogenase (NpRdhA) from *Nitratireductor pacificus* pH-3B showed the two [4Fe–4S] clusters located in a row between the active site harboring the cobamide cofactor and the protein

surface allowing for the uptake of electrons from an external electron donor [4,5]. The proton required for halogen substitution was suggested to be donated from a highly conserved tyrosine residue located in close proximity to the substrate-binding site [4,5]. Exchange of the Tyr by Phe in NpRdhA completely hampered its dehalogenating activity when 3,5-dibromo-4-hydroxybenzoate was used as substrate for halogen substitution. Whether proton transfer is also involved in dihaloelimination remains to be elucidated. According to the equation of the overall reaction (Fig. 1B, reaction I), protons might be dispensable. However, a two-step catalysis combining the β-elimination of one halogen and the substitution of another halogen, which would require a proton transfer, is also feasible (Fig. 1B, reactions II and III).

Here, we report on the investigation of the molecular basis for halogen substitution and dihaloelimination reactions. So far, organohalide-respiring bacteria and their RDase genes cannot be genetically modified. However, recently a platform for functional heterologous production of PceA from *D. hafniense* Y51 in *Shimwellia blattae* was described [16]. In this study, the expression system was optimized for the functional production of the cytoplasmic precursor of PceA and of DcaA of *D. dichloroeliminans* DCA1. By determining the substrate range of both enzymes and the exchange of the potential proton-donating tyrosine, the two types of cobamide-mediated reductive dehalogenation reactions have been clearly delineated from each other as two different mechanisms. Based on *in silico* structural models of DcaA and PceA, site-directed mutagenesis was applied to unravel the functional role of amino acids forming the active site and having direct influence on the conversion of the substrate.

Results and Discussion

Functional heterologous production of DcaA and PceA

For the characterization of DcaA from *D. dichloroeliminans* DCA1 and its comparison with PceA from *D. hafniense* Y51, DcaA was tested for functional heterologous production in accordance to a protocol established earlier for the formation of catalytically active PceA [16]. The coexpression of RDases from *D. hafniense* strains with their corresponding trigger-factor-like chaperones RdhTs was shown to increase the production of soluble protein [16,29] and expected to ensure accurate folding of the RDases [29,30]. Therefore, DcaA was produced together with its dedicated chaperone DcaT [25] in *S. blattae*. DcaA activity was tested in crude extract of the *S. blattae* cells using 1,2-DCA as substrate. The protein was detected by SDS/PAGE and subsequent immunological analysis.

In first experiments of this survey, the *dcaA* gene, bearing a Strep-tag encoding sequence at the 3′-end, and the nontagged *dcaT* gene were expressed from two separate plasmids. Dimethylbenzimidazole (DMB) and hydroxocobalamin ($OH–B_{12}$) were added to the growth medium in order to support the cobamide cofactor supply. Under these conditions, a 1,2-DCA conversion rate of 1.5 nkat·mg^{-1} cell protein was measured in crude extract of cells harvested 6 h after induction of protein production. The DcaA activity was increased to 2.5 nkat·mg^{-1} cell protein by cloning the *dcaA* and the *dcaT* gene onto a single plasmid, extending the cultivation time after induction of gene expression from 6 to 18 h, and cultivating *S. blattae* (Strep-*dcaA*p*dcaT*) in the presence of 5-methoxybenzimidazole (OMeBza) instead of DMB plus $OH–B_{12}$. The presence of 5-OMeBza (10 μM) rather than DMB in the growth medium increased both, the amount of DcaA protein and also the specific DcaA activity in the crude extract. Cobamide purification and identification revealed the formation of methoxybenzimidazolyl-cobamide under these conditions, which might be supportive for DcaA production and maturation. Predictions on the flexibility or restrictiveness of DcaA in cobamide cofactor utilization could not have been made, since nothing is known yet about cobamide production in *D. dichloroeliminans* DCA1. To prevent the presence of two different cobamides in the expression host, $OH–B_{12}$ was omitted from further cultivations of *S. blattae* in the presence of 5-OMeBza.

The same plasmid construction was used for the expression of *pceA* from *D. hafniense* Y51. The *dcaT* gene was not exchanged, because the chaperone $PceT_{Y51}$ [30] shares 99% protein sequence identity to DcaT [25]. In this case, cultivation of the *S. blattae* (Strep-*pceA*p*dcaT*) strain was performed in the presence of DMB and in the absence of $OH–B_{12}$. Cells were cultivated for 6 h after induction of gene expression, which resulted in a PceA activity of 0.35 nkat·mg^{-1} cell protein measured in crude extracts with PCE as substrate. The positive effect of an elongated incubation time, as shown for DcaA, was not observed for PceA (A. Mac Nelly, personal information). The replacement of DMB by 5-OMeBza did not influence PceA production or activity; hence, we continued using DMB for PceA production. The two generated strains obtained during these initial experiments, *S. blattae* (Strep-*dcaA*p*dcaT*) and

S. blattae (Strep-*pceA*p*dcaT*), were used as a platform for comparative analysis of DcaA and PceA substrate ranges and for site-directed mutagenesis of both RDases.

Substrate range of DcaA and PceA

The substrate range of DcaA from *D. dichloroeliminans* DCA1 was determined using crude extract of the *S. blattae* (Strep-*dcaA*p*dcaT*) strain. In the enzyme assay, 1,2-DCA was converted to ethene by DcaA with a specific activity of about 2.5 nkat·mg^{-1} cell protein (Fig. 2A). VC or monochloroethane (MCA), both potential intermediates of 1,2-DCA dechlorination, was not detected. This observation is consistent with the inability of DcaA to convert VC or MCA as substrate and is also in line with earlier studies on growing cultures of *D. dichloroeliminans* DCA1 [26]. Taken together, these results argue against a sequential two-step reaction mechanism in which a proton transfer is involved (Fig. 1). Besides 1,2-DCA, also 1,2-dibromoethane (DBA) was converted in crude extract. While the conversion of 1,2-DCA was strictly dependent on intact DcaA, a significant portion of the 1,2-DBA turnover was still measured (about 70%) with heat-inactivated sample. It was concluded that the active site architecture of DcaA plays a crucial role in the reductive dehalogenation of 1,2-DCA, but has only little importance for 1,2-DBA conversion. When using native or heat-inactivated crude extract of the *S. blattae* (Strep-*pceA*p*dcaT*) strain producing PceA, ethene formation from 1,2-DBA was observed with identical turnover rates, which uncovered a complete abiotic conversion mediated by cobamides. Therefore, 1,2-DBA was excluded from further analyses. The differences in the abiotic turnover rate for 1,2-DBA measured in *S. blattae* (Strep-*pceA*p*dcaT*) compared with the *S. blattae* (Strep-*dcaA*p*dcaT*) strain might be explained by the production of different cobamides in both types of cells under the applied cultivation conditions. The chlorinated counterpart of 1,2-DBA, namely 1,2-DCA, was neither converted by intact PceA nor abiotically. In addition, 1,2-difluoroethane (DFA) was tested but not converted at all, neither by DcaA or PceA nor abiotically. The elevated stability of chlorinated and fluorinated compounds over brominated organohalides is based on the increase in electronegativity of the halogen substituents from bromine to fluorine and the resulting differences in the partial negative charges of the respective substituents [28,31,32]. DcaA also converted 1,1,2-TCA to VC via dihaloelimination that was strictly enzyme-dependent (Fig. 2A). In contrast, the isomer 1,1,1-TCA was not utilized, suggesting that the enzyme is not able to perform β-eliminations, where only one halide substituent is removed as a result of proton abstraction. So far, an RDase-mediated conversion of 1,1,1-TCA was only reported for chloroform RDases, which are distantly related to DcaA and PceA [14,33,34]. In these cases, 1,1,1-TCA was converted to 1,1-DCA and subsequently MCA via halogen substitution. However, 1,1-DCA was not detected as product in the DcaA assay.

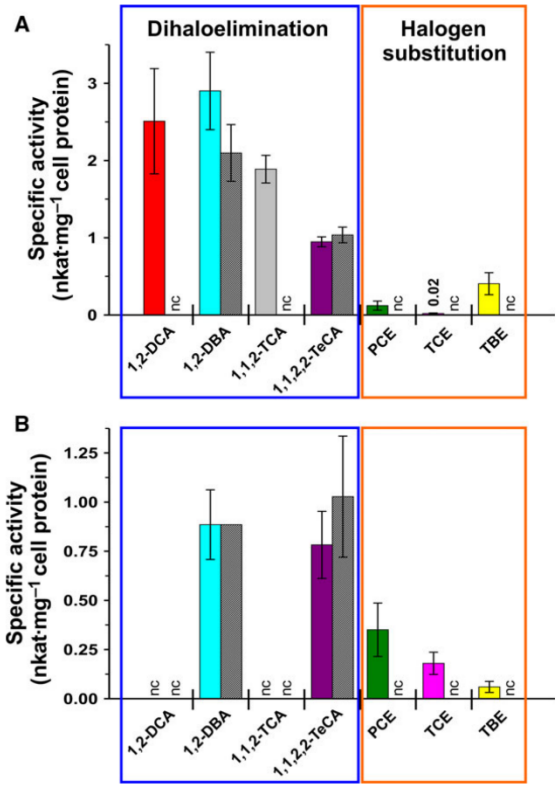

Fig. 2. Substrate range of DcaA (A) and PceA (B). The specific activity was determined using crude extracts of the *Shimwellia blattae* (Strep-*dcaA*p*dcaT*) or *S. blattae* (Strep-*pceA*p*dcaT*) strains. Conversion rates that were measured abiotically (heat-inactivated crude extract) are shown as shaded bars. All substrates for a dihaloelimination reaction are framed blue. Substrate conversion via halogen substitution is framed orange. The specific activities are represented as mean ± standard deviation from maximal nine biological replicates. nc, no conversion.

PceA was not able to convert 1,1,2- or 1,1,1-TCA, but was reported earlier to dihaloeliminate higher chlorinated alkanes such as 1,1,2,2- and 1,1,1,2-tetrachloroethane (TeCA) [24]. In the enzyme assays conducted in the study presented here, a mixture of *cis*- and *trans*-1,2-DCE was formed from 1,1,2,2-TeCA

with an activity of 0.78 nkat·mg^{-1} cell protein (Fig. 2B). However, an even higher conversion rate was measured with heat-inactivated crude extract indicating an exclusively abiotic conversion. In crude extracts of the DcaA-producing *S. blattae* (Strep-*dcaA*p*dcaT*), 1,1,2,2-TeCA dihaloelimination was also detected and proven to be completely enzyme-independent. Therefore, 1,1,2,2-TeCA was excluded from further analyses.

All potential substrates that could have been subject to dihaloelimination catalyzed by PceA were either not converted by the enzyme or the conversion was based on a cobamide-mediated abiotic reaction. Hence, PceA appears to be optimized for the catalysis of halogen substitution. PCE and TCE were converted with specific activities of 0.35 and 0.18 nkat·mg^{-1} cell protein in crude extracts of strain *S. blattae* (Strep-*pceA*p*dcaT*). The difference in turnover rates was most probably based on the higher apparent K_m for TCE conversion compared with PCE conversion, since both substrates were added in a concentration close to the K_m for TCE [24]. The product *cis*-1,2-DCE was not dehalogenated. The TCE analog tribromoethene (TBE) was dehalogenated to *cis*-1,2-dibromoethene (DBE) as end product, albeit with a 67% lower turnover rate. PceA of *D. hafniense* Y51 shares 98% amino acid sequence identity with PceA of *D. hafniense* PCE-S, which was described to dehalogenate TBE to all isomers of DBE and subsequently further to vinyl bromide and ethene [35]. It seems that the exchange of 2% of the protein sequence (11 out of 512 amino acids), spread across the whole $PceA_{PCE\text{-}S}$ sequence, can alter the RDase structure in a way that leads to a different substrate range and dehalogenation pattern. Interestingly, although no growth was observed upon cultivation of *D. dichloroeliminans* DCA1 in the presence of chlorinated ethenes as electron acceptors [26], the DcaA protein was also able to dechlorinate PCE to TCE and further to *cis*-1,2-DCE with specific activities of 0.12 and 0.02 nkat·mg^{-1} cell protein. TBE was converted to *cis*-1,2-DBE, 3.3 times faster than PCE. None of these conversions were detectable with heat-inactivated crude extract. Apparently, DcaA is able to perform both halogen substitution and dihaloelimination, but appears to be specialized on the latter, while PceA seems to be restricted to halogen substitution reactions.

The heterologous production of DcaA and PceA as Strep-tag fusion proteins allowed for their enrichment via affinity chromatography, although the binding efficiency was weak (shown for Strep-DcaA in Fig. 3). All ratios in substrate specificities measured in the crude extracts of the *S. blattae* (Strep-*dcaA*p*dcaT*) and *S. blattae* (Strep-*pceA*p*dcaT*) strains were also detected for the enriched DcaA and PceA and thus have been clearly attributed to the RDase proteins (data not shown). However, the low yield and the copurification of a substantial amount of DcaT hampered the definite determination of kinetic parameters for the enzymes.

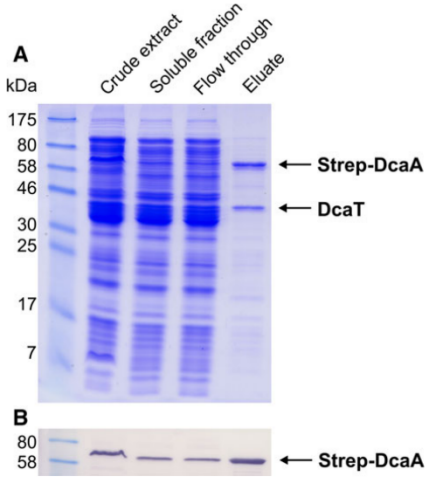

Fig. 3. Enrichment of recombinant Strep-DcaA. (A) Strep-DcaA was isolated from soluble extract of *Shimwellia blattae* (*dcaA*p*dcaT*) via Strep-Tactin affinity chromatography and analyzed on a 12.5% SDS/PAGE (Coomassie-stained). (B) The enriched enzyme was identified by immunological analysis using Strep-tag specific antibodies (IBA). Strep-DcaA was copurified with DcaT. DcaT was detected using specific antibodies raised against PceT of *Desulfitobacterium hafniense* strain Y51 (kindly provided by T. Futagami, Kagoshima University, Japan; data not shown). With the exception of the eluates, for which 2 μg protein were applied, 20 μg protein was separated on each lane.

In silico structural models of DcaA and PceA

To allow for the study of structural determinants in DcaA and PceA, which might be involved in either halogen substitution or dihaloelimination as well as in defining the substrate range, *in silico* structural models of both RDases were generated using the I-TASSER server for protein structure and function prediction [36,37]. For this purpose, the amino acid sequences for the mature RDase proteins lacking the Tat signal peptides were used. The process of structure prediction is based on a comparative analysis of the protein sequence of interest with template proteins of similar fold or secondary structures found in the protein data bank (PDB). For each RDase, the structural model was predicted twice to test for its reliability. The model displaying the higher confidence level was chosen for

further analysis. The selected threading templates found in the PDB library, which were used for the prediction of the RDase structures, were PceA of *S. multivorans* ($PceA_{Smul}$) [4] and NpRdhA of *N. pacificus* pH-3B [5]. Even though PceA and DcaA share only 28% and 36% overall amino acid sequence identities with $PceA_{Smul}$, the RDases share high global fold similarities with an average template modeling (TM) score of 0.794, whereby a TM score of 1 describes a perfect match. NpRdhA was still assigned as a structural analog with a TM score of 0.587. Distant structural homologs outside of the RDase family were found in the epoxyqueuosine reductases from *Streptococcus thermophilus* (TM score 0.372) [38] and *Bacillus subtilis* (TM score 0.371) [39]. These enzymes are also classified within cobamide-containing iron–sulfur proteins, whereby the structural similarity to RDases is mostly limited to the mode of cofactor binding. The quality of the DcaA model was calculated with a confidence (C) score of −0.87. C scores typically range from −5 to 2 with higher values expressing higher confidence. The structure model of PceA had a C score of −1.0. Looking in detail on the residue-specific quality (RSQ) of the predictions [40], differences in the local accuracy between single domains get obvious. RSQ values describe the estimated deviation of the residue in the generated model from the native structure. The domains responsible for binding of the cobamide cofactor and the two iron–sulfur clusters as well as amino acids involved in the formation of the substrate-binding pocket showed high local accuracies with RSQ values below 5 Å (Fig. 4). These good-quality structural models were used as basis for the investigation of structural and functional relations. In contrast, termini regions and domains involved in the formation of the substrate channel were less reliable with highly varying estimated distances of up to 24.9 Å. Here, also the two separately generated models

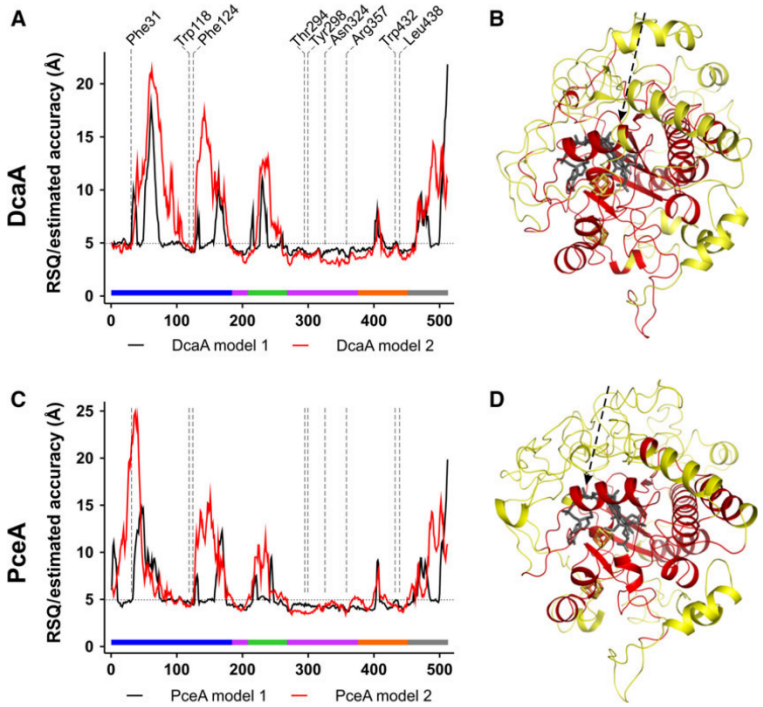

Fig. 4. *In silico* structural models of DcaA and PceA. (A,C) RSQ values of two structural models of DcaA and PceA, respectively. The models were generated independent from each other using the I-TASSER server for protein structure and function prediction. Positioning of amino acid residues with RSQ values below 5 Å were reliable. Amino acids involved in the active site formation are labeled by dashed lines. Structure domains are colored as follows: N terminus/substrate channel (blue), cobamide-binding (purple), insertion unit (green), Fe–S cluster-binding (orange), C terminus (gray). (B,D) Overall structures. The model with higher confidence for each RDase is shown. Amino acid residues with RSQ values < 5 Å in both models of each RDase are colored red, and residues with RSQ values > 5 Å are colored yellow. Each enzyme harbors two [4Fe–4S] cluster (colored sticks) and a cobamide cofactor (gray sticks). The cobamide shown here is norpseudo-B_{12}, since it is the natural cofactor of $PceA_{Smul}$ [4,61], which was used as template for model generation. The arrow indicates the substrate channel.

of each RDase showed major differences; hence, these parts were omitted from further analyses.

In comparison to the known RDases structures of $PceA_{Smul}$ and NpRdhA, the metal cofactors are located at the same position in DcaA and PceA (Fig. 5A–D). Indeed, the cofactor-binding domains are highly similar in all four RDases, while most of the differences in the protein sequences were detected in the substrate channel forming parts of the enzyme. The cobamide cofactor is positioned in the center of the protein with the active site cavity shaped by mainly aromatic amino acids above the corrin ring in DcaA or PceA (Fig. 5C,D). The proximal iron sulfur cluster in both enzymes was located about 6 Å from the cobalt ion of the cobamide and the distal iron sulfur cluster about 7.6 Å (DcaA) or 4.9 Å (PceA) away from the proximal cluster allowing for the sequential electron transfer to the active site. Also the residues forming the active site above the corrin ring of the cobamide cofactor are rather similar in DcaA and PceA. The highly conserved tyrosine residue, which was proposed as the putative proton donor in halogen substitution, is present in PceA (Tyr298). It might be essential for the dehalogenation of its substrates PCE, TCE and TBE. Interestingly, the tyrosine residue was located at the same position in DcaA, although dihaloelimination was proposed to be proton independent. The deprotonated tyrosine might be stabilized by the positive charge of a neighboring arginine residue highly conserved in $PceA_{Smul}$ [4] as well as in DcaA and PceA or a lysine in NpRdhA [5]. The Thr294 residue, which is located closely to the Tyr298 in DcaA, represents another potential proton donor in DcaA's active site. It is replaced by a valine in PceA. Two further differences become obvious when comparing DcaA and PceA. Phe124 of DcaA is replaced by Tyr124 in PceA. Although the aromatic ring of both amino acids is located in the same plane, its orientation differs in both enzymes. Nevertheless, the hydroxyl group of Tyr124 is not facing the substrate-binding pocket and no effect on substrate binding or conversion was expected for this residue. Instead of Leu438

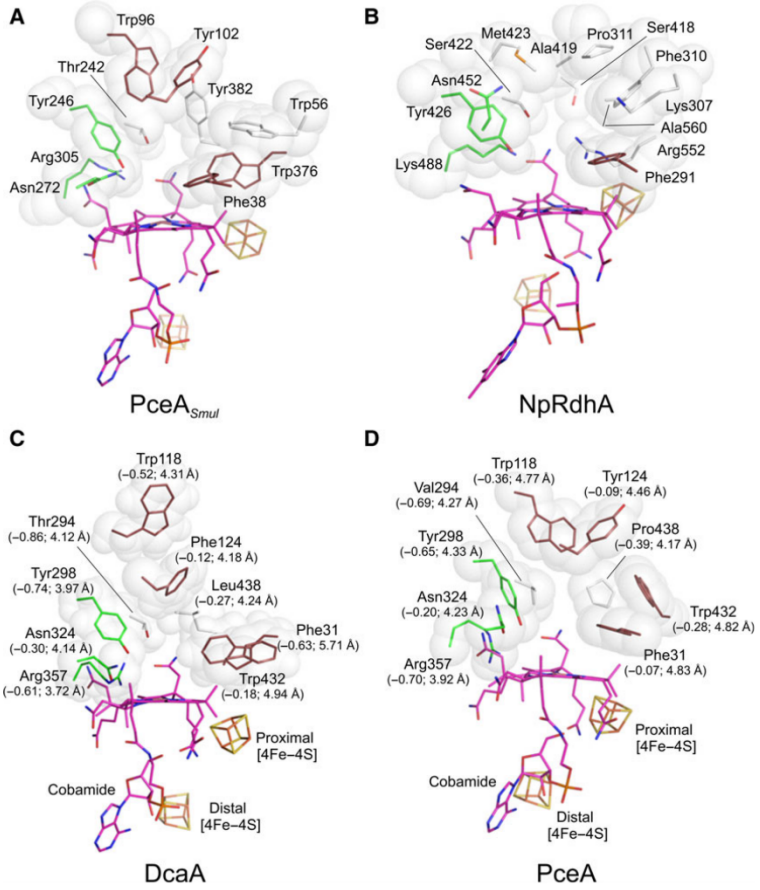

Fig. 5. Active site cavities of $PceA_{Smul}$ (A), NpRdhA (B), DcaA (C) and PceA (D). The *in silico* structural model with higher confidence is shown for DcaA and PceA. With the exception of Phe31 in DcaA and PceA, all residues belong to the regions with a high degree of reliability (red) in Fig. 4B,D. Highly conserved residues are depicted in green, less conserved residues in brown, variable residues in white, the cobamide cofactor in pink and the [4Fe–4S] clusters in yellow/orange. The normalized B-factor and the RSQ values are given in brackets. B-factor describes the fluctuation of atoms around their average position.

in DcaA, a proline residue was found in PceA. However, both amino acids cannot serve as proton donors. In general, this position is highly variable among different RDases (Fig. S1). An asparagine residue (Asn324) is the only amino acid in the active sites of DcaA and PceA that is placing its side chain in hydrogen bonding distance of about 3.4 Å to the carboxamide side chain of the cobamide, an arrangement that seems to be conserved in many other RDases (Fig. S1), and might be involved in binding of the cobamide cofactor together with further residues of the protein backbone. The orientations of Phe31 and Trp118 in DcaA have to be considered with caution. Their RSQ values allow for precise predictions of their position in the protein backbone, while the orientation of the amino acid side chains differed in the two models generated separately.

Site-directed mutagenesis in DcaA and PceA

Based on the *in silico* structural models, single amino acids forming the active sites in DcaA and PceA were exchanged to study their involvement in substrate conversion. Effects on RDase production and substrate turnover were verified by immunoblot and activity measurements using the crude extract of the mutant strains. In separate cultivation experiments of the *S. blattae* (Strep-*dcaA*p*dcaT*) strain, varying amounts of cobamide (47.2–124 nmol cobamide·g^{-1} cell protein) were determined, which resulted in variations in the DcaA activities in crude extracts (Fig. 2). However, within a single set of cultures, even when different *dcaA* mutant strains of *S. blattae* were cultivated in the same batch of medium, their cobamide content was similar. In order to allow for a direct comparison of different cultivation attempts, the *S. blattae* (Strep-*dcaA*p*dcaT*) strain or the *S. blattae* (Strep-*pceA*p*dcaT*) strain producing the wild-type enzymes were always included and the respective RDase activity was set as 100%.

Proton transfer

PceA was described to be specialized on halogen substitution, which requires a proton besides two electrons. The highly conserved Tyr298 is located in a position ideally suited to function as proton donor. Replacement of the Tyr298 by other potential proton donors, namely His, Thr and Ser as well as Phe, which resembles Tyr but lacks the proton donor function, completely suppressed PceA activity for halogenated ethenes. The amount of PceA produced by the cells was not affected by the mutations (Fig. 6A). This result highlights the essential role of Tyr298 as

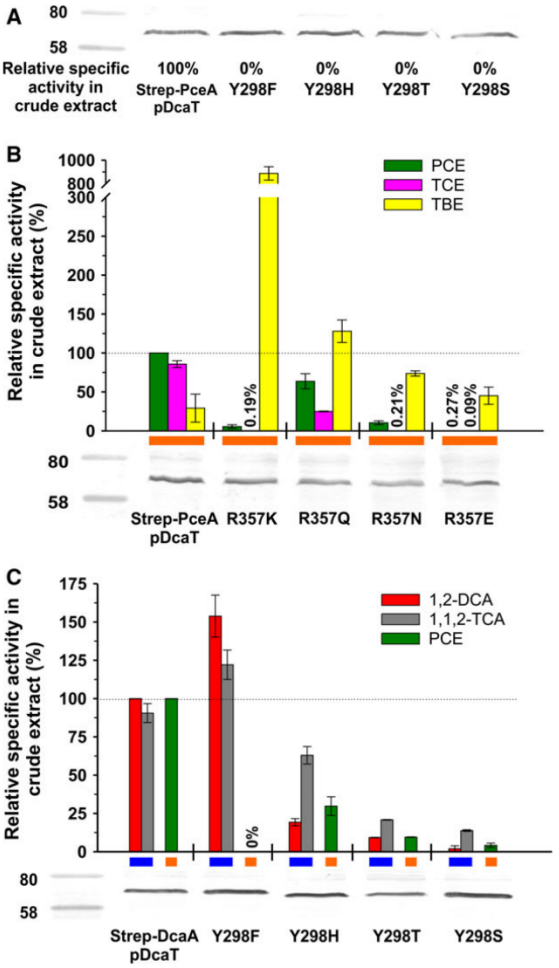

Fig. 6. Site-directed mutagenesis of the highly conserved Tyr298 and Arg357 residues in PceA (A,B) and DcaA (C). Specific activities were determined in crude extracts of *Shimwellia blattae* mutant strains that produced modified variants of the RDases. The conversion rate for 1,2-DCA in the recombinant wild-type RDase was set to 100% and used as reference for all dihaloeliminated substrates (blue). In parallel, PCE conversion in the wild-type RDase was set to 100% and used as reference for all substrates in which the halogen is substituted (orange). The RDase proteins were identified via immunoblot analysis (25 µg cell protein per lane) using Strep-tag-specific antibodies. The 80 and 58 kDa bands of the protein standard are shown. The specific activities are represented as mean ± standard deviation from a maximum of four independent experiments.

potential proton donor during halogen substitution in PceA and is in accordance with the loss of activity in the equivalent Y426F mutant of NpRdhA, which is catalyzing halogen substitution at aryl halides [5]. The positive charge of the amino groups of a closely positioned highly conserved arginine was postulated to stabilize the deprotonated tyrosine in the course of the

reaction [4]. Exchanging the Arg357 in the mutant strains R357Q and R357K led to reduced PCE and TCE conversion rates (Fig. 6B). While the presence of Gln still allowed for substantial PCE and TCE turnover, the replacement by Lys caused a drastic decrease in chloroethene conversion. The absence of a positive charge at all in R357E prevented product formation almost completely, underpinning the supportive role of a nearby amino group for proton transfer from Tyr298. Evidence has been presented before that Lys might serve as a stabilizer of the deprotonated Tyr in NpRdhA [5], but could not be functionally replaced by Gln. An improper orientation of the amino acid side chain in the mutant R357K of DcaA might be the reason for the impairment of the enzyme function in this case. Surprisingly, the TBE conversion rate was 30 times higher in the R357K mutant compared with the wild-type protein. The expanded space at the active site generated by the R357K exchange might enhance conversion rates for bigger substrates or selectively for brominated organohalides. Further side chain truncations in the R357Q and R357E mutants, however, led to a decrease of the elevated TBE activity again. About 35% of the TBE activity was still measureable in R357E lacking an amino group, compared to the R357Q analog indicating that a positive charge is not supporting TBE turnover to an extent observed for PCE and TCE. All PCE-RDases characterized so far harbor an arginine at this position [18–24] (Fig. S1). In contrast, a lysine can be found in NpRdhA and the *ortho*-chlorophenol RDase of *Desulfitobacterium dehalogenans*, which both showed higher turnover rates for bulky brominated substrates rather than for their chlorinated analogs [5,41] (Fig. S1).

The involvement of proton transfer steps in the dihaloelimination reaction is rather unlikely due to the fact that no intermediates have been detected during substrate conversion. Nevertheless, the *in silico* structural model of DcaA showed a tyrosine and arginine residue at the same positions as in PceA. Replacing the Tyr298 in DcaA by Phe, which cannot supply a proton, led to a complete loss in conversion of halogenated ethenes, while the activities for the dihaloelimination of 1,2-DCA and 1,1,2-TCA were not affected. While the Tyr298 residue is the only putative proton donor in PceA, a threonine is located in close distance to the Tyr298 in DcaA, which might be an alternative source for protons. However, an additional exchange of Thr294 against Val in the Y298F mutant of DcaA still showed dihaloeliminating activity of 0.62 nkat·mg^{-1} cell protein for 1,2-DCA. Hence, the decrease in the conversion rate seemed to be caused by other structural changes rather than a loss of the protonation capacity (see below). In this DcaA variant, no other putative proton-donating amino acid side chain was present in the active site, yet dihaloelimination reactions were detected. Although the possibility of proton donation by a water molecule in the active site cavity cannot be excluded completely, the results strongly support the assumption that no proton transfer step is involved in the dihaloelimination mechanism.

The halogen substitution mediated by DcaA was not completely disabled when Tyr298 was replaced by other potential proton donors, as it was shown for PceA. In DcaA, increasing the distance of the hydroxyl group from its original position in the mutants Y298H, Y298T and Y298S rather led to a stepwise decrease in PCE conversion rates to 4%, while the amount of DcaA was not altered in the mutant strains (Fig. 6C). The same trend was also observed for the dihaloelimination, indicating an effect on substrate binding rather than a loss of the proton donor function. The exchange of Arg357 to Gln displayed a rather negligible effect on both mechanisms (Fig. 7A). In addition, the positive effect on TBE conversion, as it was shown for the respective PceA mutant, was not observed in this case, indicating structural differences at the active sites of both enzymes leading to a different substrate positioning. The presence of the tyrosine and the arginine in dihaloeliminating RDases might reflect the general ability of these enzymes to catalyze also halogen substitution. The proton-donating function might be taken over by a histidine found at this position in several putative 1,2-DCA-dihaloeliminating RDases, e.g., in DcaA of *Dehalobacter* sp. WL [42–44] (Fig. S1). Whether these enzymes are also able to perform both mechanisms has not yet been tested. Until today, no PCE-converting RDase was found that lacks the tyrosine residue [18–24]. However, comparison of protein sequences revealed the replacement of the tyrosine by a cysteine or phenylalanine in RDases specialized on the halogen substitution at chloromethanes [14,33,34] (Fig. S1). The role of these alternative amino acids for the active site architecture and/or the catalytic mechanism remains to be elucidated.

Since the dimensions of the PceA or DcaA active site and the distances between the highly conserved tyrosine and the cobalt are similar in the *in silico* structural models, the different effects observed when the type of the proton donor changed are most probably caused by alterations in substrate positioning. The eminent importance of the substrate positioning at the active site became obvious in a previous study investigating the mode of the initial attack onto the substrate leading to halogen substitution [28]. PceA$_{Smul}$ places the substrates at a distance from the cobamide

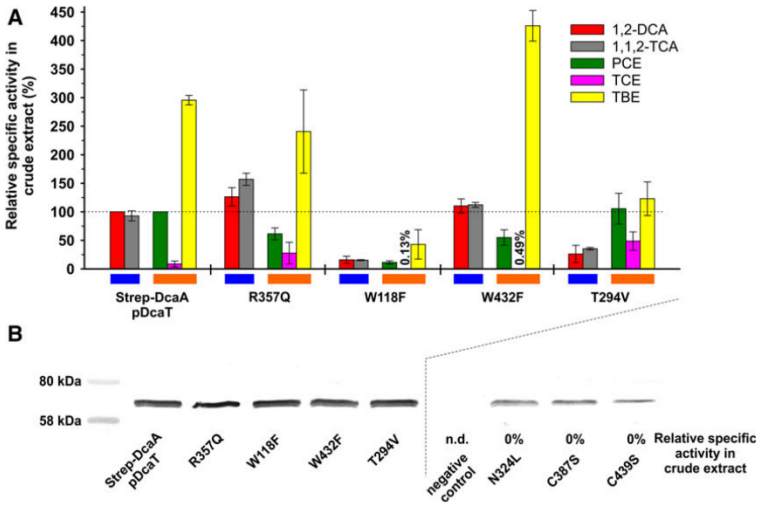

Fig. 7. Site-directed mutagenesis of amino acids involved in the architecture of DcaA's active site. (A) Specific activities were determined in crude extracts of *Shimwellia blattae* mutant strains that produced variants of DcaA. The conversion rate for 1,2-DCA in the recombinant wild-type DcaA was set to 100% and used as reference for all dihaloeliminated substrates (blue). In parallel, PCE conversion in the wild-type DcaA was set to 100% and used as reference for all substrates in which the halogen is substituted (orange). (B) The RDase protein in the crude extracts was identified via immunoblot analysis (25 μg cell protein per lane) using Strep-tag specific antibodies. The mutant strains N324L, C387S und C439S did not show any activity. The specific activities are represented as mean ± standard deviation from two independent experiments. The *S. blattae* (p*dcaT*) strain was used as negative control. n.d., not determined.

cofactor, and based on this finding, it was proposed that the enzyme attacks the substrate via long-range electron transfer [4,28]. In contrast, NpRdhA attacks the substrate at the halogen substituent and forms a cobalt–halogen bond, which is allowed by an appropriate positioning of the organohalide toward the cobalt ion [5]. In a third case, compound-specific isotope analyses of dehalogenating cultures of *Desulfitobacterium* sp. strain Viet1 and *Geobacter lovleyi* strain SZ indicated a direct nucleophilic attack by [Co^{I}] onto the carbon atom, even though a dissociative single electron transfer could not be excluded [45]. The latter would require an intimate interaction of both reaction partners, but the actual positioning of the substrates at the active site of the enzymes involved is not known so far. Results obtained in a very recent study by Elsner *et al.* [46], who applied dual-element isotope analysis, pointed out that an intimate interaction between both reaction partners might be a common theme in enzymatic reductive dehalogenation of chlorinated ethenes. However, data from electron paramagnetic resonance spectroscopy of $PceA_{Smul}$ equipped with various substrates did not support this assumption [28].

Active site cavity of DcaA

The active site cavity of DcaA and PceA is mainly lined by aromatic amino acids such as tryptophan and phenylalanine. The Trp118 residue in DcaA is involved in encapsulating the active site cavity. Although Trp118 points with its side chain away from the active site as shown in the *in silico* structural model in Fig. 5C, the side chain orientation differed in separately generated models. It is also feasible that the indole ring is exposed toward the cobamide cofactor and that the benzene ring of the indol moiety is directly involved in active site formation of DcaA, as it was described for the crystal structure of $PceA_{Smul}$ [4] and for the *in silico* model of PceA (Fig. 5D). When Trp118 was replaced by Phe in the W118F mutant, the overall reductive dehalogenation activity decreased drastically, while the DcaA amount in the crude extract remained stable (Fig. 7B). Widening of the active site toward the top might result in a higher flexibility of the substrate's orientation and position in the cavity, which can have a negative effect on its conversion. While the Trp118 residue is frequently conserved in the protein sequences of PCE- and putative 1,2-DCA-converting RDases [18–20,22–24,43,44], enzymes specialized on aryl halides or chloromethanes show a higher variability at this position [5,14,33,34,47–50] (Fig. S1). For halogenated ethenes and ethanes, a densely packed cavity seems to be crucial for correct substrate positioning and thus efficient conversion. The conservative exchange of Trp432, which is involved in forming one side of the active site

cavity (Fig. 5C,D), by Phe did not hamper the overall DcaA activity, but led to a shift in substrate specificity. While the conversion of 1,2-DCA and 1,1,2-TCA was not affected in W432F, TBE turnover increased by 44% reaching a final activity of about 0.47 nkat·mg^{-1} cell protein (Fig. 7A). In contrast, PCE and TCE conversion decreased by 45% and 94%, respectively. In this case, the widened active site cavity seemed to slightly shift the haloethene specificity toward bulkier molecules such as TBE and disfavored smaller molecules like PCE and TCE. Similar to the Trp118 mutant, the lack of stabilization by the indole ring in W432F might hamper correct positioning, here especially of smaller substrates such as TCE. The finding that the conversion rate of the larger chloroethanes compared to that of TBE was not increased might indicate a different positioning in the active site of DcaA. In RDases converting aryl halides, the tryptophan is mostly replaced by an arginine or phenylalanine, both amino acids providing more space for larger substrates [5,16,41,48–52] (Fig. S1). The opposite effect was observed in the T294V mutant. Exchange of the Thr294 against the slightly larger Val slowed down conversion of the larger substrates 1,2-DCA, 1,1,2-TCA and TBE by a factor of 2.4–3.8, while TCE conversion increased 5.6 times (Fig. 7A). In this case, already a slightly narrowed active site supports positioning and conversion of smaller molecules. While the overall RDase protein sequence does not allow for substrate predictions, the active site's architecture shows a high adaptation to its substrates and already conservative amino acid replacements change the substrate preferences. Especially His298 or K357 equivalents were found to be good indicators for either a specialization on dihaloelimination or a preference for larger brominated organohalides as substrates, respectively.

Cofactor binding in DcaA

The protein sequence of RDases does not encode for a typical cobamide-binding motif. In structural analysis, the cobamide cofactor was shown to be noncovalently bound to the protein backbone [4,5]. The Asn324 residue in the active site is located within hydrogen bonding distance to the carboxamide side chain of the corrin ring and might be involved in binding of the cobamide cofactor. The feasibility of the Asn residue to participate in cobamide binding was already shown in the crystal structure of $PceA_{Smul}$ [4]. The DcaA mutant N324L completely lost its ability of reductive dehalogenation. An alteration of the cobamide content in the cells was excluded by testing for the abiotic conversion of 1,2-DBA that was not affected in comparison to other strains tested. However, none of the enzyme-dependent activities were measurable. The DcaA amount in the crude extract was detected by immunoblot that showed a weaker band compared to the wild-type enzyme (Fig. 7B), indicating a degradation of the protein most probably due to a hampered cobamide incorporation and an improper folding of DcaA. Whether the cobamide cofactor is bound improperly or not bound at all in the N324L enzyme variant has to be analyzed with pure enzyme in further studies, in which other amino acids involved in cobamide cofactor-binding should also be tested. In the catalytic cycle, the cobamide cofactor has to be reduced with electrons from an external electron donor via the two cubane Fe–S clusters. The Fe–S cluster-binding motifs are highly conserved among all RDases. In the folded protein, the clusters are located between the surface of the protein and the active site, thus allowing for intramolecular electron transfer from the external electron donor to the cobamide cofactor [4,5]. An identical positioning was also observed in the *in silico* structural model of DcaA (Fig. 5C). Destruction of the [4Fe–4S] cluster proximal to the cobamide and the distal [4Fe–4S] cluster in the mutant strains C439S and C387S, respectively, completely hampered dehalogenating activity and showed weaker DcaA bands in the immunoblot (Fig. 7B). The latter observation might again indicate degradation of misfolded protein. The proximal cluster is in close distance to both, the cobamide cofactor and the protein surface, and in principle would allow for an electron transfer in the C387S mutant that lacks the distal cluster. The absence of any detectable dehalogenating activity measured in the crude extract indicated that the reduced methyl viologen, which serves as external electron mediator in the assay, was not able to reduce the proximal [4Fe–4S] cluster directly or that the enzyme was not loaded with cofactors at all. The physiological electron donor interacting with the RDases in the organohalide respiratory chain is not known so far. Several models exist for *S. multivorans* and *Dehalococcoides* spp., which all involve exoplasmic as well as integral membrane proteins in the electron transfer chain [53–55]. It is unclear, whether the electrons enter the RDase at the distal or the proximal [4Fe–4S] cluster. To elucidate the exact route of the intramolecular electron transfer, spectroscopic studies with pure enzymes are required.

Conclusion

In this study, comparative functional analysis of PceA specialized on halogen substitution and the dihaloeliminating DcaA allowed for a clear separation between

two types of dehalogenation reactions by means of involvement or nonparticipation of proton transfer steps. In addition, the presence of both types of reaction within a single RDase has been shown, thus, making predictions on the presence of a certain mechanism in a specific RDase difficult. In contrast to DcaA from *D. dichloroeliminans* DCA1, the chloroform and 1,1,1-TCA-RDase of *Desulfitobacterium* sp. strain PR [56] and an enrichment culture containing *Desulfomonile tiedjei* DCB-1 [57] were found to convert 1,1,2-TCA and 1,2-DCA in a halogen substitution reaction rather than via dihaloelimination. The trichloromethane RDase of *Dehalobacter* sp. strain UNSWDHB is even able to reduce a single substrate, 1,1,2-TCA, either via dihaloelimination to VC or via halogen substitution to 1,2-DCA [14]. From these observations and the results of the study presented, one has to assume that every cobamide-containing RDase can probably catalyze halogen substitution or dihaloelimination until a specialization most probably achieved by small alterations in the active site architecture has been proven.

Materials and methods

Bacterial strains, plasmids

Plasmids used in this study are presented in Table S1. *Shimwellia blattae* (ATCC 33430) was used as heterologous expression host for the production of RDases. The mutant strains *S. blattae* (Strep-*dcaA*p*dcaT*) and *S. blattae* (Strep-*pceA*p*dcaT*) are derivatives of the wild-type strain carrying RDase and chaperone genes, which were introduced into the plasmid pASK-IBA63c-plus (IBA, Göttingen, Germany). The mutant strain *S. blattae* (p*dcaT*) carries exclusively the chaperone gene and served as negative control for RDase production.

Plasmid construction and transformation of *S. blattae*

All cloning steps were conducted according to standard techniques described in Sambrook *et al.* [58]. The genes encoding for DcaA (WP_015261904.1) and DcaT (WP_015261906.1) of *D. dichloroeliminans* DCA1 (synonym *D. dichloroeliminans* LMG P-21439) and PceA (BAC00915.1) of *D. hafniense* Y51 were amplified via PCR from purified genomic DNA. The DNA sequences of all primers used in this study are listed in Table S2. Primers used to amplify the genes of interest contained restriction sites for selected endonucleases (for details, see Table S2). The primer T493 additionally contained the sequence encoding for a Strep-tag and an *Nhe*I site. The *dcaA* PCR product was cut with *Pci*I/*Xho*I and cloned into the *Nco*I and *Xho*I sites of the pASK-IBA63c-plus plasmid. The *dcaT* PCR product was cloned downstream of *dcaA* into the *Xho*I and *Afe*I sites of the plasmid 'Strep-*dcaA*'. Finally, the *tet*-promotor region and ribosome-binding site of pASK-IBA63c-plus was amplified, cut with *Xho*I/*Sal*I, and additionally introduced into the plasmid 'Strep-*dcaA_dcaT*' upstream of *dcaT* using the *Xho*I site resulting in 'Strep-*dcaA*p*dcaT*'. The *dcaA* gene was exchanged by *pceA* using the *Nhe*I and *Xho*I sites to generate the plasmid 'Strep-*pceA*p*dcaT*'. For testing a negative control in expression experiments, *dcaA* was removed from the 'Strep-*dcaA*p*dcaT*' plasmid by digestion with *Xba*I and religation of the plasmid. All constructs were transformed into competent cells of *S. blattae* (ATCC33430), whereby the ampicillin resistance cassette was used as selection marker. The validity of all plasmid constructs shown in Table S1 was confirmed by DNA sequencing. For site-directed mutagenesis, *dcaA* and *pceA* were amplified by overlap extension PCR [59] using primers, which contained the modified sequences. The genetically modified PCR product was cut with *Nhe*I/*Nco*I or *Nco*I/*Xho*I, ligated into the correspondingly digested 'Strep-*dcaA*p*dcaT*' or 'Strep-*pceA*p*dcaT*' plasmids and transformed into *S. blattae*. The presence of the desired mutation was again confirmed by DNA sequencing.

Cultivation of bacteria

For the heterologous production of the RDases together with DcaT, *S. blattae* strains were cultivated anaerobically in a defined mineral medium [16] in the presence of 0.02% yeast extract. Instead of 1 mL SL4, 0.2 mL of the SL10 trace element solution was added to the medium. The $CoCl_2$ concentration was adjusted to 8.66 μM using a 50-mM stock solution in ultrapure water. Glycerol (300 mM) was used as growth substrate and ampicillin (100 $\mu g \cdot mL^{-1}$) was added. For each cultivation, an LB (Luria-Bertani, [59])-grown preculture, which was cultivated overnight aerobically at 28 °C, was used for inoculation of a 20 mL LB-preculture grown aerobically at 28 °C for 7–8 h. From this second culture, a third preculture, which was grown anaerobically at 24 °C on the defined mineral medium described above, was inoculated. The initial optical density at 578 nm (OD_{578}) was adjusted to 0.1. At an OD_{578} of 1.2–2.1, the third preculture served as inoculum for the main culture [initial OD_{578} = 0.02 for *S. blattae* (Strep-*dcaA*p*dcaT*) or OD_{578} = 0.01 for *S. blattae* (Strep-*pceA*p*dcaT*)]. For strains producing variants of DcaA, 10 μM 5-OMeBza was added to the main culture, and for strains producing modified PceA proteins 10 μM DMB was amended. Both benzimidazoles were added from sterile and anaerobized 5 mM 5-OMeBza or 4 mM DMB stock solutions in ultrapure water. The cells were cultivated at 18 °C until an OD_{578} of 0.2–0.4 was reached. Recombinant protein production was induced by the addition of 200 $ng \cdot mL^{-1}$ anhydrotetracycline. *Shimwellia blattae* (Strep-*pceA*p*dcaT*) strains were harvested after 6 h by centrifugation (12 000 ***g***, 10 min, 10 °C) under aerobic conditions. *Shimwellia blattae* (Strep-*dcaA*p*dcaT*) strains were harvested 18 h after induction. The cell pellets

were stored at −20 °C. For strain maintenance *S. blattae* was cultivated in LB medium and stored at −80 °C in the presence of 15% glycerol.

RDase enzyme activity measurement and immunoblot

Activity measurements were performed with crude extract of the *S. blattae* strains. Therefore, cells of *S. blattae* were transferred into an anaerobic glove box (CoyLab, Grass Lake, MI, USA) and resuspended in anoxic 100 mM Tris/HCl buffer (pH 8.0; 2 mL per 1 g wet cells) amended with protease inhibitor (cOmplete Mini EDTA-free Protease Inhibitor Cocktail; Roche Diagnostics, Mannheim, Germany). With the addition of an equal volume of glass beads (0.25–0.5 mm diameter, Carl Roth GmbH, Karlsruhe, Germany), the cells were disrupted in a bead mill (Mixer Mill MM400; Retsch, Haan, Germany) at 30 Hz for 10 min. The supernatant obtained after centrifugation (2560 ***g***, 5 min), henceforth referred to as crude extract, was stored at −20 °C. Enzyme activity measurements were performed in technical triplicates as described previously [28]. The amount of protein from crude extract applied in the assay ranged from 43 to 560 μg. Enriched enzyme was present in concentrations of 1.3–41 μg. To test for the abiotic conversion of the substrates the crude extract was incubated anoxically at 95 °C for 15 min and protein debris was removed by centrifugation at 11 750 ***g*** for 5 min. The volume of heat-inactivated crude extract applied in the assay was the same as for the corresponding enzymatic activity measurement with native crude extract. After an incubation time of 20–60 min the reaction was stopped by oxidizing the remaining Ti(III) citrate with oxygen. The samples were transferred into GC vials and stored at −20 °C. The conversion of halogenated ethenes and ethanes was monitored by gas chromatography[16]. Retention times were as follows: 1,1,2,2-TeCA 12.8 min; 1,1,2-TCA 9.4 min; 1,2-DCA 5.8 min; 1,2-DBA 10.0 min; 1,2-DFA 1.6 min; PCE 9.8 min; TCE 6.9 min; *cis*-1,2-DCE 4.3 min; *trans*-1,2-DCE 3.5 min; VC 1.7 min; ethene 1.35 min; TBE 13.7 min; *cis*-1,2-DBE 9.0 min. All chemicals used in this study were purchased in highest available purity from Sigma-Aldrich (Munich, Germany) or abcr (Karlsruhe, Germany). Whenever mutant strains were tested for activity, the corresponding wild-type strain was cultivated in parallel and included in the activity assays as a reference allowing for direct comparison of specific activities. Each mutant was cultivated at least twice independently from each other. The protein concentrations were measured with the Bradford assay [60] using the Roti-Nanoquant reagent (Roth). Crude extracts of *S. blattae* strains (25 μg protein/lane) or enriched protein (2 μg protein/lane) were subjected to sodium dodecyl sulfate polyacrylamide gel electrophoresis (SDS/PAGE; 12.5%). The immunological analysis was conducted in accordance with Kunze *et al.* (2017) [28].

Generation of *in silico* structural models

The structural models of DcaA and PceA were generated using the I-TASSER server for protein structure and function prediction [36,37]. The best threading template used for structure prediction was $PceA_{Smul}$, which contains one norpseudo-B_{12} and two [4Fe–4S] cluster. The topology of the metal cofactors in the structural models was automatically defined by the I-TASSER platform based on their positioning in the threading template.

Enrichment of Strep-tagged RDases

The recombinant Strep-RDases were purified via affinity chromatography using Strep-Tactin Superflow column material (IBA). All steps were performed in an anaerobic glove box. The cells of the *S. blattae* strains were resuspended in anoxic 100 mM Tris/HCl buffer (pH 8.0; 2 mL per 1 g wet cells) amended with protease inhibitor, disrupted in a French Press at 2000 Psi (French Pressure Cell Press; Thermo Fisher Scientific, Germany) and subjected to ultracentrifugation (100 000 ***g***, 45 min, 4 °C; L8-M Ultracentrifuge, Rotor Ti70; Beckman Coulter, Krefeld, Germany). The supernatant was transferred to a Strep-Tactin column and eluted with 2.5 mM desthiobiotin (IBA). The RDase was copurified together with the DcaT chaperone. The eluate was concentrated to about 300–400 μL and subjected to SDS/PAGE and activity assay as described above or stored at −20 °C.

Cobamide extraction and analysis

The cobamide cofactor was extracted from crude extract of *S. blattae* strains and analyzed via HPLC according to a protocol reported by Keller *et al.* (2014) [61]. Cells were disrupted as described above in the RDase enzyme activity measurement section. The purified cobamides were analyzed via HPLC using a reverse phase column (Kinetex, 5 μM, C18, 100 Å, LC column, 250 × 4.6 mm; Phenomenex, Aschaffenburg, Germany). Separation was performed via isocratic elution at 30 °C using 14% methanol/0.2% acetic acid with a flow rate of 0.5 $mL \cdot min^{-1}$.

Acknowledgements

This work was financially supported by the DFG Research Unit FOR1530 (grant DI 314/14-2) and the Ernst Abbe Foundation. Peggy Brand-Schön is acknowledged for skillful technical assistance. *D. dichloroeliminans* DCA1 strain was kindly provided by Hauke Smidt (Wageningen University, The Netherlands) and Nico Boon (Ghent University, Belgium).

Author contributions

CK and TS conceived and designed the study. CK performed all experiments. All authors participated in data analysis, discussion, and writing of the manuscript.

References

1 Agency for Toxic Substances and Disease Registry (2013) Summary Data for 2013 Priority List of Hazardous Substances. US Department of Health and Human Services, Atlanta, Georgia, online at https://www.atsdr.cdc.gov/spl/resources/atsdr_2013_SPL_detailed_data_table.pdf, accessed May 17, 2017.

2 Agency for Toxic Substances and Disease Registry (2015) Summary Data for 2015 Priority List of Hazardous Substances. US Department of Health and Human Services, Atlanta, Georgia, online at https://www.atsdr.cdc.gov/spl/resources/atsdr_2015_spl_detailed_data_table.pdf, accessed May 17, 2017.

3 Adrian L & Löffler FE, eds (2016) Organohalide-Respiring Bacteria. Springer Verlag, Berlin Heidelberg.

4 Bommer M, Kunze C, Fesseler J, Schubert T, Diekert G & Dobbek H (2014) Structural basis for organohalide respiration. *Science* **346**, 455–458.

5 Payne KAP, Quezada CP, Fisher K, Dunstan MS, Collins FA, Sjuts H, Levy C, Hay S, Rigby SEJ & Leys D (2015) Reductive dehalogenase structure suggests a mechanism for B_{12}-dependent dehalogenation. *Nature* **517**, 513–516.

6 Nijenhuis I & Zinder SH (2005) Characterization of hydrogenase and reductive dehalogenase activities of *Dehalococcoides ethenogenes* strain 195. *Appl Environ Microbiol* **71**, 1664–1667.

7 John M, Schmitz RPH, Westermann M, Richter W & Diekert G (2006) Growth substrate dependent localization of tetrachloroethene reductive dehalogenase in *Sulfurospirillum multivorans*. *Arch Microbiol* **186**, 99–106.

8 Reinhold A, Westermann M, Seifert J, von Bergen M, Schubert T & Diekert G (2012) Impact of vitamin B_{12} on formation of the tetrachloroethene reductive dehalogenase in *Desulfitobacterium hafniense* Y51. *Appl Environ Microbiol* **78**, 8025–8032.

9 Palmer T & Berks BC (2012) The twin-arginine translocation (Tat) protein export pathway. *Nat Rev Microbiol* **10**, 483–496.

10 Hug LA, Maphosa F, Leys D, Löffler FE, Smidt H, Edwards EA & Adrian L (2013) Overview of organohalide-respiring bacteria and a proposal for a classification system for reductive dehalogenases. *Philos Trans R Soc Lond B Biol Sci* **368**, 20120322.

11 Judger B-E, Ertan H, Lee M, Manefield M & Marquis CP (2015) Reductive dehalogenases come of age in biological destruction of organohalides. *Trends Biotechnol* **33**, 595–610.

12 Schubert T & Diekert G (2016) Comparative biochemistry of organohalide respiration. In *Organohalide-Respiring Bacteria* (Adrian L & Löffler FE, eds), pp. 397–427. Springer Verlag, Berlin Heidelberg.

13 Fincker M & Spormann AM (2017) Biochemistry of catabolic reductive dehalogenation. *Annu Rev Biochem* **86**, 357–386.

14 Judger BE, Bohl S, Lebhar H, Healey RD, Manefield M, Marquis CP & Lee M (2017) A bacterial chloroform reductive dehalogenase: purification and biochemical characterization. *Microb Biotechnol* 1–9. https://doi.org/10.1111/1751-7915.12745

15 Alfán-Guzmán R, Ertan H, Manefield M & Lee M (2017) Isolation and characterization of *Dehalobacter sp.* strain TeCB1 including identification of TcbA: a novel tetra- and trichlorobenzene reductive dehalogenase. *Front Microbiol* **8**, 558.

16 Mac Nelly A, Kai M, Svatos A, Diekert G & Schubert T (2014) Functional heterologous production of reductive dehalogenases from *Desulfitobacterium hafniense* strains. *Appl Environ Microbiol* **80**, 4313–4322.

17 Parthasarathy A, Stich TA, Lohner ST, Lesnefsky A, Britt RD & Spormann AM (2015) Biochemical and EPR-spectroscopic investigation into heterologously expressed vinyl chloride reductive dehalogenase (VcrA) from *Dehalococcoides mccartyi* strain VS. *J Am Chem Soc* **137**, 3525–3532.

18 Neumann A, Wohlfarth G & Diekert G (1996) Purification and characterization of tetrachloroethene reductive dehalogenase from *Dehalospirillum multivorans*. *J Biol Chem* **271**, 16515–16519.

19 Schumacher W, Holliger C, Zehnder AJ & Hagen WR (1997) Redox chemistry of cobalamin and iron-sulfur cofactors in the tetrachloroethene reductase of *Dehalobacter restrictus*. *FEBS Lett* **409**, 421–425.

20 Maillard J, Schumacher W, Vazquez F, Regeard C, Hagen WR & Holliger C (2003) Characterization of the corrinoid iron-sulfur protein tetrachloroethene reductive dehalogenase of *Dehalobacter restrictus*. *Appl Environ Microbiol* **69**, 4628–4638.

21 Magnuson JK, Stern RV, Gossett JM, Zinder SH & Burris DR (1998) Reductive dechlorination of tetrachloroethene to ethene by a two-component enzyme pathway. *Appl Environ Microbiol* **64**, 1270–1275.

22 Miller E, Wohlfarth G & Diekert G (1998) Purification and characterization of the tetrachloroethene reductive dehalogenase of strain PCE-S. *Arch Microbiol* **169**, 497–502.

23 van de Pas BA, Gerritse J, de Vos WM, Schraa G & Stams AJM (2001) Two distinct enzyme systems are responsible for tetrachloroethene and chlorophenol

reductive dehalogenation in *Desulfitobacterium* strain PCE1. *Arch Microbiol* **176**, 165–169.
24 Suyama A, Yamashita M, Yoshino S & Furukawa K (2002) Molecular characterization of the PceA reductive dehalogenase of *Desulfitobacterium* sp. strain Y51. *J Bacteriol* **184**, 3419–3425.
25 Marzorati M, de Ferra F, Van Raemdonck H, Borin S, Allifranchini E, Carpani G, Serbolisca L, Verstraete W, Boon N & Daffonchio D (2007) A novel reductive dehalogenase, identified in a contaminated groundwater enrichment culture and in *Desulfitobacterium dichloroeliminans* strain DCA1, is linked to dehalogenation of 1,2-dichloroethane. *Appl Environ Microbiol* **73**, 2990–2999.
26 De Wildeman S, Diekert G, Van Langenhove H & Verstraete W (2003) Stereoselective microbial dehalorespiration with vicinal dichlorinated alkanes. *Appl Environ Microbiol* **69**, 5643–5647.
27 Miller E, Wohlfarth G & Diekert G (1997) Studies on tetrachloroethene respiration in *Dehalospirillum multivorans*. *Arch Microbiol* **166**, 379–387.
28 Kunze C, Bommer M, Hagen WR, Uksa M, Dobbek H, Schubert T & Diekert G (2017) Cobamide-mediated enzymatic reductive dehalogenation via long-range electron transfer. *Nat Commun* **8**, 15858.
29 Maillard J, Genevaux P & Holliger C (2011) Redundancy and specificity of multiple trigger factor chaperones in *Desulfitobacteria*. *Microbiology* **157**, 2410–2421.
30 Morita Y, Futagami T, Goto M & Furukawa K (2009) Functional characterization of the trigger factor protein PceT of tetrachloroethene-dechlorinating *Desulfitobacterium hafniense* Y51. *Appl Microbiol Biotechnol* **83**, 775–781.
31 Cooper M, Wagner A, Wondrousch D, Sonntag F, Sonnabend A, Brehm M, Schüürmann G & Adrian L (2015) Anaerobic microbial transformation of halogenated aromatics and fate prediction using electron density modeling. *Environ Sci Technol* **49**, 6018–6028.
32 Liao R-Z, Chen S-L & Siegbahn PEM (2015) Which oxidation state initiates dehalogenation in the B_{12}-dependent enzyme NpRdhA, Co^{I}, Co^{II} or Co^{0}? *ACS Catal* **5**, 7350–7358.
33 Tang S & Edwards EA (2013) Identification of *Dehalobacter* reductive dehalogenases that catalyse dechlorination of chloroform, 1,1,1-trichloroethane and 1,1-dichloroethane. *Philos Trans R Soc Lond B Biol Sci* **368**, 20120318.
34 Ding C, Zhao S & He J (2014) A *Desulfitobacterium* sp. strain PR reductively dechlorinates both 1,1,1-trichloroethane and chloroform. *Environ Microbiol* **16**, 3387–3397.
35 Ye L, Schilhabel A, Bartram S, Boland W & Diekert G (2010) Reductive dehalogenation of brominated ethenes by *Sulfurospirillum multivorans* and *Desulfitobacterium hafniense* PCE-S. *Environ Microbiol* **12**, 501–509.
36 Zhang Y (2008) I-TASSER server for protein 3D structure prediction. *BMC Bioinformatics* **9**, 40.
37 Roy A, Kucukural A & Zhang Y (2010) I-TASSER: a unified platform for automated protein structure and function prediction. *Nat Protoc* **5**, 725–738.
38 Payne KAP, Fisher K, Sjuts H, Dunstan MS, Bellina B, Johannissen L, Barran P, Hay S, Rigby SEJ & Leys D (2015) Epoxyqueuosine reductase structure suggests a mechanism for cobalamin-dependent tRNA modification. *J Biol Chem* **290**, 27572–27581.
39 Dowling DP, Miles ZD, Köhrer C, Maiocco SJ, Elliott SJ, Bandarian V & Drennan CL (2016) Molecular basis of cobalamin-dependent RNA modification. *Nucleic Acids Res* **44**, 9965–9976.
40 Yang J, Wang Y & Zhang Y (2016) ResQ: an approach to unified estimation of B-factor and residue-specific error in protein structure prediction. *J Mol Biol* **428**, 693–701.
41 van de Pas BA, Smidt H, Hagen WR, van der Oost J, Schraa G, Stams AJM & de Vos WM (1999) Purification and molecular characterization of *ortho*-chlorophenol reductive dehalogenase, a key enzyme of halorespiration in *Desulfitobacterium dehalogenans*. *J Biol Chem* **274**, 20287–20292.
42 Grostern A & Edwards EA (2009) Characterization of a *Dehalobacter* coculture that dechlorinates 1,2-dichloroethane to ethene and identification of the putative reductive dehalogenase gene. *Appl Environ Microbiol* **75**, 2684–2693.
43 Marzorati M, Balloi A, de Ferra F, Corallo L, Carpani G, Wittebolle L, Verstraete W & Daffonchio D (2010) Bacterial diversity and reductive dehalogenase redundancy in a 1,2-dichloroethane-degrading bacterial consortium enriched from a contaminated aquifer. *Microb Cell Fact* **9**, 12.
44 Merlino G, Balloi A, Marzorati M, Mapelli F, Rizzi A, Lavazza D, de Ferra F, Carpani G & Daffonchio D (2015) Diverse reductive dehalogenases are associated with *Clostridiales*-enriched microcosms dechlorinating 1,2-dichloroethane. *Biomed Res Int* **2015**, 242856.
45 Cretnik S, Bernstein A, Shouakar-Stash O, Löffler F & Elsner M (2014) Chlorine isotope effects from isotope ratio mass spectrometry suggest intramolecular C-Cl bond competition in trichloroethene (TCE) reductive dehalogenation. *Molecules* **19**, 6450–6473.
46 Heckel B, Cretnik S, Kliegman S, Shouakar-Stash O, McNeill K & Elsner M (2017) Reductive outer-sphere single electron transfer is an exception rather than the rule in natural and engineered chlorinated ethene dehalogenation. *Environ Sci Technol* **51**, 9663–9673.

47 Adrian L, Rahnenführer J, Gobom J & Hölscher T (2007) Identification of a chlorobenzene reductive dehalogenase in *Dehalococcoides* sp. strain CBDB1. *Appl Environ Microbiol* **73**, 7717–7724.
48 Boyer AB, Pagé-Bélanger R, Saucier M, Villemur R, Lépine F, Juteau P & Beaudet R (2003) Purification, cloning and sequencing of an enzyme mediating the reductive dechlorination of 2,4,6-trichlorophenol from *Desulfitobacterium frappieri* PCP-1. *Biochem J* **373**, 297–303.
49 Thibodeau J, Gauthier A, Duguay M, Villemur R, Lépine F, Juteau P & Beaudet R (2004) Purification, cloning and sequencing of a 3,5-dichlorophenol reductive dehalogenase from *Desulfitobacterium frappieri* PCP-1. *Appl Environ Microbiol* **70**, 4532–4537.
50 Chen K, Huang L, Xu C, Liu X, He J, Zinder SH, Li S & Jiang J (2013) Molecular characterization of the enzymes involved in the degradation of a brominated aromatic herbicide. *Mol Microbiol* **89**, 1121–1139.
51 Christiansen N, Ahring BK, Wohlfarth G & Diekert G (1998) Purification and characterization of the 3-chloro-4-hydroxy-phenylacetate reductive dehalogenase of *Desulfitobacterium hafniense*. *FEBS Lett* **436**, 159–162.
52 Krasotkina J, Walters T, Maruya KA & Ragsdale SW (2001) Characterization of the B_{12}- and iron-sulfur-containing reductive dehalogenase from *Desulfitobacterium chlororespirans*. *J Biol Chem* **276**, 40991–40997.
53 Goris T, Schiffmann CL, Gadkari J, Schubert T, Seifert J, Jehmlich N, von Bergen M & Diekert G (2015) Proteomics of the organohalide-respiring Epsilonproteobacterium *Sulfurospirillum multivorans* adapted to tetrachloroethene and other energy substrates. *Sci Rep* **5**, 13794.
54 Kublik A, Deobald D, Hartwig S, Schiffmann CL, Andrades A, von Bergen M, Sawers RG & Adrian L (2016) Identification of a multi-protein reductive dehalogenase complex in *Dehalococcoides mccartyi* strain CBDB1 suggests a protein-dependent respiratory electron transport chain obviating quinone involvement. *Environ Microbiol* **18**, 3044–3056.
55 Mayer-Blackwell K, Sewell H, Fincker M & Spormann AM (2016) Comparative physiology of organohalide-respiring bacteria. In *Organohalide-Respiring Bacteria* (Adrian L & Löffler FE, eds), pp. 259–280. Springer Verlag, Berlin Heidelberg.
56 Zhao S, Ding C & He J (2015) Detoxification of 1,1,2-trichloroethane to ethene by *Desulfitobacterium* and identification of its functional reductase gene. *PLoS ONE* **10**, e0119507.
57 Fathepure BZ & Tiedje JM (1994) Reductive dechlorination of tetrachloroethylene by a chlorobenzoate-enriched biofilm reactor. *Environ Sci Technol* **28**, 746–752.
58 Sambrook J, Fritsch EF & Maniatis T (1989) Molecular Cloning: A Laboratory Manual, 2nd edn. Cold Spring Harbor Laboratory Press, Cold Spring Harbor, NY, USA.
59 Higuchi R, Krummel B & Saiki RK (1988) A general method of *in vitro* preparation and specific mutagenesis of DNA fragments: study of protein and DNA interactions. *Nucleic Acids Res* **16**, 7351–7367.
60 Bradford MM (1976) A rapid and sensitive method for the quantification of microgram quantities of protein utilizing the principle of protein-dye binding. *Anal Biochem* **72**, 248–254.
61 Keller S, Ruetz M, Kunze C, Kräutler B, Diekert G & Schubert T (2014) Exogenous 5,6-dimethylbenzimidazole caused production of a non-functional tetrachloroethene reductive dehalogenase in *Sulfurospirillum multivorans*. *Environ Microbiol* **16**, 3361–3369.

Supporting information

Additional Supporting Information may be found online in the supporting information tab for this article:

Table S1. Plasmids used in this study.

Table S2. Oligonucleotides used for plasmid constructions.

Fig. S1. Amino acid sequence alignment of selected RDases.

2.5 Selective, light-driven enzymatic dehalogenations of organic compounds

Siritanaratkul B, Islam STA, Schubert T, Kunze C, Goris T, Diekert G, Armstrong FA (2016) *RSC Adv* 6, 84882-84886.

So far, activity assays with RDases were conducted using chemical electron mediators, whereby the entry point of the electrons into the RDase and its mechanism was not known. In this study, evidence for the interfacial electron transfer from an external electron source via the iron-sulfur cluster to the active site is given for PceA of *S. multivorans*. In addition, a setup was established allowing for reductive dehalogenation of chlorinated ethenes by PceA bound to an electrode that is driven by UV light, thus offering a future perspective for its use in bioremediation of organohalide-contaminated sites, which still belong to the most frequently detected and most toxic and hazardous pollutants in the environment.

My own contribution to this publication covers about 10%.
This includes the cultivation of the mutant strain *S. multivorans* GD21 and the purification of PceA. During a two week stay at the University of Oxford I participated in electrochemical measurements (cyclic voltammograms) using PceA bound to a PGE electrode. Furthermore, I participated in the revision of the manuscript.

For supplementary information see appendix, pp. lxv - lxvii.

RSC Advances

PAPER

View Article Online
View Journal | View Issue

Cite this: *RSC Adv.*, 2016, **6**, 84882

Selective, light-driven enzymatic dehalogenations of organic compounds†

Bhavin Siritanaratkul,[a] Shams T. A. Islam,[a] Torsten Schubert,[b] Cindy Kunze,[b] Tobias Goris,[b] Gabriele Diekert[b] and Fraser A. Armstrong*[a]

Received 4th August 2016
Accepted 24th August 2016

DOI: 10.1039/c6ra19777a

www.rsc.org/advances

Tetrachloroethene reductive dehalogenase (PceA), a corrinoid-containing enzyme from *Sulfurospirillum multivorans*, is highly active for the sequential reduction of the organohalide tetrachloroethene (PCE) to trichloroethene (TCE), then regiospecifically to *cis*-1,2-dichloroethene (cDCE). We demonstrate direct electron transfer from graphite and semiconductor electrodes to PceA adsorbed onto the electrode surface. Colloidal TiO_2 nanoparticles modified with PceA efficiently carry out the sequence of dehalogenation reactions under UV light irradiation.

Introduction

Enzymes can be coupled to semiconductors that provide electrons or holes under light irradiation, thus directing catalysis of highly selective redox reactions. So far, most of these reactions have been related to solar fuels (artificial photosynthesis). Systems based upon non-toxic TiO_2 have been constructed for H_2 production and CO_2 reduction, using hydrogenases[1] and carbon monoxide dehydrogenases (CODH),[2,3] respectively. As part of a program to extend research to alternative organic targets, a flavocytochrome c_3 fumarate reductase was recently used to demonstrate C=C hydrogenation using electrons from dye-sensitized TiO_2 nanoparticles.[4]

In a completely different context, semiconductors have been studied for their application in light-driven decomposition of chlorinated organic compounds that are common toxic contaminants in water. For example, trichloroethene (TCE) has been used as a model target for studying photocatalytic decomposition of organohalides on TiO_2.[5,6] This non-specific process is enhanced by the presence of O_2, as the mechanism probably proceeds by generation of oxygen radicals on the bare TiO_2 surface. These radicals react with TCE through a complex series of steps to yield a mixture of products such as phosgene, HCl, CO and CO_2.

Enzymes offer possibilities for highly controlled dehalogenation reactions, some of which could have analytical or synthetic use. *Sulfurospirillum multivorans* (previously known as *Dehalospirillum multivorans*) is a bacterium that can use tetrachloroethene (commonly known as perchloroethylene, or PCE) or trichloroethene (TCE) as electron acceptors in anaerobic respiration.[7,8] Tetrachloroethene is thereby selectively reduced *via* trichloroethene (TCE) to *cis*-1,2-dichloroethene (*c*DCE), as shown in eqn (1) and 2.

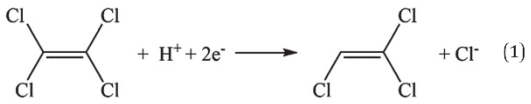

(1)

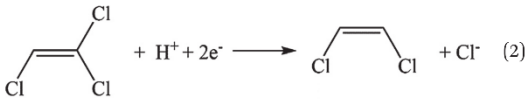

(2)

The terminal reductase in this process, the PCE reductive dehalogenase (PceA),[9] contains a corrinoid (norpseudo-B_{12})[10] and iron sulfur clusters as cofactors; its structure was recently determined.[11] Two [4Fe–4S] clusters are located close to the co-containing norpseudo-B_{12}, allowing electron transport from the enzyme surface to the buried active site.

By analogy with ongoing strategies in artificial photosynthesis, the highly specific reductive dechlorination reactions catalysed by reductive dehalogenases should be possible using light-activated semiconductors. Unlike artificial photosynthesis, however, chemical energy is not stored: sequential conversions of PCE to TCE and TCE to *c*DCE are both thermodynamically favourable, based on estimated reduction potentials (pH 7) of +0.58 V and +0.54 V respectively.[12] As well as greatly accelerating rates, the enzyme ensures both substrate specificity and regiospecificity (the latter for eqn (2)).

We have now explored the extension of enzyme-semiconductor strategies to achieve selective reductive dehalogenation of

[a]*Inorganic Chemistry Laboratory, Department of Chemistry, University of Oxford, South Parks Road, Oxford OX1 3QR, Oxfordshire, UK*

[b]*Institut für Mikrobiologie, Friedrich-Schiller-Universität Jena, Lehrstuhl für Angewandte und Ökologische Mikrobiologie, Philosophenweg 12, 07743 Jena, Germany*

† Electronic supplementary information (ESI) available. See DOI: 10.1039/c6ra19777a

View Article Online
Paper RSC Advances

compounds such as PCE and TCE, using UV light and colloidal anatase TiO_2 (bandgap 3.2 eV). The activity of PceA has previously been studied by chemical assays[9] and cyclic voltammetry in the presence of electron mediators, but no evidence for direct interfacial electron transfer with a conducting surface has been reported.[13] Therefore, we first investigated the direct adsorption of PceA onto different electrodes, in order to establish that direct interfacial electron transfer to PceA is feasible.

Results and discussion

All electrochemical measurements were performed under anaerobic conditions in a glove box (Belle Technologies, O_2 < 3 ppm). Fig. 1 shows cyclic voltammograms obtained with PceA adsorbed on a stationary pyrolytic graphite edge (PGE) electrode. Briefly, the surface of the PGE electrode was abraded with sandpaper, then 1 μL of PceA solution (21 μM) was applied. Upon injection of an aliquot of TCE, dissolved in ethanol, yielding 0.8 mM final concentration in the aqueous cell solution, a sharp reduction wave appears with an onset potential of −0.45 V *vs.* SHE at pH 7. At an electrode such as PGE that shows metallic conductivity properties, the onset potential for an adsorbed enzyme catalyzing an irreversible reaction is related to the potential of the redox centre at which electrons enter or leave the enzyme:[14] in this case one of the two [4Fe–4S] clusters is the likely entry site. The decrease in reduction current that is observed on subsequent cycles is mainly due to evaporation of the volatile substrate, and to a lesser extent due to film loss. The isolated norpseudo-B_{12} cofactor was also tested with a PGE electrode, but did not show any activity towards catalytic TCE reduction.

To establish that PceA adsorbs on TiO_2 nanoparticles (P25: anatase/rutile ratio approx. 3/1), the UV-vis absorbance of a solution of PceA was recorded before and after stirring with TiO_2 particles (1 mg mL^{-1}) for 20 min (Fig. 2). At the enzyme concentration for the photochemical reaction described in the following section (21 nM), the UV-vis absorbance of the enzyme was too low to be observed clearly, therefore a more concentrated solution was used (0.1 μM). Even at this higher concentration, the enzyme was almost totally adsorbed from solution onto the TiO_2 particles after stirring for 20 min. It is therefore reasonable to assume that at the lower enzyme concentration used for the photochemical experiments, the adsorption of PceA onto TiO_2 is at least 90% complete, although it is unlikely that all enzyme molecules are attached in an optimal way for interfacial electron transfer.

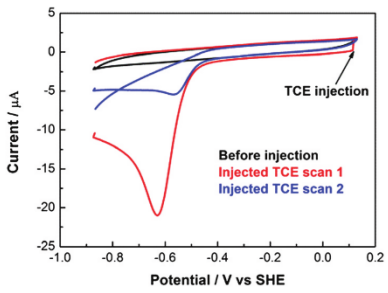

Fig. 1 Cyclic voltammograms of PceA on a pyrolytic graphite 'edge' (PGE) electrode, before and after injection of the substrate, trichloroethene (TCE). Reaction conditions: Tris buffer 0.1 M, pH 7.0, 25 °C, scan rate 20 mV s^{-1}, electrode is stationary.

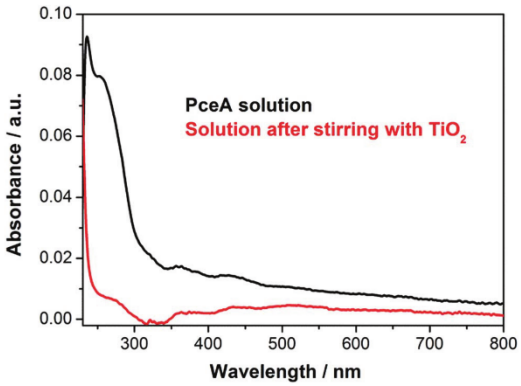

Fig. 2 UV-vis absorbance of PceA (0.1 μM) in Tris buffer pH 7.0, before and after stirring with TiO_2 particles (1 mg mL^{-1}).

Fig. 3 shows the activity of PceA adsorbed on a TiO_2 electrode. The electrode was constructed by depositing TiO_2 nanoparticles on an conducting indium tin oxide (ITO) surface, as described previously.[15] Compared to metallic-like PGE, n-type TiO_2 attains significant conductivity only when a more negative potential is applied (the flat-band potential is a guide[15]) and background cycles each show a prominent trumpet-like shape that shifts to more negative potential with increasing pH. Adsorption of enzyme does not alter the voltammetric response compared to bare TiO_2. As shown in Fig. 3A, injections of TCE (0.8 mM) result in a catalytic net reduction current that commences once the electrode potential has entered the conductive region of TiO_2. The background-subtracted cyclic voltammograms shown in Fig. 3B confirm that PceA is active in the pH range 6–8, and that pH 7 is a suitable condition for experiments with TiO_2. In similar experiments, using PCE (0.8 mM) as the substrate instead of TCE (Fig. 3C and D), reduction currents were also observed. Control experiments with no enzyme confirmed that neither PCE or TCE were reduced on either bare PGE or TiO_2 electrodes; therefore the observed reduction current is due to enzyme catalysis. These measurements showed that PceA can receive electrons from TiO_2 and use the electrons in the reductive dehalogenation of TCE and PCE.

Light-driven conversion of TCE or PCE to *c*DCE under anaerobic conditions was demonstrated in a colloidal system. Irradiation with UV light generates electron–hole pairs in TiO_2 particles. The electrons are transferred to PceA to drive the reduction of PCE or TCE, and the holes are quenched by electrons from the amine buffer, Tris.[1] Particular care was taken to minimize losses of chlorinated ethenes by using a gas-tight

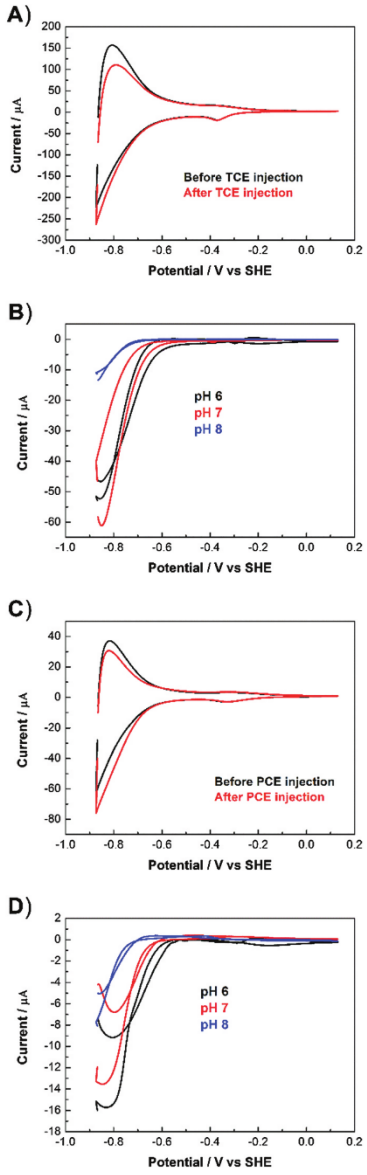

Fig. 3 Cyclic voltammograms of PceA adsorbed on a TiO_2 electrode. Panel (A) shows the current before (black line) and after (red line) injection of TCE (final concentration 0.8 mM). Panel (B) shows the blank-subtracted voltammograms at pH 6–8. Panels (C) and (D) are the same experiments, but with injection of 0.8 mM PCE instead of TCE. Reaction conditions: Tris buffer, 25 °C, 20 mV s^{-1}, stationary electrode, no gas flow.

vessel and avoiding rubber septa that absorb the volatile compounds. In a typical experiment, a solution of PceA (0.17 nmol) in 8 mL of Tris buffer (Tris 100 mM, pH 7.0), was mixed with TiO_2 particles (P25, 8 mg) and the suspension was placed in a vial suitable for near-UV transmission and closed tightly with a Teflon seal. A solution of the substrate, either tetrachloroethene (PCE) or trichloroethene (TCE) in ethanol, was injected into the suspension before sealing the vial and commencing irradiation with a UV lamp (365 nm, 8 W, 1.5 cm distance). Small aliquots (0.5 mL) of the solution were sampled periodically by syringe extraction through the Teflon seal, and the product was detected and quantified by GC-MS headspace analysis. The temperature of the suspension increased by 5–6 °C (typical values being 24 °C to 30 °C) over 4 h of irradiation (it was not practical to thermostat the vial). Errors arising from the sample transfers for GC-MS analysis and calibration were minimized as far as practically feasible.

Fig. 4A shows the consumption of TCE and concurrent production of *c*DCE under UV irradiation, reproducibly reaching 85% conversion after 2 h. The subsequent decrease in activity varied from one experiment to another but is likely due

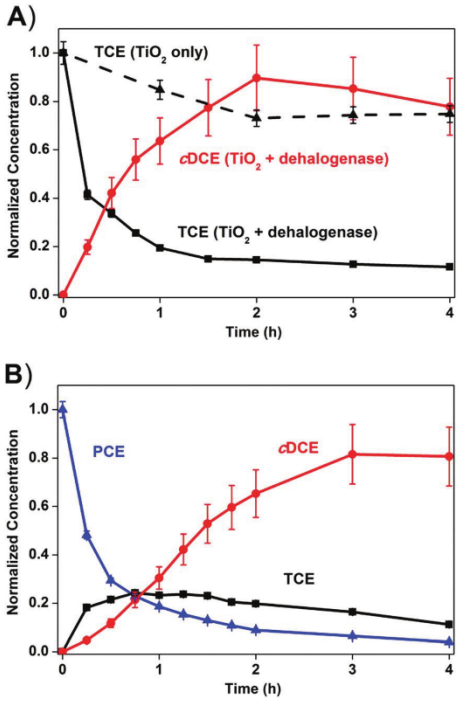

Fig. 4 Enzymatic reductive dechlorination by UV irradiation of TiO_2–PceA. (A) Time courses of concentrations of trichloroethene (TCE, solid black line) and *cis*-1,2-dichloroethene (*c*DCE, red line) in sealed, aqueous TiO_2–PceA suspensions, under UV irradiation, commencing from an initial TCE concentration of 0.55 mM. The control reaction with no enzyme is shown in dashed black line; no *c*DCE was detected in the control. (B) A similar set up, but starting with tetrachloroethene (PCE, blue line) in solution at 0.26 mM. Normalized concentrations of TCE and *c*DCE are shown as black and red lines, respectively. In the control reaction without enzyme (not shown), neither TCE nor *c*DCE could be detected. Conditions given in text.

View Article Online
Paper RSC Advances

to slow enzyme deactivation caused by oxidative damage from the valence-band holes. Control experiments with TiO_2 but no enzyme showed a decrease to *ca.* 70% of the starting TCE concentration after 4 h: the latter is ascribed to decomposition on bare TiO_2 and, to a lesser extent, losses during sampling. It is known that chlorinated organic compounds undergo slow photo-decomposition on TiO_2 under anaerobic conditions, giving CO_2 and HCl as final products.[16] In our own study (see control reaction included in Fig. 4A) we also noted that TCE undergoes decomposition[5] on bare TiO_2, albeit at a much slower rate than the enzymatic pathway. Photocatalysis of TCE on bare TiO_2 does not produce *c*DCE,[5] and PceA is required for the specific reduction of TCE to *c*DCE to occur.

For the experiment starting with PCE in the solution (Fig. 4B), production of both TCE and *c*DCE was observed after irradiation, with the TCE concentration reaching a maximum value after approximately 0.75 h, before decreasing due to conversion to *c*DCE. When only *c*DCE was present at the start of the reaction, no difference between reaction solutions with and without the enzyme was observed (see ESI, Fig. S1†), showing that some of the slight decrease in *c*DCE concentration (after more than 2 h referring to Fig. 4A) is due to slow decomposition on bare TiO_2. Reductive dechlorination by PceA thus terminates at *c*DCE, which is not reduced further. Cyclic voltammograms of PceA with *c*DCE injections also showed no reduction current (see ESI, Fig. S2†), in agreement with previous reports that *c*DCE is not a substrate for this enzyme.[9]

Together, the results demonstrate rapid and sequential photo-driven conversion of PCE to TCE and finally *c*DCE by PceA.

From the maximum product concentration obtained and the molecular mass of PceA based on crystallography (52.3 kDa calculated for a monomer),[11] we estimated the turnover number (TON) at 18 000 per enzyme active site for *c*DCE production after 4 h, and an average turnover frequency (TOF) of 2.4 s^{-1} (per enzyme active site). Both TON and TOF are lower limits for their true values, because not all enzyme molecules are likely to be adsorbed onto TiO_2 in an electroactive configuration, and the product *c*DCE is slowly decomposed on bare TiO_2. The TOF from the photochemical experiments is an order of magnitude lower than the TOF value (*ca.* 90 s^{-1}) measured by a chemical assay using reduced methyl viologen.[11]

In an attempt to see if visible light could be utilized, we modified the TiO_2 nanoparticles with a Ru-based dye [$(Ru(bpy)_2(4,4\text{-}(PO_3H_2)_2bpy))Br_2$ (bpy = 2,2-bipyridine)] as used in previous systems with CODH or flavocytochrome c_3 fumarate reductase.[2,4] Upon visible light irradiation ($\lambda > 420$ nm), the dye–TiO_2–PceA system was able to convert TCE to *c*DCE, although at a much lower rate (see ESI, Fig. S3†). It may be possible to replace the dye–TiO_2 system with a native visible-light active semiconductor, and this is currently under investigation.

This report provides proof of principle that reductive dehalogenases can be harnessed for solar-driven transformations of halogenated organic compounds. Several reductive dehalogenases have been characterized, each one displaying a characteristic spectrum of substrates and products,[17,18] and future research could incorporate these various enzymes into similar semiconductor-based light systems for selective halogen/H substitutions.

Conclusions

We have established the scope for selective light-driven reductive dehalogenation of organohalides using enzyme-modified semiconductor nanoparticles. Specifically, our discovery of a hybrid enzyme/materials pathway for the direct conversion of PCE to TCE and *c*DCE provides an interesting and conceptually valuable addition to the library of solar-to-chemical processes currently being studied.

Experimental

Materials

Tris buffer solutions were prepared by dissolving Tris (Tris(hydroxymethyl)aminomethane, Fisher, 99.8%) and $(NH_4)_2SO_4$ (Fisher, 99.8%) in purified water (Millipore, 18 MΩ cm) and titrating to the desired pH using HCl or NaOH.

Tetrachloroethene (PCE, Sigma Aldrich, 99%), trichloroethene (TCE, Sigma Aldrich, 99.5%), *cis*-1,2-dichloroethene (*c*DCE, Sigma Aldrich, 97%), and ethanol (Sigma Aldrich, 99.8%) were used without further purification.

Enzyme purification

The dehalogenase PceA was purified from a *Sulfurospirillum multivorans* mutant strain producing PceA with a C-terminal Strep-Tag. The strain was cultivated in 12 L pyruvate/fumarate-containing medium[8] in the presence of 0.72 mM $FeSO_4$ and kanamycin. The cells were harvested under oxic conditions before disruption *via* French Press under anaerobic conditions. The $PceA_{strep}$ product was purified under anoxic conditions *via* gravity flow using Strep-Tactin (IBA, Göttingen, Germany) as described previously.[9,11] A total of 2.3 mg of PceA-Strep were obtained from 1.9 g cell protein. The enzyme was stored at −80 °C.

Protein film electrochemistry

All electrochemical measurements were conducted in a glove box under an N_2 atmosphere (Belle Technologies, $O_2 < 3$ ppm). A single-compartment cell with a water jacket was used with a 3-electrode setup: PGE or TiO_2 (as working electrodes), Pt wire (as counter electrode), and Ag/AgCl (as reference electrode). An Autolab PGSTAT30 potentiostat controlled by Nova software (EcoChemie) was used to record voltammograms. The surface of the PGE electrode was abraded with sandpaper (P400 Tufbak Durite) and rinsed with deionized water before applying enzyme solution (typically 1 μL) to the electrode surface. After waiting for approximately 30 s, the electrode was placed in the cell and measurements were initiated. The compounds PCE, TCE, and *c*DCE were dissolved in EtOH before injecting into the cell.

Electrode preparation

Pyrolytic graphite 'edge' (PGE) electrodes were fabricated in-house; a small piece of pyrolytic graphite was embedded in

epoxy resin within a Teflon casing containing a metal contact rod. The graphite was oriented so that the basal planes were perpendicular to the surface (approximately 0.03 cm^2).

The TiO_2 electrodes were fabricated with TiO_2 particles (P25, Degussa) on ITO slides (SPI Supplies, 1.1 mm thick, 8–12 Ω) using the doctor's blade method. The TiO_2 coated ITO slides were calcined in air at 450 °C for 30 min. A copper wire was attached with silver paint, then the exposed surfaces were covered with epoxy.

UV-vis spectroscopy

Absorbance spectra were recorded with a Perkin-Elmer Lambda 19 UV-vis spectrometer using quartz cuvettes. The spectrum of the PceA solution (5.95 μg mL^{-1} in Tris buffer pH 7) was measured before and after stirring (following centrifugation) with TiO_2 particles (1 mg mL^{-1}) for 20 min.

Photochemical reactions

A sample of TiO_2 particles (P25, Degussa, 7 mg) was sonicated in Tris buffer (pH 7, 7 mL) for 15 min, then 7 μL of PceA solution (1.19 mg mL^{-1}) was added to the suspension which was stirred for a further 20 min. The substrate solution, either PCE or TCE in EtOH, was added and the reaction vessel was sealed with a Teflon cap. Note that TCE is known to dissolve rubber, therefore rubber stoppers should be avoided for prolonged reactions. A UV lamp (UVL-28 EL series, 365 nm, 8 W, held at 1.5 cm distance) was used to illuminate the vessel under continuous stirring. Periodically, a 0.5 mL sample of the liquid phase was taken for product detection by GC-MS headspace analysis (Agilent 7890B, HP5 column, He carrier gas). The GC sampling vial was incubated at 60 °C for 5 min before a sample of the headspace was taken. The GC oven was held at 40 °C for 5 min from injection, then ramped up to 290 °C at a rate of 50 °C min^{-1}. Calibration was established with standard solutions of PCE, TCE, and *c*DCE. The cell was not thermostatted: during irradiation, the temperature of the solution increased from 24 °C to 30 °C over the course of 4 h.

Acknowledgements

We thank James Wickens for assistance with GC-MS measurements. Financial support for CK, TS, GD and TG in the framework of the German Research Foundation (DFG) Research Unit FOR 1530 is gratefully acknowledged. FAA is a Royal Society-Wolfson Research Merit Award holder.

References

1 E. Reisner, D. J. Powell, C. Cavazza, J. C. Fontecilla-Camps and F. A. Armstrong, *J. Am. Chem. Soc.*, 2009, **131**, 18457–18466.
2 T. W. Woolerton, S. Sheard, E. Reisner, E. Pierce, S. W. Ragsdale and F. A. Armstrong, *J. Am. Chem. Soc.*, 2010, **132**, 2132–2133.
3 A. Bachmeier and F. Armstrong, *Curr. Opin. Chem. Biol.*, 2015, **25**, 141–151.
4 A. Bachmeier, B. J. Murphy and F. A. Armstrong, *J. Am. Chem. Soc.*, 2014, **136**, 12876–12879.
5 J. Fan and J. T. Yates, *J. Am. Chem. Soc.*, 1996, **118**, 4686–4692.
6 M. D. Driessen, A. L. Goodman, T. M. Miller, G. A. Zaharias and V. H. Grassian, *J. Phys. Chem. B*, 1998, **102**, 549–556.
7 A. Neumann, H. Scholz-Muramatsu and G. Diekert, *Arch. Microbiol.*, 1994, **162**, 295–301.
8 H. Scholz-Muramatsu, A. Neumann, M. Meßmer, E. Moore and G. Diekert, *Arch. Microbiol.*, 1995, **163**, 48–56.
9 A. Neumann, G. Wohlfarth and G. Diekert, *J. Biol. Chem.*, 1996, **271**, 16515–16519.
10 B. Kräutler, W. Fieber, S. Ostermann, M. Fasching, K.-H. Ongania, K. Gruber, C. Kratky, C. Mikl, A. Siebert and G. Diekert, *Helv. Chim. Acta*, 2003, **86**, 3698–3716.
11 M. Bommer, C. Kunze, J. Fesseler, T. Schubert, G. Diekert and H. Dobbek, *Science*, 2014, **346**, 455–458.
12 T. M. Vogel, C. S. Criddle and P. L. McCarty, *Environ. Sci. Technol.*, 1987, **21**, 722–736.
13 G. Diekert, D. Gugova, B. Limoges, M. Robert and J.-M. Savéant, *J. Am. Chem. Soc.*, 2005, **127**, 13583–13588.
14 S. V. Hexter, T. F. Esterle and F. A. Armstrong, *Phys. Chem. Chem. Phys.*, 2014, **16**, 11822.
15 A. Bachmeier, V. C. C. Wang, T. W. Woolerton, S. Bell, J. C. Fontecilla-Camps, M. Can, S. W. Ragsdale, Y. S. Chaudhary and F. A. Armstrong, *J. Am. Chem. Soc.*, 2013, **135**, 15026–15032.
16 P. Calza, C. Minero and E. Pelizzetti, *Environ. Sci. Technol.*, 1997, **31**, 2198–2203.
17 B.-E. Jugder, H. Ertan, S. Bohl, M. Lee, C. P. Marquis and M. Manefield, *Front. Microbiol.*, 2016, **7**.
18 T. Schubert and G. Diekert, in *Organohalide Respiring Bacteria*, ed. L. Adrian and F. E. Loffler, Springer-Verlag Berlin Heidelberg, in press.

3 Discussion

Organohalides belong to the most abundant pollutants in the environment. Due to their recalcitrant carbon-halide bonds and toxicity, bioremediation attempts have to be intensified. A potential solution is provided by a special group of bacteria, called organohalide-respiring bacteria, which is able to utilize these halogenated compounds as electron acceptors in a respiratory chain (summarized in Adrian and Löffler, 2016). The use of a cobamide cofactor for the reductive dehalogenation of these compounds makes RDases unique among terminal reductases. However, their in-depth biochemical investigation was still pending.

3.1 RDases as a new class of cobamide-dependent enzymes with a unique three-dimensional structure

In this study, the cultivation of *S. multivorans* and the isolation of its tetrachloroethene-converting PceA was optimized to provide the required quantity of protein in a quality to allow for detailed structural and functional analysis. Thus, the first crystal structure for a respiratory RDase was resolved by X-ray crystallography. The PceA crystal structure showed the enzyme in a homodimeric arrangement with a large interface formed mainly by the cobamide binding domains with their typical nitroreductase fold, whereby each monomer harbors all cofactors and is independently active (ch. 2.1). In parallel to the results obtained here, the crystal structure of the non-respiratory *ortho*-dibromophenol reductase (NpRdhA) from *Nitratireductor pacificus* pHt-3B, described to reduce 3,5-dibromo-4-hydroxybenzoate in a halogen substitution reaction, was elucidated (Payne *et al.*, 2015a). Although the NpRdhA structure is monomeric, the protein sequence is about 50% longer than PceA and encodes two duplicated cobamide-binding domains, which are positioned in a way that they resemble the PceA dimer. Here, only one of the two domains binds the cofactor, the other one is likely a consequence of gene duplication and divergence (Payne *et al.*, 2015a). Both RDase structures, a PceA monomer compared to NpRdhA, displayed the same arrangement of the cofactors. Given the fact that the enzymes share only 28% protein sequence identity and represent distinct classes of RDases with regard to main substrate ranges, cofactor positioning is assumed to be a conserved feature

in RDases. The cobamide is non-covalently bound in the center of the protein in the 'base-off' conformation in the [Co^{II}]-state (Fig. 3.1; ch. 2.1; Payne *et al.*, 2015a). The cobalt ion is neither coordinated to the lower ligand base as typical for isolated cobamides, nor to an alternative lower base such as a histidine of the protein backbone as shown for the well-characterized cobamide-dependent methyltransferases and most adenosylcobalamin-dependent enzymes (Fig. 3.1 A-D; Banerjee and Ragsdale, 2003; Gruber *et al.*, 2011; Bridwell-Rabb and Drennan, 2017a). The 5-coordinated 'base-off' cobamide was confirmed by EPR spectroscopy of the as-isolated enzymes (see appendix p. xliv; Payne *et al.*, 2015a) and is consistent with previous EPR studies of PceA of *D. restrictus* and CprA of *D. dehalogenans* (Schumacher *et al.*, 1997; van de Pas *et al.*, 1999). Furthermore, instead of a methyl group or a 5'-deoxyadenosyl group typical for methyltransfereases, mutases and eliminases (Banerjee and Ragsdale, 2003; Gruber *et al.*, 2011; Bridwell-Rabb and Drennan, 2017a), the RDase cofactor was found to bind a water molecule, or alternatively a hydroxyl group, as upper axial ligand to the cobalt ion (called aquocobamide or hydroxocobamide) (Fig. 3.1 B-D; ch. 2.1; Payne *et al.*, 2015a). So far, only the reconstituted VcrA of *Dehalococcoides mccartyi* strain VS was shown to bind the cobamide in a 5-coordinated [Co^{II}]-state in the 'base-on' conformation (Parthasarathy *et al.*, 2015). Here, the lower ligand base is coordinated towards the cobalt ion, while an upper axial ligand is missing. In 1,2-dichloropropane RDases (DcpAs) from dehalogenating Chloroflexi a putative cobamide-binding motif (DHXG-X_{39}-S-X_{32}-G) was identified (Padilla-Crespo *et al.*, 2014). However, detailed biochemical characterization of these enzymes is not available up to now. It remains to be seen, whether DcpAs might bind the cobamide cofactor in a 'base-off/His-on' conformation. All in all, the global protein fold, the more common mode of 'base-off' cobamide binding and the presence of a water/hydroxyl group as upper axial ligand of the cobalt clearly differentiate RDases from adenosylcobalamin-dependent enzymes and methyltransferases and places RDases in a novel class of cobamide-containing oxidoreductases.

Structural homologs in the cobamide binding domain of RDases were first found in the previously reported human B_{12} binding protein methylmalonic aciduria *cblC* type with homocysteinuria (MMACHC) (Kim *et al.*, 2008). Later, the crystal structures of the epoxyqueuosine reductases (QueG) from *Streptococcus thermophilus* (Payne *et al.*, 2015b) and *Bacillus subtilis* (Dowling *et al.*, 2016) were resolved. The enzymes are classified together with RDases within cobamide-containing iron-sulfur proteins and share protein sequence similarities in the C-terminal part including the two iron-sulfur cluster binding motifs (Miles *et al.*, 2011). Both QueG structures resemble the aquocobamide- and the two [4Fe-4S] cluster binding

module of the RDases (Fig. 3.1 E; Payne *et al.*, 2015b; Dowling *et al.*, 2016), thus suggesting a conserved electron transfer pathway in both cobamide-containing iron-sulfur proteins. However, while the overall features of cobamide binding are similar, the detailed hydrogen bonding networks differ among the proteins. This might be based on the lack of a conserved cobamide binding motif in their protein sequences.

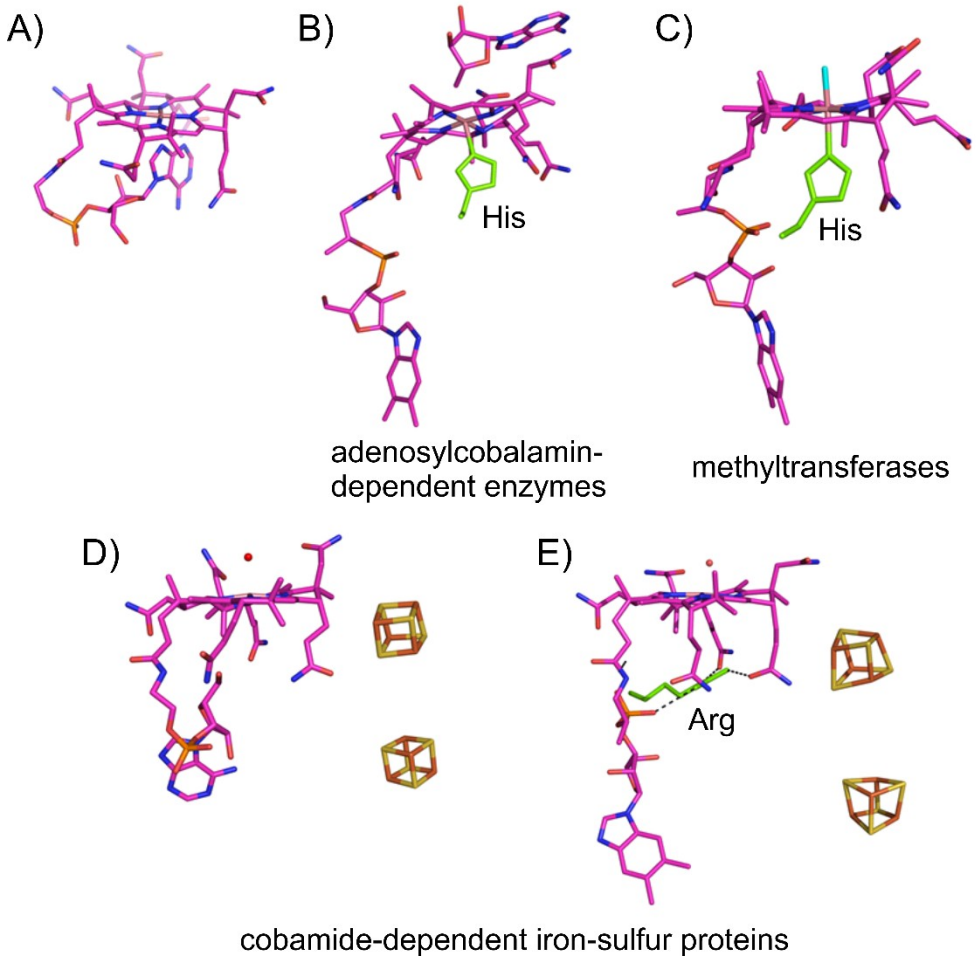

Figure 3.1: Mode of cobamide binding in different classes of cobamide-dependent enzymes. A) Isolated cobamide (here norpseudo-B_{12}; Kräutler *et al.*, 2003) in the 'base-on' conformation binding the nucleotide base as lower ligand. B) 'Base-off/His-on' adenosylcobalamin from human methylmalonyl-CoA mutase (Froese *et al.*, 2010). The highly light-sensitive Co-C5' bond between the Co and the 5'-deoxyadenosyl group as upper ligand was likely broken in the X-ray beam. C) 'Base-off/His-on' methylcobalamin from *E. coli* (Drennan *et al.*, 1994). The methyl group is colored cyan. D) 'Base-off' aquocobamide from RDases (here norpseudo-B_{12} from PceA of *S. multivorans*) with a curled linker moiety. E) 'Base-off' aquocobalamin from epoxyqueuosine reductase (QueG) from *B. subtilis* with an arginine in the protein backbone blocking access to the lower face of the cobalt ion. In D+E the water molecule/hydroxyl group as upper ligand is shown as red sphere.

In QueG of *B. subtilis* a conformational change of the cobamide cofactor to its 'base-on' state is prevented by an arginine that is blocking the access to the lower axial position and may preorganize the cofactor for reduction to the catalytically active square-planar [Co^{I}] species (Dowling *et al.*, 2016). Exchange of the arginine to alanine led to strongly reduced turnover rates. Also in QueG of *S. thermophilus* access to the cobalt is prevented by the protein backbone (Payne *et al.*, 2015b). Unique for PceA and NpRdhA is the stabilized curled linker moiety in the nucleotide loop of the cobamide compared to the typically rather extended conformation (Fig. 3.1 B-E; ch. 2.1; Payne *et al.*, 2015a; Svetlitchnaia *et al.*, 2006). It is expected that the curled arrangement prevents a reorientation of the lower ligand base towards to cobalt and hence the formation of [Co^{III}] and an impact on the reaction mechanism. In addition, the protein environment makes the binding of an alternative lower ligand such as a histidine residue impossible. Stability of the [Co^{II}]-signal in EPR measurements upon oxidation of PceA of *S. multivorans* and *D. restrictus* and CprA of *D. dehalogenans* up to a redox potential of about +300 mV supports this assumption (see appendix p. xliv; Schumacher *et al.*, 1997; van de Pas *et al.*, 1999). If the 'base-on' conformation in the [Co^{III}]-state should emerge in the course of the reaction, the midpoint redox potential of the [Co^{III}]/[Co^{II}] redox pair would be unusually high. The midpoint redox potential of the [Co^{II}]/[Co^{I}] couple was shown to be about -380 mV at pH 7.5 in PceA of *S. multivorans* (Kräutler *et al.*, 2003) and thus about 100 mV more positive than for the [Co^{II}]/[Co^{I}] couple of the isolated norpseudo-B_{12} (-490 mV at pH 7, Kräutler *et al.*, 2003). Apparently, the fixed 'base-off' conformation together with the weak water/hydroxyl group as upper ligand strongly supports the reduction of the protein-bound cobamide cofactor to the catalytically active [Co^{I}]-state in PceA. So far, *S. multivorans* and the closely related *Sulfurospirillum halorespirans* are the only organisms found that produce norpseudo-B_{12} (Kräutler *et al.*, 2003; Goris *et al.*, 2017). The atypical norcobamide showed a significant higher abiotic reductive dehalogenation activity when compared to norcobalamin or cobalamin (Neumann *et al.*, 2002; Keller *et al.*, 2014), which were reported to be much harder reducible with a midpoint redox potential of the [Co^{II}]/[Co^{I}] couple of about -610 mV (Lexa and Saveant, 1983). This was attributed to the higher tendency of the adenine moiety in cobamides to stay in the 'base-off' conformation in solution compared to DMB-containing cobamides, and thus facilitating cobalt reduction in the course of the abiotic reaction mechanism (Fieber *et al.*, 2002; Krone and Thauer, 1989a). In contrast, reduction of the 5-coordinated 'base-off' cobamide cofactor bound in PceA of *D. restrictus* and CprA of *D. dehalogenans*, which was at least in PceA expected to be cobalamin (Holliger *et al.*, 1998; Rupakula *et al.*, 2013), showed the same

midpoint redox potential like the norpseudo-B_{12} cofactor in PceA of *S. multivorans* (Schumacher *et al.*, 1997; van de Pas *et al.*, 1999). This further strengenths the assumption that the fixed curled nucleotide loop of the cobamide and the protein environment in RDases permanently prevent the formation of the 'base-on' state of the cobamide cofactor and the involvement of the lower ligand in the RDase-mediated reaction mechanism at all. Hence, in this respect a clear mechanistic difference exists between abiotic and biotic cobamide-mediated reductive dehalogenation.

Structural variability in the PceA-bound cobamide was shown by generating different norcobamides in *S. multivorans* (ch. 2.2). Next to norpseudo-B_{12}, also 5-OMeBza- and 6-OHBza-NCba were incorporated into PceA without any loss in enzyme activity or maturation, all occupying a conserved position in the crystal structure. Interestingly, *S. multivorans* only produced these isomers of the norcobamides. Whether the unusual regioselectivity in the cobamide biosynthesis reflects an adaptation to the needs of the PceA enzyme remains speculative. According to the crystal structure of PceA, the protein would also allow for an inverse substitution pattern in the lower ligand base, since no sterical constraints with the protein environment get obvious. On the other hand, the incorporation of methylated benzimidazolyl-NCbas strongly affected PceA maturation and activity (ch. 2.2; Keller *et al.*, 2014). Since the lower ligand of the cobamide in PceA was shown to be not involved in the RDase mechanism (see above), it can be assumed that the character of the lower ligand base is rather important for correct binding of the cofactor and protein folding and that the loss of activity is only a consequence of incorrect PceA maturation. It is not known whether the cofactor has to attain a specific conformation prior to the incorporation into the RDase proteins or whether nucleotide loop arrangement intertwines with the PceA folding process. Either way, the hydrophic character of the methylated benzimidazoles might be incompatible with the lower ligand positioning in a solvent accessible cavity. The DMB base of the cobalamin cofactor in NpRdhA is buried within the protein and protected from solvent (Payne *et al.*, 2015a). Next to NpRdhA, also VcrA of *D. mccartyi* VS is fully active with cobalamin as cofactor (Parthasarathy *et al.*, 2015). And organohalide-dependent growth of further cobamide-auxotrophic *D. mccartyi* strains was shown to depend on cobamides with DMB, 5-MeBza or 5-OMeBza as lower ligand, while 5-OHBza, Bza or adenine did not allow for dehalogenating activity (Yi *et al.*, 2012; Yan *et al.*, 2012; Yan *et al.*, 2013; Yan *et al.*, 2016). However, no structural data are available here, leaving open the question whether the lower ligand base is protected from solvent as described for NpRdhA. Beyond that, generalists and specialists in cobamide cofactor utilization were

identified. PceA of *D. hafniense* Y51 remained active in the presence of various benzimidazolyl- and purinyl-cobamides, while the heterologously produced DcaA of *D. dichloroeliminans* DCA1 displayed an unexpected specificity for OMeBza-Cba as cofactor, showing about nine times higher activities compared to the presence of other benzimidazolyl- or purinyl-cobamides (T. Schubert; unpublished data). Whether OMeBza-Cba is also the natural cobamide cofactor in *D. dichloroeliminans* DCA1 is not known so far. The organism possesses a full set of genes required for cobamide biosynthesis, but genes for benzimidazole biosynthesis are not included (NC_019903). Among all these RDases PceA of *S. multivorans* is unique by binding norcobamides lacking a methyl group in the nucleotide loop at C176 (Kräutler *et al.*, 2003). Whether the cobamide cofactor structure was adapted to the PceA protein, which three-dimensional structure revealed special constraints not allowing for a methyl group at this position (ch. 2.1), or the PceA protein was adapted to the norpseudo-B_{12} cofactor remains speculation. In the presence of mainly methyl group containing pseudo-B_{12} with only a small fraction of norpseudo-B_{12} left production of active PceA was observed, although at lower rates (Keller *et al.*, 2016). It has not yet been tested if pseudo-B_{12} was effectively incorporated into the protein and whether it causes a rearrangement of the protein environment, or if the reduced activity rather results from PceA occupied with remaining norpseudo-B_{12}. Further structural analysis are required to figure out how RDases achieve cofactor specificity or flexibility. To get a better understanding of the diversity in natural cobamide cofactors used in RDases, further wide-ranging biochemical studies of RDases from phylogenetically diverse organisms will be necessary. Apparently, organohalide-respiring bacteria like *S. multivorans* or *D. mccartyi* strains are able to produce a variety of different cobamide derivatives, which does not necessarily reflect the needs of their RDase proteins (ch. 2.2; Yi *et al.*, 2012; Yan *et al.*, 2012; Yan *et al.*, 2013; Keller *et al.*, 2014; Keller *et al.*, 2016; Yan *et al.*, 2016). It is conceivable that the evolution of RDases, especially of cobamide-auxotrophic organohalide-respiring bacteria, adapted to the presence or limitation of cobamide building blocks in their surrounding environment.

To allow for the reduction of the cobamide cofactor at the active site, the structural analysis of PceA and NpRdhA (ch. 2.1; Payne *et al.*, 2015a), as well as the structural analysis of the QueGs from *S. thermophilus* (Payne *et al.*, 2015b) and *B. subtilis* (Dowling *et al.*, 2016) as further representatives of the new class of cobamide-dependent enzymes, suggest a consecutive electron transfer via the two [4Fe-4S] cluster. These are positioned in close distance between the protein surface and the cobamide cofactor allowing for the intramolecular electron transfer

from an external electron donor to the cobamide (Fig. 3.1 D, E; ch. 2.1; Payne *et al.*, 2015a; Payne *et al.*, 2015b; Dowling *et al.*, 2016). By binding the isolated PceA protein on a redox electrode the electron transfer chain could be emulated, assuming the electrode as the direct electron donor in the respiratory chain (ch. 2.5). Thus, one of the two cubane iron-sulfur cluster could be identified as the entry site for electrons at an onset potential of -450 mV vs. SHE at pH 7. This was confirmed by EPR-coupled redox titration showing midpoint redox potentials for the $[4Fe\text{-}4S]^{1+}/[4Fe\text{-}4S]^{2+}$ redox pair of -440 mV at pH 7.5 (unpublished data). A similar potential was also determined for the two [4Fe-4S]-cluster in PceA of *D. restrictus* (Schumacher *et al.*, 1997). The redox potentials for the two cubane iron-sulfur cluster in NpRdhA, as well as in VcrA of D. *mccartyi* VS, were not determined (Payne *et al.*, 2015a; Parthasarathy *et al.*, 2015). Since the midpoint redox potential of the $[Co^{II}]/[Co^{I}]$ couple of the cobamide cofactor was determined to be about -370 mV at pH 7.5-8 (Schumacher *et al.*, 1997; van de Pas *et al.*, 1999; Kräutler *et al.*, 2003) electron transfer within the protein is quaranteed. A previously proposed splitted electron flow to the cobamide cofactor in the active site, whereby each electron enters the protein separately via a single [4Fe-4S] cluster (Neumann *et al.*, 1996) cannot be excluded, but seems rather unlikely after elucidation of the cofactor positioning in the enzyme. In addition, the splitted electron flow was suggested on the assumption that $[Co^{III}]$ is formed in the course of the catalytic cycle (Neumann *et al.*, 1996). However, the presence of the oxidized $[Co^{III}]$ state was not observed so far (see above). An exception might be CprA of *D. dehalogenans* that harbors a [3Fe-4S] cluster with a midpoint redox potential of +70 mV next to one low-potential [4Fe-4S] cluster (van de Pas *et al.*, 1999). The positive potential of the [3Fe-4S] cluster would form a thermodynamic barrier within the consecutive electron transfer chain. Its function in CprA remains to be elucidated. Whether the electrons enter the RDase at the distal or the proximal [4Fe-4S] cluster could not be resolved with the methods applied. The PceA crystal structure suggests a membrane attachment of the PceA protein via two highly flexible regions, one in each monomer, which would place the distal [4Fe-4S] cluster in proximity to putative membrane-integral respiratory chain components (ch. 2.1). Such a highly flexible region was not described for the crystal structure of the non-respiratory, cytoplasmic NpRdhA (Payne *et al.*, 2015a), highlighting its role in membrane orientation of PceA. Up to date, the physiological electron donor for RDases in the organohalide respiratory chain is not known, but several models for divers organohalide-respiring bacteria exist, which all involve putative membrane-integral electron carrier (Schumacher and Holliger, 1996; Goris *et al.*, 2015; Kruse *et al.*, 2015; Kublik *et al.*, 2016;

Fincker and Spormann, 2017). Further biochemical and spectroscopic studies will be necessary to elucidate the electron transfer route within the respiratory chain.

The iron-sulfur cluster binding domain in PceA and NpRdhA is tightly packed against the cobamide binding unit (ch. 2.1; Payne *et al.*, 2015a). This suggests, moreover, a close interplay between all cofactors during RDase maturation. The Strep-tagged PceA variant produced in the mutant strain *S. multivorans* GD21 was lacking about 62% of its cofactors under standard cultivation conditions including 90 µM $FeSO_4$ in the medium (see appendix p. xlix). A complete occupation of PceA with all [4Fe-4S] cluster was attained by increasing the $FeSO_4$ concentration in the growth medium, which indicated an iron limitation during PceA maturation. The concomitant increase in the cobamide cofactor content in PceA, although the cobamide biosynthesis was not altered, highlights thereby the close coupling between iron-sulfur cluster and cobamide incooperation, only allowing for cobamide binding if the [4Fe-4S] cluster are present too. The importance of the two [4Fe-4S] cluster for RDase folding and activity was confirmed in the inactivated C387S and C439S mutants of the heterologously produced DcaA from *D. dichloroeliminans* DCA1 (ch. 2.4). In the same way, already the exchange of one of the hydrogen bonding partners for the cobamide cofactor, a frequently conserved asparagine in the active site, abolished enzyme activity most probably due to improper folding of the protein (ch. 2.4). This intertwine cofactor binding might also partially explain the difficulties in reconstitution of RDase apoproteins with cofactors, which was described in several attempts for heterologous production of these enzymes (Neumann *et al.*, 1998; Sjuits *et al.*, 2012; Payne *et al.*, 2015a).

3.2 Reaction mechanism of RDases

The well-known adenosylcobalamin-dependent enzymes and methyltransferases were described to rely on cobalt-carbon chemistry during the catalytic cycle (Banerjee and Ragsdale, 2003; Gruber *et al.*, 2011; Bridwell-Rabb and Drennan, 2017a). Also the abiotic dehalogenation of alkyl halides by isolated cobamides was proposed to involve Co-C bond formation (alkylation) via a nucleophilic attack of [Co^I] on the electron-deficient halogen-binding carbon (Schrauzer and Deutsch, 1968; Krone *et al.*, 1989a). However, the protein environments of PceA and NpRdhA, as representatives for RDases catalyzing halogen substitution reactions, exclude such a mechanism and requests another explanation for the enzyme-mediated catalytic

cycle for reductive dehalogenation. On the one hand, the protein prohibits the formation of a 'base-on' cobamide cofactor, which was described as a transient state within alkylation reactions (ch.2.1; Payne *et al.*, 2015a). On the other hand, access to the upper face of the cobalt is restricted by the active site architecture not allowing for a direct binding of the substrate's carbon to the [Co^{I}] (ch.2.1; ch. 2.3; Payne *et al.*, 2015a). While X-ray structural analysis of PceA crystals soaked with TCE did not allow for an unambiguous deduction on the cobalt-substrate interaction and thus the reaction mechanism, positioning of larger bromophenols in the active site was more defined and allowed for further structure-function analysis (ch. 2.3). Based on the distant positioning of the substrates with the halide substituents out of the axial position of the cobalt ion in the crystal structures of PceA and the absence of PceA-substrate interaction signals during turnover tracked by EPR spectroscopy, a dissociative long-range electron transfer mechanism was proposed that involves radical formation upon transfer of a first electron on the electron-deficient substrate and elimination of a halogen substituent (Fig. 3.2 A; ch. 2.3). The close interaction between the cobamide and the proximal [4Fe-4S] cluster would either allow for the transfer of the second electron to the substrate radical directly from the [4Fe-4S] cluster, or would ensure rapid supply of further electrons for the cobalt ion. Both might be putative precautions to avoid long residence times for the radicals. How the enzyme recognizes the substrate to avoid oxidative damage by transferring electrons in an empty active site, remains elusive. In adenosylcobalamin-dependent enzymes the homolytic [Co^{III}]-carbon bond cleavage in the cofactor and thus generation of the catalytically active 5'-deoxyadenosyl radical was proposed to be initiated by a conformational change upon substrate binding (Gruber *et al.*, 2011; Bridwell-Rabb and Drennan, 2017a). However, the positioning of the substrates in PceA's active site does not involve the formation of any substrate-enzyme bonds and no conformational change, other than the disappearance of the upper water/hydroxyl group ligand, was observed upon reduction of the PceA crystals to the catalytically active [Co^{I}]-state. The proposed dissociative long-range electron transfer mechanism without direct cobalt-substrate binding is consistent with the absence of a [Co^{III}] signal in EPR measurements so far (see above; see appendix p. xliv; Schumacher *et al.*, 1997; van de Pas *et al.*, 1999) and would allow for successive switches between [Co^{I}] and [Co^{II}] only. Substrate conversion and dehalogenation pattern are thereby mainly decided by internal charge distribution (bond energies and partial negative charges) within the substrate (ch. 2.3). A rather undirected electron transfer in PceA is furthermore supported by the production of all three isomers of dibromoethene from tribromoethene (Ye *et al.*, 2010), while only *cis*-1,2-DCE was formed from TCE (Neumann *et*

al., 1996). During the reductive dehalogenation of 2,3-dichloropropene substrate radical formation was observed leading to adduct formation with methyl viologen radicals, the artificial electron donor applied in the enzyme assay (Schmitz *et al.*, 2007). However, the positive effect of ammonium ions on the turnover rates for selected substrates in PceA still remains mysterious (ch. 2.3; Neumann *et al.*, 1996; Ye *et al.*, 2010). So far, only propyl iodide seem to overcome the structural barrier above the cobamide cofactor at the active site of PceA and directly interact with the cobalt. However, propyl iodide inhibited PceA function (ch. 2.3; Neumann *et al.*, 1995).

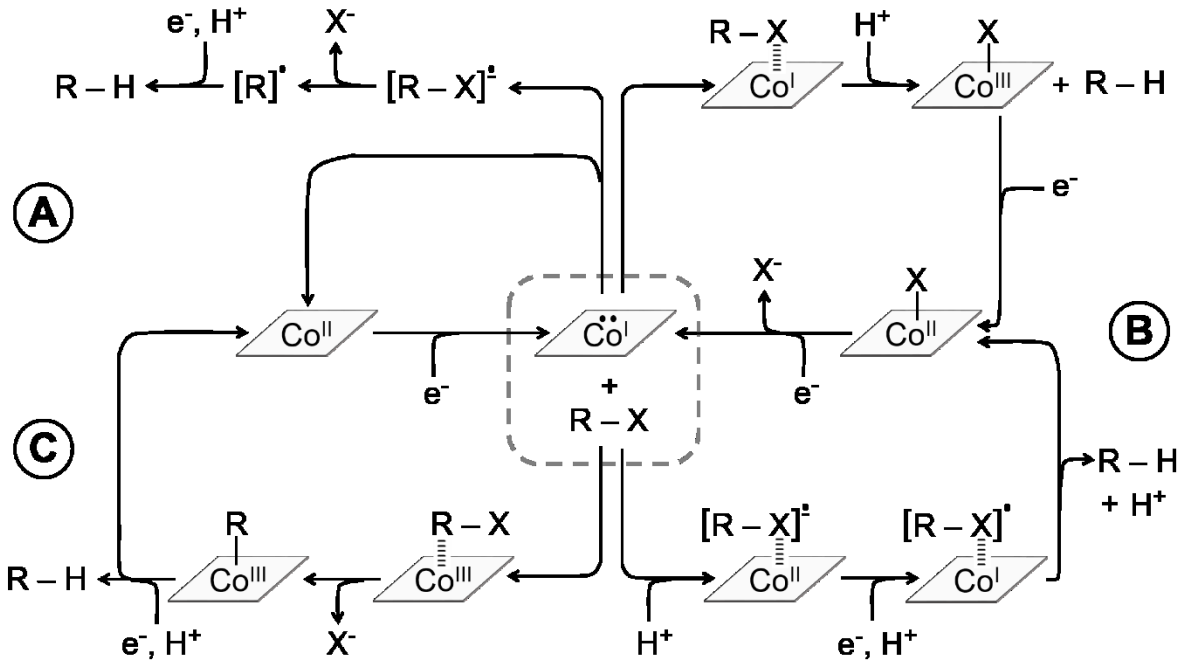

Fig. 3.2: Proposed catalytic mechanisms of RDases. A) Dissociative long-range electron transfer mechanism from [Co^{I}] leading to substrate radical formation and finally to the formation of a carbanion after elimination of the halogen substituent. B) Formation of a cobalt-halogen bond after [Co^{I}] attack directly at the halogen substituent followed by either heterolytic (top) or homolytic (bottom) cleavage of the carbon-halogen substrate bond. C) Alkylation of the cobalt by a nucleophilic attack of [Co^{I}] on the carbon backbone of the organohalide.
[Co^{I-III}]: oxidation states of the cobalt ion in the cobamide cofactor; R: hydrocarbon backbone; X: halogen substituent.

In contrast to PceA, spectroscopic analysis of substrate-enzyme complexes in NpRdhA revealed a direct interaction between the cobalt ion and a bromine substituent of the substrate 3,5-dibromo-4-hydroxybenzoate (Payne *et al.*, 2015a). Based on these findings a reaction mechanism was proposed, which involves direct nucleophilic attack of [Co^{I}] at the halogen substituent of the substrate leading to cobalt-halogen bond formation (Fig. 3.2 B). So far, crystal structures of NpRdhA-substrate complexes are not available, and *in silico* predictions of the substrate positioning show the substrate oriented with either the bromine substituent *ortho* to the hydroxyl group above the cobalt or out of the axial position with the hydrogen in *meta*-position closest to the cobalt (Payne *et al.*, 2015a; Pietra, 2015). Nevertheless, in both cases the substrate might be located closer to the cobalt in relation to the distance in PceA, allowing for cobalt-halogen interaction in NpRdhA. The fact that both enzymes, NpRdhA and PceA, convert bromophenols facilitate a direct comparison of their dehalogenation patterns. Apparently, NpRdhA selectively converts substrates that resemble the structure of 2,6-dihalogenated phenols (Payne *et al.*, 2015a). In contrast, the substitution pattern in substrates for PceA is much more diverse and also *meta*- and *para*- substituents were removed (ch. 2.3). In addition, the positive effect of a decreasing electronegativity of the halogen substituents from chlorine to iodine on the substrate conversion in PceA (ch. 2.3) was not observed for NpRdhA (Payne *et al.*, 2015a). This emphasizes a difference between both RDases, which might originate from two distinct reaction mechanisms. In *D. mccartyi* CBDB1 a reductive dehalogenation mechanism initiated through single electron transfer from [Co^{I}] to the halogen site of various aryl halides as substrates was proposed, similar to the mechanism described in Fig. 3.2 B(bottom) (Cooper *et al.*, 2015). Also here, different partial charge models suggest that the regioselective dehalogenation is based on halogen-carbon bond polarization, removing the halogen substituent with the least negative partial charge. A restriction in substrate utilization based on the halogen substituent pattern as described for NpRdhA was thereby not observed. Only recently, Johannissen and colleagues reported on the probability that, according to molecular docking and density functional theory calculations, also the PceA-mediated dehalogenation of TCE follows adduct formation due to cobalt-halogen interaction (2017). However, such an intimate cobalt-substrate interaction was not observed in EPR spectroscopy after addition of substrates to the isolated PceA, neither for PCE or TCE, nor for bromophenols. Furthermore, the reductive dehalogenation of chloroanillines in *Dehalobacter* strain 14DCB1 was proposed to be the result of an initial attack on a carbon-attached hydrogen atom (Zhang *et al.*, 2017). Further biochemical studies will be necessary to elucidate the reaction mechanism

of the RDases involved here. And data obtained from compound-specific isotope analysis indicate a further mechanism via direct nucleophilic attack by [Co^I] at the carbon backbone of the substrate in dehalogenating cultures of *Desulfitobacterium* sp. strain Viet1 and *Geobacter lovleyi* strain SZ, which would require an intimate cobalt-substrate interaction (Fig. 3.1 C), even though a dissociative single electron transfer could not be excluded (Cretnik *et al.*, 2014). However, the actual positioning of the substrates at the active site of the enzymes involved is not known so far. Apparently, RDases are highly versatile and all four mechanisms proposed for the halogen substitution reaction might be found in the phylogenetically diverse organohalide-utilizing bacteria. It remains a mystery whether there was a mechanistic diversity already in the progenitor RDase that was adapted differently in individual RDases, or whether mechanistically different RDases evolved independently from each other. Very recent results obtained from dual-element isotope analysis propose an intimate cobalt-carbon bond formation as described for *Desulfitobacterium* sp. Viet1 and *G. lovleyi* SZ as the common mode in enzymatic reductive dehalogenation of chlorinated ethenes (Fig. 3.2 C; Heckel *et al.*, 2017). These data are in contrast to the observations in PceA of *S. multivorans* described above and are currently under debate. The fact, that PceA of *S. multivorans* shows exceptional high activities, not only for halogenated ethenes, but also for bromophenols when comparing the dehalogenating activities between all so far purified RDases (ch. 2.3; see references in Tab. 1.1), implicate differences between haloethene-utilizing RDases. The assumption that the specialties in the nucleotide loop structure of the norpseudo-B_{12} cofactor might be responsible for the high turnover rate of PceA seems rather unlikely since the cobamide's tail is not involved in catalysis and the enzyme-bound norspeudo-B_{12} shows the same behavior like other cobamide cofactors (see above; see appendix p. xliv; Schumacher *et al.*, 1997; van de Pas *et al.*, 1999). Thus, the increased activity might be based on a differing reaction mechanism, however, other structural reasons can not be excluded. Further detailed mechanistic studies including RDase representatives from diverse organisms and for the conversion of all substrate classes (halogenated alkenes, halogenated alkanes, aryl halides) will be necessary to evaluate the distribution of the different proposed modes for initializing the cobamide-mediated enzymatic halogen substitution reaction.

Nevertheless, RDases display an unprecedented way of utilizing a cobamide cofactor for the enzymatic reductive dehalogenation. The proposed dissociative long-range electron transfer mechanism initiated directly from [Co^I] in PceA as well as the cobalt-halogen chemistry in NpRdhA clearly differ from classical cobamide-dependent biochemistry in enzymatic systems

(Banerjee and Ragsdale, 2003; Gruber *et al.*, 2011; Bridwell-Rabb and Drennan, 2017a). The distantly related QueG was shown to share the conserved electron transfer chain via the two [4Fe-4S] cluster to the 'base-off' aquocobamide cofactor described for RDases. In contrast, the protein environment and its active site show major differences (Payne *et al.*, 2015b; Dowling *et al.*, 2016). Here, the substrate binding pocket allows for the access of the substrate to the cobalt ion. Structural and spectroscopic analysis of QueG from *S. thermophilus* and *B. subtilis* propose a nucleophilic attack of the [Co^{I}]-state of the cobamide cofactor leading an alkylation (Payne *et al.*, 2015b; Dowling *et al.*, 2016). Thus, the proposed RDase-mechanisms for PceA and NpRdhA appears to be unique also among other cobamide-containing iron-sulfur proteins. It would be interesting to see whether QueGs would be able to utilize organohalides such as PCE and how they would do this.

What all RDases have in common, is the protonation step in the halogen substitution reaction, which is necessary to replace the eliminated halogen substituent. A highly conserved tyrosine and arginine/lysine pair in the active sites of PceA and NpRdhA was found to be ideally positioned with the hydroxyl group of the tyrosine and the stabilizing positive charge of the arginine (PceA) / lysine (NpRdhA) in close distance towards the substrate above the cobamide cofactor allowing for proton donation (ch. 2.1; ch. 2.3; ch. 2.4; Payne *et al.*, 2015a). Exchange of both residues in the Y426F and K488Q mutants of NpRdhA, respectively, led to a complete loss of the dehalogenating activity (Payne *et al.*, 2015a). The introduction of mutations into PceA of *S. multivorans* is hardly practicable, and its heterologous production in *E. coli* BL21 (Neumann *et al.*, 1998) or *S. blattae* (data not shown) resulted in nonfunctional apoprotein. Instead, the chloroethene-utilizing PceA of *D. hafniense* Y51 (Suyama *et al.*, 2002) could be functionally produced in *S. blattae* and subjected to site-directed mutagenesis. Also here, replacement of the tyrosine homolog completely hampered its dehalogenating activity. While the homologous R357Q mutant remained active, replacement of the arginine against glutamate, which is lacking a positive charge, abolished chloroethene-conversion ability. This supports the stabilizing function of the arginine in the protonation reaction of the tyrosine also in $PceA_{Y51}$, but reveals a more flexibility in the type or position of the positive charge in the active site. A tyrosine resembling the one in RDases was also found in the crystal structures of QueGs (Payne *et al.*, 2015b; Dowling *et al.*, 2016). However, it does not seem to be involved in the reaction mechanism. Instead, an asparagine is located close by and ideally positioned in close distance to the cobalt-carbon/substrate bond and expected to deliver the two protons required for epoxide

reduction (Schrauzer and Windgassen, 1967; Dowling *et al.*, 2016). Knock-out of the asparagine showed drastically decreased product formation (Dowling *et al.*, 2016).
The dihaloelimination reaction found in a distinct group of organohalide-respiring bacteria could be clearly separated from the halogen substitution reaction by the need of a proton donor (ch. 2.4). The inability of the heterologoulsy produced DcaA of *D. dichloroeliminans* DCA1 to convert putative substrate intermediates produced if a halogen substitution step is involved within the dihaloelimination reaction, together with the maintained dihaloeliminating activity after knock-out of the putative proton donors in the active site excluded the involvement of proton transfer steps in this type of reductive dehaogenation reaction (ch. 2.4).

3.3 Structural versatility in RDases reflected in substrate ranges?

Up to date, more than 300 putative RDase genes are deposited in databases (Hug *et al.*, 2013). Their broad range of protein sequences shows a high variability. Yet, this study revealed similar key structural and biochemical features involved in the cofactor positioning and the internal electron transfer chain between PceA and NpRdhA (see above). Further *in silico* predictions of the crystal structures of DcaA from *D. dichloroeliminans* DCA1 and PceA from *D. hafniense* Y51 ($PceA_{Y51}$) showed highest accuracy in cofactor positioning and partially in the active site arrangement, supporting the assumption that these regions are conserved among RDases (ch. 2.4). In contrast, larger differences between the crystal structures of PceA and NpRdhA were found in the composition and folding of the N-terminal regions that are mainly involved in the formation of the hydrophobic substrate channel as well as in selected amino acids involved in the formation of the active site (ch. 2.1; ch. 2.4; Payne *et al.*, 2015a). In line with this, predictions of the substrate channel forming regions in the *in silico* structural models of DcaA and $PceA_{Y51}$ proved to be unreliable, due to the lack of protein sequence similarities to PceA and NpRdhA, which were used as templates for model generation (ch. 2.4). This diversity might reflect an adaptation of the various RDases to the wide range of alkyl and aryl halides serving as substrates, whereby an increasing protein sequence similarity in this regions might indicate overlapping substrate spectra. Indeed, RDase protein sequences weakly align in clusters placing all RDases in four groups converting either halogenated alkenes, aryl halides, halogenated alkanes in a halogen substitution reaction or haloalkanes in a dihaloelimination reaction (for an alignment with selected representatives of each group see appendix p. xi and pp. lx-lxiv).

Nevertheless, there are still large sequence differences within each group, as for PceAs the protein sequence similarities range from 99% to 27% (see references Tab. 1.1). Vice versa, high sequence similarity does not necessarily mean that the RDases share a common substrate spectrum or a common pattern in product formation (ch. 2.4; Buttet *et al.*, 2013; Alfán-Guzmán *et al.*, 2017). To get a global overview structure-function relationship analysis was further expanded towards a haloalkane dehalogenating RDase and a respiratory aryl halide converting RDase next to the nonrespiratory aryl halide converting NpRdhA, the haloalkene utilizing PceAs of *S. multivorans* and *D. hafniense* Y51, and the dihaloeliminating DcaA investigated in this study so far. Therefore, the *in silico* structural models of the chloroform and 1,1,1-trichloroethane RDase (CtrA) from *Desulfitobacterium* sp. strain PR and of the chlorophenol RDase (CprA) from *D. dehalogenans* were generated using the iTASSER server for protein structure and function prediction (Fig. 3.3; Zhang, 2008; Roy *et al.*, 2010).

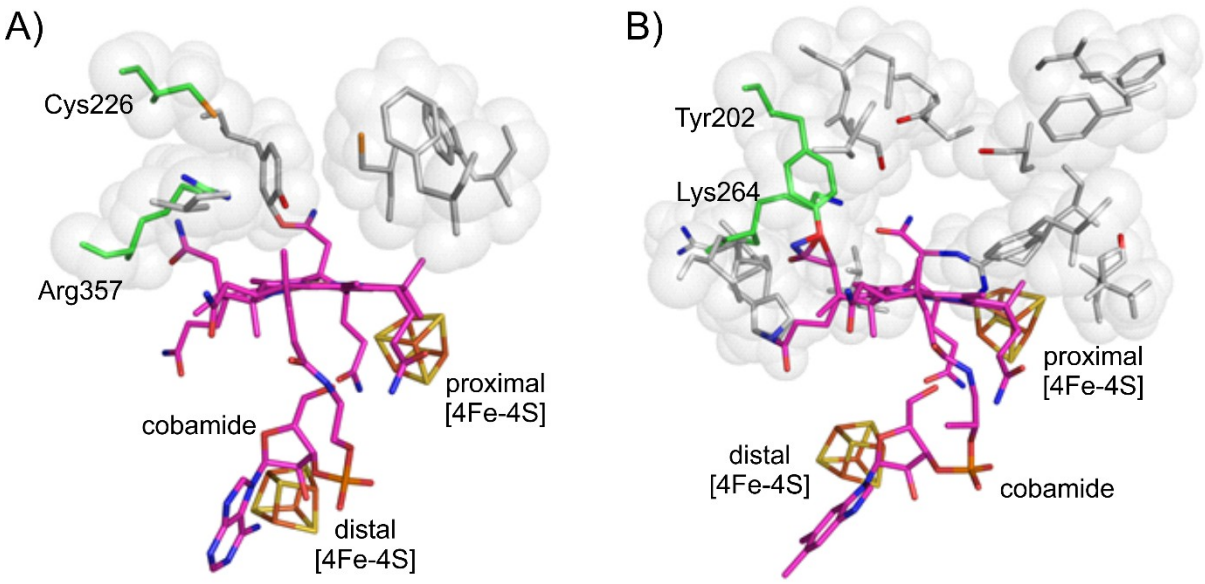

Figure 3.3: *In silico* structural models of the active site cavities and electron transfer chains of CtrA of *Desulfitobacterium* sp. PR (A; C-score: 0.15) and CprA of *D. dehalogenans* (B; C-score: 0.83). The cobamide shown in CtrA is norpseudo-B_{12}, since this is the natural cofactor of $PceA_{Smul}$ (ch. 2.1; Kräutler *et al.*, 2003), which was used as template for model generation. For CprA the crystal structure of NpRdhA (Payne *et al.*, 2015a) was mainly used in model generation, thus cobalamin was incorporated as cobamide cofactor. The highly conserved tyrosine and arginine/lysine positions are depicted in green, the cobamide cofactor in pink and the [4Fe-4S] clusters in yellow/orange. Due to the lack of sequence similarity, prediction of the *in silico* model of CtrA was partially difficult and only reliable amino acid residues involved in active site formation are shown.

In general, the active sites of RDases converting alkyl halides have smaller dimensions than the active sites of aryl halide utilizing RDases and according to PceA from *S. multivorans*, are restricted to smaller substrates up to the size of monoaromatic organohalides (ch. 2.3). In the same way, the entrance of the substrate channel in the chloroethene converting PceA of *S. multivorans* is defined by a small letterbox entry (ch. 2.1), while access to the bromohydroxybenzoate-utilizing NpRdhA seems to be less restricted (Payne *et al.*, 2015a). Dihaloelimating DcaAs as well as RDases converting haloalkanes in a halogen substitution reaction share similar dimensions in the active site like PceAs. The substrate binding pockets in these RDase groups are characterized by mainly aromatic and hydrophobic amino acids with tryptophanes, phenylalanines and tyrosines as the more frequently conserved residues.

The active site arrangements of PceA of *S. multivorans* and *D. hafniense* Y51 look highly similar although they share only 28% protein sequence similarity, indicating a partially conserved active site among all PceAs (ch. 2.4). On the other hand, $PceA_{Y51}$ and PceA of *D. hafniense* PCE-S share 98% protein sequence identity and the same amino acids involved in the active site formation (see appendix pp. lx-lxiv), but they still show different patterns in product formation. While $PceA_{Y51}$ is limited to *cis*-1,2-DBE formation from TBE (ch. 2.4), $PceA_{PCE\text{-}S}$ was described to dehalogenate TBE to all isomers of DBE and subsequently further to vinyl bromide and ethene (Ye *et al.*, 2010). Thus, further structural elements have to be involved in substrate binding or the reaction mechanism that causes different substrate spectra and dehalogenation patterns. Furthermore, PceA of *S. multivorans* shares 92% protein sequence identity with PceA of *S. halorespirans* and with $PceA_{TCE}$ from the enriched *Sulfurospirillum* sp. SL2 (Neumann *et al.*, 1996; Luijten *et al.*, 2003; Buttet *et al.*, 2013; Goris *et al.*, 2017). However, while the first two PceAs convert PCE via TCE to *cis*-1,2-DCE, the latter enzyme accumulates TCE as end product. Comparison of their protein sequences and their *in silico* structural models revealed two amino acid exchanges in the active sites between $PceA_{Smul}$/$PceA_{Shaf}$ and $PceA_{TCE}$, namely the replacement of Phe38 by Leu and of Thr242 by Ala (data not shown; for comparison see active site of $PceA_{Smul}$ in ch. 2.1). It remains to be tested if these residues might be involved in substrate binding by using comparable site-directed mutagenesis. In general, most haloalkene converting RDases stop PCE dehalogenation at *cis*-1,2-DCE. It was suggested, that the enzymes are not able to overcome the barrier of the high energy level required for further dehalogenation (ch. 2.4; Liao *et al.*, 2016). However, the VcrA of *D. mccartyi* VS is known to catalyze the halogen substitution of 1,1-DCE and its dehalogenation product VC further to ethene (Müller *et al.*, 2004; Parthasarathy *et al.*, 2015).

This is so far the only RDase known, which binds the cobamide cofactor in the 'base-on' conformation (Parthasarathy *et al.*, 2015). Isolated 'base-on' cobamides were described to have lower midpoint redox potentials for the [Co^{II}]/[Co^{I}] couple than 'base-off' cobamides (Banerjee *et al.*, 1990). The redox properties of the cobamide cofactor bound to VcrA have not yet been determined. However, it is feasible, that the redox potential of the VcrA-bound 'base-on' cobamide is also lower compared to the so far described RDase-bound 'base-off' cobamides (see above). This might probably lead to different catalytic properties that can overcome the energetic barrier to dehalogenate DCE and VC. It is not known, whether the 'base-on' conformation of the cobamide cofactor might be a general feature for dichloroethene and vinyl chloride utilizing RDases. So far VcrA is the only protein for this substrate class that was biochemically characterized in more detail.

So far it was assumed that RDases catalyzing dihaloelimination reactions represent a distant group of these enzymes. However, DcaAs align with high scores to $PceA_{Y51}$-like haloethene utilizing RDases and the active site architectures of both RDase groups look highly similar (ch. 2.4). In this study DcaA of *D. dichloroeliminans* DCA1 was shown to catalyze both types of dehalogenation reactions depending on the substrate. Next to the dihaloelimination of halogenated alkanes, the enzyme was able to perform halogen substitution reactions like described for PceAs using halogenated ethenes as substrates. This raises the question why the highly similar $PceA_{Y51}$ does not show a similar substrate range and is not also able to perfom enzyme-dependent dihaloelimination reactions. However, with the methods applied here, this could not be clarified. Marzorati and coworkers identified two small and defined regions, where most of the sequence differences between DcaAs and PceAs are concentrated (2007). Further amino acid exchanges in these regions might be necessary to identify key elements for dihaloelimination reactions. In contrast, VcrA was shown to convert 1,2-DCA in a dihaloelimination reaction next to the halogen substitution of DCE and VC (Parthasarathy *et al.*, 2015). Within the active site, DcaAs can only be differentiated from PceAs if a histidine is found at the highly conserved tyrosine position, as shown for DcaA from the 1,2-DCA dihaloeliminating *Dehalobacter* sp. WL (Grostern and Edwards, 2009) and for further putative DcaA proteins detected in dihaloeliminating enrichment cultures (Marzorati *et al.*, 2010; Merlino *et al.*, 2015). Whether these enzymes are also able to perform dihaloelimination and halogen substitution reactions in parallel remains to be tested. Exchange of the Tyr298 in DcaA of *D. dichloroeliminans* DCA1 against His still showed about 30% of its original halogen substitution activity next to 100% dihaloeliminating activity (ch. 2.4). So far, no PceA was

found that is lacking the tyrosine residue (see appendix p. xi, pp. lx-lxiv) and the mutant Tyr298His from $PceA_{Y51}$ complete lost its activity (ch. 2.4). In contrast to DcaAs, CtrA from *Desulfitobacterium* sp. PR is known to convert 1,1,2-TCA and 1,2-DCA in a halogen substitution reaction rather than via dihaloelimination. The trichloromethane RDase of *Dehalobacter* sp. strain UNSWDHB is even able to reduce a single substrate, 1,1,2-TCA, either via dihaloelimination to VC or via halogen substitution to 1,2-DCA (Wong *et al.*, 2016). In general, chloromethane-converting RDases have similar dimensions in their active sites compared to PceAs and DcaAs, but display major differences in the protein sequences (Fig. 3.3 A). Thus, prediction of defined amino acids involved in the formation of the active site in CtrA was not always unambiguously assignable. In this RDase group the highly conserved tyrosine is replaced by a cysteine or phenylalanine (see appendix pp. lx-lxiv; Wong *et al.*, 2016; Tang and Edwards, 2013; Ding *et al.*, 2014). In addition, a highly conserved asparagine involved in cobamide binding in PceAs and DcaA is exchanged against alanine or serine in chloromethane converting RDases (ch. 2.1; ch. 2.4; see appendix pp. lx-lxiv). Whether these residues are involved in the halogen substitution reaction of haloalkanes or in substrate positioning in the active site remains to be elucidated. Another tyrosine in close proximity might be able to function as the proton donor in these RDases.

The *in silico* active site structural model of the CprA from *D. dehalogenans*, as representative of an aryl halide specialized respiratory RDase, shows high similarity to the non-respiratory NpRdhA (Fig. 3.3B; Payne *et al.*, 2015a). In both RDases amino acids involved in the active site formation are located in similar positions in the protein backbone like in PceAs. However, their active sites are shaped by mainly smaller, short-chained residues, instead of aromatic amino acids like in alkyl halide converting RDases, thus forming a larger active site that allows for the uptake of bigger aryl halides as substrates. This might be a general feature only for aryl halide utilizing RDases. The mutant W118F of DcaA mimics an only slightly larger active site volume by expanding the active site towards the ceiling. Thus, the halogen substitution as well as the dihaloelimination activity in DcaA was drastically decreased, underlining the necessity of a smaller active site for correct positioning of smaller alkyl halides as substrates (ch. 2.4). The highly conserved tyrosine and arginine/lysine pair is thereby located at the same position in CprA and NpRdhA like in PceAs and ensures the proton transfer step during halogen substitution. While all alkyl halide converting RDases encode for an arginine at the highly conserved position, the presence of a lysine seems to be restricted to aryl halide utilizing RDases (see appendix pp. lx-lxiv). Exchange of the Arg357 in $PceA_{Y51}$ against Lys led to significantly

higher turnover rates for the larger brominated ethenes, but drastically decreased conversion rates for smaller chlorinated analogs (ch. 2.4). Therefore, the presence of a lysine might furthermore support conversion of larger aromatic substrates in aryl halide converting RDases. In this study several differences in the protein sequences could be highlighted, which might allow for a cautious assignment of so far uncharacterized putative RDases to their possible substrate classes. Basically three different modes of active site arrangements for RDases were found, one mode for PceAs and DcaAs, one type for RDases converting haloalkanes in a halogen substitution reaction and one mode for larger aryl halide converting RDases. And in case of the presence of a histidine at the highly conserved tyrosine position, DcaAs could be differentiated from PceAs. Nevertheless, predictions of substrate spectra of so far unknown RDases solely based on protein sequence or structural model comparison have to be considered with caution, since their might be overlapping substrate ranges. Monoaromatic benzenes and phenols as substrates might thereby represent an intermediate size fitting into the active sites of PceAs and aryl halide converting RDases. Over 20 years, PceA of *S. multivorans* was described to be restricted to the dehalogenation of alkyl halides including halogenated ethenes and propenes (Neumann *et al.*, 1996; Neumann *et al.*, 2002; Ye *et al.*, 2010). However, in this study the enzyme was shown to convert also bromophenols (ch. 2.3). The other way around might be possible for the tetrachlorobenzene RDase from *Dehalobacter* sp. strain TeCB1 that was shown to convert tetra-and trichlorobenzene, although the protein shares 95% protein sequence identity with $PceA_{Y51}$ (Alfán-Guzmán *et al.*, 2017). Whether the enzyme is also able to convert haloethenes was not tested. Furthermore, it could have been shown that already minimal changes in the active site, like conservative single amino acid exchanges in DcaA and $PceAY_{51}$, led to significant shifts in the substrate spectrum (ch. 2.4). Even if an organism is not growing on individual organohalides, the isolated RDase protein might be able to convert it, as shown for haloethenes in DcaA of *D. dichloroeliminans* DCA1 (ch. 2.4; De Wildemann *et al.*, 2003). Although isolated PceA of *S. multivorans* was shown to convert bromophenols with high specific activities, the organism is not able to use it as growth substrate (data not shown). Therefore, substrates from all classes have to be tested in activity assays to elucidate the substrate range of a new found RDase. This should also include representatives of all types of halogen substituents, since some RDases, like PceA of *S. multivorans*, might prefer brominated or iodinated substrates over their chlorinated analogs (ch. 2.3). So far, no RDase was found that is able to convert fluorinated organohalides. The strong carbon-fluorine bond appears to remain persistent against cobamide-mediated catalytic mechanisms. Only very few dehalogenating

enzyme systems have been described to reduce organofluorides, e.g. the 4-fluorobenzoate utilizing ATP-dependent class I benzoyl-CoA reductase (Tiedt *et al.*, 2016). Further systematic structural analysis of relevant RDases as well as systematic analysis of RDase substrate spectra including all substrate classes will be necessary to fully understand the flexibility and versatility of these enzymes and to identify the structural determinants that define substrate preferences or also reaction mechanisms.

The fact that the reductive dehalogenation by PceA of *S. multivorans* can be coupled to light-driven electrochemical reactors offers an opportunity for future application of RDases in bioremediation of contaminated sites. Successful bioaugmentation of a tetrachloroethene-contaminated field site was shown using the KB-1 consortium, which contains mainly *Dehalococcoides* spp. and *Geobacter* spp. (Duhamel *et al.*, 2002; Major *et al.*, 2002; Duhamel and Edwards, 2006). A direct application of the RDases in the field or their use as biochemical sensors would be a great alternative to expand bioremediation approaches. We were able to identify variable substrate binding regions, which may be exploited to combine different RDases and thus broaden the substrate spectrum for application in different contaminated sites. However, further protein engineering and design of optimized RDases will be necessary to realize this vision. A better in-depth understanding of cobamide utilization in RDases will thereby facilitate the functional production of different so far uncharacterized RDases or can be directly applied for stimulation of bioremediation by native dehalogenating communities at contaminated sites.

4 References

Abrahamson K, Ekdahl A, Collén J, Petersén M (1995) Marine algae - a source of trichloroethylene and perchloroethylene. *Limnol Oceanogr* 40, 1321-1326.

Adrian L, Rahnenführer J, Gobom J, Hölscher T (2007) Identification of a chlorobenzene reductive dehalogenase in *Dehalococcoides* sp. strain CBDDB1. *Appl Environ Microbiol* 73, 7717-7724.

Adrian L and Löffler FE (eds.) (2016) *Organohalide-respiring bacteria*, Springer-Verlag Berlin Heidelberg, doi: 10.1007/978-3-662-49875-0

Afonine PV, Grosse-Kunstleve RW, Echols N, Headd JJ, Moriarty NW, Mustyakimov M, Terwilliger TC, Urzhumtsev A, Zwart PH, Adams PD (2012) Towards automated crystallographic structure refinement with phenix.refine. *Acta Crystallogr D Biol Crystallogr* 68, 352–367.

Alfán-Guzmán R, Ertan H, Manefield M, Lee M (2017) Isolation and characterization of *Dehalobacter sp.* strain TeCB1 including identification of TcbA: a novel tetra- and trichlorobenzene reductive dehalogenase. *Front Microbiol* 8, 558.

Atashgahi S, Lu Y, Smidt H (2016) Overview of known organohalide-respiring bacteria-phylogenetic diversity and environmental distribution. In *Organohalide-respiring bacteria* (Adrian L and Löffler FE, eds), pp. 63-106. Springer-Verlag Berlin Heidelberg, doi: 10.1007/978-3-662-49875-0_5

ATSDR: Agency for Toxic Substances and Disease Registry (2013) Summary Data for 2013 priority list of hazardous substances. U.S. Department of Health and Human Services, Atlanta, Georgia, online at *https://www.atsdr.cdc.gov/spl/resources/ATSDR_2013_SPL_Detailed_Data_Table.pdf*, accessed May 17, 2017.

ATSDR: Agency for Toxic Substances and Disease Registry (2015) Summary Data for 2015 priority list of hazardous substances. U.S. Department of Health and Human Services, Atlanta, Georgia, online at *https://www.atsdr.cdc.gov/spl/resources/atsdr_2015_spl_detailed_data_table.pdf*, accessed May 17, 2017.

Bachmeier A, Wang VCC, Woolerton TW, Bell S, Fontecilla-Camps JC, Can M, Ragsdale SW, Chaudhary YS, Armstrong FA (2013) How light-harvesting semiconductors can alter the bias of reversible electrocatalysts in favor of H_2 production and CO_2 reduction. *J Am Chem Soc* 135, 15026-15032.

Bachmeier A, Murphy BJ, Armstrong FA (2014) A multi-heme flavoenzyme as a solar conversion catalyst. *J Am Chem Soc* 136, 12876-12879.

Bachmeier A and Armstrong F (2015) Solar-driven proton and carbon dioxide reduction to fuels – lessons from metalloenzymes. *Curr Opin Chem Biol* 25, 141-151.

Banerjee R and Ragsdale SW (2003) The many faces of vitamin B_{12}: catalysis by cobalamin-dependent enzymes. *Annu Rev Biochem* 72, 209-247.

Banerjee RV, Harder SR, Ragsdale SW, Matthews RG (1990) Mechanism of reductive activation of cobalamin-dependent methionine synthase: an electron paramagnetic resonance spectroelectrochemical study. *Biochemistry* 29, 1129–1135.

Benjdia A, Pierre S, Gherasim C, Guillot A, Carmona M, Amara P, Banerjee R, Berteau O (2015) The thiostrepton A tryptophan methyltransferase TsrM catalyses a cob(II)alamin-dependent methyl transfer reaction. *Nat Commun* 6, 8377, doi:10.1038/

ncomms9377.
Benning MM, Wesenberg MM, Wesenberg G, Liu R, Taylor KL, Dunaway-Mariano D, Holden HM (1998) The three-dimensional structure of 4-hydroxybenzoyl-CoA thioesterase from *Pseudomonas* sp. strain CBS-3. *J Biol Chem* 273, 33572-33579.
Berglund GI, Carlsson GH, Smith AT, Szöke H, Henriksen A, Hajdu J (2002) The catalytic pathway of horseradish peroxidase at high resolution. *Nature* 417, 463-468.
Bisaillon A, Beaudet R, Lépine F, Dézel E, Villemur R (2010) Identification and characterization of a novel CprA reductive dehalogenase specific to highly chlorinated phenols from *Desulfitobacterium hafniense* strain PCP-1. *Appl Environ Microbiol* 76, 7536-7540.
Blanksby SJ and Ellison GB (2003) Bond dissociation energies of organic molecules. *Acc Chem Res* 36, 255-263.
Board PG, Baker RT, Chelvanayagam G, Jermiin LS (1997) Zeta, a novel class of glutathione transferases in a range of species from plants to humans. *Biochem J* 328, 929-935.
Bobyk KD, Ballou DP, Rokita SE (2015) Rapid kinetics of dehalogenation promoted by iodotyrosine deiodinase from human thyroid. *Biochemistry* 54, 4487-4494.
Bolivar F, Rodriquez RL, Greene PJ, Betlach MC, Heyneker HL, Boyer HW, Crosa JH, Falkow S (1977) Construction and characterization of new cloning vehicles. II. A multipurpose cloning system. *Gene* 2, 95–113.
Bollet C, Gevaudan MJ, de Lamballerie X, Zandotti C, de Micco P (1991) A simple method for the isolation of chromosomal DNA from gram positive or acid-fast bacteria. *Nucleic Acids Res* 19, 1955.
Bommer M, Kunze C, Fesseler J, Schubert T, Diekert G, Dobbek H (2014) Structural basis for organohalide respiration. *Science* 346, 455-458.
Boyer AB, Pagé-Bélanger R, Saucier M, Villemur R, Lépine F, Juteau P, Beaudet R (2003) Purification, cloning and sequencing of an enzyme mediating the reductive dechlorination of 2,4,6-trichlorophenol from *Desulfitobacterium frappieri* PCP-1. *Biochem J* 373, 297-303.
Bradford MM (1976) A rapid and sensitive method for the quantification of microgram quantities of protein utilizing the principle of protein-dye binding. *Anal Biochem* 72, 248-254.
Bridwell-Rabb J and Drennan CL (2017a) Vitamin B_{12} in the spotlight again. *Curr Opin Chem Biol* 37, 63-70.
Bridwell-Rabb J, Zhong A, Sun HG, Drennan CL, Liu HW (2017b) A B_{12}-dependent radical SAM enzyme involved in oxetanocin A biosynthesis. *Nature* 544, 322-326.
Brot N and Weissbach H (1965) Enzymatic synthesis of methionine: chemical alkylation of the enzyme-bound cobamide. *J Biol Chem* 240, 3064-3070.
Buckel W and Golding BT (2008) Chemistry of B_{12}-Dependent Enzyme Reactions. *Wiley Encyclopedia of Chemical Biology* 1-9.
Burkhardt A, Pakendorf T, Reime B, Meyer J, Fischer P, Stübe N, Panneerselvam S, Lorbeer O, Stachnik K, Warmer M, Rödig P, Göries D, Meents A (2016) Status of the crystallography beamlines at PETRA III. *Eur Phys J Plus* 131, 56.
Buttet GF, Holliger C, Maillard J (2013) Functional genotyping of *Sulfurospirillum* spp. in mixed cultures allowed the identification of a new tetrachloroethene reductive dehalogenase. *Appl Environ Microbiol* 79, 6941-6947.
Cabrita MT, Vale C, Rauter AP (2010) Halogenated compounds from marine algae. *Mar Drug* 8, 2301-2317.
Calza P, Minero C, Pelizzetti E (1997) Photocatalytically assisted hydrolysis of chlorinated methanes under anaerobic conditions. *Environ Sci Technol* 31, 2198-2203.

Castanié-Cornet MP, Bruel N, Genevaux P (2014) Chaperone networking facilitates protein targeting to the bacterial cytoplasmic membrane. *Biochim Biophys Acta* 1843, 1442-1456.

Castro CE (1998) Environmental dehalogenation: chemistry and mechanism. In *Reviews of environmental contamination and toxicology* (Ware G, ed), vol. 155, p. 1. Springer Verlag Berlin Heidelberg

Champloy F, Gruber K, Jogl G, Kratky C (2000) XAS spectroscopy reveals X-ray-induced photoreduction of free and protein-bound B_{12} cofactors. *J Synchrotron Rad* 7, 267-273.

Chan CH, Newmister SA, Talyor K, Claas KR, Rayment I, Escalante-Semerena JC (2014) Dissecting cobamide diversity through structural and functional analyses of the base-activating CobT enzyme of *Salmonella enterica*. *Biochim Biophys Acta* 1840, 464-475.

Chen K, Huang L, Xu C, Liu X, He J, Zinder SH, Li S, Jiang J (2013) Molecular characterization of the enzymes involved in the degradation of a brominated aromatic herbicide. *Mol Microbiol* 89, 1121-1139.

Chen VB, Arendall WB 3rd, Headd JJ, Keedy DA, Immormino RM, Kapral GJ, Murray LW, Richardson JS, Richardson DC (2010) MolProbity: all-atom structure validation for macromolecular crystallography. *Acta Crystallogr D Biol Crystallogr* 66, 12–21.

Christiansen N, Ahring BK, Wohlfarth G, Diekert G (1998) Purification and characterization of the 3-chloro-4-hydroxy-phenylacetate reductive dehalogenase of Desulfitobacterium hafniense. *FEBS Lett* 436, 159-162.

Claas KR, Parrish JR, Maggio-Hall LA, Escalante-Semerena JC (2010) Functional analysis of the nicotinate mononucleotide:5,6-dimethylbenzimidazole phosphoribosyl-transferase (CobT) enzyme, involved in the late steps of coenzyme B_{12} biosynthesis in *Salmonella enterica*. *J Bacteriol* 192, 145-154.

Cooper M, Wagner A, Wondrousch D, Sonntag F, Sonnabend A, Brehm M, Schüürmann G, Adrian L (2015) Anaerobic microbial transformation of halogenated aromatics and fate prediction using electron density modeling. *Environ Sci Technol* 49, 6018-6028.

Cretnik S, Bernstein A, Shouakar-Stash O, Löffler F, Elsner M (2014) Chlorine isotope effects from isotope ratio mass spectrometry suggest intramolecular C-Cl bond competition in trichloroethene (TCE) reductive dehalogenation. *Molecules* 19, 6450-6473.

Crofts TS, Seth EC, Hazra AB, Taga ME (2013) Cobamide structure depends on both lower ligand availability and CobT substrate specificity. *Chem Biol* 20, 1265-1274.

Crofts TS, Hazra AB, Tran JL, Sokolovskaya OM, Osadchiy V, Ad O, Pelton J, Bauer S, Taga ME (2014) Regiospecific formation of cobamide isomers is directed byCobT. *Biochemistry* 53, 7805-7815.

Crooks GP, Xu L, Barkley RM, Copley SD (1995) Exploration of possible mechanisms for 4-chlorobenzoyl CoA dehalogenase: evidence for an aryl-enzyme intermediate. *J Am Chem Soc* 117, 10791-10798.

de Jong E and Field JA (1997) Sulfur tuft and turkey tail: biosynthesis and degradation of organohalogens by basidiomycetes. *Annu Rev Microbiol* 51, 375-414.

De Wildeman S, Diekert G, Van Langenhove H, Verstraete W (2003) Stereoselective microbial dehalorespiration with vicinal dichlorinated alkanes. *Appl Environ Microbiol* 69, 5643-5647.

Diederichs K and Karplus PA (1997) Improved R-factors for diffraction data analysis in macromolecular crystallography. *Nat Struct Biol* 4, 269–275.

Diekert G, Gugova D, Limoges B, Robert M, Savéant J-M (2005) Electroenzymatic reactions. Investigation of a reductive dehalogenase by means of electrogenerated redox cosubstrates. *J Am Chem Soc* 127, 13583-13588.

Dijk JA, Stams AJ, Schraa G,Ballerstedt H, de Bont JA, Gerritse J (2003) Anaerobic oxidation of 2-chloroethanol under denitrifying conditions by Pseudomonas stutzeri strain JJ. *Appl Environ Microbiol* 63, 68-74.

Ding C, Zhao S, He J (2014) A *Desulfitobacterium* sp. strain PR reductively dechlorinates both 1,1,1-trichloroethane and chloroform. *Environ Microbiol* 16, 3387-3397.

Ding W, Li Q, Jia Y, Ji X, Qianzhu H, Zhang Q (2016) Emerging diversity of the cobalamin-dependent methyltransferases involving radical-based mechanisms. *ChemBioChem* 17, 1191-1197.

Dolfing J and Janssen DB (1994) Estimates of Gibbs free energies of formation of chlorinated aliphatic compounds. *Biodegradation* 5, 21-28.

Dolfing J and Novak I (2015) The Gibbs free energy of formation of halogenated benzenes, benzoates and phenols and their potential role as electron acceptors in anaerobic environments. *Biodegradation* 26, 15-27.

Dowling DP, Miles ZD, Köhrer C, Maiocco SJ, Elliott SJ, Bandarian V, Drennan CL (2016) Molecular basis of cobalamin-dependent RNA modification. *Nucleic Acids Res* 44, 9965-9976.

Drennan CL, Huang S, Drummond JT, Matthews RG, Ludwig ML (1994) How a protein binds B_{12}: A 3.0 Å x-ray structure of the B_{12} binding domains of methionine synthase. *Science* 266, 1669-1674.

Driessen MD, Goodman AL, Miller TM, Zaharias GA, Grassian VH (1998) Gas-phase photooxidation of trichloroethylene on TiO_2 and ZnO: influence of trichloroethylene pressure, oxygen pressure, and the photocatalyst surface on the product distribution. *J Phys Chem B* 102, 549-556.

Duhamel M and Edwards EA (2006) Microbial composition of chlorinated ethene-degrading cultures dominated by *Dehalococcoides*. *FEMS Microbiol Ecol* 58, 538-549.

Duhamel M, Wehr SD, Yu L, Rizvi H, Seepersad D, Dworatzek S, Cox EE, Edwards EA (2002) Comparison of anaerobic dechlorinating enrichment cultures maintained on tetra-chloroethene, trichloroethene, *cis*-dichloroethene and vinyl chloride. *Water Res* 36, 4193-4202.

Emsley P, Lohkamp B, Scott WG, Cowtan K (2010) Features and development of Coot. *Acta Crystallogr D Biol Crystallogr* 66, 486–501.

Ensley BD (1991) Biochemical diversity of trichloroethylene metabolism. *Annu Rev Microbiol* 45, 283-299.

Fan J and Yates JT (1996) Mechanism of photooxidation of trichloroethylene on TiO2: detection of intermediates by infrared spectroscopy. *J Am Chem Soc* 118, 4686-4692.

Fathepure BZ and Tiedje JM (1994) Reductive dechlorination of tetrachloroethylene by a chlorobenzoate-enriched biofilm reactor. *Environ Sci Technol* 28, 746-752.

Fetzner S and Lingens F (1994) Bacterial dehalogenases: biochemistry, genetics, and biotechnological applications. *Microbiol Mol Biol Rev* 58, 641-685.

Fieber W, Hoffmann B, Schmidt W, Stupperich E, Konrat R, Kräutler B (2002) Pseudocoenzyme B_{12} and Adenosyl-Factor A: Electrochemical Synthesis and Spectroscopic Analysis of Two Natural B_{12} Coenzymes with Predominantly 'Base-off' Constitution. *Helv Chim Acta* 85, 927-944.

Field JA and Wijnberg JBPA (2003) An update on organohalogen metabolites produced by basidiomycetes. In *Natural production of organohalogen compounds* (Gribble GW, ed), vol 3, pp 103-119. Springer-Verlag Berlin Heidelberg, doi: 10.1007/978-3-540-45293-5

Fincker M and Spormann AM (2017) Biochemistry of catabolic reductive dehalogenation. *Annu Rev Biochem* 86, 357-386.

Fish WW (1988) Rapid colorimetric micromethod for the quantitation of complexed iron in biological samples. *Methods Enzymol* 158, 357-364.

Fontecave M and Ollagnier-de-Choudens S (2008) Iron-sulfur cluster biosynthesis in bacteria: mechanisms of cluster assembly and transfer. *Arch Biochem Biophys* 474, 226-237.

Fox BR, Borneman JG, Wackett LP, Lipscomb JD (1990) Haloalkene oxidation by the soluble methane monooxygenase from *Methylosinus trichosporium* OB3b. *Appl Environ Microbiol* 29, 6419-6427.

Frey B, McCloskey J, Kersten W, Kersten H (1988) New function of vitamin B_{12}: cobamide-dependent reduction of epoxyqueuosine to queuosine in tRNAs of Escherichia coli and Salmonella typhimurium. *J Bacteriol* 170, 2078-2082.

Friedrich W and Bernhauer K (1958) Zur Chemie und Biochemie der „Cobalamine", VIII. Über die 5- und 6-Methyl-benzimidazol-cobalamin-Analoga. *Chemische Berichte* 91, 1665-1670.

Froese DS, Kochan GT, Muniz JRC, Wu X, Gileadi C, Ugochukwu E, Krysztofinska E, Gravel RA, Oppermann UCT, Yue WW (2010) Structures of the human GTPase MMMA and vitamin B_{12}-dependent methylmalonyl-CoA mutase and insight into their complex formation. *J Biol Chem* 285, 38204-38213.

Froese DS, Krojer T, Wu X, Shrestha R, Kiyani W, von Delft F, Gravel RA, Oppermann U, Yue WW (2012) Structure of MMACHC reveals an arginine-rich pocket and a domain-swapped dimer for its B_{12} processing function. *Biochemistry* 51, 5083-5090.

Fuchs G (2008) Anaerobic metabolism of aromatic compounds. *Ann N Y Acad Sci* 1125, 82-99.

Fung JM, Morris RM, Adrian L, Zinder SH (2007) Expression of reductive dehalogenase genes in *Dehalococcoides ethenogenes* strain 195 growing on tetrachloroethene, trichloroethene, or 2,3-dichlorophenol. *Appl Environ Microbiol* 73, 4439-45.

Futagami T, Goto M, Furukawa K (2008) Biochemical and genetic bases of dehalorespiration. *Chem Rec* 8, 1-12.

Gälli R, Stucki G, Leisinger T (1982) Mechanism of dehalogenation of dichloromethane by cell extracts of Hyphomicrobium DM2. *Experientia* 38, 1378.

Gantzer CJ and Wackett LP (1991) Reductive dechlorination catalysed by bacterial transition-metal coenzymes. Environ Sci Technol 25, 715-722.

Gerritse J, Renard V, Pedro-Gomes TM, Lawson PA, Collins MD, Gottschal JC (1996) *Desulfitobacterium* sp. strain PCE1, an anaerobic bacterium that can grow by reductive dechlorination of tetrachloroethene or *ortho*-chlorinated phenols. *Arch Microbiol* 165, 132-140.

Giese B, Laturnus F, Adams FC, Wiencke C (1999) Release of volatile iodinated C_1-C_4 hydrocarbons by marine macroalgae from various climate zones. *Environ Sci Technol* 33, 2432-2439.

Glod G, Angst W, Holliger C, Schwarzenbach RP (1997) Corrinoid-mediated reduction of tetrachloroethene, trichloroethene, and trichlorofluoroethene in homogeneous aqueous solution: reaction kinetics and reaction mechanisms. *Environ Sci Technol* 31, 253-260.

Goris T, Schubert T, Gadkari J, Wubet T, Tarkka M, Buscot F, Adrian L, Diekert G (2014) Insights into organohalide respiration and the versatile catabolism of *Sulfuospirillum multivorans* gained from comparative genomics and physiological studies. *Environ Microbiol* 16, 3562-3580.

Goris T, Schiffmann CL, Gadkari J, Schubert T, Seifert J, Jehmlich N, von Bergen M, Diekert G (2015) Proteomics of the organohalide-respiring Epsilonproteobacerium *Sulfurospirillum multivorans* adapted to tetrachloroethene and other energy substrates. *Sci Rep* 5, 13794.

Goris T, Schenz B, Zimmermann J, Lemos M, Hackermüller J, Schubert T, Diekert G (2017) The complete genome of the tetrachloroethene-respiring epsilonproteobacterium *Sulfurospirillum halorespirans*. *J Biotechnol* 255, 33-36.

Gray HB and Winkler JR (2005) Long-range electron transfer. *Proc Natl Acad Sci U.S.A.* 102, 3534-3539.

Gribble GW (1992) Naturally occurring organohalogen compounds - a survey. *J Nat Prod* 55, 1353-1395.

Gribble GW (2003) The diversity of naturally produced organohalogens. *Chemosphere* 52, 289-297.

Gribble GW (2004) Amazing organohalogens. *Am Sci* 92, 342-349.

Gribble GW (2012) Recently discovered naturally occuring heterocyclic organohalogen compounds. *Heterocycles* 84, 157-207.

Grostern A and Edwards EA (2009) Characterization of a *Dehalobacter* coculture that dechlorinates 1,2-dichloroethane to ethene and identification of the putative reductive dehalogenase gene. *Appl Environ Microbiol* 75, 2684-2693.

Gruber K, Puffer B, Kräutler B (2003) Vitamin B_{12}-derivatives-enzyme cofactors and ligands of proteins and nucleic acids. *Chem Soc Rev* 40, 4346-4363.

Gruber K, Puffer B, Kräutler B (2011) Vitamin B_{12}-derivatives enzyme cofactors and ligands of proteins and nucleic acids. *Chem Soc Rev* 40, 4346-4363.

Hagen WR (2006) EPR spectroscopy as a probe of metal centres in biological systems. Dalton Trans 37, 4415–4434.

Hagen WR (2009) *Biomolecular EPR spectroscopy*. CRC Press / Taylor & Francis Group, Boca Raton, Fl, USA.

Häggblom MM and Young LY (1999) Anaerobic degradation of 3-halobenzoates by a denitrifying bacterium. *Arch Microbiol* 171, 230-236.

Harper DB and Hamilton JTG (2003) The global cycles of the naturally-occuring monohalomethanes. In *Natural production of organohalogen compounds* (Gribble GW, ed), vol 3, pp 17-41. Springer-Verlag Berlin-Heidelberg, doi: 10.1007/978-3-540-45293-5

Hazra AB, Tran JL, Crofts TS, Taga ME (2013) Analysis of substrate specificity in CobT homologs reveals widespread preference for DMB, the lower axial ligand of vitamin B_{12}. *Chem Biol* 20, 1275-1285.

Hazra AB, Han AW, Mehta AP, Mok KC, Osadchiy V, Begley TP, Taga ME (2015) Anaerobic biosynthesis of the lower ligand of vitamin B_{12}. *Proc Natl Acad Sci U S A* 112, 10792-10797.

Heckel B, Cretnik S, Kliegman S, Shouakar-Stash O, McNeill K, Elsner M (2017) Reductive outer-sphere single electron transfer is an exception rather than the rule in natural and engineered chlorinated ethene dehalogenation. *Environ Sci Technol*, doi: 10.1021/acs.est.7b01447.

Hexter SV, Esterle TF, Armstrong FA (2014) A unified model for surface electrocatalysis based on observations with enzymes. *Phys Chem Chem Phys* 16, 11822-11833.

Higuchi R, Krummel B, Saiki RK (1988) A general method of *in vitro* preparation and specific mutagenesis of DNA fragments: study of protein and DNA interactions. *Nucleic Acids Res* 16, 7351-7367.

Holliger C, Hahn D, Harmsen H, Ludwig W, Schumacher W, Tindall B, Vazquez F, Weiss N, Zehnder AJB (1998) *Dehalobacter restrictus* gen. nov. and sp. nov., a strictly anaerobic bacterium that reductively dechlorinates tetra- and trichlroethene in an anaerobic respiration. *Arch Microbiol* 169, 313-321.

Holliger C, Wohlfarth G, Diekert G (1999) Reductive dechlorination in the energy metabolism of anaerobic bacteria. *FEMS Microbiol Rev* 22, 383-398.

Holliger C, Regeard C, Diekert G (2003) Dehalogenation by anaerobic bacteria. In *Dehalogenation: Microbial Processes and Environmental Applications* (Häggblom MM and Bossert ID, eds), pp. 115-157. Kluwer Academic Publisher, Dordrecht, the Netherlands, doi: 10.1007/b101852

Holm L and Rosenström P (2010) Dali server: Conservation mapping in 3D. *Nucleic Acids Res* 38 (Web Server issue), W545–W549.

Holton JM (2009) A beginner's guide to radiation damage. *J Synchrotron Radiat* 16, 133-142.

Hu J, Chuenchor W, Rokita SE (2015) A switch between one- and two-electron chemistry of the human flavoprotein iodotyrosine deiodinase is controlled by substrate. *J Biol Chem* 290, 590-600.

Hug LA, Maphosa F, Leys D, Löffler FE, Smidt H, Edwards EA, Adrian L (2013) Overview of organohalide-respiring bacteria and a proposal for a classification system for reductive dehalogenases. *Phil Trans R Soc B* 368, 20120322.

Johannissen LO, Leys D, Hay S (2017) A common mechanism for coenzyme cobalamin-dependent reductive dehalogenases. *Phys Chem Chem Phys* 19, 6090-6094.

John M, Schmitz RPH, Westermann M, Richter W, Diekert G (2006) Growth substrate dependent localization of tetrachloroethene reductive dehalogenase in *Sulfurospirillum multivorans*. *Arch Microbiol* 186, 99-106.

John M, Rubick R, Schmitz RPH, Rakoczy J, Schubert T, Diekert G (2009) Retentive memory of bacteria: Long-term regulation of dehalorespiration in *Sulfurospirillum multivorans*. *J Bacteriol* 191, 1650-1655.

Jordan A, Harnisch J, Borchers R, Guern F, Shinohara H (2000) Volcanogenic halocarbons. *Environ Sci Technol* 34, 1122-1124.

Judger B-E, Ertan H, Lee M, Manefield M, Marquis CP (2015) Reductive dehalogenases come of age in biological destruction of organohalides. *Trends Biotechnol* 33, 595-610.

Jugder B-E, Ertan H, Bohl S, Lee M, Marquis CP, Manefield M (2016) Organohalide respiring bacteria and reductive dehalogenases: key tools in organohalide bioremediation. *Front Microbiol* 7, 249.

Judger BE, Bohl S, Lebhar H, Healey RD, Manefield M, Marquis CP, Lee M (2017) A bacterial chloroform reductive dehalogenase: purification and biochemical characterization. *Microb Biotechnol*, doi: 10.1111/1751-7915.12745.

Justicia-Leon SD, Ritalahti KM, Mack EE, Löffler FE (2012) Dichloromethane fermentation by a *Dehalobacter* sp. in an enrichment culture derived from pristine river sediment. *Appl Environ Microbiol* 78, 1288-1291.

Kabsch W (2010) XDS. *Acta Crystallogr D Biol Crystallogr* 66, 125–132.

Karplus PA, Diederichs K (2012) Linking crystallographic model and data quality. *Science* 336, 1030–1033.

Keller S, Ruetz M, Kunze C, Kräutler B, Diekert G, Schubert T (2014) Exogenous 5,6-dimethylbenzimidazole caused production of a non-functional tetrachloroethene reductive dehalogenase in *Sulfurospirillum multivorans*. *Environ Microbiol* 16, 3361-3369.

Keller S, Treder A, von Reuss SH, Escalante-Semerena JC, Schubert T (2016) The SMUL_1544 Gene Product Governs Norcobamide Biosynthesis in the Tetrachloroethene-Respiring Bacterium *Sulfurospirillum multivorans*. *J Bacteriol* 198, 2236-2243.

Kennes C, Pries F, Krooshof GH, Bokma E, Kingma J, Janssen DB (1995) Replacement of tryptophan residues in haloalkane dehalogenase reduces halide binding and catalytic

activity. *Eur J Biochem* 228, 403-407.

Kiefer Jr. PM, McCarthy DL, Copley SD (2002) The reaction catalyzed by tetrachlorohydroquinone dehalogenase does not involve nucleophilic aromatic substitution. *Biochemistry* 41, 1308-1314.

Kiel M and Engesser KH (2015) The biodegradation vs. biotransformation of fluorosubstituted aromatics. *Appl Microbiol Biotechnol* 99, 7433-7464.

Kim J, Gherasim C, Banerjee R (2008) Decyanation of vitamin B_{12} by a trafficking chaperone. *Proc Natl Acad Sci U.S.A.* 105, 14551-14554.

Kim S-H, Harzman C, Davis JK, Hutcheson R, Broderick JB, Marsh TL, Tiedje JM (2012) Genome sequence of *Desulfitobacterium hafniense* DCB-2, a Gram-positive anaerobe capable of dehalogenation and metal reduction. *BMC Microbiol* 12:21.

Kim YE, Hipp MS, Bracher A, Hayer-Hartl M, Hartl FU (2013) Molecular chaperone functions in protein folding and proteostasis. *Annu Rev Biochem* 82, 323-355.

Kleindienst S, Higgins SA, Tsementzi D, Chen G, Konstantinidis KT, Mack EE, Löffler FE (2017) 'Candidatus *Dichloromethanomonas elyunquensis*' gen. nov., sp. nov., a dichloromethane-degrading anaerobe of the Peptococcaceae family. *Syst Appl Microbiol* 40, 150-159.

Kohler-Staub D and Leisinger T (1985) Dichloromethane dehalogenase of *Hyphomicrobium* sp. strain DM2. *J Bacteriol* 162, 676-681.

Kohler-Staub D, Hartmans S, Gälli R, Suter F, Leisinger T (1986) Ecidence for identical dichloromethane dehalogenases in different methylotrophic bacteria. *J Gen Microbiol* 132, 2837-2843.

Krasotkina J, Walters T, Maruya KA, Ragsdale SW (2001) Characterization of the B_{12}- and iron-sulfur-containing reductive dehalogenase from *Desulfitobacterium chlororespirans*. *J Biol Chem* 276, 40991-40997.

Kräutler B, Moll J, Thauer RK (1987) The corrinoid from *Methanobacterium thermoautotrophicum* (Marburg strain). Spectroscopic structure analysis and identification as Coβ-cyano-5'-hydroxybenzimidazolyl-cobamide (factor III). *Eur J Biochem* 162, 275-278.

Kräutler B, Fieber W, Ostermann S, Fasching M, Ongania K-H, Gruber K, Kratky C, Mikl C, Siebert A, Diekert G (2003) The cofactor of tetrachloroethene reductive dehalogenase of *Dehalospirillum multivorans* is norpseudo-B_{12}, a new type of a natural corrinoid. *Helv Chim Acta* 86, 3698-3716.

Krone UE, Thauer RK, Hogenkamp HPC (1989a) Reductive dehalogenation of chlorinated C_1-hydrocarbons mediated by corrinoids. *Biochemistry* 28, 4908-4914.

Krone UE, Laufer K, Thauer RK, Hogenkamp HPC (1989b) Coenzyme F430 as a possible catalyst for the reductive dehalogenation of chlorinated C1 hydrocarbons in methanogenic bacteria. *Biochemistry* 28: 10061-10065.

Krug M, Weiss MS, Heinemann U, Mueller U (2012) XDSAPP: a graphical user interface for the convenient processing of diffraction data using XDS. *J Appl Cryst* 45, 568–572.

Kruse T, van de Pas BA, Atteia A, Krab K, Hagen WR, Goodwin L, Chain P, Boeren S, Maphosa F, Schraa G, de Vos WM, van der Oost J, Smidt H, Stams AJ (2015) Genomic, proteomic, and biochemical analysis of the organohalide respiratory pathway in *Desulfitobacterium dehalogenans*. *J Bacteriol* 197, 893-904.

Kublik A, Deobald D, Hartwig S, Schiffmann CL, Andrades A, von Bergen M, Sawers RG, Adrian L (2016) Identification of a multi-protein reductive dehalogenase complex in Dehalococcoides mccartyi strain CBDB1 suggests a protein-dependent respiratory electron transport chain obviating quinone involvement. *Environ Microbiol* 18, 3044-3056.

Kuntze K, Kiefer P, Baumann S, Seifert J, von Bergen M, Vorholt JA, Boll M (2011) Enzymes involved in the anaerobic degradation of metasubstituted halobenzoates. *Mol Microbiol* 82, 758-769.

Kunze C, Bommer M, Hagen WR, Uksa M, Dobbek H, Schubert T, Diekert G (2017) Cobamide-mediated enzymatic reductive dehalogenation via long-range electron transfer. *Nat Commun*, in press.

Leisinger T, Bader R, Hermann R, Schmid-Appert M, Vuilleumier S (1994) Microbes, enzymes and genes involved in dichloromethane utilization. *Biodegradation* 5, 237-248.

Lenhert PG and Hodgkin DC (1961) Structure of the 5,6-dimethylbenzimidazolylcobamide coenzyme. *Nature* 192, 937-938.

Leri AC, Marcus MA, Myneni SCB (2007) X-ray spectromicroscopic investigation of natural organochlorine distribution in weathering plant material. *Geochim Cosmochim Acta* 71, 5834-5846.

Lexa D and Saveant JM (1983) The electrochemistry of vitamin B_{12}. *Acc Chem Res* 16, 235-243.

Liao R-Z, Chen S-L, Siegbahn PEM (2015) Which oxidation state initiates dehalogenation in the B_{12}-dependent enzyme NpRdhA, Co^{I}, Co^{II} or Co^{0}? *ACS Catal* 5, 7350-7358.

Liao R-Z, Chen S-L, Siegbahn PEM (2016) Unraveling the mechanism and regioselectivity of the B_{12}-dependent reductive dehalogenase PceA. *Chem Eur J* 22, 12391-12399.

Löffler FE, Cole JR, Ritalahti KM, Tiedje JM (2003) Diversity of dechlorinating bacteria. In *Dehalogenation – Microbial processes and environmental applications* (Häggblom MM and Bossert ID, eds), pp. 53-87. Kluwer Academics Publisher, Boston/Dordrecht/London

Löffler FE, Yan J, Ritalahti KM, Adrian L, Edwards EA, Konstantinidis KT, Müller JA, Fullerton H, Zinder SH, Spormann AM (2013) *Dehalococcoides mccartyi* gen. nov., sp. nov., obligately organohaliderespiring anaerobic bacteria relevant to halogen cycling and bioremediation, belong to a novel bacterial class, *Dehalococcoidia* classis nov., order *Dehalococcoidales* ord. nov. and family *Dehalococcoidaceae* fam. nov., within the phylum *Chloroflexi*. *Int J Syst Evol Microbiol* 63, 625-635.

Ludwig ML and Matthews RG (1997) Structure-based perspectives on B_{12}-dependent enzymes. *Annu Rev Biochem* 66, 269-313.

Luijten ML, de Weert J, Smidt H, Boschker HT, de Vos WM, Schraa G, Stams AJ (2003) Description of *Sulfurospirillum halorespirans* sp. nov., an anaerobic, tetrachloroethene-respiring bacterium, and transfer of *Dehalospirillum multivorans* to the genus *Sulfurospirillum* as *Sulfurospirillum multivorans* comb. nov. *Int J Syst Evol Microbiol* 53, 787-793.

Mac Nelly A, Kai M, Svatos A, Diekert G, Schubert T (2014) Functional heterologous production of reductive dehalogenases from *Desulfitobacterium hafniense* strains. *Appl Environ Microbiol* 80, 4313-4322.

Maggio-Hall LA and Escalante-Semerena JC (1999) *In vitro* synthesis of the nucleotide loop of cobalamin by *Salmonella typhimurium* enzymes. *Proc Natl Acad Sci USA* 96, 11798-11803.

Mägli A, Wendt M, Leisinger T (1996) Isolation and characterization of *Dehalobacter formicoaceticum* gen. nov. sp. nov., a strictly anaerobic bacterium utilizing dichloromethane as source of carbon and energy. *Arch Microbiol* 166, 101-108.

Magnuson JK, Stern RV, Gossett JM, Zinder SH, Burris DR (1998) Reductive dechlorination of tetrachloroethene to ethene by a two-component enzyme pathway. *Appl Environ Microbiol* 64, 1270-1275.

Magnuson JK, Romine MF, Burris DR, Kingsley MT (2000) Trichloroethene reductive dehalogenase from *Dehalococcoides ethenogenes*: sequence of *tceA* and substrate range characterization. *Appl Environ Microbiol* 66, 5141-5147.

Maillard J, Schumacher W, Vazquez F, Regeard C, Hagen WR, Holliger C (2003) Characterization of the corrinoid iron-sulfur protein tetrachloroethene reductive dehalogenase of *Dehalobacter restrictus*. *Appl Environ Microbiol* 69, 4628-4638.

Maillard J, Genevaux P, Holliger C (2011) Redundancy and specificity of multiple trigger factor chaperones in Desulfitobacteria. *Microbiology* 157, 2410-2421.

Major DW, McMaster ML, Cox EE, Edwards EA, Dworatzek SM, Hendrickson ER, Starr MG, Payne JA, Buonamici LW (2002) Field demonstration of successful bioaugmentation to achieve dechlorination of tetrachloroethene to ethene. *Environ Sci Technol* 36, 5106-5116.

Mancia F, Keep NH, Nakagawa A, Leadlay PF, McSweeney S, Rasmussen B, Boseck P, Diat O, Evans PR (1996) How coenzyme B_{12} radicals are generated: The crystal structure of methylmalonyl-coenzyme A mutase at 2Å resolution. *Structure* 4, 339-350.

Maphosa F, de Vos WM, Smidt H (2010) Exploiting the ecogenomics toolbox for environmental diagnostics of organohalide-respiring bacteria. *Trends Biotechnol* 28, 308-316.

Marzorati M, de Ferra F, Van Raemdonck H, Borin S, Allifranchini E, Carpani G, Serbolisca L, Verstraete W, Boon N, Daffonchio D (2007) A novel reductive dehalogenase, identified in a contaminated groundwater enrichment culture and in *Desulfitobacterium dichloroeliminans* strain DCA1, is linked to dehalogenation of 1,2-dichloroethane. *Appl Environ Microbiol* 73, 2990-2999.

Marzorati M, Balloi A, de Ferra F, Corallo L, Carpani G, Wittebolle L, Verstraete W, Daffonchio D (2010) Bacterial diversity and reductive dehalogenase redundancy in a 1,2-dichloroethane-degrading bacterial consortium enriched from a contaminated aquifer. *Microb Cell Fact* 9, 12, doi: 10.1186/1475-2859-9-12.

Matthews RG (2001) Cobalamin-dependent methyltransferases. *Acc Chem Res* 34, 681-689.

Mayer-Blackwell K, Sewell H, Fincker M, Spormann AM (2016) Comparative physiology of organohalide-respiring bacteria. In *Organohalide-respiring bacteria* (Adrian L and Löffler FE, eds), pp. 259-280. Springer-Verlag Berlin Heidelberg, doi: 10.1007/978-3-662-49875-0_12

Maymó-Gatell X, Anguish T, Zinder SH (1999) Reductive dechlorination of chlorinated ethenes and 1,2-dichloroethane by *Dehalococcoides ethenogenes* 195. *Appl Environ Microbiol* 65, 3108-3113.

McCarthy DL, Louie DF, Copley SD (1997) Identification of a covalent intermediate between glutathione and cysteine13 during during catalysis by tetrachlorohydroquinone dehalogenase. *J Am Chem Soc* 119, 11337-11338.

McCauley KM, Pratt DA, Wilson SR, Shey J, Burkey TJ, van der Donk WA (2005) Properties and reactivity of chlorovinylcobalamin and vinylcobalamin and their implications for vitamin B_{12}-catalyzed reductive dechlorination of chlorinated alkenes. *J Am Chem Soc* 127, 1126-1136.

McConnell O and Fenical W (1977) Halogen chemistry of the red algae *Asparagopsis*. *Phytochemistry* 16, 367-374.

Meents A, Reime B, Stuebe N, Fischer P, Warmer M, Goeries D, Roever J, Meyer J, Fischer J, Burkhardt A, Vartiainen I, Karvinen P, David C (2013) Development of an in-vacuum x-ray microscope with cryogenic sample cooling for beamline P11 at PETRA III. *Proceedings of SPIE* 8851, X-Ray Nanoimaging: Instruments and Methods, 88510K.

Merlino G, Balloi A, Marzorati M, Mapelli F, Rizzi A, Lavazza D, de Ferra F, Carpani G, Daffonchio D (2015) Diverse reductive dehalogenases are associated with Clostridiales-enriched microcosms dechlorinating 1,2-dichloroethane. *BioMed Res Int* 2015, 242856.

Meyer DJ, Coles B, Pemble SE, Gilmore KS, Fraser GM, Ketterer B (1991) Theta, a new class of glutathione transferases purified from rat and man. *Biochem J* 274, 409-414.

Miles ZD, McCarty RM, Molnar G, Bandarian V (2011) Discovery of epoxyqueuosine (oQ) reductase reveals parallels between halorespiration and tRNA modification. *Proc Natl Acad Sci USA* 108, 7368-7372.

Miles ZD, Myers WK, Kincannon WM, Britt RD, Bandarian V (2015) Biochemical and spectroscopic studies of epoxyqueosine reductase: a novel iron-sulfur cluster and cobalamin containing protein involved in the biosynthesis of queosine. *Biochemistry* 54, 4927-4935.

Miller E, Wohlfarth G, Diekert G (1997) Studies on tetrachloroethene respiration in *Dehalospirillum multivorans*. *Arch Microbiol* 166, 379-387.

Miller E, Wohlfarth G, Diekert G (1998) Purification and characterization of the tetrachloroethene reductive dehalogenase of strain PCE-S. *Arch Microbiol* 169, 497-502.

Mohn WW and Tiedje JM (1992) Microbial reductive dehalogenation. *Microbiol Mol Biol Rev* 56, 482-507.

Moore SJ, Lawrence AD, Biedendieck R, Deery E, Frank S, Howard MJ, Rigby SE, Warren MJ (2013) Elucidation of the anaerobic pathway for the corrin component of cobalamin (vitamin-B_{12}). *Proc Natl, Acad Sci U S A* 110, 14906-14911.

Moore TC and Escalante-Semerena JC (2016) Corrinoid metabolism in dehalogenating pure cultures and microbial communities. In *Organohalide-respiring bacteria* (Adrian L and Löffler FE, eds), pp. 455-484. Springer-Verlag Berlin Heidelberg, doi: 10.1007/978-3-662-49875-0_19

Moriarty NW, Grosse-Kunstleve RW, Adams PD (2009) electronic Ligand Builder and Optimization Workbench (eLBOW): a tool for ligand coordinate and restraint generation. *Acta Crystallogr D Biol Crystallogr* 65, 1074–1080.

Morita Y, Futagami T, Goto M, Furukawa K (2009) Functional characterization of the trigger factor protein PceT of tetrachloroethene-dechlorinating *Desulfitobacterium hafniense* Y51. *Appl Microbiol Biotechnol* 83, 775-781.

Müller R, Thiele J, Klages U, Lingens F (1984) Incorporationof [18O] water into 4-hydroxybenzoic acid in the reaction of 4-chlorobenzoate dehalogenase from *Pseudomonas* sp. CBS3. *Biochem Biophys Res Commun* 124, 178-182.

Müller JA, Rosner BM, von Abendroth G, Meshulam-Simon G, McCarty PL, Spormann AM (2004) Molecular identification of the catabolic vinyl chloride reductase from *Dehalococcoides* sp. strain VS and its environmental distribution. *Appl Environ Microbiol* 70, 4880-4888.

Mueller U, Darowski N, Fuchs MR, Förster R, Hellmig M, Paithankar KS, Pühringer S, Steffien M, Zocher G, Weiss MS (2012) Facilities for macromolecular crystallography at the Helmholtz-Zentrum Berlin. *J Synchrotron Radiat* 19, 442–449.

Neumann A, Scholz-Muramatsu H, Diekert G (1994) Tetrachloroethene metabolism of *Dehalospirillum multivorans*. *Arch Microbiol* 162, 295-301.

Neumann A, Wohlfarth G, Diekert G (1995) Properties of tetrachloroethene and trichloroethene dehalogenase of *Dehalospirillum multivorans*. *Arch Microbiol* 163, 276-281.

Neumann A, Wohlfarth G, Diekert G (1996) Purification and characterization of tetrachloroethene reductive dehalogenase from *Dehalospirillum multivorans*. *J Biol Chem* 271, 16515-16519.

Neumann A, Wohlfarth G, Diekert G (1998) Tetrachloroethene dehalogenase from *Dehalospirillum multivorans*: cloning, sequencing of the encoding genes, and expression of the pceA gene in *Escherichia coli*. *J Bacteriol* 180, 4140–4145.

Neumann A, Siebert A, Trescher T, Reinhardt S, Wohlfarth G, Diekert G (2002) Tetrachloroethene reductive dehalogenase of *Dehalospirillum multivorans*: substrate specificity of the native enzyme and its corrinoid cofactor. *Arch. Microbiol* 177, 420-426.

Ni S, Fredrickson JK, Xun L (1995) Purification and characterization of a novel 3-chlorobenzoate reductive dehalogenase from the cytoplasmic membrane of *Desulfomonile tiedjei* DCB-1. *J Bacteriol* 177, 5135-39.

Nijenhuis I and Zinder SH (2005) Characterization of hydrogenase and reductive dehalogenase activities of *Dehalococcoides ethenogenes* strain 195. *Appl Environ Microbiol* 71, 1664-1667.

Orser CS, Dutton J, Lange C, Jablonski P, Xun L, Hargis M (1993) Characterization of a Flavobacterium glutathione-S-transferase gene involved in reductive dehalogenation. *J Bacteriol* 175, 2640-2644.

Orser CS and Lange CC (1994) Molecular analysis of pentachlorophenol degradation. Biodegradation 5, 277-288.

Padilla-Crespo E, Yan J, Swift C, Wagner DD, Chourev K, Hettich RL, Ritalahti KM, Löffler FE (2014) Identification and environmental distribution of dcpA, which encodes the reductive dehalogenase catalyzing the dichloroelimination of 1,2-dichloropropane to propene in organohalide-respiring chloroflexi. *Appl Environ Microbiol* 80, 808-818.

Padovani D, Labunska T, Palfey BA, Ballou DP, Banerjee R (2008) Adenosyltransferase tailors and delivers coenzyme B_{12}. *Nat Chem Biol* 4, 194-196.

Palmer T and Berks BC (2012) The twin-arginine translocation (Tat) protein export pathway. *Nat Rev Microbiol* 10, 483-496.

Parthasarathy A, Stich TA, Lohner ST, Lesnefsky A, Britt RD, Spormann AM (2015) Biochemical and EPR-spectroscopic investigation into heterologously expressed vinyl chloride reductive dehalogenase (VcrA) from *Dehalococcoides mccartyi* strain VS. *J Am Chem Soc* 137, 3525-3532.

Paul C and Pohnert G (2011) Production and role of volatile halogenated compounds from marine algae. *Nat Prod Rep* 28, 186-195.

Payne KAP, Quezada CP, Fisher K, Dunstan MS, Collins FA, Sjuts H, Levy C, Hay S, Rigby SEJ, Leys D (2015a) Reductive dehalogenase structure suggests a mechanism for B_{12}-dependent dehalogenation. *Nature* 517, 513-516.

Payne KAP, Fisher K, Sjuts H, Dunstan MS, Bellina B, Johannissen L, Barran P, Hay S, Rigby SEJ, Leys D (2015b) Epoxyqueuosine reductase structure suggests a mechanism for cobalamin-dependent tRNA modification. *J Biol Chem* 290, 27572-27581.

Phatarphekar A, Buss JM, Rokita SE (2014) Iodotyrosine deiodinase: a unique flavoprotein present in organisms of diverse phyla. *Mol BioSyst* 10, 86-92.

Picardal FW, Arnold RG, Couch H, Little AM, Smith ME (1993) Involvement of cytochromes in the anaerobic biotransformation of tetrachloromethane by *Shewanella putrefaciens* 200. *Appl Environ Microbiol* 59, 3763-3770.

Pietra F (2015) Uptake of organohalide pollutants, and release of partially dehalogenated products, by NpRdhA, a 'base-off' cob(II)alamin-dependent reductive dehalogenase from a deep sea bacterium. A molecular dynamics investigation. *Chem Biodivers* 12, 1945-1953.

Pries F, Kingma J, Pentenga M, van Pouderoyen G, Jeronimus-Stratingh CM, Bruins AP, Janssen DB (1994) Site-directed mutagenesis and oxygen isotope incorporation studies

of the nucleophilic aspartate of haloalkane dehalogenase. *Biochemistry* 33, 1242-1247.

Ragsdale SW (2006) Metals and their scaffolds to promote difficult enzymatic reactions. *Chem Rev* 106, 3317-3337.

Ragsdale SW (2008) Catalysis of methyl group transfers involving tetrahydrofolate and B_{12}. *Vitam Horm* 79, 293-324.

Reinhold A, Westermann M, Seifert J, von Bergen M, Schubert T, Diekert G (2012) Impact of vitamin B_{12} on formation of the tetrachloroethene reductive dehalogenase in *Desulfitobacterium hafniense* Y51. *Appl Environ Microbiol* 78, 8025-8032.

Reisner E., Powell DJ, Cavazza C., Fontecilla-Camps JC, Armstrong FA (2009) Visible light-driven H_2 production by hydrogenases attached to dye-sensitized TiO_2 nanoparticles. *J Am Chem Soc* 131, 18457-18466.

Renz P (1999) Biosynthesis of the 5,6-dimethylbenzimidazole moiety of cobalamin and of the other bases found in natural corrinoids. In *Chemistry and Biochemistry of B12* (Banerjee R, ed), pp. 557-576. John Wiley & Sons, New York, USA

Rokita SE, Adler JM, McTamney PM, Watson Jr. JA (2010) Efficient use and recycling of the micronutrient iodide in mammals. *Biochimie* 92, 1227-1235.

Roy A, Kucukural A, Zhang Y (2010) I-TASSER: a unified platform for automated protein structure and function prediction. *Nat Protoc* 5, 725-738.

Rupakula A, Kruse T, Boeren S, Holliger C, Smidt H, Maillard J (2013) The restricted metabolism of the obligate organohalide respiring bacterium *Dehalobacter restrictus*: lessons from tiered functional genomics. *Phil Trans R Soc B* 368, 20120325.

Sambrook J, Fritsch EF, Maniatis T (1989) *Molecular Cloning: A Laboratory Manual*, 2nd ed, Cold Spring Harbor Laboratory Press, Cold Spring Harbor, NY, USA.

Saporito-Irwin SM, Geist RT, Gutmann DH (1997) Ammonium acetate protocol for the preparation of plasmid DNA suitable for mammalian cell transfections. Biotechniques 23, 424–427.

Schanke CA and Wackett LP (1992) Environmental reductive elimination reactions of polychlorinated ethanes mimicked by transition-metal coenzymes. *Environ Sci Technol* 26, 830-833.

Schlichting I, Berendzen J, Chu K, Stock AM, Maves SA, Benson DE, Sweet RM, Ringe D, Petsko GA, Sligar SG (2000) The catalytic pathway of cytochrome P450cam at atomic resolution. *Science* 287, 1615-1622.

Schmitz RPH, Wolf J, Habel A, Neumann A, Ploss K, Svatos A, Boland W, Diekert G (2007) Evidence for a radical mechanism of the dechlorination of chlorinated propenes mediated by the tetrachloroethene reductive dehalogenase of *Sulfurospirillum multivorans*. *Environ Sci Technol* 41, 7370-7375.

Scholz-Muramatsu H, Neumann A, Messmer M, Moore E, Diekert G (1995) Isolation and characterization of *Dehalospirillum multivorans* gen. nov., sp. nov., a tetrachloroethene-utilizing, strictly anaerobic bacterium. *Arch Microbiol* 163, 48-56.

Schrauzer GN and Windgassen RJ (1967) On hydroxyalkyl-cobaloximes and the mechanism of a cobamide-dependent diol dehydrase. *J Am Chem Soc* 89, 143-147.

Schrauzer GN and Deutsch E (1969) Reactions of cobalt(I) supernucleophiles. The alkylation of vitamin B_{12}s, cobaloximes(I), and related compounds. *J Am Chem Soc* 91, 3341-3350.

Schubert T and Diekert G (2016) Comparative biochemistry of organohalide respiration. In *Organohalide-respiring bacteria* (Adrian L and Löffler FE, eds), pp. 397-427. Springer-Verlag Berlin Heidelberg, doi: 10.1007/978-3-662-49875-0_17

Schubert T (2017) The organohalide-respiring bacterium *Sulfurospirillum multivorans*: a natural source for unusual cobamides. *World J Microbiol Biotechnol* 33, 93.

Schühle K, Gescher J, Feil U, Paul M, Jahn M, Schägger H, Fuchs G (2003) Benzoate-coenzyme A ligase from Thauera aromatica: an enzyme acting in anaerobic and aerobic pathways. *J Bacteriol* 185, 4920-4929.

Schumacher W and Holliger C (1996) The proton/electron ratio of the menaquinone-dependent electron transport from dihydrogen to tetrachloroethene in "*Dehalobacter restrictus*". *J Bacteriol* 178, 2328-2333.

Schumacher W, Holliger C, Zehnder AJ, Hagen WR (1997) Redox chemistry of cobalamin and iron-sulfur cofactors in the tetrachloroethene reductase of *Dehalobacter restrictus*. *FEBS Lett* 409, 421-425.

Shey J and van der Donk WA (2000) Mechanistic studies on the vitamin B_{12}-catalyzed dechlorination of chlorinated alkenes. *J Am Chem Soc* 122, 12403-12404.

Sievers F, Wilm A, Dineen DG, Gibson TJ, Karplus K, Li W, Lopez R, McWilliam H, Remmert M, Söding J, Thompson JD, Higgins DG (2011) Fast, scalable generation of high-quality protein multiple sequence alignments using Clustal Omega. *Mol Syst Biol* 7, 539.

Simon J, Gross R, Ringel M, Schmidt E, Kröger A (1998) Deletion and site-directed mutagenesis of the *Wolinella succinogenes* fumarate reductase operon. *Eur J Biochem* 251, 418–426.

Sjuts H, Fisher K, Dunstan MS, Rigby SE, Leys D (2012) Heterologous expression, purification and cofactor reconstitution of the reductive dehalogenase PceA from *Dehalobacter restrictus*. *Protein Expr Purif* 85, 224-229.

Song BK, Palleroni NJ, Häggblom MM (2000) Isolation and characterization of diverse halobenzoate-degrading denitrifying bacteria from soils and sediments. *Appl Environ Microbiol* 66, 3446-3453.

Stupperich E, Steiner I, Rühlemann M (1986) Isolation and analysis of bacterial cobamides by high performance liquid chromatography. *Anal Biochem* 155, 365-370.

Suyama A, Iwakiri R, Kai K, Tokunaga T, Sera N, Furukawa K (2001) Isolation and characterization of *Desulfitobacterium* sp. strain Y51 capable of efficient dehalogenation of tetrachloroethene and polychloroethane. *Biosci Biotechnol Biochem* 65, 1474-1481.

Suyama A, Yamashita M, Yoshino S, Furukawa K (2002) Molecular characterization of the PceA reductive dehalogenase of *Desulfitobacterium* sp. strain Y51. *J Bacteriol* 184, 3419-3425.

Svetlitchnaia T, Svetlitchnyi V, Meyer O, Dobbek H (2006) Structural insights into methyltransfer reactions of a corrinoid iron-sulfur protein involved in acetyl-CoA synthesis. *Proc Natl Acad Sci U.S.A.* 103, 14331-14336.

Swarts HJ, Verhagen FJM, Field JA, Wijnberg JBPA (1996) Novel chlorometabolites produced by *Bjerkandera* species. *Phytochemistry* 42, 1699-1701.

Swarts HJ, Verhagen FJM, Field JA, Wijnberg JBPA (1998) Trichlorinated phenols from *Hypholoma elongatum*. *Phytochemistry* 49, 203-206.

Taga ME, Larsen NA, Howard-Jones AR, Walsh CT, Walker GC (2007) BluB cannibalizes flavin to form the lower ligand of vitamin B_{12}. *Nature* 446, 449-453.

Tang S, Chan WWM, Fletcher KE, Seifert J, Liang X, Löffler FE, Edwards EA, Adrian L (2012) Functional characterization of reductive dehalogenases by using blue native polyacrylamide gel electrophoresis. *Appl Environ Microbiol* 79, 974-981.

Tang S and Edwards EA (2013) Identification of *Dehalobacter* reductive dehalogenases that catalyse dechlorination of chloroform, 1,1,1-trichloroethane and 1,1-dichloroethane. *Phil Trans R Soc B* 368, 20120318.

Terwilliger TC, Adams PD, Read RJ, McCoy AJ, Moriarty NW, Grosse-Kunstleve RW, Afonine PV, Zwart PH, Hung LW (2009) Decision-making in structure solution using Bayesian estimates of map quality: The PHENIX AutoSol wizard. *Acta Crystallogr D Biol Crystallogr* 65, 582-601.

Thauer RK (1998) Biochemistry of methanogenesis: a tribute to Marjory Stephenson. 1998 Marjory Stephensol Prize Lecture. *Microbiol* 144, 2377-2406.

Thibodeau J, Gauthier A, Duguay M, Villemur R, Lépine F, Juteau P, Beaudet R (2004) Purification, cloning and sequencing of a 3,5-dichlorophenol reductive dehalogenase from *Desulfitobacterium frappieri* PCP-1. *Appl Environ Microbiol* 70, 4532-4537.

Thomas SR, McTamney PM, Adler JM, LaRonde-LeBlanc N, Rokita SE (2009) Crystal structure of iodotyrosine deiodinase, a novel flavoprotein responsible for iodide salvage in thyroid glands. *J Biol Chem* 284, 19659-19667.

Tiedt O, Mergelsberg M, Boll K, Müller M, Adrian L, Jehmlich N, von Bergen M, Boll M (2016) ATP-dependent C-F bond cleavage allows the complete degradation of 4-fluroaromatics without oxygen. *MBio* 7, pii: e00990-16.

Tobiszewski M and Namieśnik J (2012) Abiotic degradation of chlorinated ethanes and ethenes in water. *Environ Sci Pollut Res* 19, 1994-2006.

Totten LA and Assaf-Anis NM (2003) Abiotic dehalogenation by metals. In *Dehalogenation – Microbial processes and environmental applications* (Häggblom MM and Bossert ID, eds), pp. 261-287. Kluwer Academics Publisher, Boston/Dordrecht/London

Traunecker J, Preuss A, Diekert G (1991) Isolation and characterization of a methyl chloride utilizing, strictly anaerobic bacterium. *Arch Microbiol* 156, 416-421.

Trzebiatowski JR and Escalante-Semerena JC (1997) Purification and characterization of CobT, the nicotinate-mononucleotide:5,6-dimethylbenzimidazole phosphoribosyl-transferase enzyme from *Salmonella typhimurium* LT2. *J Biol Chem* 272, 17662-17667.

van de Pas BA, Smidt H, Hagen WR, van der Oost J, Schraa G, Stams AJM, de Vos WM (1999) Purification and molecular characterization of *ortho*-chlorophenol reductive dehalogenase, a key enzyme of halorespiration in *Desulfitobacterium dehalogenans*. *J Biol Chem* 274, 20287-20292.

van de Pas BA, Gerritse J, de Vos WM, Schraa G, Stams AJM (2001) Two distinct enzyme systems are responsible for tetrachloroethene and chlorophenol reductive dehalogenation in *Desulfitobacterium* strain PCE1. *Arch Microbiol* 176, 165-169.

Verschueren KHG, Seljée F, Rozeboom HJ, Kalk KH, Dijkstra BW (1993) Crystallographic analysis of the catalytic mechanism of haloalkane dehalogenase. *Nature* 363, 693-698.

Vieira J and Messing J (1982) The pUC plasmids, an M13mp7-derived system for insertion mutagenesis and sequencing with synthetic universal primers. *Gene* 19, 259–268.

Vogel TM, Criddle CS, McCarty PL (1987) ES&T critical reviews: transformations of halogenated aliphatic compounds. *Environ Sci Technol* 21, 722-736.

Wackett LP, Logan MSP, Blocki FA, Bao-li C (1992) A mechanistic perspective on bacterial metabolism of chlorinated methanes. *Biodegradation* 3, 19-36.

Walker MC and Chang MCY (2014) Natural and engineered biosynthesis of fluorinated natural products. *Chem Soc Rev* 43, 6527-6536.

Warren MJ, Raux E, Schubert HL, Escalante-Semerena JC (2002) The biosynthesis of adenosylcobalamin (vitamin B_{12}). *Nat Prod Rep* 19, 390-412.

Weiss MS (2001) Global indicators of X-ray data quality. *J Appl Cryst* 34, 130-135.

Weissbach H, Redfield BG, Dickerman H, Brot N (1965) Studies on methionine biosynthesis: effect of alkylcobamide derivatives on the formation of holoenzyme. *J Biol Chem* 240, 856-862.

Wong YK, Holland SI, Ertan H, Manefield M, Lee M (2016) Isolation and characterization of *Dehalobacter sp.* strain UNSWDHB capable of chloroform and chlorinated ethane respiration. *Environ Microbiol* 18, 3092-3105.

Woolerton TW, Sheard S, Reisner E, Pierce E, Ragsdale SW and Armstrong FA (2010) Efficient and clean photo-reduction of CO_2 to CO by enzyme-modified TiO_2 nanoparticles using visible light. , *J Am Chem Soc* 132, 2132-2133.

Xun L, Topp E, Orser C (1992) Purification and characterization of a tetrachloro-*p*-hydroquinone reductive dehalogenase from a Flavobacterium sp. *J Bacteriol* 174, 8003-8007.

Yan J, Ritalahti KM, Wagner DD, Löffler FE (2012) Unexpected specificity of interspecies cobamide transfer from *Geobacter* spp. to organohalide-respiring *Dehalococcoides mccartyi* strains. *Appl Environ Microbiol* 78, 6630-6636.

Yan J, Im J, Yang Y, Löffler FE (2013) Guided cobalamin biosynthesis supports *Dehalococcoides mccartyi* reductive dechlorination activity. *Philos Trans R Soc B* 368, 20120320.

Yan J, Şimşir B, Farmer AT, Bi M, Yang Y, Campagna SR, Löffler FE (2016) The corrinoid cofactor of reductive dehalogenases affects dechlorination rates and extents in organohalide-respiring *Dehalococcoides mccartyi*. *ISME J* 10, 1092-1101.

Yang G, Liang P-H, Dunaway-Mariano D (1994) Evidence for nucleophilic catalysis in the aromatic substitution reaction catalysed by (4-chlorobenzoyl)coenzyme A dehalogenase. *Biochemistry* 33, 8527-8531.

Yang J, Wang Y, Zhang Y (2016) ResQ: An approach to unified estimation of B-factor and residue-specific error in protein structure prediction. *J Mol Biol* 428, 693-701.

Ye L, Schilhabel A, Bartram S, Boland W, Diekert G. (2010) Reductive dehalogenation of brominated ethenes by *Sulfurospirillum multivorans* and *Desulfitobacterium hafniense* PCE-S. *Environ Microbiol* 12, 501-509.

Yi S, Seth EC, Men YJ, Stabler SP, Allen RH, Alvarez-Cohen L, Taga ME (2012) Versatility in corrinoid salvaging and remodeling pathways supports corrinoid-dependent metabolism in *Dehalococcoides mccartyi*. *Appl Environ Microbiol* 78, 7745–7752.

Zayas CL and Escalante-Semerena JC (2007) Reassessment of the late steps of coenzyme B_{12} synthesis in *Salmonella enterica*: evidence that dephosphorylation of adenosylcobalamin-5′-phosphate by the CobC phosphatase is the last step of the pathway. *J Bacteriol* 189, 2210–2218.

Zeldin OB, Gerstel M, Garman EF (2013) *RADDOSE-3D*: time- and space-resolved modelling of dose in macromolecular crystallography. *J Appl Cryst* 46, 1225-1230.

Zhang Y (2008) I-TASSER server for protein 3D structure prediction. *BMC Bioinformatics* 9, 40.

Zhang S, Wondrousch D, Cooper M, Zinder SH, Schüürmann G, Adrian L (2017) Anaerobic dehalogenation of chloroanilines by *Dehalococcoides mccartyi* strain CBDB1 and *Dehalobacter* strain 14DCB1 via different pathways as related to molecular electronic structure. *Environ Sci Technol* 51, 3714-3724.

Zhao S, Ding C, He J (2015) Detoxification of 1,1,2-trichloroethane to ethene by *Desulfitobacterium* and identification of its functional reductase gene. *PLoS One* 10, e0119507.

Appendix / Supplementary Information for Manuscripts

www.sciencemag.org/cgi/content/full/science.1258118/DC1

Supplementary Materials for

Structural basis for organohalide respiration

Martin Bommer, Cindy Kunze, Jochen Fesseler, Torsten Schubert, Gabriele Diekert,* Holger Dobbek*

*Corresponding author. E-mail: holger.dobbek@biologie.hu-berlin.de (H.D.); gabriele.diekert@uni-jena.de (G.D.)

Published 2 October 2014 on *Science* Express
DOI: 10.1126/science.1258118

This PDF file includes:

Materials and Methods

Purification of the tetrachloroethene reductive dehalogenase (PceA)

The enzyme was purified from a *Sulfurospirillum multivorans* mutant strain. The mutant strain produced a PceA variant, which contained a C-terminal Strep-tag (PceA-Strep). *S. multivorans* was cultivated in 30 L pyruvate/PCE-containing medium (*9*). We obtained 4 mg of PceA-Strep from 3 g cell protein. All steps were conducted under anoxic conditions. The PceA-Strep was isolated from cell extracts via gravity flow using the Strep-Tactin Superflow column material (IBA, Göttingen, Germany). The Strep-Tactin column was equilibrated with buffer A (100 mM Tris-HCl, pH 8). PceA-Strep was eluted from the column material with buffer B (100 mM Tris-HCl, pH 8, 2.5 mM desthiobiotin, 5 mM Tris(2-carboxyethyl)phosphine). The elution buffer was replaced by the storage buffer (30 mM Tris-HCl, pH 7.5, 5 mM TCEP) via repeated concentration and resuspension of PceA-Strep in a Vivaspin 6 (30K) ultrafiltration unit (Sartorius, Göttingen, Germany). The enzyme was stored at -80°C. The PceA enzyme activity in the protein fractions used for crystallization (~1,800 nat/mg protein) was measured with methyl viologen (reduced with Ti(III) citrate) as low potential electron donor (*8*).When PceA-Strep was incubated under air (18°C), 50% of the enzyme activity was lost after three hours. This process was significantly slowed down by the addition of 5 mM TCEP, which resulted in a half-life time of 19 hours.

Crystallization and incubation with ligands

Crystallization, ligand incubation and flash cooling of crystals were performed under anoxic conditions in a glove box (model B; COY Laboratory Products, Grass Lake, MI) under an atmosphere of 95% N_2/5% H_2. Crystals were grown by the sitting drop vapor diffusion method at room temperature. To obtain the $P2_1$ crystal form, 12 mg/ml of PceA in 30 mM Tris-HCl, pH 7.5, 5 mM TCEP was mixed at 1:1 ratio with a crystallization solution containing 15% (w/v) PEG 3350 and 0.2 M sodium malonate. The more robust $P4_1$ crystal form used for substrate soaking experiments was grown by supplementing 2% benzamidine. Crystals were flash cooled in liquid nitrogen after protection in the crystallization solution supplement with 20% (v/v) glycerol and PEG 3350 to bring its

final concentration to 25%. For the iodide soak, 0.5 M NH_4I was added to the cryoprotectant. TCE-containing cryoprotectant not including benzamidine was saturated with tricholoroethene (Sigma-Aldrich, St. Louis, MO) by vigorous shaking overnight and crystals were incubated in the solution for 5-10 minutes. Soaking with dibromoethene was performed in two steps: a 30-minute incubation in cryoprotectant without glycerol and a 5-minute soak with glycerol. For this purpose solutions were saturated with the commercially available *cis-/trans*-dibromoethene mixture (Sigma-Aldrich). Frozen crystals were removed from the anoxic atmosphere and from thereon stored and handled at 100K.

Data collection and refinement

Diffraction data were collected on BL14.1 operated by the Helmholtz-Zentrum Berlin (HZB), BL14.2 operated by the Joint Berlin MX-Laboratory at the BESSY II electron storage ring (Berlin-Adlershof, Germany) (*23*) and at beamline P11 at the light source PETRA III at DESY (Hamburg, Germany). Data were indexed and integrated with the XDS package (*24*) and XDSAPP (*25*), see Table S1. The structure of the $P2_1$ crystal form was solved by native Fe,Co-SAD phasing with Phenix AutoSol (*26*).
Restraints for norpseudo-B_{12} were derived from the publicly available Vitamin B_{12} dictionary prepared by Dr. Oliver Smart (Global Phasing Inc., Cambridge, UK) using the Grade Server v1.001. Other ligand restraints were generated using eLBOW (*27*) and the structure built in COOT (*28*), refined with *phenix.refine* (*29*) and validated with Molprobity (*30*). Residues 1-411 and 431-462 were placed in the $P4_1$ and $P2_1$ crystal forms, while residues 412-430 were modeled only in chain A of the $P2_1$ form. TCE was modeled into the *F*o-*F*c difference map, while *cis*-dibromoethene and iodide were modeled into the anomalous difference map for the halide. Structural homologues were identified using the Dali server (*31*).

Fig. S1.

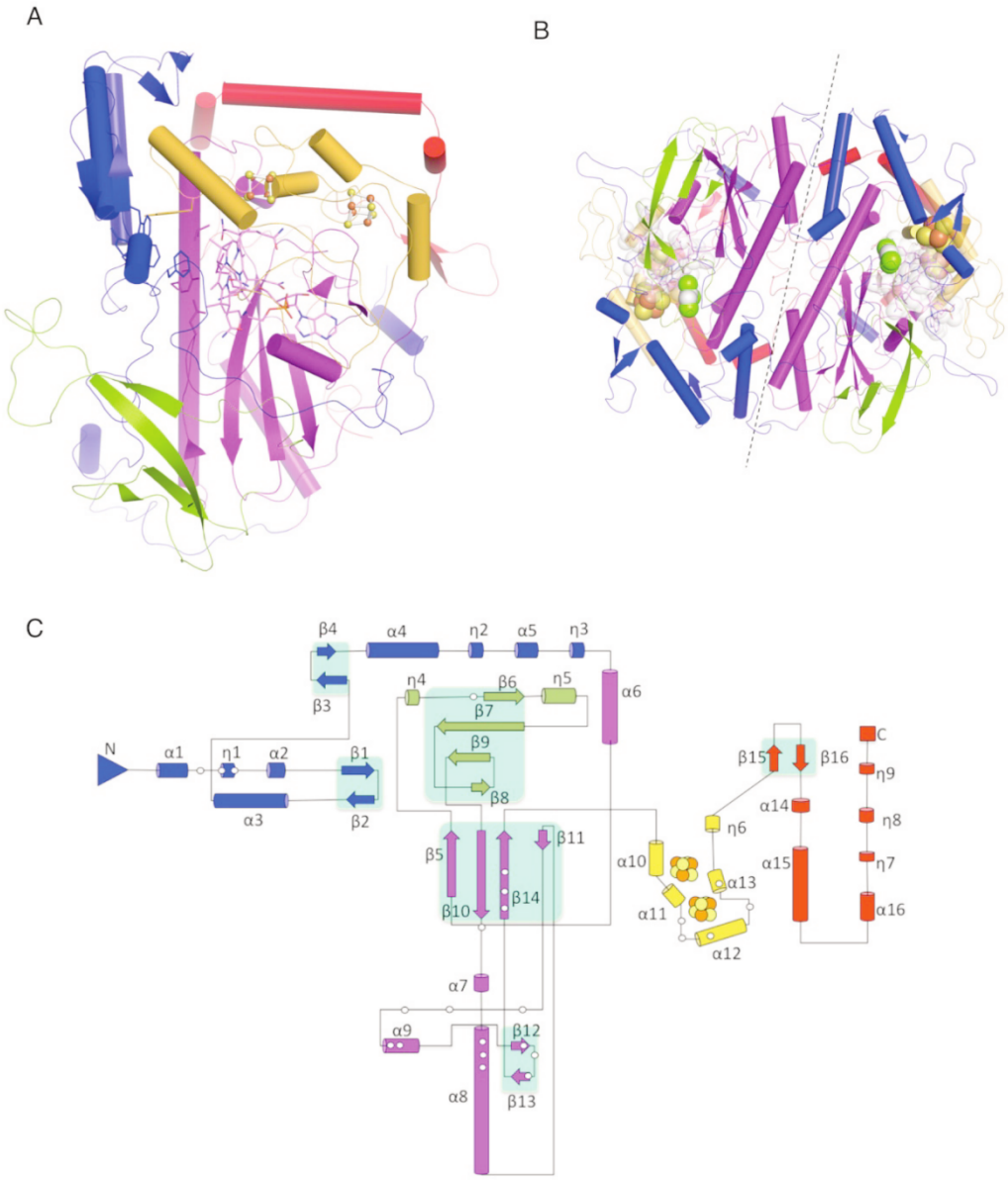

Fig. S1. The PceA fold. Regions are colored throughout as follows: N-terminal unit (blue, residues 1-138), norpseudo-B_{12} binding core (purple, residues 139-163 and 216-323), insertion unit (green, residues 164-215), iron-sulfur cluster binding unit (yellow, residues 324-394) and C-terminal unit (red, residues 395-462), containing helix 15 not observed in all protomers. **A)** Secondary structure representation of a PceA protomer. The norpseudo-B_{12} cofactor (purple) and residues forming the substrate-binding pocket (blue, yellow, purple) are shown as sticks and [4Fe-4S] clusters as ball and stick. **B)**

Representation of the dimer viewed down the non-crystallographic two-fold axis, additionally showing the bound TCE substrate (spheres). **C)** Topology diagram, norpseudo-B_{12} binding residues are indicated by void circles.

Fig. S2

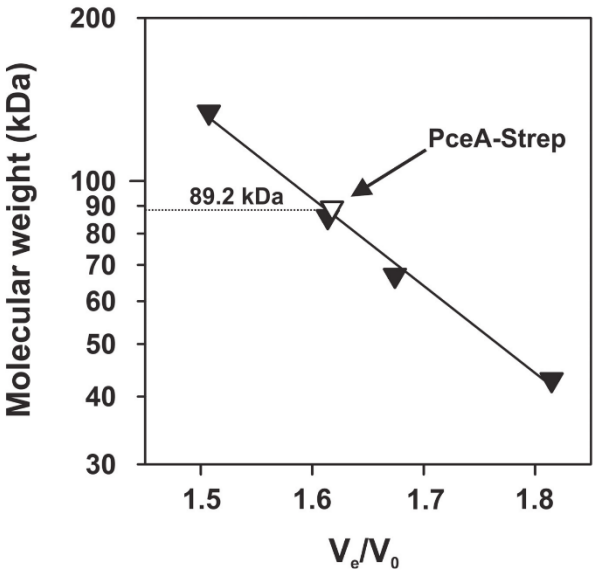

Fig. S2. Determination of the apparent molecular mass of PceA-Strep. Size-exclusion chromatography was conducted with the concentrated eluate from the Strep-Tactin affinity chromatography, which was loaded onto a HiLoad 16/60 Superdex 75 prep grade column (GE Healthcare) equilibrated with the following buffer: 50 mM Tris-HCl (pH 7.5), 100 mM KCl, 0.5 mM DTT, 5 mM TCEP. The apparent molecular mass of the protein (void triangle) was calculated from its retention [elution volume/void volume (V_e/V_0)] in comparison with those of standard proteins (filled triangles). The shown data represent the average of two independent experiments with two replicates, respectively. As standard proteins albumin (dimer 134 kDa, monomer 67 kDa) and ovalbumin (dimer 86 kDa, monomer 43 kDa) were used.

Fig. S3

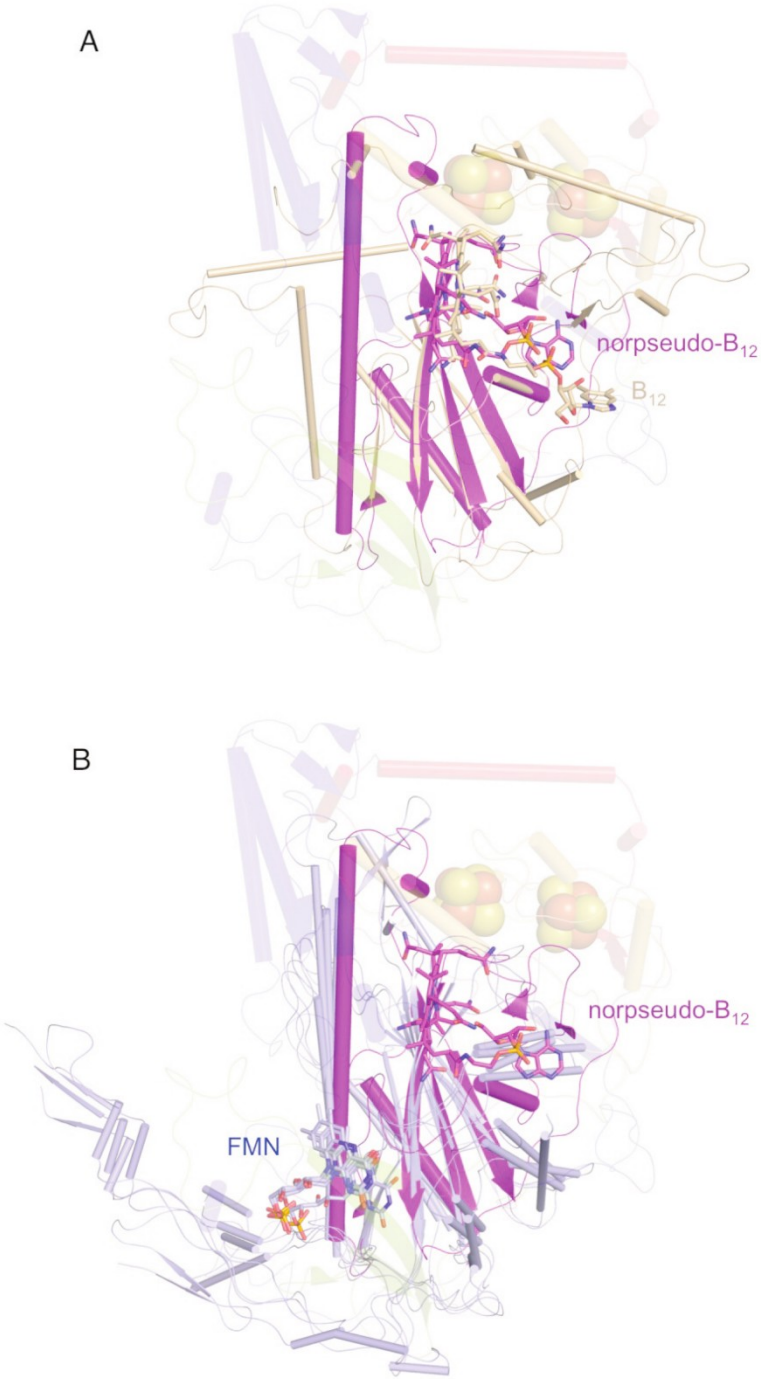

Fig. S3. Structure alignment of the central B_{12}-binding core. Residues 139-163 and 216-323 of PceA (purple) were aligned with **A)** Human methylmalonic aciduria *cblC* type with homocystinuria type C protein (cream, PDB: 3SOM, Dali server Z-score: 7.0)

and **B)** members of the nitroreductase-family: *Escherichia coli* FMN-dependent flavoprotein nitroreductase (PDB: 1DS7, Z: 4.2), *Agrobacterium tumefaciens* FMN-containing oxidoreductase (PDB: 2FRE, Z: 4.1), *Lactococcus lactis* copper-induced nitroreductase CinD (PDB: 2WQF, Z: 4.5) and *Helicobacter pylori* metronidazole activating nitroreductase RdxA (PDB: 3QDL, Z: 4.4), all colored light blue. Other structural elements of PceA as well as the [4Fe4S]-clusters (spheres) are shown as faint outlines.

Fig. S4

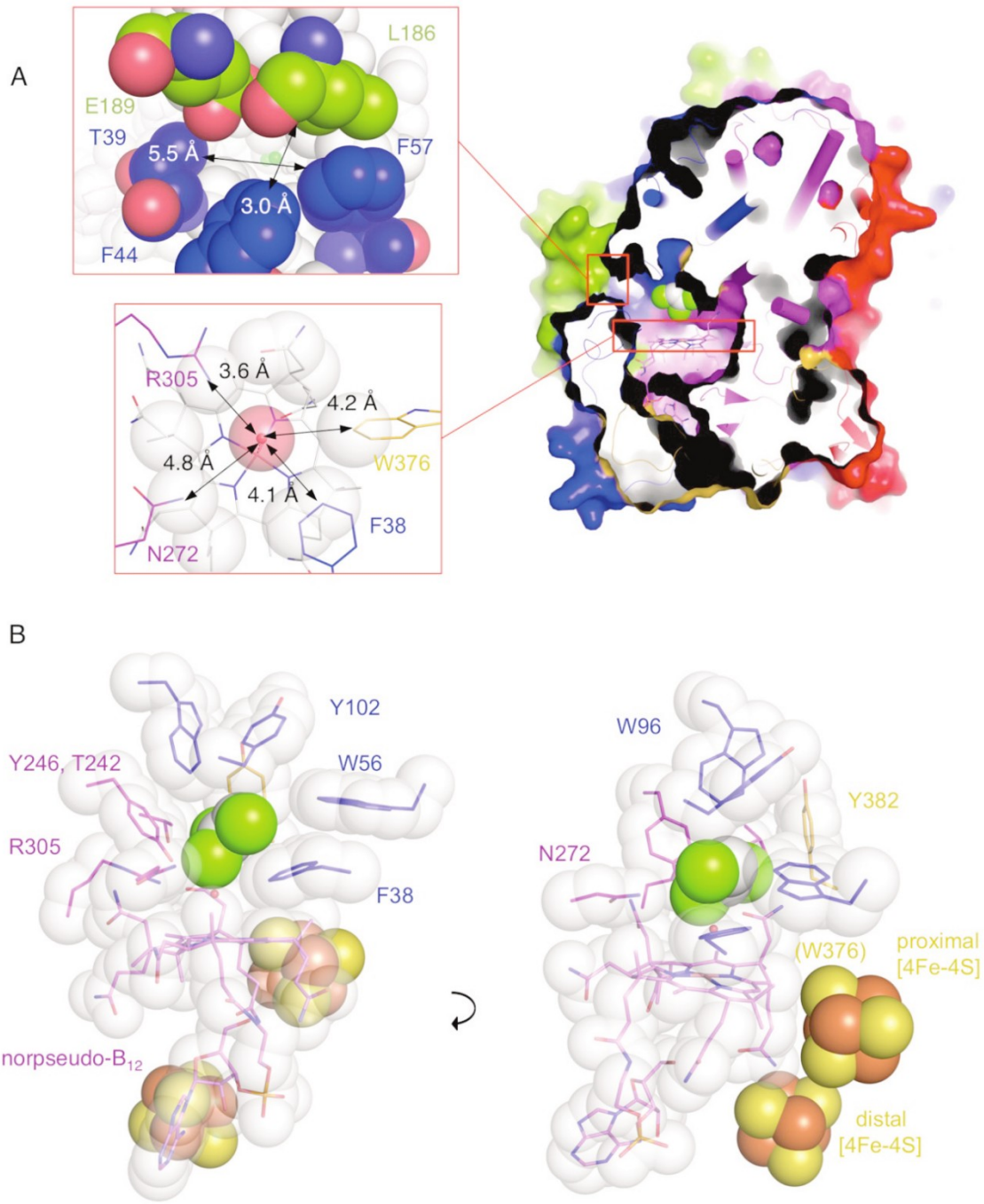

Fig. S4. Substrate channel and pocket of PceA. **A)** Cut surface representation colored as in Fig. S1, showing the norpseudo-B_{12} cofactor as sticks and TCE as spheres. The top insert shows the entrance to the substrate channel - the letter box - constrained by Thr39,

Phe44, Phe57 (N-terminal), Leu186 and Glu189 (Insertion). Residues lining the substrate pocket and channel are additionally shown as white spheres. The lower insert shows a perimeter fence formed by Arg305, Asn272, Trp376, Phe38 and norspeudo-B_{12} side chains just above the corrin ring, restricting access to the cobalt to water / small ions. Atoms closest to and in plane with the water ligand are shown as spheres and their distances indicated. **B)** Van-der-Waals representation of hydrophobic amino acid side chains forming the substrate-binding pocket. TCE and the [4Fe-4S] cluster are shown as spheres. Trp376 was omitted for clarity, but its position is indicated.

Fig. S5

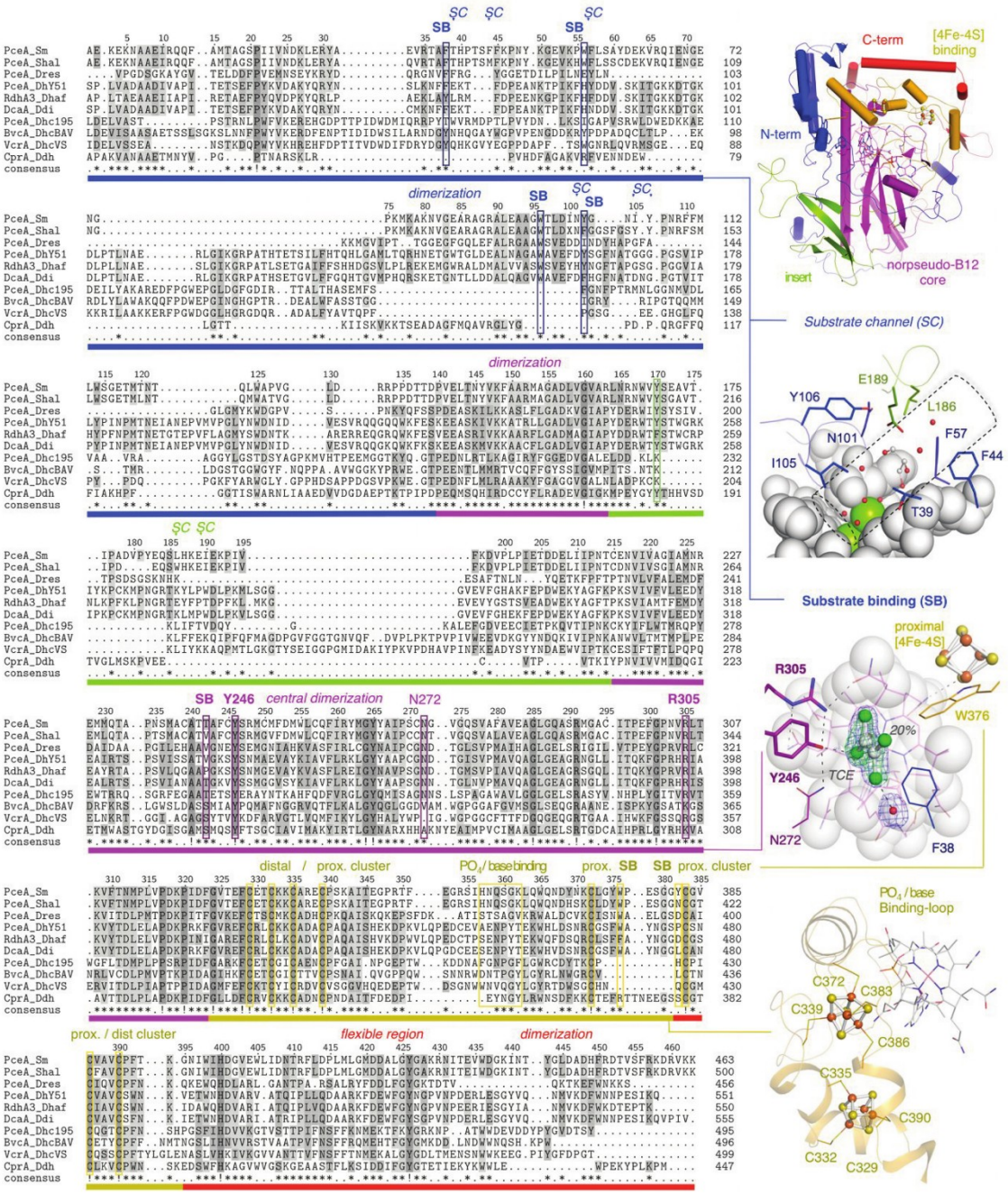

Fig. S5. Sequence alignment of known RDases. Regions are colored and residues binding substrate and cofactors indicated in reference to *S. multivorans* PceA. Selected RDases from the following organohalide-respiring microorganisms were aligned with Clustal Omega (*32*): PceA_Sm - *Sulfurospirillum multivorans* PCE/TCE RDase

(AF022812), PceA_SmSL2 *Sulfurospirillum* sp. SL2 PCE-only RDase (AGW23615), PceA_Dres *Dehalobacter restrictus* DSM 9455 PCE/TCE RDase (AHF10423), PceA_DhY51 *Desulfitobacterium hafniense* Y51 PCE/TCE RDase (YP519072), RdhA3_Dhaf *Desulfitobacterium hafniense* DCB-2 dichlorophenol (DCP)/PCE RDase (YP002457196), DcaA_Ddi *Desulfitobacterium dichloroeliminans* LMG P-21439 dichloroethane (DCA) RDase (CAJ75430), PceA_Dhc195 *Dehalococcoides mccartyi* 195 PCE/TCE RDase (DET0318), BvcA_DhcBAV *Dehalococcoides mccartyi* BAV1 TCE/DCE/DCA RDase (AAT48558), VcrA_DhcVS *Dehalococcoides mccartyi* VS vinylchloride reductase (AAQ94119), CprA_Ddh *Desulfitobacterium* sp. PCE-1 o-chlorophenol reductive RDase (AF259790). (!) Indicate strictly conserved, (*) partially conserved residues.

Fig. S6

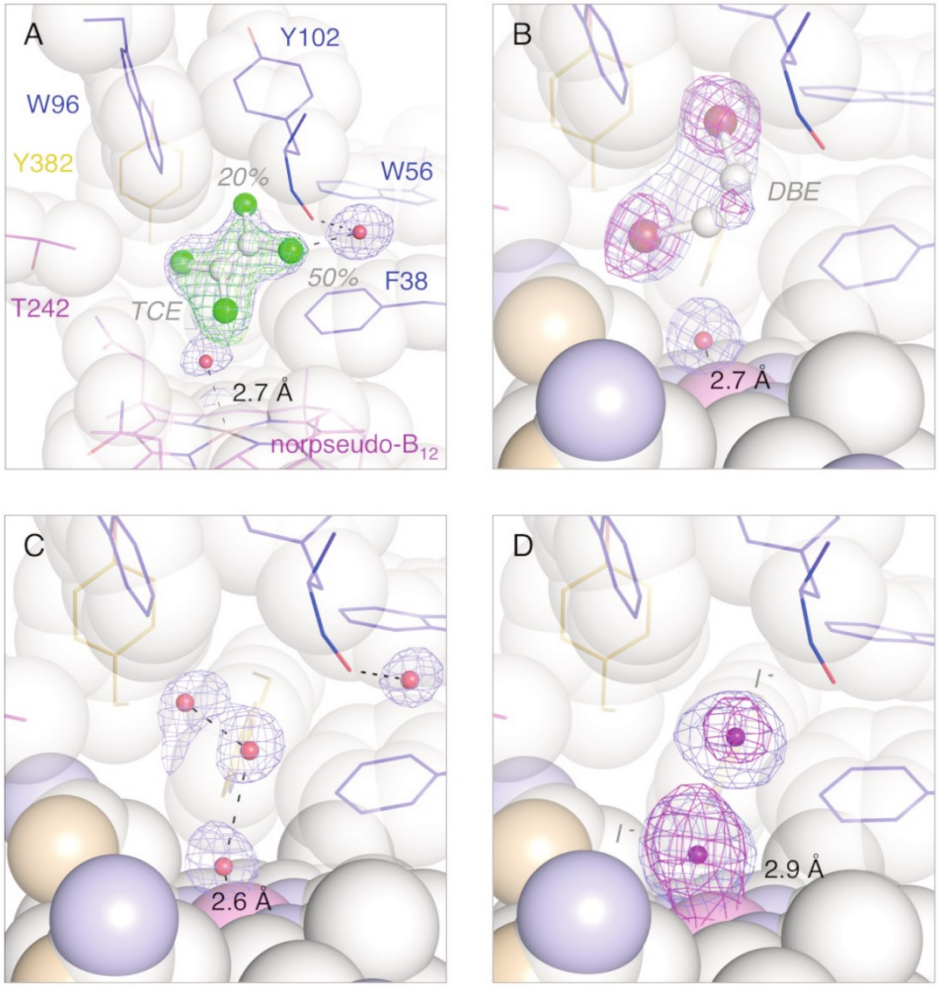

Fig. S6. Active-site electron density maps A) TCE (Two orientations, modeled with 20% and 50% occupancy are overlaid. Of the chloride atoms closest to W56, only the one adjacent to the label is present in each case). **B)** *cis*-DBE, **C)** water/empty binding site, **D)** iodide. In detail: 1σ 2_mFo-_DFc (**A**, blue, TCE and water), 4σ $_mFo\text{-}_DFc$ (**A**, green, TCE), 8σ anomalous difference (**B**, purple, *cis*-DBE), 1σ 2_mFo-_DFc (**B**, blue, *cis*-DBE), 1.2σ 2_mFo-_DFc (**C**, blue, water), 5σ anomalous difference (**D**, purple, iodide), 1σ 2_mFo-_DFc (**D**, blue, iodide). Distances between cobalt and β-ligand are indicated.

Table S1.

Data collection and refinement statistics

	6 protomers/ASU	no substrate	trichloroethene	dibromoethene	0.5M NH_4I
Data collection					
Beamline	HZB 14.2	HZB 14.1	HZB 14.1	DESY P11	HZB 14.1
Detector	MarCCD 225	Pilatus 6M	Pilatus 6M	Pilatus 6M	Pilatus 6M
Wavelength (Å)	1.600	0.9184	0.9184	0.9184	1.3776
Resolution range (Å) (highest resolution shell)	48.76 - 2.24 (2.32 - 2.24)	46.86 - 1.60 (1.65 - 1.60)	45.55 - 1.80 (1.86 - 1.80)	47.34 - 1.65 (1.71 - 1.65)	47.05 - 2.10 (2.17 - 2.10)
Space group	$P\,2_1$	$P\,4_1$	$P\,4_1$	$P\,4_1$	$P\,4_1$
Unit cell *a,b,c* (Å)	74.3, 110.6, 178.8	73.1, 73.1, 183.1	73.9, 73.9, 185.4	73.7, 73.7, 185.3	73.2, 73.2, 184.2
α,β,γ (°)	90, 95.9, 90	90, 90, 90	90, 90, 90	90, 90, 90	90, 90, 90
Total reflections	1665430 (126553)	1585257 (138075)	1271048 (111500)	3252352 (306451)	1544194 (147489)
Unique reflections	137023 (11986)	126647 (12157)	91944 (9090)	118228 (11696)	56502 (5507)
Multiplicity	12.1 (10.6)	12.5 (11.4)	13.8 (12.3)	27.5 (26.2)	27.3 (26.8)
Completeness (%)	98.47 (84.77)	99.59 (96.00)	99.92 (99.26)	99.88 (98.84)	99.81 (98.16)
Mean I/sigma(I)[a]	12.26 (2.59)	15.70 (1.95)	16.02 (1.93)	29.99 (2.38)	17.62 (2.31)
Wilson B-factor ($Å^2$)	28.03	17.43	20.14	21.84	28.87
R_{meas}[b]	0.178 (1.100)	0.116 (1.028)	0.1522 (1.307)	0.09769 (1.565)	0.2401 (1.666)
R_{pim}[c]	0.051 (0.340)	0.032 (0.298)	0.041 (0.369)	0.019 (0.303)	0.046 (0.319)
CC1/2[d]	0.996 (0.893)	0.999 (0.755)	0.999 (0.652)	1 (0.76)	0.998 (0.74)
Refinement					
R_{work}	0.1793 (0.4413)	0.1517 (0.2308)	0.1359 (0.2161)	0.1342 (0.2410)	0.1420 (0.2365)
R_{free}	0.2177 (0.4975)	0.1830 (0.2741)	0.1649 (0.2452)	0.1573 (0.2606)	0.1859 (0.2601)
Number of non-H atoms	22528	7983	8187	8220	7732
macromolecules	20813	6985	7097	7097	6842
ligands	630	261	283	305	263
water	1085	737	807	818	627
Protein residues	2655	884	893	893	870
RMS deviation (bonds) (Å)	0.008	0.007	0.011	0.007	0.012
RMS deviation (angles) (°)	1.81	1.15	1.92	1.15	1.97
Ramachandran favored (%)	97	97	98	98	98
Ramachandran outliers (%)	0.19	0	0	0	0
Clashscore	5	1.6	1.5	1.9	2.9
Average B-factor (all $Å^2$)	35.2	25.2	26.4	29.6	32.7
macromolecules	35.3	24.5	25.4	28.6	32.2
ligands	28.6	22.1	26.7	30.2	29.4
solvent	37.1	32.7	34.9	38.8	40.1

[a] Criterion for resolution cut-off: Mean I/sigma(I) > 2.
[b] Redundancy-independent merging R-factor (*33*)
[c] Precision-indicating merging R-factor (*34*)
[d] Pearson correlation coefficient of half data sets (*35*)
Values in parentheses refer to the highest resolution shell

References and Notes

1. C. Holliger, G. Wohlfarth, G. Diekert, Reductive dechlorination in the energy metabolism of anaerobic bacteria. *FEMS Microbiol. Rev.* **22**, 383–398 (1998). doi:10.1111/j.1574-6976.1998.tb00377.x

2. B. Kräutler, W. Fieber, S. Ostermann, M. Fasching, K.-H. Ongania, K. Gruber, C. Kratky, C. Mikl, A. Siebert, G. Diekert, The Cofactor of Tetrachloroethene Reductive Dehalogenase of *Dehalospirillum multivorans* Is Norpseudo-B12, a New Type of a Natural Corrinoid. *Helv. Chim. Acta* **86**, 3698–3716 (2003). doi:10.1002/hlca.200390313

3. L. A. Hug, F. Maphosa, D. Leys, F. E. Löffler, H. Smidt, E. A. Edwards, L. Adrian, Overview of organohalide-respiring bacteria and a proposal for a classification system for reductive dehalogenases. *Philos. Trans. R. Soc. Lond. B Biol. Sci.* **368**, 20120322 (2013). Medline doi:10.1098/rstb.2012.0322

4. A. Mac Nelly, M. Kai, A. Svatoš, G. Diekert, T. Schubert, Functional heterologous production of reductive dehalogenases from *Desulfitobacterium hafniense* strains. *Appl. Environ. Microbiol.* **80**, 4313–4322 (2014). Medline doi:10.1128/AEM.00881-14

5. A. Neumann, G. Wohlfarth, G. Diekert, Purification and characterization of tetrachloroethene reductive dehalogenase from *Dehalospirillum multivorans*. *J. Biol. Chem.* **271**, 16515–16519 (1996). Medline doi:10.1074/jbc.271.28.16515

6. H. Scholz-Muramatsu, A. Neumann, M. Messmer, E. Moore, G. Diekert, Isolation and characterization of *Dehalospirillum multivorans* gen. nov., sp. nov., a tetrachloroethene-utilizing, strictly anaerobic bacterium. *Arch. Microbiol.* **163**, 48–56 (1995). doi:10.1007/BF00262203

7. Materials and methods are available on *Science* Online

8. T. Goris, T. Schubert, J. Gadkari, T. Wubet, M. Tarkka, F. Buscot, L. Adrian, G. Diekert, Insights into organohalide respiration and the versatile catabolism of *Sulfurospirillum multivorans* gained from comparative genomics and physiological studies. *Environ. Microbiol.* n/a (2014). 10.1111/1462-2920.12589 Medline doi:10.1111/1462-2920.12589

9. E. Miller, G. Wohlfarth, G. Diekert, Studies on tetrachloroethene respiration in *Dehalospirillum multivorans*. *Arch. Microbiol.* **166**, 379–387 (1996). Medline doi:10.1007/BF01682983

10. L. Ye, A. Schilhabel, S. Bartram, W. Boland, G. Diekert, Reductive dehalogenation of brominated ethenes by *Sulfurospirillum multivorans* and *Desulfitobacterium hafniense* PCE-S. *Environ. Microbiol.* **12**, 501–509 (2010). Medline doi:10.1111/j.1462-2920.2009.02093.x

11. C. L. Drennan, S. Huang, J. T. Drummond, R. G. Matthews, M. L. Lidwig, How a protein binds B12: A 3.0 A X-ray structure of B12-binding domains of methionine synthase. *Science* **266**, 1669–1674 (1994). Medline doi:10.1126/science.7992050

12. F. Mancia, N. H. Keep, A. Nakagawa, P. F. Leadlay, S. McSweeney, B. Rasmussen, P. Bösecke, O. Diat, P. R. Evans, How coenzyme B12 radicals are generated: The crystal structure of methylmalonyl-coenzyme A mutase at 2 A resolution. *Structure* **4**, 339–350 (1996). Medline doi:10.1016/S0969-2126(96)00037-8

13. J. Kim, C. Gherasim, R. Banerjee, Decyanation of vitamin B12 by a trafficking chaperone. *Proc. Natl. Acad. Sci. U.S.A.* **105**, 14551–14554 (2008). Medline doi:10.1073/pnas.0805989105

14. D. S. Froese, T. Krojer, X. Wu, R. Shrestha, W. Kiyani, F. von Delft, R. A. Gravel, U. Oppermann, W. W. Yue, Structure of MMACHC reveals an arginine-rich pocket and a domain-swapped dimer for its B12 processing function. *Biochemistry* **51**, 5083–5090 (2012). Medline doi:10.1021/bi300150y

15. H. B. Gray, J. R. Winkler, Long-range electron transfer. *Proc. Natl. Acad. Sci. U.S.A.* **102**, 3534–3539 (2005). Medline doi:10.1073/pnas.0408029102>

16. T. Svetlitchnaia, V. Svetlitchnyi, O. Meyer, H. Dobbek, Structural insights into methyltransfer reactions of a corrinoid iron-sulfur protein involved in acetyl-CoA synthesis. *Proc. Natl. Acad. Sci. U.S.A.* **103**, 14331–14336 (2006). Medline doi:10.1073/pnas.0601420103

17. M. John, R. P. H. Schmitz, M. Westermann, W. Richter, G. Diekert, Growth substrate dependent localization of tetrachloroethene reductive dehalogenase in *Sulfurospirillum multivorans*. *Arch. Microbiol.* **186**, 99–106 (2006). Medline doi:10.1007/s00203-006-0125-5

18. J. Shey, W. A. van der Donk, Mechanistic Studies on the Vitamin B 12 -Catalyzed Dechlorination of Chlorinated Alkenes. *J. Am. Chem. Soc.* **122**, 12403–12404 (2000). doi:10.1021/ja0055965

19. R. P. H. Schmitz, J. Wolf, A. Habel, A. Neumann, K. Ploss, A. Svatos, W. Boland, G. Diekert, Evidence for a radical mechanism of the dechlorination of chlorinated propenes mediated by the tetrachloroethene reductive dehalogenase of *Sulfurospirillum muftivorans*. *Environ. Sci. Technol.* **41**, 7370–7375 (2007). Medline doi:10.1021/es071026u<jrn>20. G. Glod, W. Angst, C. Holliger, R. P. Schwarzenbach, Corrinoid-Mediated Reduction of Tetrachloroethene, Trichloroethene, and Trichlorofluoroethene in Homogeneous Aqueous Solution: Reaction Kinetics and Reaction Mechanisms. *Environ. Sci. Technol.* **31**, 253–260 (1997). doi:10.1021/es9603867

21. W. Schumacher, C. Holliger, A. J. Zehnder, W. R. Hagen, Redox chemistry of cobalamin and iron-sulfur cofactors in the tetrachloroethene reductase of Dehalobacter restrictus. *FEBS Lett.* **409**, 421–425 (1997). Medline doi:10.1016/S0014-5793(97)00520-6

22. K. M. McCauley, D. A. Pratt, S. R. Wilson, J. Shey, T. J. Burkey, W. A. van der Donk, Properties and reactivity of chlorovinylcobalamin and vinylcobalamin and their implications for vitamin B12-catalyzed reductive dechlorination of chlorinated alkenes. *J. Am. Chem. Soc.* **127**, 1126–1136 (2005). Medline doi:10.1021/ja048573p

23. U. Mueller, N. Darowski, M. R. Fuchs, R. Förster, M. Hellmig, K. S. Paithankar, S. Pühringer, M. Steffien, G. Zocher, M. S. Weiss, Facilities for macromolecular crystallography at the Helmholtz-Zentrum Berlin. *J. Synchrotron Radiat.* **19**, 442–449 (2012). Medline doi:10.1107/S0909049512006395

24. W. Kabsch, Xds. *Acta Crystallogr. D Biol. Crystallogr.* **66**, 125–132 (2010). Medline doi:10.1107/S0907444909047337

25. M. Krug, M. S. Weiss, U. Heinemann, U. Mueller, XDSAPP : A graphical user interface for the convenient processing of diffraction data using XDS. *J. Appl. Cryst.* **45**, 568–572 (2012). doi:10.1107/S0021889812011715

26. T. C. Terwilliger, P. D. Adams, R. J. Read, A. J. McCoy, N. W. Moriarty, R. W. Grosse-Kunstleve, P. V. Afonine, P. H. Zwart, L. W. Hung, Decision-making in structure solution using Bayesian estimates of map quality: The PHENIX AutoSol wizard. *Acta Crystallogr. D Biol. Crystallogr.* **65**, 582–601 (2009). Medline doi:10.1107/S0907444909012098

27. N. W. Moriarty, R. W. Grosse-Kunstleve, P. D. Adams, electronic Ligand Builder and Optimization Workbench (eLBOW): A tool for ligand coordinate and restraint generation. *Acta Crystallogr. D Biol. Crystallogr.* **65**, 1074–1080 (2009). Medline doi:10.1107/S0907444909029436

28. P. Emsley, B. Lohkamp, W. G. Scott, K. Cowtan, Features and development of Coot. *Acta Crystallogr. D Biol. Crystallogr.* **66**, 486–501 (2010). Medline doi:10.1107/S0907444910007493

29. P. V. Afonine, R. W. Grosse-Kunstleve, N. Echols, J. J. Headd, N. W. Moriarty, M. Mustyakimov, T. C. Terwilliger, A. Urzhumtsev, P. H. Zwart, P. D. Adams, Towards automated crystallographic structure refinement with phenix.refine. *Acta Crystallogr. D Biol. Crystallogr.* **68**, 352–367 (2012). Medline doi:10.1107/S0907444912001308

30. V. B. Chen, W. B. Arendall 3rd, J. J. Headd, D. A. Keedy, R. M. Immormino, G. J. Kapral, L. W. Murray, J. S. Richardson, D. C. Richardson, MolProbity: All-atom structure validation for macromolecular crystallography. *Acta Crystallogr. D Biol. Crystallogr.* **66**, 12–21 (2010). Medline doi:10.1107/S0907444909042073

31. L. Holm, P. Rosenström, Dali server: Conservation mapping in 3D. *Nucleic Acids Res.* **38** (Web Server), W545–W549 (2010). Medline doi:10.1093/nar/gkq366

32. F. Sievers, A. Wilm, D. Dineen, T. J. Gibson, K. Karplus, W. Li, R. Lopez, H. McWilliam, M. Remmert, J. Söding, J. D. Thompson, D. G. Higgins, Fast, scalable generation of high-quality protein multiple sequence alignments using Clustal Omega. *Mol. Syst. Biol.* **7**, 539 (2011). Medline doi:10.1038/msb.2011.75

33. K. Diederichs, P. A. Karplus, Improved R-factors for diffraction data analysis in macromolecular crystallography. *Nat. Struct. Biol.* **4**, 269–275 (1997). Medline doi:10.1038/nsb0497-269

34. M. S. Weiss, Global indicators of X-ray data quality. *J. Appl. Cryst.* **34**, 130–135 (2001). doi:10.1107/S0021889800018227

35. P. A. Karplus, K. Diederichs, Linking crystallographic model and data quality. *Science* **336**, 1030–1033 (2012). Medline doi:10.1126/science.1218231

Selective utilization of benzimidazolyl-norcobamides as cofactors by the tetrachlororethene reductive dehalogenase of *Sulfurospirillum multivorans*

Sebastian Keller, Cindy Kunze, Martin Bommer, Christian Paetz, Riya C. Menezes, Aleš Svatoš, Holger Dobbek, and Torsten Schubert

SUPPORTING INFORMATION

NMR data (extended)

Structure analysis of the 6-OHBza-*N*-α-ribofuranosyl moiety of 6-OHBza-norcobamide. All norcobamide (NCba) structures were analyzed by NMR spectroscopy with focus on the various benzimidazoles incorporated during the cultivation experiments. In the following, the structure analysis of the 6-OHBza-*N*-α-ribofuranosyl moiety of 6-OHBza-NCba is described as a typical example (Fig. S1-8). In an analogous manner the structures and chemical shifts of the 5-OMeBza-NCba (Fig. S9-14), the 5-MeBza-NCba (Fig. S15-20), and the 6-MeBza-NCba (Fig. S21-26) have been worked out.

The ^{1}H NMR spectrum showed six signals in the low field range, three of them attributable to an aromatic AMX spin system. However, a deviation of the chemical shifts compared to the literature (1) was observed and thus the structure was elucidated *de novo*. Starting point was a ^{1}H-^{13}C HSQC cross signal at δ_H 6.17, *m*/δ_C 86.6 (Fig. S6), which was assigned to position 1' of the α-ribofuranose moiety. By means of ^{1}H-^{1}H DQFCOSY, selective ^{1}H-^{1}H TOCSY (offset on H-1') and ^{1}H-^{13}C HSQC all remaining positions of the α-ribofuranose were assigned (Fig. S4) The ^{1}H-^{13}C HMBC (Fig. S7) correlation of H-1' with C-2 (δ_C 141.8) was proving the connection of the α-ribofuranosyl with the benzimidazolyl part. In order to elucidate the position of the hydroxyl group at the benzimidazole, a ^{1}H-^{1}H ROESY experiment was conducted (Fig. S8). Correlation of H-1' with the broad singlet of H-7 (δ_H 6.80) was observed, and ^{1}H-^{13}C HSQC revealed the corresponding C-7 at δ_C 96.8. Furthermore, H-4' (δ_H 4.02, *m*) showed a ROE-correlation to H-2 (δ_H 7.03), indicating that the α-ribofuranosyl and benzimidazolyl systems

have a perpendicular orientation towards each other. Because no ^{1}H-^{1}H DQFCOSY correlation of H-7 was observed, the position of the hydroxyl group in the benzimidazolyl moiety had to be in position 6. The remaining protonated positions of the benzimidazole were assigned from ^{1}H-^{13}C HMBC and ^{1}H-^{1}H DQFCOSY correlations, respectively. ^{1}H-^{13}C HMBC correlations from H-7 revealed the chemical shifts of position 5 (δ_H 6.73, *d*, $^{3}J_{HH}$=8.9 Hz /δ_C 113.2) and position 9 (δ_C 132.2). H-4 (δ_H 6.49, *d*, $^{3}J_{HH}$=8.9 Hz) was determined from a ^{1}H-^{1}H DQFCOSY correlation with H-5. The corresponding ^{13}C chemical shift C-4 (δ_C 117.4) was determined by ^{1}H-^{13}C HSQC. The ^{13}C chemical shifts of position 8 (δ_C 132.5) and 6 (δ_C 153.7) were determined from the ^{1}H-^{13}C HMBC correlation with H-4. Finally, the ^{1}H-^{13}C HMBC correlation of H-2 with C-8 and C-9, the evidence for the linkage of the imidazolyl moiety with the phenyl moiety of benzimidazole, completed the structure elucidation of the 6-OHBza-NCba.

References:

1. Crofts TS, Hazra AB, Tran JL, Sokolovskaya OM, Osadchiy V, Ad O, Pelton J, Bauer S, Taga ME. 2014. Regiospecific formation of cobamide isomers is directed by CobT. Biochemistry 53:7805-7815.

Supplementary Table 1. Data collection and refinement statistics

	PceA harbouring **6-OHBza**-norcobamide	PceA harbouring **5-OMeBza**-norcobamide
Data Collection	PETRA III P11	HZB-MX 14.1
Wavelength	0.9184	0.9184
Resolution range	36.1 - 1.59 (1.65 - 1.59)	39.8 - 1.60 (1.66 - 1.60)
Space group	$P\,4_1$	$P\,4_1$
Unit cell (Å, °)	73.6 73.6 184.7 90 90 90	73.6 73.6 185.3 90 90 90
Unique reflections	129361 (12146)	129127 (12767)
Multiplicity	13.2 (12.6)	13.8 (13.6)
Completeness (%)	99 (93)	100 (99)
I/sigma(I)	14.9 (1.9)	19.0 (1.7)
Wilson B-factor	19.0	20.2
R-merge	0.114 (0.931)	0.098 (1.57)
R-pim	0.033 (0.270)	0.027 (0.436)
$CC_{1/2}$	1.00 (0.80)	1.00 (0.62)
Refinement		
R-work	0.152 (0.257)	0.151 (0.260)
R-free	0.177 (0.285)	0.172 (0.289)
Number of non-H atoms	7945	7820
macromolecules	6838	6843
ligands	243	251
solvent	864	726
Protein residues	862	865
RMS(bonds, Å)	0.007	0.007
RMS(angles, °)	0.93	0.93
Ramachandran favored (%)	98	98
Ramachandran outliers (%)	0	0
Rotamer outliers (%)	0	0
Clashscore	2.7	2.4
Average B-factor	26.5	26.2
macromolecules	25.5	25.4
ligands	21.7	21.7
solvent	36.0	35.1

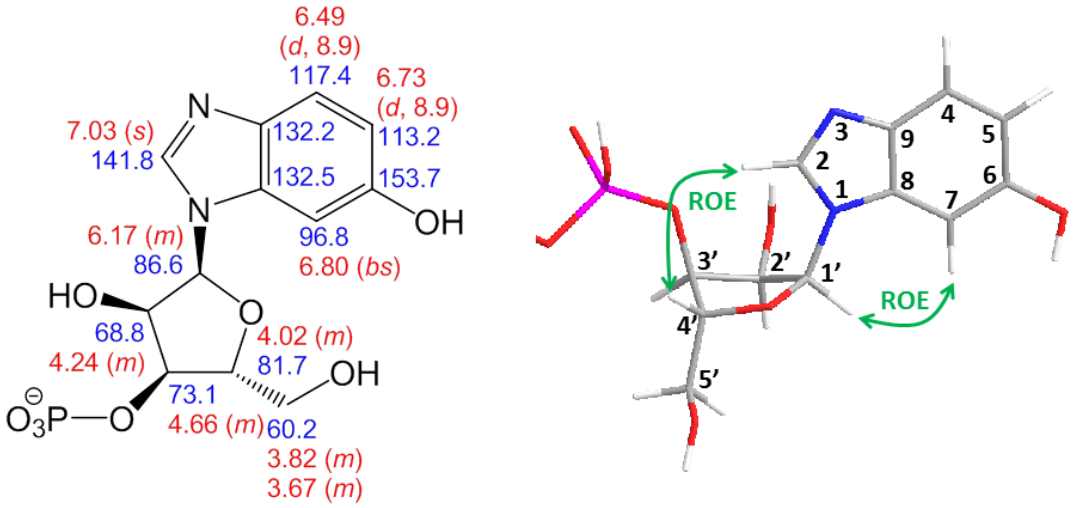

Fig. S1: Chemical shifts (δ_H red, δ_C blue) of the 6-OHBza-*N*-α-ribofuranosyl-fragment and the ^{1}H-^{1}H ROESY key correlations for determination of the position of the hydroxyl group.

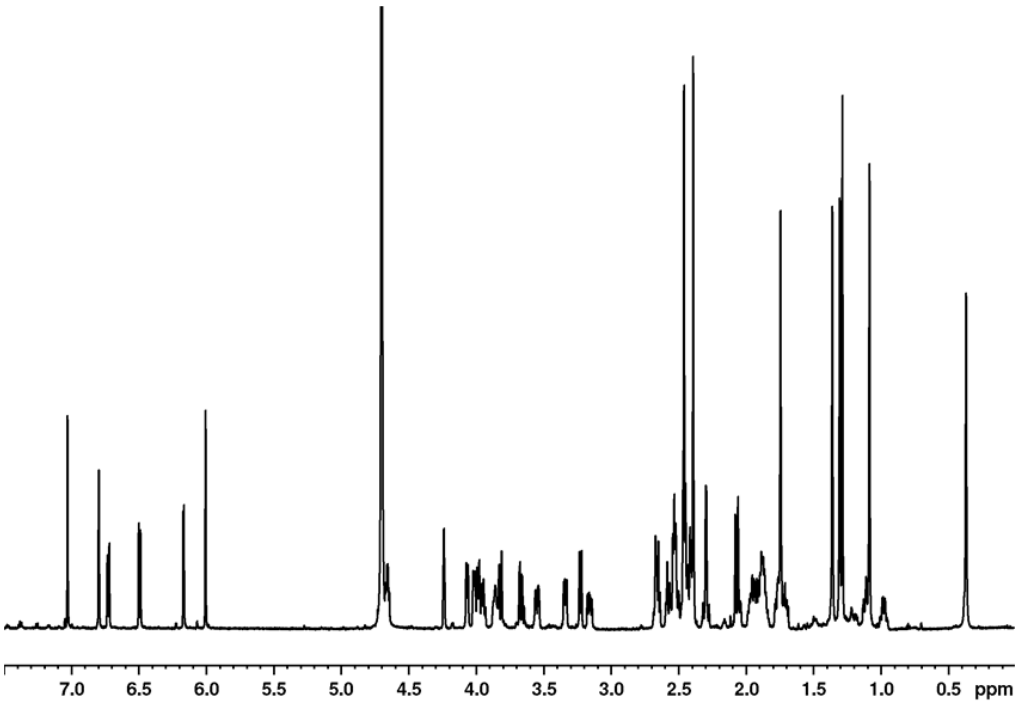

Fig. S2: ^{1}H-NMR spectrum of the 6-OHBza-NCba.

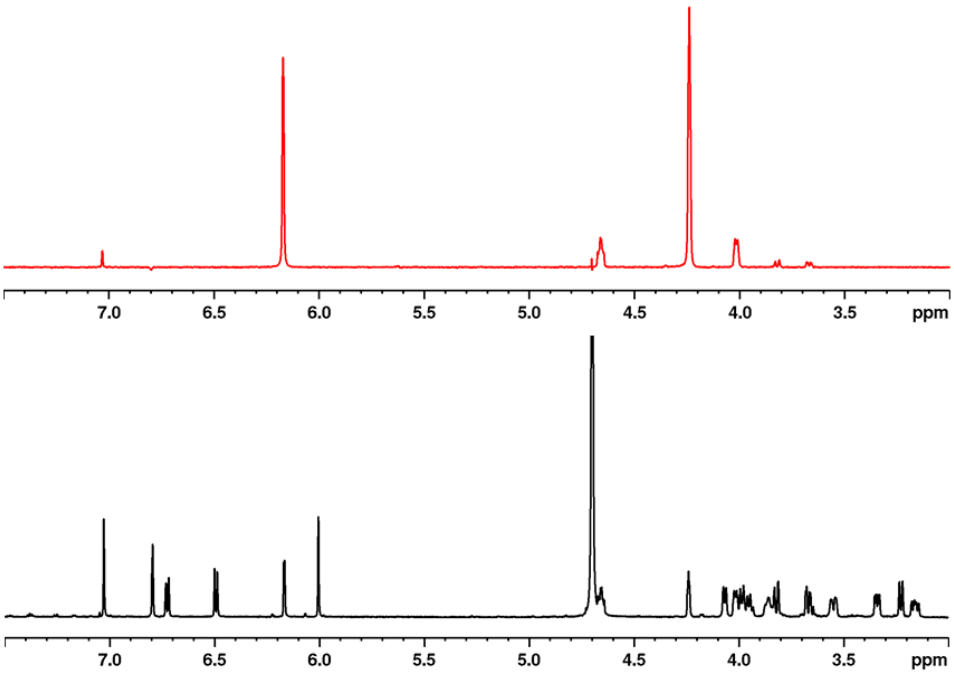

Fig. S3: ^{1}H-SELTOCSY spectrum of the α-ribofuranosyl moiety (red) of the 6-OHBza-NCba compared to the ^{1}H-NMR spectrum (black) of the 6-OHBza-NCba.

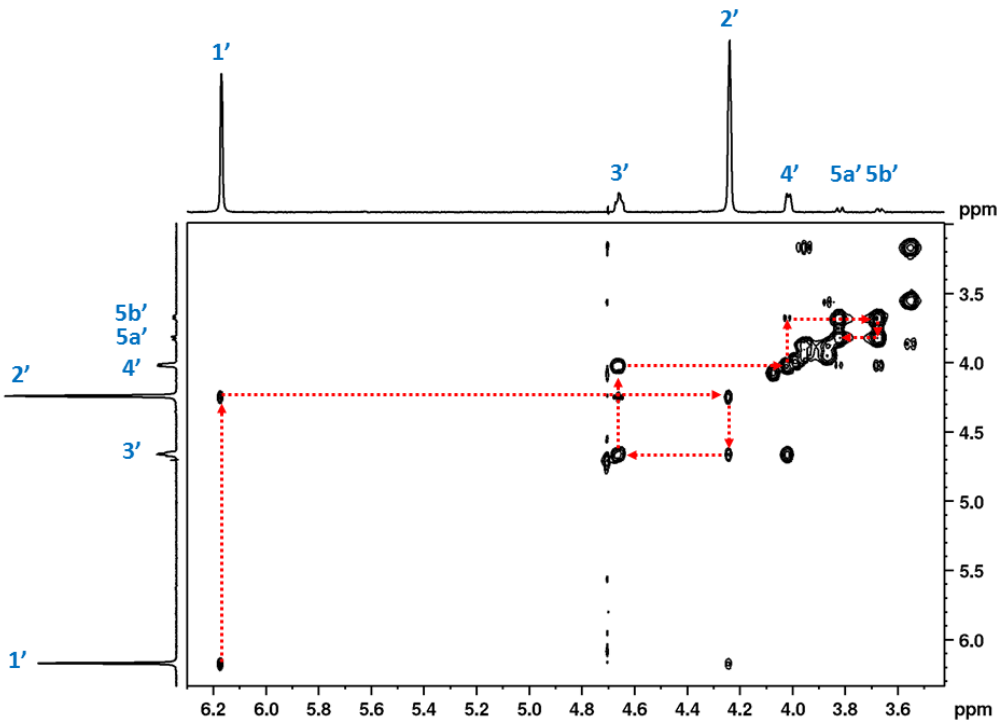

Fig. S4: ^{1}H-^{1}H DQFCOSY spectral detail of the α-ribofuranosyl unit of 6-OHBza-NCba with SELTOCSY spectra as projections.

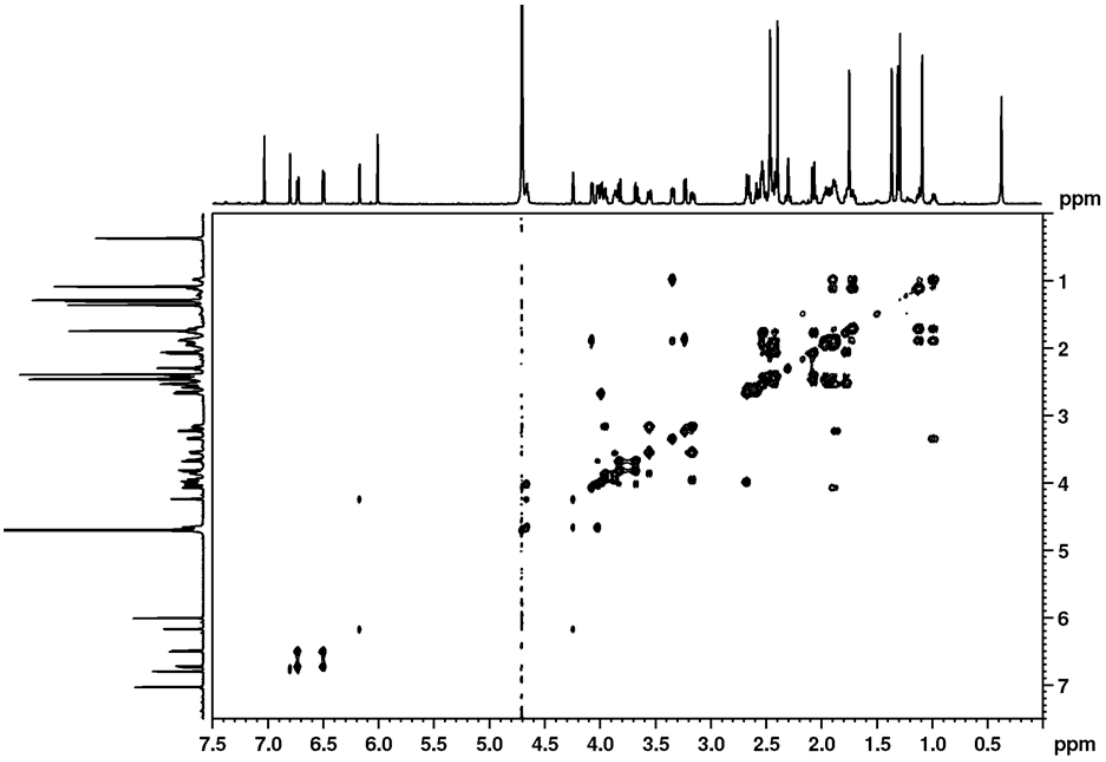

Fig. S5: Full ^{1}H-^{1}H-DQFCOSY spectrum of the 6-OHBza-NCba.

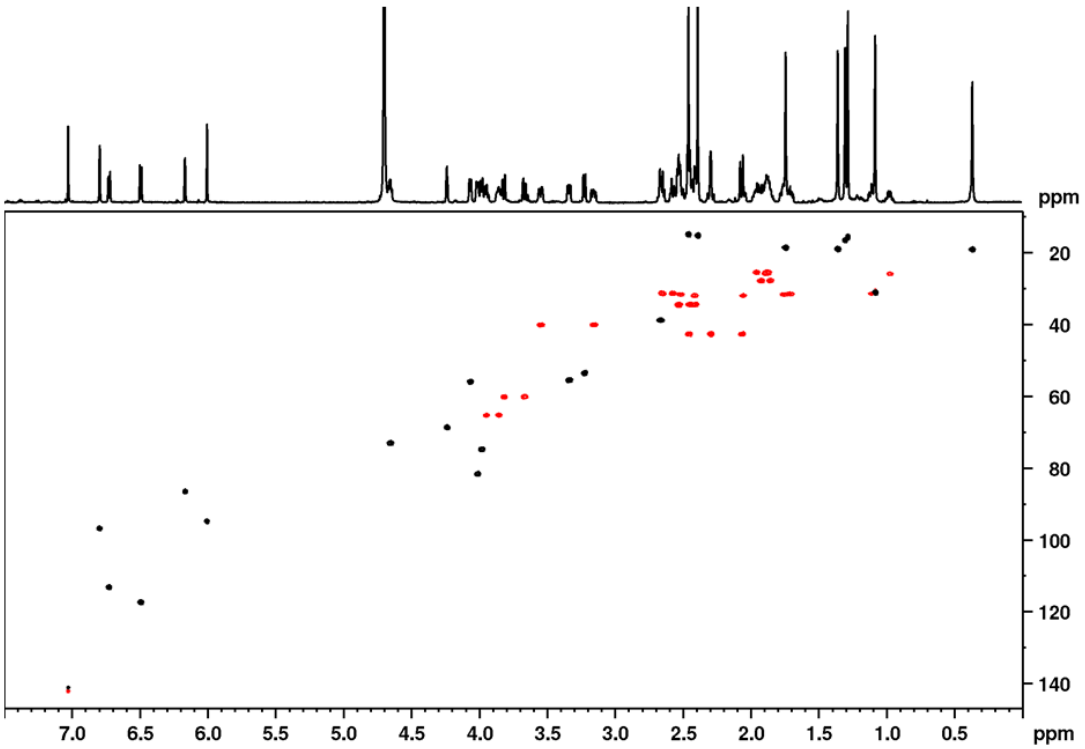

Fig. S6: ^{1}H-^{13}C HSQC spectrum of 6-OHBza-NCba.

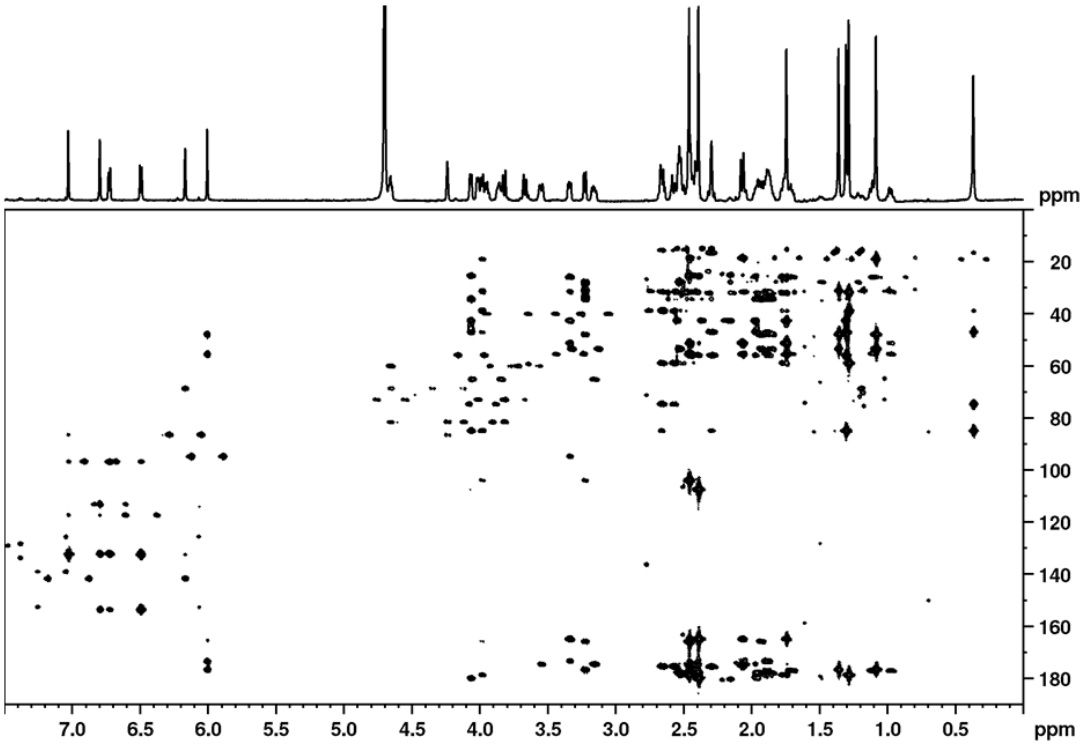

Fig. S7: ^{1}H-^{13}C HMBC spectrum of the 6-OHBza-NCba.

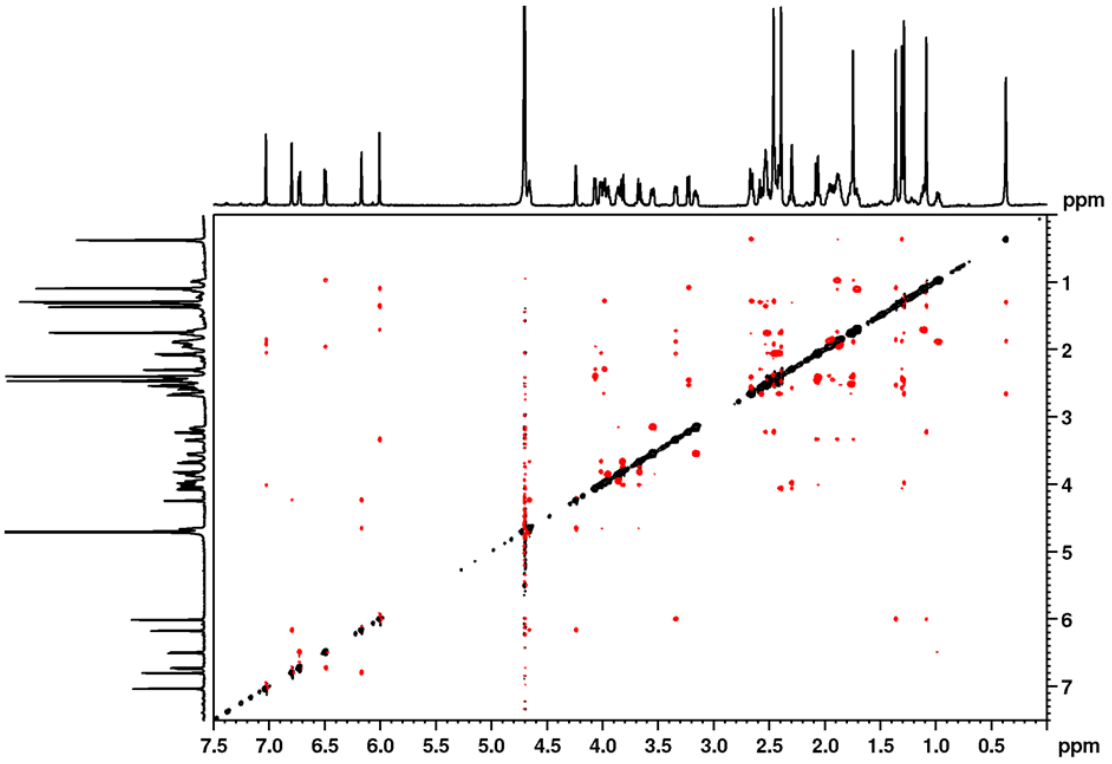

Fig. S8: ^{1}H-^{1}H ROESY spectrum of the 6-OHBza-NCba.

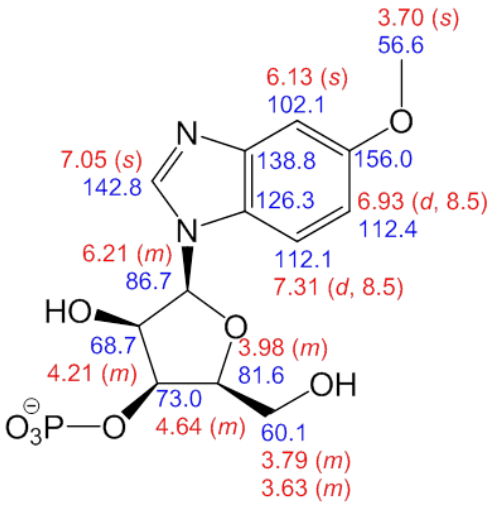

Fig. S9: Chemical shifts (δ_H red, δ_C blue) of the 5-OMeBza-*N*-α-ribofuranosyl-fragment.

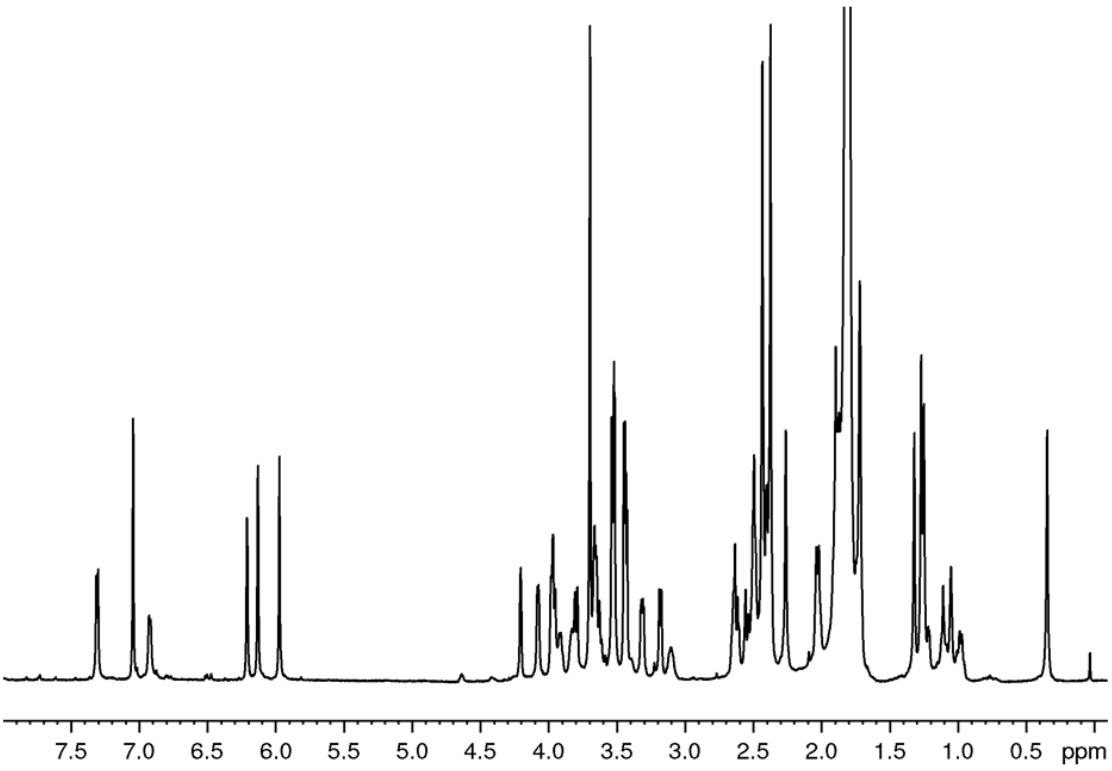

Fig. S10: ^{1}H-NMR spectrum of the 5-OMeBza-NCba.

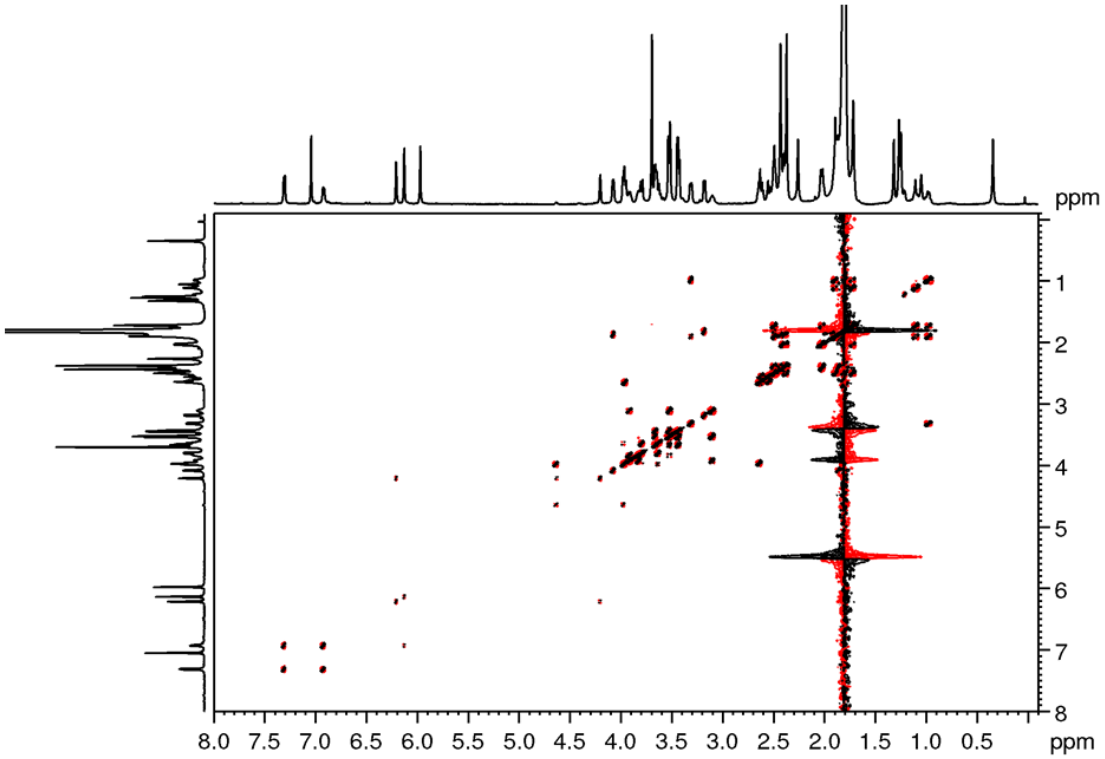

Fig. S11: ^{1}H-^{1}H-DQFCOSY spectrum of the 5-OMeBza-NCba.

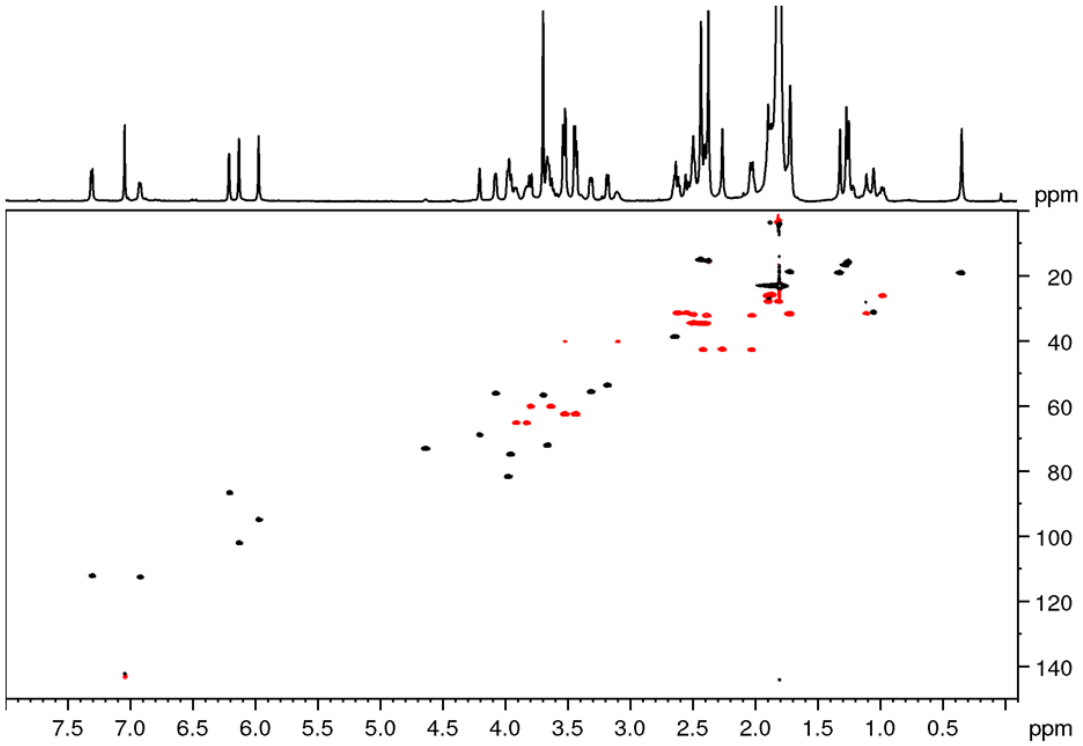

Fig. S12: ^{1}H-^{13}C HSQC spectrum of 5-OMeBza-NCba.

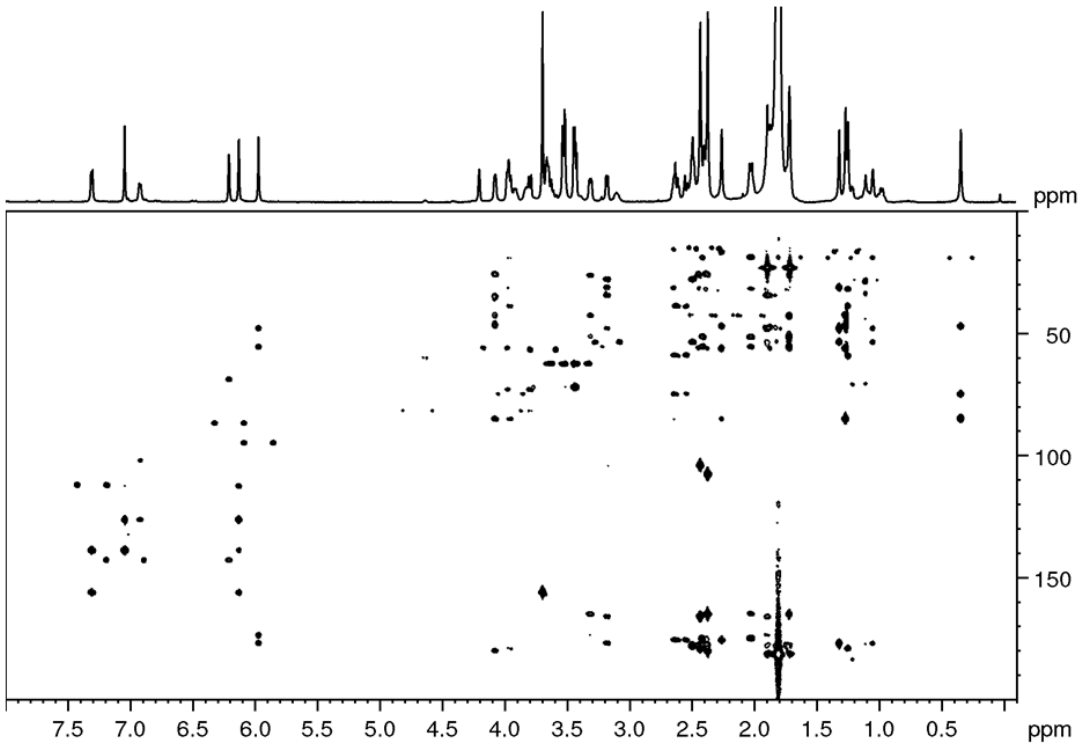

Fig. S13: ^{1}H-^{13}C HMBC spectrum of the 5-OMeBza-NCba.

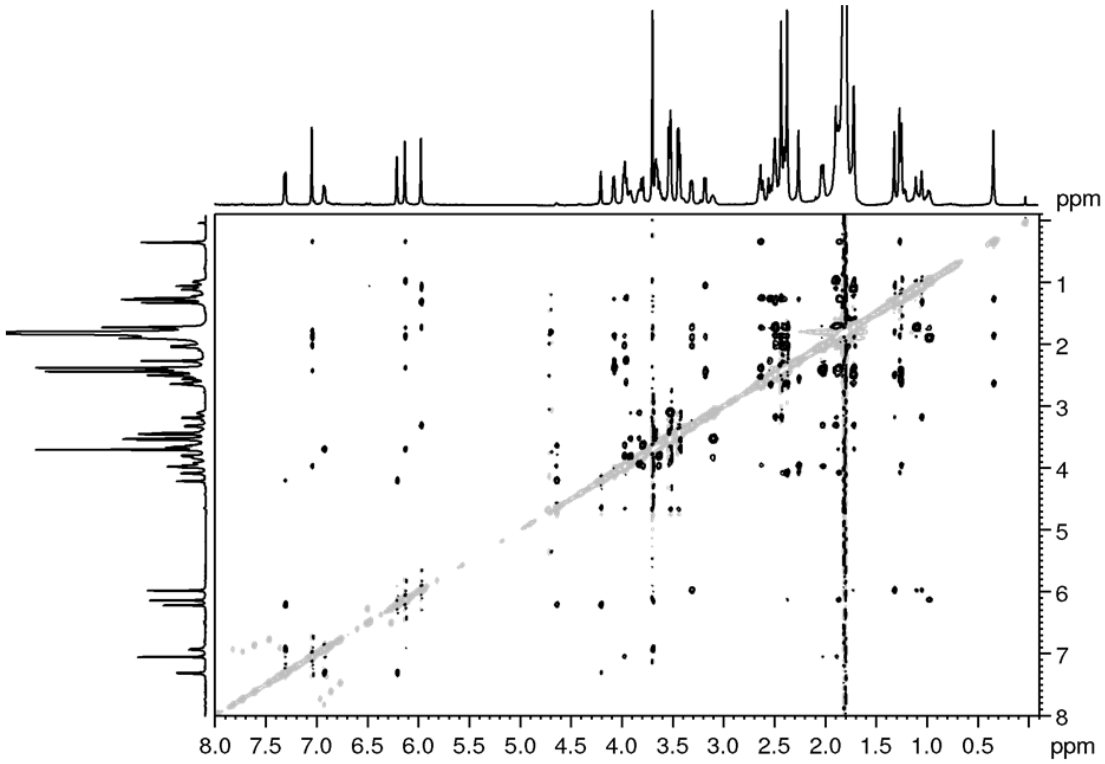

Fig. S14: ^{1}H-^{1}H ROESY spectrum of the 5-OMeBza-NCba

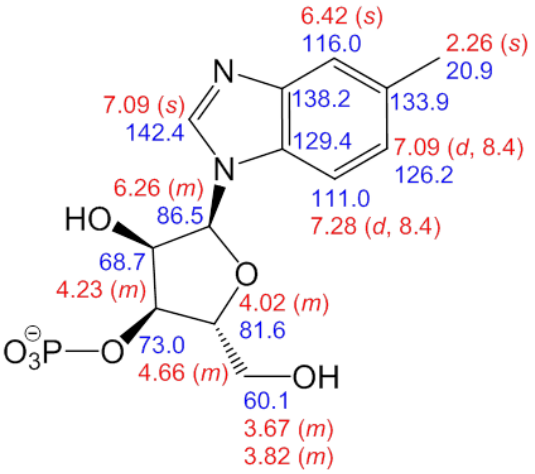

Fig. S15: Chemical shifts (δ_H red, δ_C blue) of the 5-MeBza-*N*-α-ribofuranosyl-fragment.

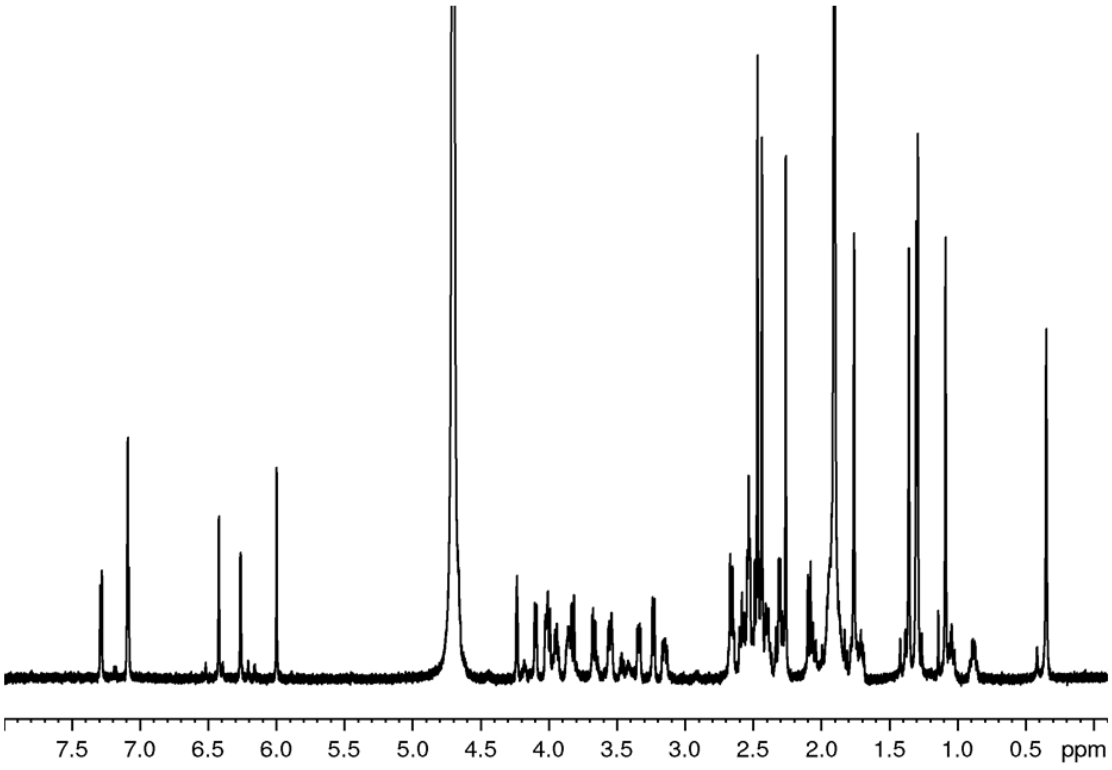

Fig. S16: ^{1}H-NMR spectrum of the 5-MeBza-NCba.

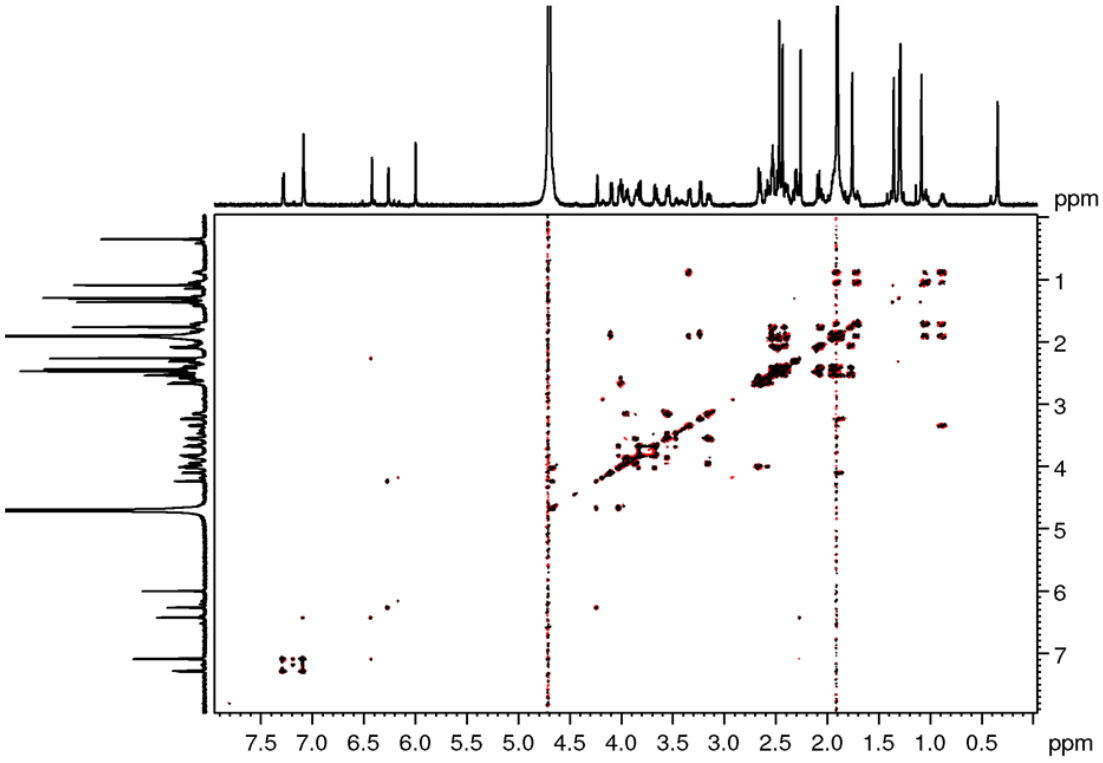

Fig. S17: ^{1}H-^{1}H-DQFCOSY spectrum of the 5-MeBza-NCba.

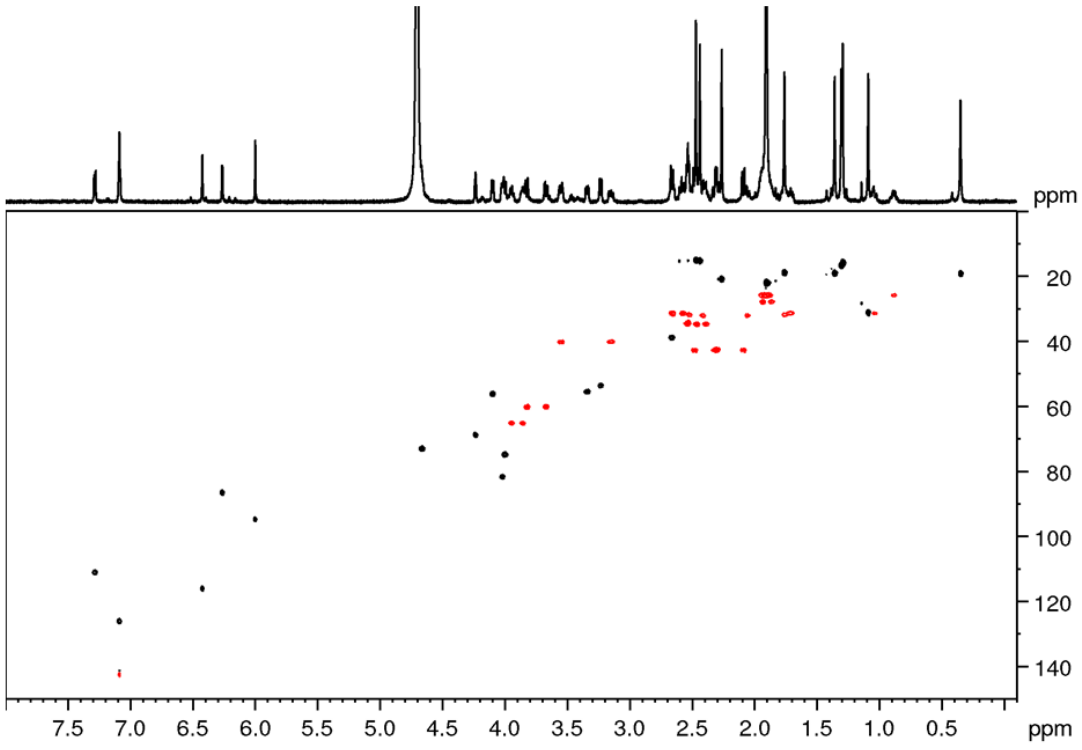

Fig. S18: ^{1}H-^{13}C HSQC spectrum of 5-MeBza-NCba.

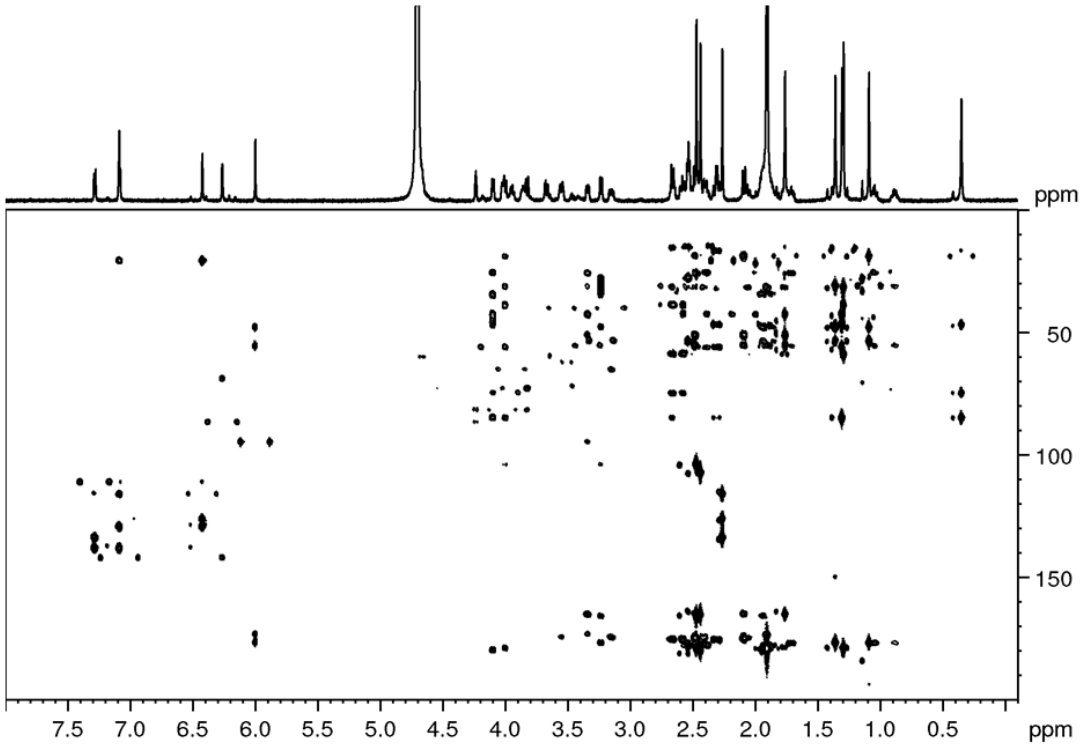

Fig. S19: ^{1}H-^{13}C HMBC spectrum of the 5-MeBza-NCba.

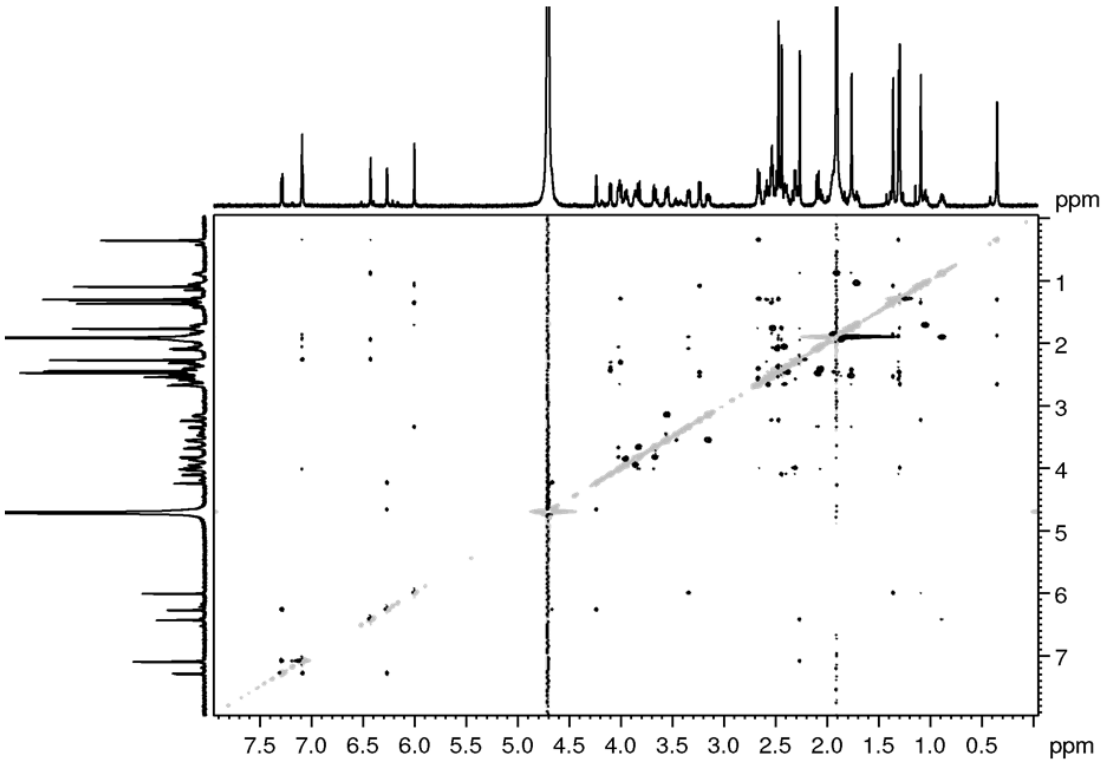

Fig. S20: ^{1}H-^{1}H ROESY spectrum of the 5-MeBza-NCba.

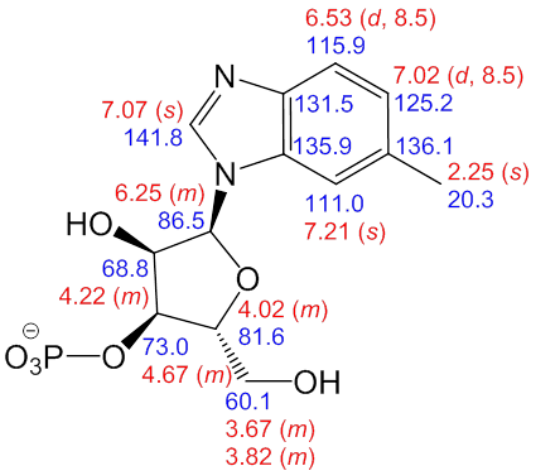

Fig. S21: Chemical shifts (δ_H red, δ_C blue) of the 6-MeBza-*N*-α-ribofuranosyl-fragment.

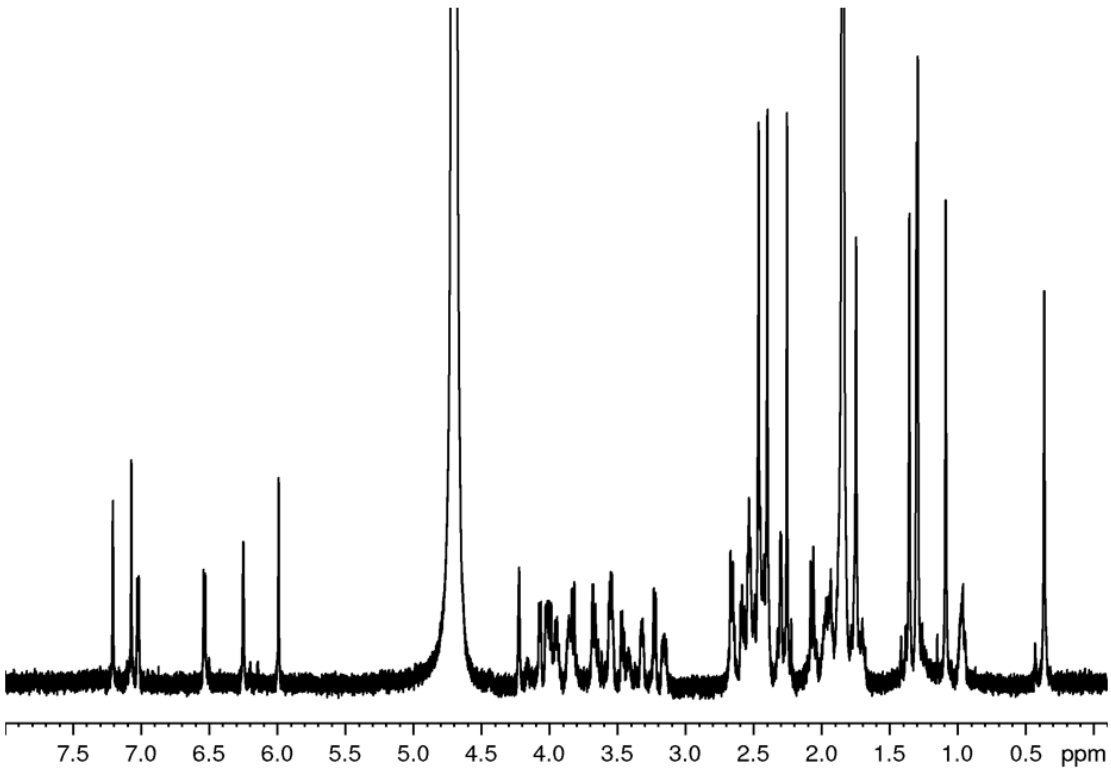

Fig. S22: ^{1}H-NMR spectrum of the 6-MeBza-NCba.

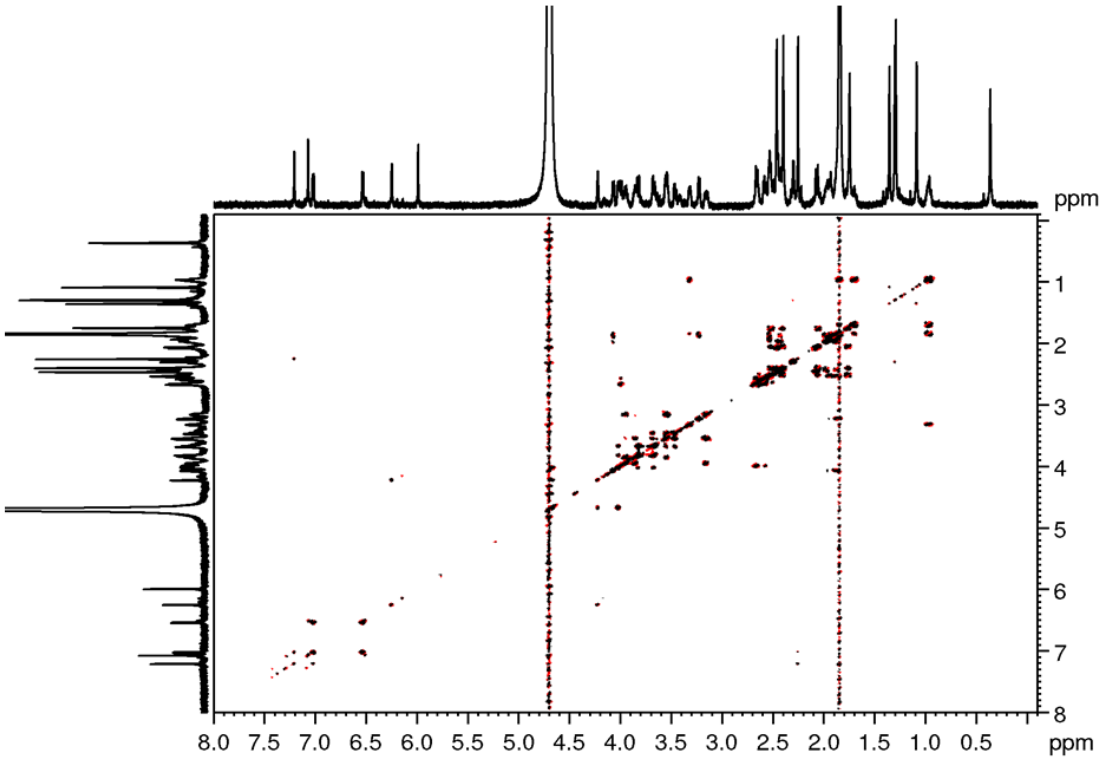

Fig. S23: ^{1}H-^{1}H-DQFCOSY spectrum of the 6-MeBza-NCba.

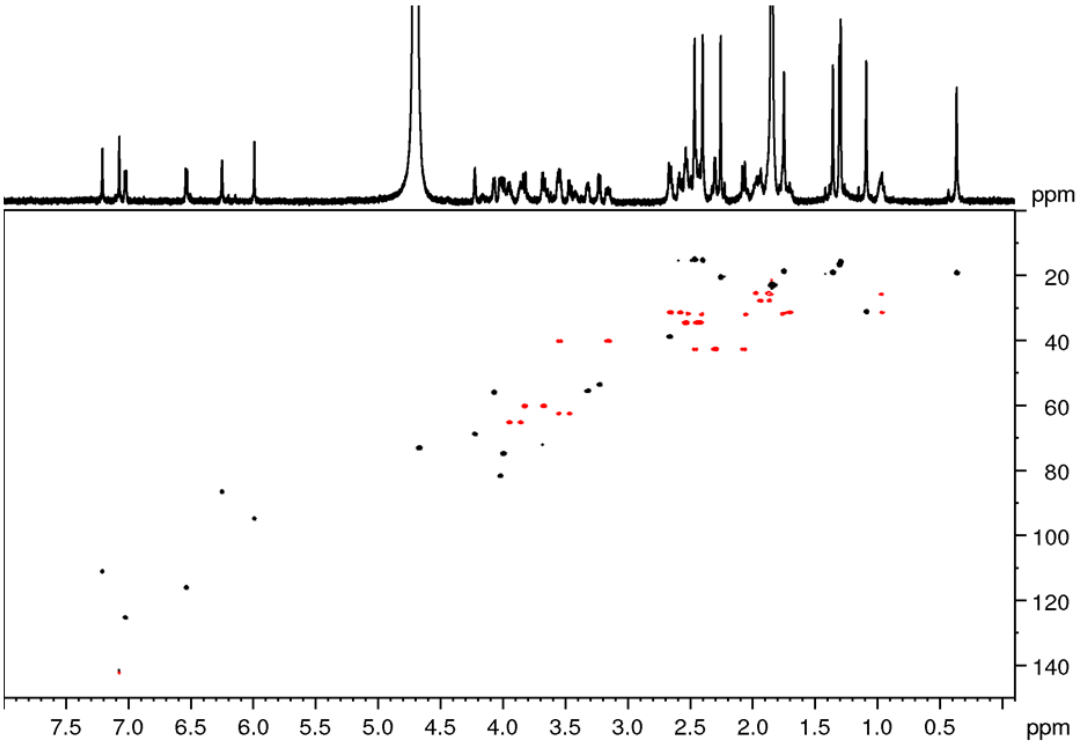

Fig. S24: ^{1}H-^{13}C HSQC spectrum of 6-MeBza-NCba.

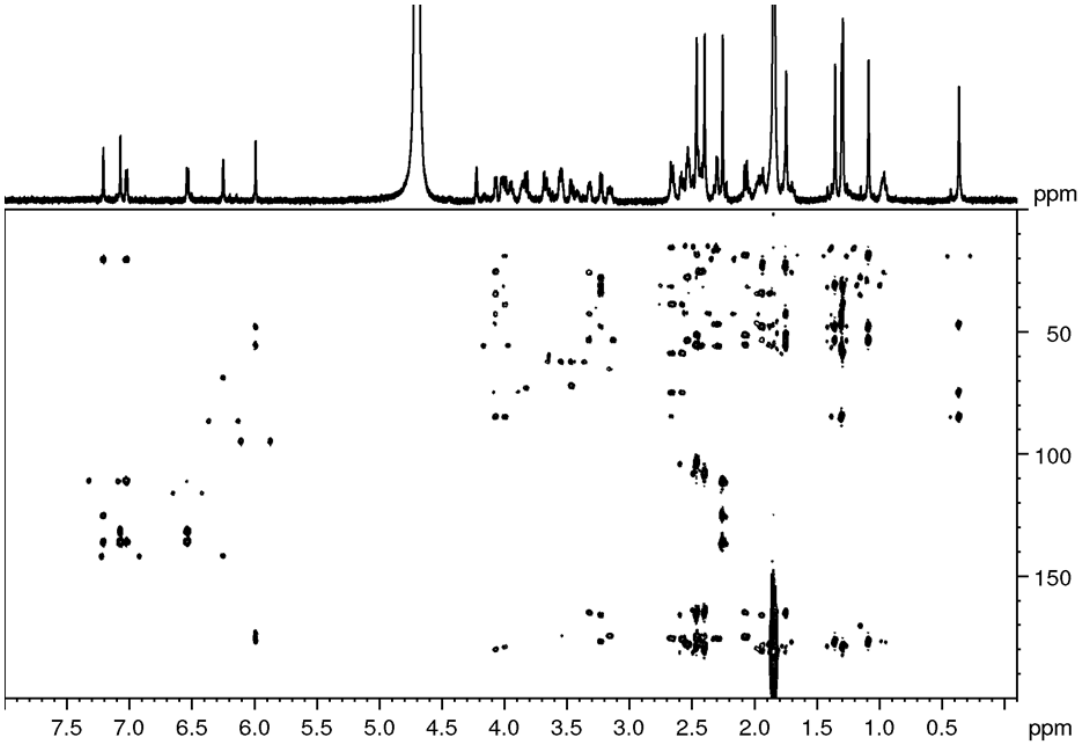

Fig. S25: ^{1}H-^{13}C HMBC spectrum of the 6-MeBza-NCba.

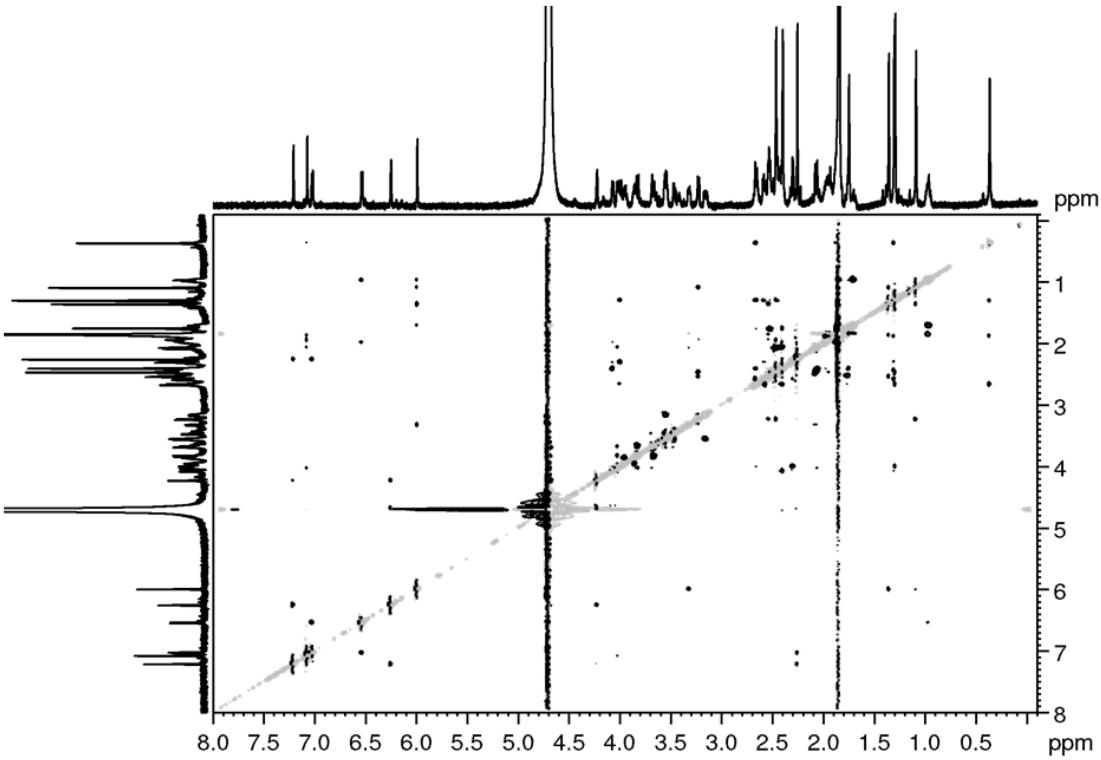

Fig. S26: ^{1}H-^{1}H ROESY spectrum of the 6-MeBza-NCba.

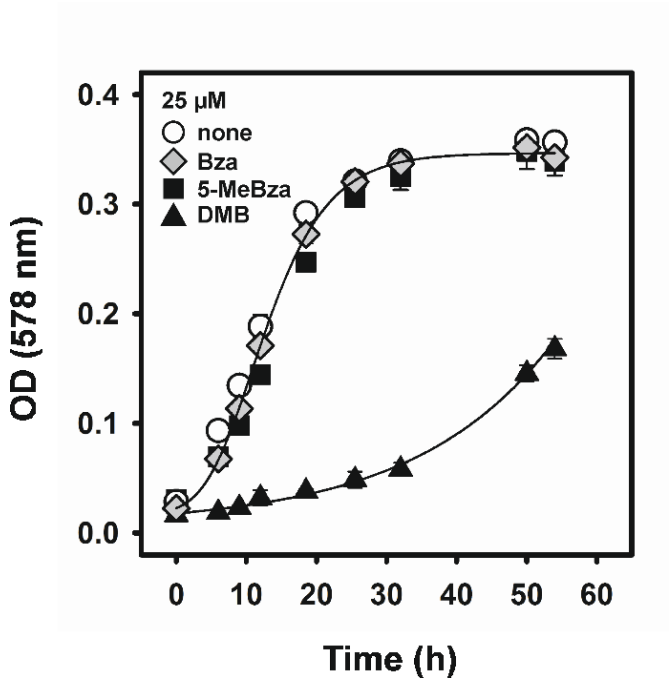

Fig. S27: PCE-dependent growth of *S. multivorans* in the presence of different benzimidazoles.

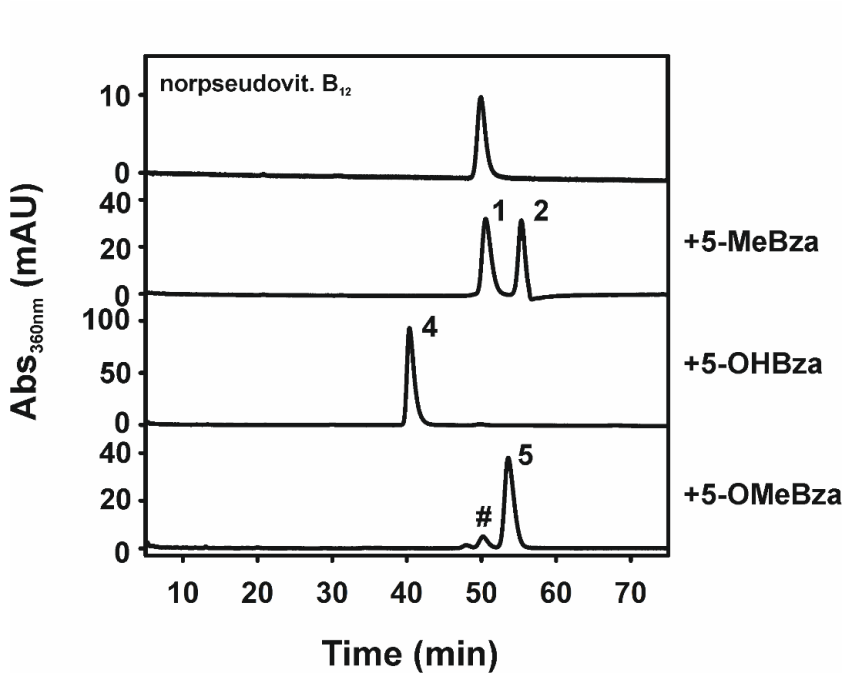

Fig. S28: HPLC-elution profiles of NCbas extracted from PceA purified from *S. multivorans* GD21 cultivated in the presence of either 5-MeBza, 5-OHBza, or 5-OMeBza. The first chromatogram shows a norpseudovitamin B_{12} standard. The designations of the signals refer to the cobamides identified in the respective cell types (see Fig. 1C). The specific activities of the purified PceA enzymes were as follows: +5-MeBZa, 687 nkat/mg; +5-OHBza, 1504 nkat/mg; +5-OMeBza, 1056 nkat/mg.

Cobamide-mediated enzymatic reductive dehalogenation via long-range electron transfer

SUPPLEMENTARY INFORMATION

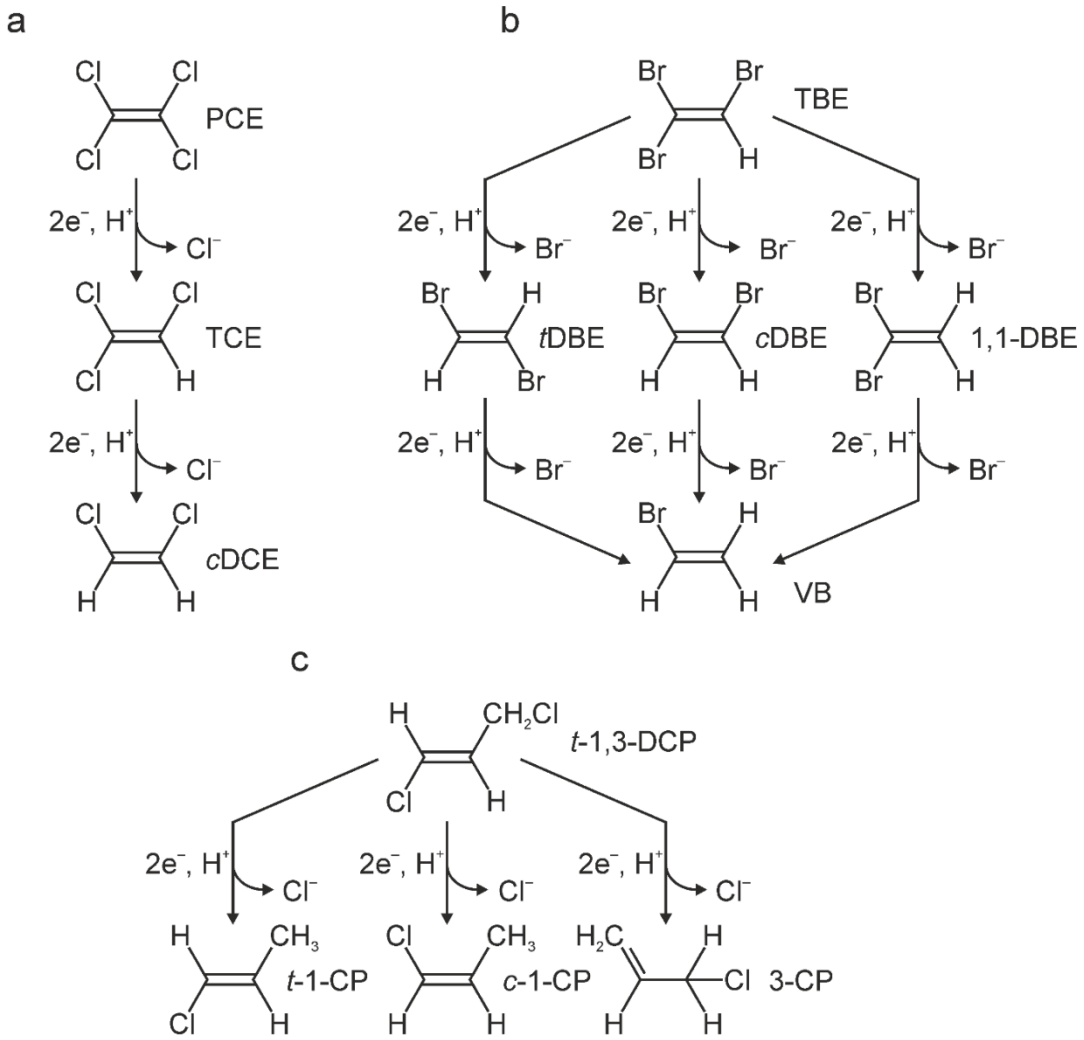

Supplementary Figure 1: Conversion of tetrachloroethene (a), tribromoethene (b), and *trans*-1,3-dichloropropene (c) by PceA. PCE: perchloroethylene / tetrachloroethene, TCE: trichloroethene, *c*DCE: *cis*-1,2-dichloroethene, TBE: tribromoethene, *t*DBE: *trans*-1,2-dibromoethene, *c*DBE: *cis*-1,2-dibromoethene, 1,1-DBE: 1,1-dibromoethene, VB: vinylbromide, *t*-1,3-DCP: *trans*-1,3-dichloropropene, *t*-1-CP: *trans*-1-chloropropene, *c*-1-CP: *cis*-1-chloropropene, 3-CP: 3-chloropropene.

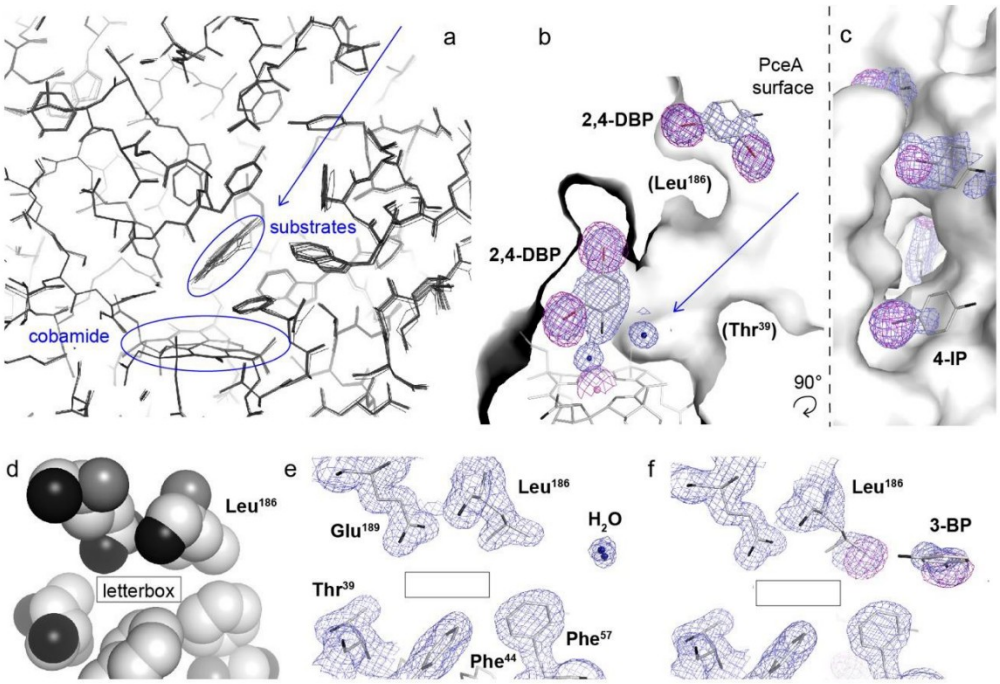

Supplementary Figure 2: Access of halogenated phenols to the substrate channel and binding pocket of PceA. (a) Slice-through PceA highlighting the substrate channel (arrow), norpseudo-B_{12} cofactor, and substrate binding site. All structures presented here (see Table 2) were overlayed. (b) Active site cavity and substrate channel with 2,4-DBP bound in both the active site and on the protein surface. Two representative water molecules (blue spheres) close to Co and the substrate are shown. Additional water and buffer molecules within the substrate channel and protein surface are omitted for clarity. The size of the substrate entrance is restricted to a maximum width of 5.5 Å by *inter alia* Leu186 and Thr39. (c) "Letter box" opening of the substrate channel of PceA with 4-IP bound to the hydrophobic groove at the protein surface. (d) Van-der-Waals radius representation of the substrate entry letter box. (e) Defined electron density for letter box residues (2,4,6-TBP bound PceA shown as representative structure). (f) Electron density for 3-BP bound PceA is perturbed at Leu186. Anomalous signal indicates partial replacement at the common Leu186 position with a 3-BP molecule.

2

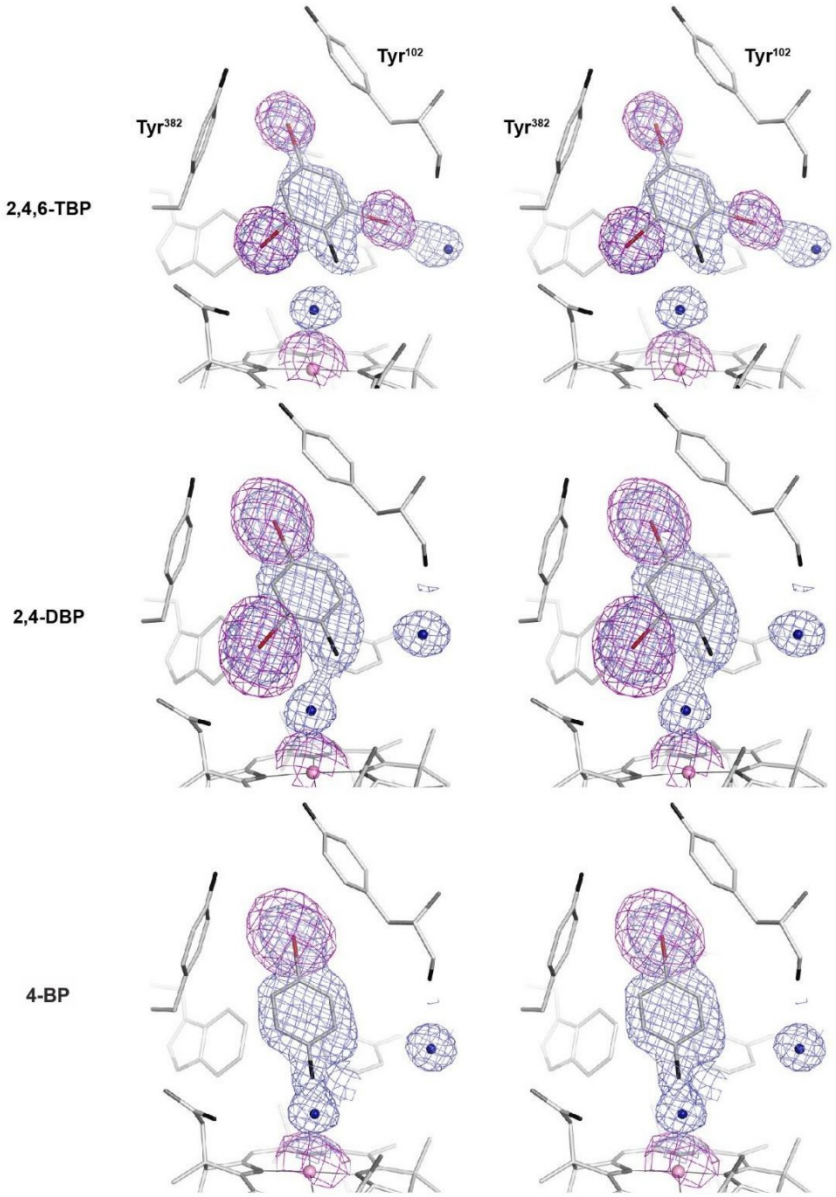

Supplementary Figure 3: Wall-eye stereo representation of 2,4,6-TBP, 2,4-DBP, and 4-BP bound to PceA. Blue mesh represents 1 σ $2F_o$-F_c electron density maps and purple mesh 5 σ anomalous difference density maps at λ = 0.918 Å, indicative of bromide (red sticks). The substrate hydroxyl group is shown in black, the cobalt atom in pink.

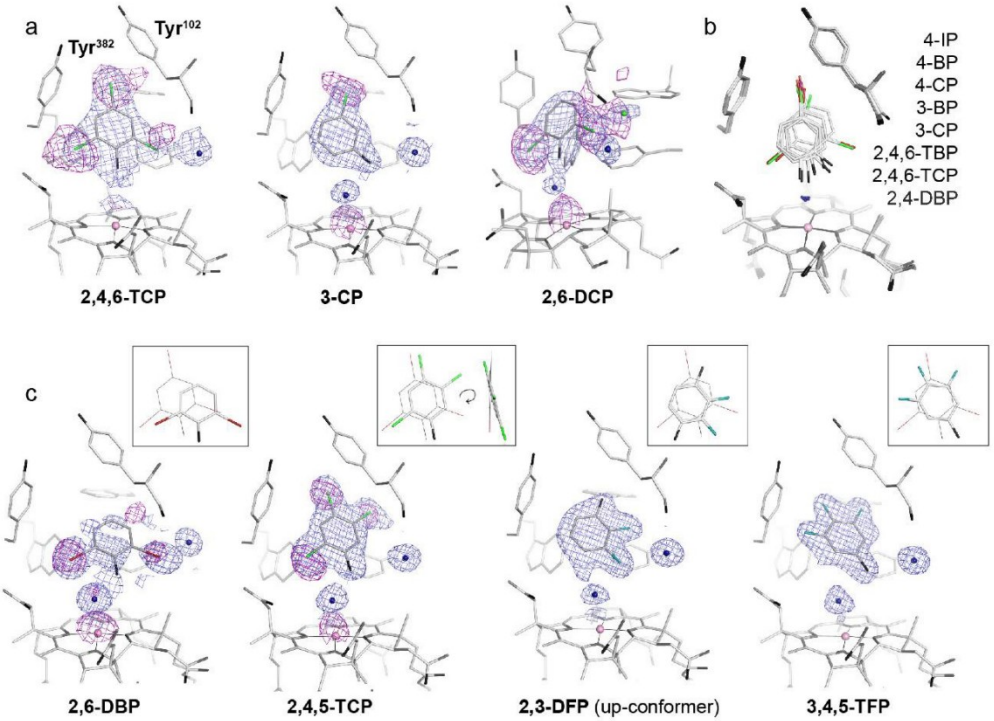

Supplementary Figure 4: Positioning of halogenated phenols in the substrate-binding pocket of PceA. (a) 2,4,6-TCP*, 3-CP*, and 2,6-DCP share the same position as their brominated analogues, but were not converted by PceA. Electron density for the chloride atom is dispersed away from C6, but not C2 in 2,6-DCP. No cobalt β-ligand was modelled for 2,4,6-TCP because of the lower resolution. (b) Overlay of tested halogenated phenols demonstrates a similar positioning in the active site. (c) Substrates bound in different orientations: 2,6-DBP* shifted towards Tyr102. 2,4,5-TCP pitched 15° backwards to circumvent the close proximity between the chlorine at C5 and Tyr102. 2,3-Difluorophenol is apparently bound in two orientations that are inverted horizontally (see inset). 3,4,5-Trifluorophenol is able to orient its *meta*-fluorines towards the inhibited position close

to Tyr382 and also towards Tyr102. The smaller fluorine substituents seem to fit into these positions.

In the direction shown, Tyr382, Tyr102, and the corrin ring encircle the binding site. For all substrates 1 sigma $2F_o$-F_c electron density (blue) for substrate, Co-ligand water, and the first water molecule in the substrate channel are shown. Anomalous difference density (indicative of a heavy atom) is shown around the substrate for bromine (5 sigma) or chlorine (3.5 sigma for 2,4,5-TCP and 3-CP, 3.0 sigma for 2,6-DCP and 2.5 sigma for 2,4,6-TCP; data were collected at 1.9 Å X-ray wavelength). Selected overlays are shown as insets. Substrates marked with * were incubated together with crystals in buffer containing 200 mM chloride as counter ion.

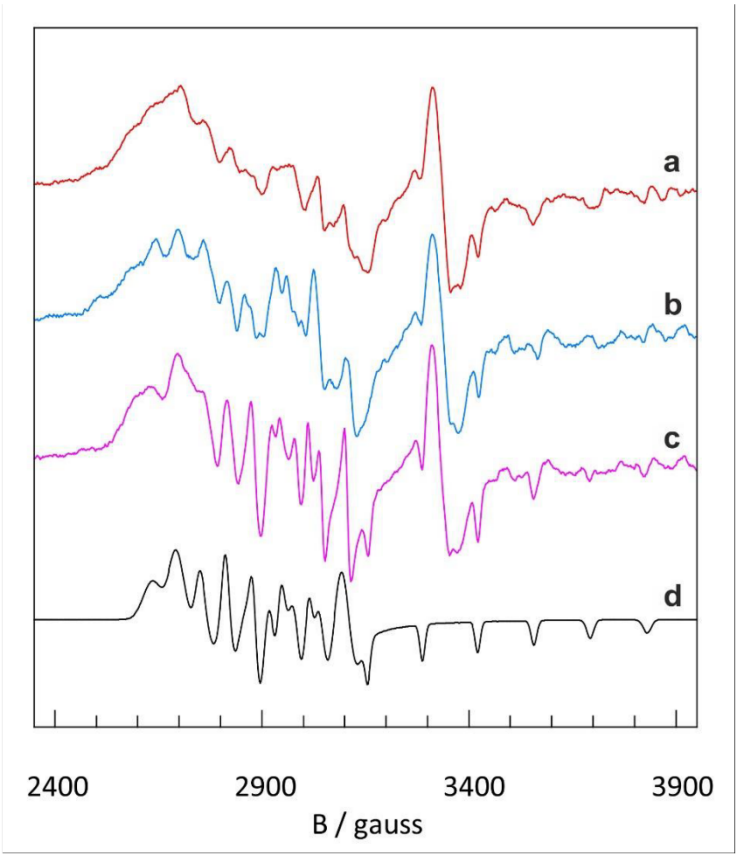

Supplementary Figure 5: Overview of spectral effects in the [Co^{II}]-EPR of PceA upon incubation with substrates. Trace a is the low-spin S = 1/2 spectrum of the cobamide cofactor in as-isolated enzyme (61 µM). The feature near g = 2 (circa 3350 gauss) is from a minor [3Fe-4S] species, a degradation product of the [4Fe-4S] clusters. Trace b shows the spectrum after 2 min incubation in a saturated PCE solution, which led to a minor increase in resolution of the I = 7/2 Co nuclear hyperfine interaction (also observed for other halogenated ethenes). A further increase in resolution in particular in the middle part of the spectrum is afforded upon incubation with the phenol derivatives; shown is 2,4-DBP (trace c). The latter spectrum is simulated in trace d with parameters (zyx-value): g-values 1.989, 2.292, 2.338; hyperfine A-values 134, 55, 65 gauss; linewidths W 10, 25, 25 gauss, line asymmetry values B 0.03, -0.04, -0.04 and C 0.03, 0.03, 0.03. The latter are defined

as total linewidth = $W(1+Bm_I+Cm_I^2)$, in which m_I is the nuclear quantum orientation running from -7/2 to 7/2 for cobalt[1]. The spectral sharpening upon substrate addition may be partly due to a general attenuating effect of the organic substrate on ice crystal growth during freezing of the samples in liquid nitrogen (*i.e.,* causing a reduction of g-strain), but the conspicuous grouping of the spectra in ethene- versus phenol-type would seem to indicate that there is also a more specific effect on active-site conformation upon substrate binding.

Experimental EPR conditions were: microwave frequency, 9338 MHz; microwave power, 12.7 mW; modulation frequency, 100 kHz, modulation amplitude, 8 gauss; temperature 22 K.

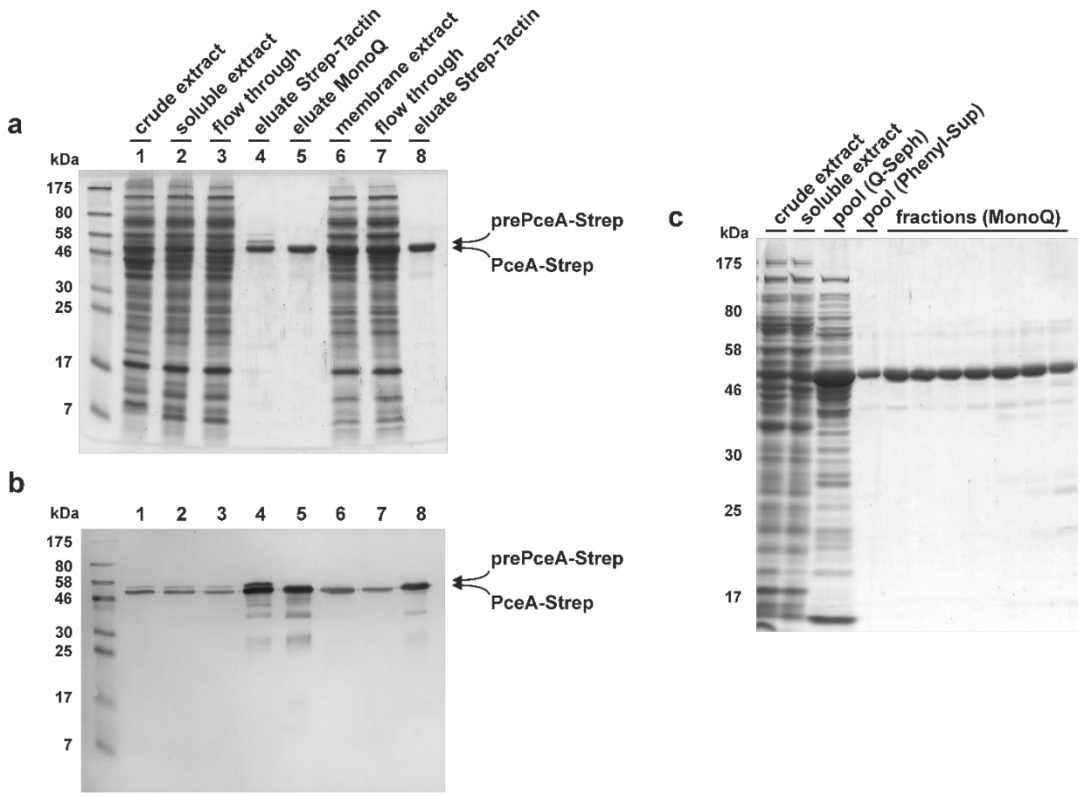

Supplementary Figure 6: Purification of recombinant PceA-Strep from *S. multivorans* GD21 and purification of PceA from the wild type strain. (a) PceA-Strep was isolated from soluble and membrane extract of *S. multivorans* GD21, grown on pyruvate/PCE medium in the presence of 720 µM $FeSO_4$, via Strep-Tactin affinity-chromatography. An apparently homogenous mature PceA-Strep protein was isolated, when the membrane extract was applied (lane 8). A mixture of the enzyme's precursor prePceA-Strep and the mature form was obtained when soluble extract was used (lane 4). The binding of the affinity-tagged enzyme to the Strep-Tactin matrix appeared to be very loose, since a significant portion of the PceA-Strep was detected in the flow through of the column. This observation has been made previously, when the C-terminally Strep-tagged PceA of *Dehalobacter restrictus* was heterologously produced and purified via affinity chromatography[2]. Both results point

towards a C-terminus of PceA enclosed by the protein structure with little access to the surrounding. Coomassie-stained 12.5% SDS-PAGE with 10 µg protein (except the eluates, of which 1 µg was applied) separated on each lane. (b) Immunoblot of the SDS-PAGE developed with an antibody against the Strep-tag. (c) PceA was conventionally isolated from the soluble extract of *S. multivorans*, grown on pyruvate/fumarate medium in the presence of 90 µM $FeSO_4$, via a combination of Q-Sepharose, Phenyl-Superose, and MonoQ column[3]. Coomassie-stained 12.5% SDS-PAGE with 10 µg protein of extract and from pooled fractions eluted from a Q-Sepharose column and 1 µg protein from pooled fractions eluted from a Phenyl-Superose column and from eluates of a MonoQ column, respectively, separated on each lane.

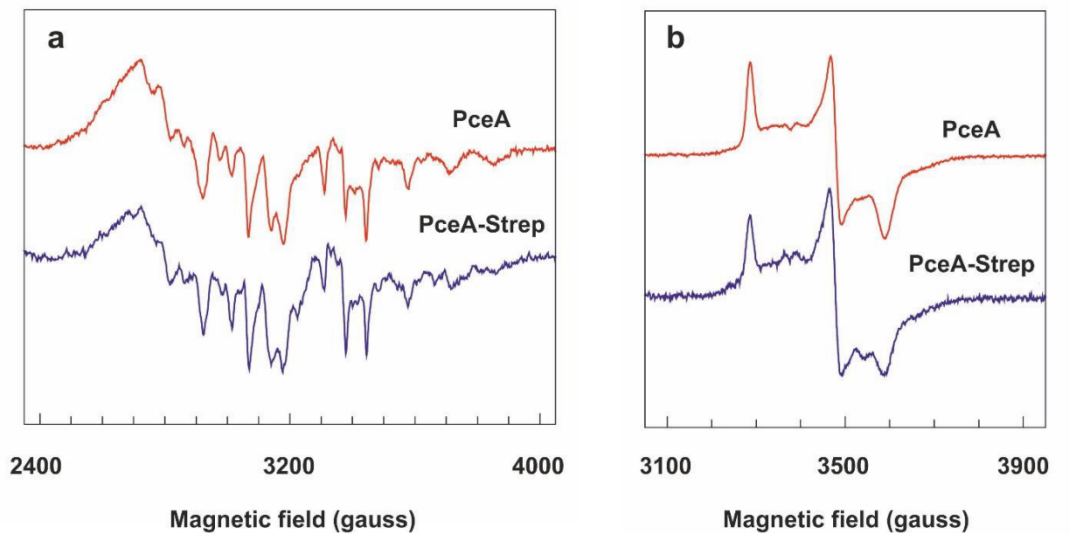

Supplementary Figure 7: Determination of the redox states of the metal-cofactors in mature PceA (red traces) and mature PceA-Strep (blue traces) by EPR spectroscopy. (a) Cob(II)alamin spectra of as-isolated enzyme. The two spectra were essentially identical and were typical for cob(II)alamin in the base-off configuration as indicated by the lack of characteristic superhyperfine splitting from an axially coordinating nitrogen base. The base-off configuration of the cobamide cofactor in the wild type PceA enzyme has been reported earlier[6]. Estimation of the spin Hamiltonian parameters by simulation[1] afforded g-values of $g_{||}$ = 2.00 and $g_{\perp} \approx$ 2.32 and cobalt hyperfine (I = 7/2) values of $A_{||}$ = 132 and $A_{\perp} \approx$ 60 gauss. These values were quite similar to those previously found for the base-off form of cob(II)alamin in the PCE reductive dehalogenase of *Dehalobacter* restrictus[7] or in the *ortho*-chlorophenol reductive dehalogenase of *Desulfitobacterium* dehalogenans[8]. Application of elevated positive redox potentials up to 309 mV by the addition of potassium hexacyanoferrate(III) did not led to the disappearance of the [Co^{II}] signal, which would indicate [Co^{III}] formation.

(b) [4Fe-4S] spectra for dithionite-reduced enzyme. Upon reduction with sodium dithionite the [Co^{II}] signal disappeared, because of [Co^{I}] formation. At 17 K the characteristic interaction pattern appeared for two $[4Fe\text{-}4S]^{1+}$ clusters with mutual dipolar coupling over a typical distance of about 10 Å. The effective g-values read from the spectra were g_z = 2.05, g_y = 1.94, g_x = 1.88, but these were likely to be shifted somewhat from the actual g-values of the cubanes by virtue of the dipolar interaction.

EPR conditions were: microwave frequency, 9448 MHz; microwave power, -22 dB (1.26 mW) for trace a and -26 dB (0.5 mW) for trace b; temperature, 31 K for trace a and 17 K for trace b.

Spin quantification versus an external copper(II)-standard gave concentrations of 166 μM cobalt and 355 μM cubane for the sample containing PceA and 83 μM cobalt and 155 μM cubane for the sample containing PceA-Strep, *i.e.,* two iron-sulfur clusters per cobamide cofactor in both preparations. These results were in accordance with previously reported 1 mol cobamide and 8 mol iron per mol PceA[4] or PceA-Strep (Supplementary Table 2). From the spectroscopic results obtained for the PceA-Strep variant in comparison to the wild type PceA a negative effect of the C-terminal Strep-tag on the maturation and activity of the enzyme was excluded.

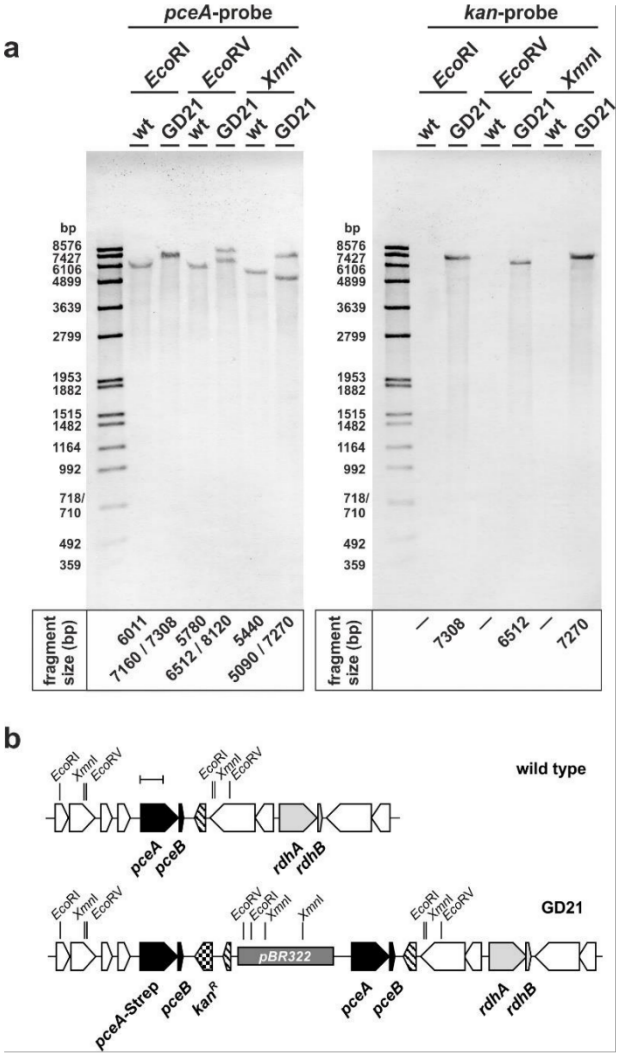

Supplementary Figure 8: Generation of the mutant strain *S. multivorans* GD21 by incorporation of a modified *pceA* gene cluster into *S. multivorans* via single homologous recombination. (a) The integration of the plasmid into the organohalide respiration region in the genome sequence of *S. multivorans* wild type (Genbank accession no. CP007201)[12] was proven by Southern hybridization analysis of *S. multivorans* GD21 in comparison to the wild type (wt) using specific DNA probes against *pceA* and *kanamycin (kan)*. No impact on PCE dependent growth was

observed for the mutant strain compared to the wild type. (b) Schematic representation of the genetic manipulation. The scale bar represents 1000 base pairs.

Supplementary Table 1: PceA activity for 4-BP in the presence of different artificial electron donors. All viologens (0.5 mM) were reduced by the addition of 1.4 mM Ti(III) citrate. Sodium dithionite was used as sole electron donor in a concentration of 1.4 mM without further addition of Ti(III) citrate. Given are relative specific activities in relation to the standardised activity with methyl viologen as electron donor (100%).

The use of sodium dithionite as reducing agent showed 14 times slower conversion rates compared to benzyl viologen as reducing agent with a similar redox potential. In PceA crystals treated with 5 mM dithionite, a heart-shaped electron density attributed to a SO_2 molecule with the sulphur atom pointing to the Co was found at the active site, which might have caused the reduced activity.

Electron donor	$E^{0'}$ (mV)	Relative specific activity (%)
Ethyl viologen	-480	167
Methyl viologen	-440	100
Sodium dithionite	-386	2.5
Benzyl viologen	-360	34

Supplementary Table 2: Cofactor content in isolated PceA-Strep from *S. multivorans* GD21 cultivated in the presence of different $FeSO_4$ concentrations. The conventionally purified PceA from *S. multivorans* wild type contained about 8 mol iron and 1 mol cobamide per mol purified PceA when grown in the presence of 90 µM $FeSO_4$[4]. Under these conditions, only 2.9±0.1 mol iron and 0.3 mol cobamide were detected per mol PceA-Strep. Since *S. multivorans* produces the cobamide cofactor *de novo* in high excess, the limitation might be due to a shortage in iron supply rather than in cobamide production. An increase of the $FeSO_4$ concentration up to 720 µM in the growth medium led to the production of mature PceA-Strep completely occupied with cofactors. The iron limitation may be caused by the parallel expression of two *pceA* genes in strain GD21 (Supplementary Fig. 8). The cobamide cofactor was extracted from PceA-Strep and analysed via high-performance liquid chromatography as described by Keller *et al.*[3]. Iron determination was performed using the method published by Fish[5].

[$FeSO_4$] (µM) in the medium	**Metals/Cofactors (mol/mol PceA-Strep)**	
	n [Fe]	**n [Cobamide]**
PceA Neumann *et al.*, 1996[4]	8	1
S. multivorans GD21		
90	2.9 ± 0.1	0.3
180	4.35 ± 0.25	n.d.
360	4.45 ± 0.25	n.d.
720	7.5 ± 0.4*	1.0*
	7.1 ± 1.2#	1.0#

At a $FeSO_4$ concentration of 720 µM the cofactors were separately extracted from PceA-Strep isolated from soluble extract (*) or membrane extract (#).
n.d.: not determined

Supplementary Table 3 part 1/4. Data collection and refinement statistics

(molecular replacement)

	3-BP (5MAA)	3-CP (5M8Y)	4-BP (5M8U)	4-IP (5MA2)
Data collection				
Space group	$P\,4_1$	$P\,4_1$	$P\,4_1$	$P\,4_1$
Cell dimensions				
a, *b*, *c* (Å)	73.8, 73.8,185.4	73.8, 73.8,185.2	73.6, 73.6, 184.6	73.8, 73.8 184.7
α, β, γ (°)	90, 90, 90	90, 90, 90	90, 90, 90	90, 90, 90
Resolution (Å)	45.5 - 1.69 (1.75 - 1.69)	47.4 - 1.86 (1.92 - 1.86)	36.8 - 1.90 (1.97 - 1.90)	45.4 - 1.88 (1.95 - 1.88)
R_{merge} (%)	9.1 (122)	5.4 (37)	9.9 (95)	8.2 (39)
$I / \sigma I$	21.6 (2.0)	29.1 (3.3)	19.9 (2.3)	19.3 (2.9)
Completeness (%)	100 (99)	97 (78)	100 (100)	99 (89)
Redundancy	13.8 (13.1)	10.8 (4.4)	7.7 (7.7)	11.0 (4.8)
Refinement				
Resolution (Å)	45.5 - 1.69	47.4 - 1.86	36.8 - 1.90	45.4 - 1.88
No. reflections	110982	80946	76762	79047
R_{work} / R_{free}	14.8 / 16.7	13.0 / 16.1	14.6 / 17.2	13.6 / 16.5
No. atoms				
Protein	6852	6857	6866	6858
Ligand/ion	277	274	299	322
Water	759	763	783	721
B-factors (Å^2)				
Protein	28	29	28	32
Ligand/ion	26	28	29	34
Water	39	40	41	43
R.m.s. deviations				
Bond lengths (Å)	0.010	0.007	0.008	0.011
Bond angles (°)	1.86	0.92	0.91	1.88

*Values in parentheses are for highest-resolution shell.

Supplementary Table 3 part 2/4. Data collection and refinement statistics (molecular replacement)

	4-CP (5M8W)	2,4-DBP (5M92)	2,6-DBP (5M91)
Data collection			
Space group	$P\,4_1$	$P\,4_1$	$P\,4_1$
Cell dimensions			
a, *b*, *c* (Å)	73.3, 73.3, 184.4	73.9, 73.9, 185.1	73.5, 73.5, 184.6
α, β, γ (°)	90, 90, 90	90, 90, 90	90, 90, 90
Resolution (Å)	39.0 - 2.28 (2.36 - 2.28)	46.3 - 1.79 (1.85 - 1.79)	30.1 - 1.72 (1.78 - 1.72)
R_{merge} (%)	15.0 (89)	9.0 (95)	6.7 (76)
$I / \sigma I$	19.3 (2.6)	22.1 (2.4)	22.1 (2.6)
Completeness (%)	100 (099)	100 (96)	100 (99)
Redundancy	7.4 (7.1)	13.6 (13.4)	7.7 (7.6)
Refinement			
Resolution (Å)	39.0 - 2.28	46.3 - 1.79	30.1 - 1.72
No. reflections	44129	93432	103500
R_{work} / R_{free}	14.0 / 19.3	14.9 / 17.8	14.6 / 17.5
No. atoms			
Protein	6837	6857	6855
Ligand/ion	301	316	279
Water	500	731	801
B-factors (Å^2)			
Protein	32	29	27
Ligand/ion	34	30	27
Water	38	41	39
R.m.s. deviations			
Bond lengths (Å)	0.008	0.029	0.008
Bond angles (°)	0.93	0.93	0.96

*Values in parentheses are for highest-resolution shell.

Supplementary Table 3 part 3/4. Data collection and refinement statistics

(molecular replacement)

	2,4,6-TBP (5M2G)	2,6-DCP (5MA0)	2,4,6-TCP (5MA1)
Data collection			
Space group	$P\,4_1$	$P\,4_1$	$P\,4_1$
Cell dimensions			
a, *b*, *c* (Å)	73.6, 73.6, 185.0	73.6, 73.6, 184.5	73.5, 73.5, 179.4
α, β, γ (°)	90, 90, 90	90, 90, 90	90, 90, 90
Resolution (Å)	47.3 - 1.80 (1.86 - 1.80)	31.0 - 1.90 (1.97 - 1.90)	33.9 - 2.6 (2.69 - 2.60)
R_{merge} (%)	7.2 (71)	6.6 (80)	17.7 (128)
$I / \sigma I$	15.1 (2.1)	32.3 (2.7)	20.0 (2.3)
Completeness (%)	100 (100)	99 (96)	100 (100)
Redundancy	4.6 (4.7)	14.1 (9.4)	15.0 (14.7)
Refinement			
Resolution (Å)	47.3 - 1.80	31.0 - 1.90	33.9 - 2.60
No. reflections	90629	76268	29139
R_{work} / R_{free}	13.4 / 16.7	13.6 / 16.7	15.0 / 21.5
No. atoms			
Protein	6863	6828	6559
Ligand/ion	290	264	242
Water	771	681	215
B-factors (Å^2)			
Protein	28	29	46
Ligand/ion	28	27	40
Water	42	40	45
R.m.s. deviations			
Bond lengths (Å)	0.010	0.007	0.010
Bond angles (°)	1.00	0.94	1.15

*Values in parentheses are for highest-resolution shell.

Supplementary Table 3 part 4/4. Data collection and refinement statistics (molecular replacement)

	2,4,5-TCP (5M8X)	2,3-DFP (5M8Z)	3,4,5-TFP (5M90)
Data collection			
Space group	$P\,4_1$	$P\,4_1$	$P\,4_1$
Cell dimensions			
a, *b*, *c* (Å)	73.8, 73.8, 185.0	73.6, 73.6, 185.0	73.6, 73.6, 185.1
α, β, γ (°)	90, 90, 90	90 90 90	90, 90, 90
Resolution (Å)	47.3 - 1.87 (1.94 - 1.87)	47.3 - 1.66 (1.72 - 1.66)	47.3 - 1.60 (1.66 - 1.60)
R_{merge} (%)	5.8 (29)	5.2 (62)	4.8 (63)
$I / \sigma I$	26.7 (4.0)	21.9 (2.8)	24.9 (2.8)
Completeness (%)	97 (75)	100 (100)	1.00 (99)
Redundancy	11.2 (5.3)	6.8 (6.5)	6.8 (6.7)
Refinement			
Resolution (Å)	47.3 - 1.87	47.3 - 1.66	47.3 - 1.60
No. reflections	78587	115504	129216
R_{work} / R_{free}	12.8 / 15.9	13.8 / 16.1	14.3 / 16.7
No. atoms			
Protein	6939	6861	6819
Ligand/ion	293	327	296
Water	732	744	793
B-factors (Å^2)			
Protein	28	27	25
Ligand/ion	28	29	25
Water	39	40	38
R.m.s. deviations			
Bond lengths (Å)	0.008	0.009	0.008
Bond angles (°)	0.95	1.03	0.98

*Values in parentheses are for highest-resolution shell.

Supplementary Table 4: Plasmids used in this study.

Plasmid	Relevant characteristic(s), construction details	Reference
pBR322	Amp^R, Tet^R	(9)
pUC4K	Amp^R, Kan^R	(10)
pY179	6-kb *Eco*RI fragment of genomic DNA of *S. multivorans* subcloned into pBluescript II SK+ cut with *Eco*RI; fragment oriented inverse to *lacZ*	(11)
pTOS001	*Bam*HI/*Bgl*II-fragment of pY179 ligated with pBR322 cut with *Bam*HI; fragment oriented inverse to *tet*	This study
pTOS012	*Bam*HI-fragment (Klenow-treated) of pUC4K ligated with pTOS001 cut with *Bst*XI (Klenow-treated); fragment oriented inverse to *pceA*	This study
pTOS024	pY179 cut with *Xho*I/*Bgl*II, treated with Klenow-fragment and re-ligated	This study
pTOS036	inverse PCR using primers T68/T69 and pTOS024 as template; cut with *Nhe*I and re-ligated	This study
pTOS071	pTOS036 cut with *Nhe*I/*Afl*II and ligated with an similarly cut PCR-fragment, which was generated using primers T110/AN38 and template pY179	This study
pTOS077	*Pml*I/*Afl*II-fragment of pTOS071 ligated with pTOS012 cut with *Pml*I/*Afl*II	This study

REFERENCES

(1) Hagen, W.R. *Biomolecular EPR spectroscopy* (CRC Press / Taylor & Francis Group, Boca Raton, Fl, USA, 2009).

(2) Sjuts, H., Fisher, K., Dunstan, M.S., Rigby, S.E., Leys, D. Heterologous expression, purification and cofactor reconstitution of the reductive dehalogenase PceA from *Dehalobacter restrictus*. *Protein Expr. Purif.* **85,** 224-229 (2012).

(3) Keller, S., *et al.* Exogenous 5,6-dimethylbenzimidazole caused production of a non-functional tetrachloroethene reductive dehalogenase in *Sulfurospirillum multivorans*. *Environ. Microbiol.* **16,** 3361-3369 (2014).

(4) Neumann, A., Wohlfarth, G., Diekert, G. Purification and characterization of tetrachloroethene reductive dehalogenase from *Dehalospirillum multivorans*. *J. Biol. Chem.* **271,** 16515-16519 (1996).

(5) Fish, W.W. Rapid colorimetric micromethod for the quantitation of complexed iron in biological samples. *Methods Enzymol.* **158,** 357-364 (1988).

(6) Kräutler, B., *et al.* The cofactor of tetrachloroethene reductive dehalogenase of *Dehalospirillum multivorans* is norpseudo-B_{12}, a new type of a natural corrinoid. *Helv. Chim. Acta.* **86,** 3698-3716 (2003).

(7) Schumacher, W., Holliger, C., Zehnder, A.J.B., Hagen, W.R. Redox chemistry of cobalamin and iron-sulfur cofactors in the tetrachloroethene reductase of *Dehalobacter restrictus*. *FEBS Letters* **409,** 421-425 (1997).

(8) van de Pas, B.A., *et al.* Purification and molecular characterization of ortho-chlorophenol reductive dehalogenase, a key enzyme of halorespiration in *Desulfitobacterium dehalogenans*. *J. Biol. Chem.* **274,** 20287-20292 (1999).

(9) Bolivar, F., *et al.* Construction and characterization of new cloning vehicles. II. A multipurpose cloning system. *Gene* **2,** 95-113 (1977).

(10) Vieira, J. and Messing, J. The pUC plasmids, an M13mp7-derived system for insertion mutagenesis and sequencing with synthetic universal primers. *Gene* **19,** 259-268 (1982).

(11) Neumann, A., Wohlfarth, G., Diekert, G. Tetrachloroethene dehalogenase from *Dehalospirillum multivorans*: Cloning, sequencing of the encoding genes, and expression of the *pceA* gene in *Escherichia coli*. *J. Bacteriol.* **180,** 4140-4145 (1998).

(12) Goris, T., *et al.* Insights into organohalide respiration and the versatile catabolism of *Sulfurospirillum multivorans* gained from comparative genomics and physiological studies. *Environ. Microbiol.* **16,** 3562-3580 (2014).

Subtle changes in the active site architecture untangled overlapping substrate ranges and mechanistic differences of two reductive dehalogenases

Cindy Kunze, Gabriele Diekert and Torsten Schubert

DOI: 10.1111/febs.14258

SUPPLEMENTARY MATERIAL

Table S1. Plasmids used in this study.

Plasmid	Description[a]	Source or reference
pASK-IBA63c-plus	Expression vector, *tet*-promoter, *tet*-repressor, Amp^r, *Strep*-tag II for C-terminal fusion, f1-origin	IBA, Göttingen, Germany
Strep-*dcaA*	PCR-fragment (primers T493/T495 on genomic DNA of *Desulfitobacterium dichloroeliminans* LMG P-21439) cut with *Pci*I/*Xho*I ligated into pASK-IBA63c-plus cut with *Nco*I/*Xho*I	This study
Strep-*dcaA_dcaT*	PCR-fragment (primers T604/605 on genomic DNA of *Desulfitobacterium dichloroeliminans* LMG P-21439) cut with *Xho*I/*Afe*I ligated into Strep-*dcaA* cut with *Xho*I/*Afe*I	This study
Strep-*dcaA*p*dcaT*	PCR-fragment (primers T634/635 on the *tet*-promotor and ribosome binding site region in Strep-*dcaA_dcaT* cut with *Xho*I/*Sal*I ligated into Strep-*dcaA_dcaT* cut with *Xho*I	This study
Strep-p*dcaT*	Strep-*dcaA*p*dcaT* cut with *Xba*I and religated	This study
Strep-*pceA*p*dcaT*	PCR-fragment (primers T628/T495 on genomic DNA of *Desulfitobacterium hafniense* Y51) cut with *Nhe*I/*Xho*I ligated into Strep-*dcaA*p*dcaT* cut with *Nhe*I/*Xho*I	This study

[a] *tet*: tetracycline; Amp^r: ampicillin resistance.

Table S2. Oligonucleotides used for plasmid constructions.

Oligonucleotide	Sequence [a] (5'-3')
T493 (Strep-NheI-*dcaA*-f)	gatcacatg**tggagccacccgcagttcgaaaaa**gctagcggcgaaatcaacaggagg
T495 (*dcaA*-r)	gatcctcgagctattgttttatagactcag
T604 (*dcaT*-f)	gttcctcgagatgaagcagttcg
T605 (*dcaT*-r)	ctccaagcgctttaacttgcc
T628 (*pceA*-f)	tgacgctagcggagaaatcaacaggaggaatttttttaaaag
T634 (*ptet*-f)	gatcctcgagttcctaatttttgttgac
T635 (*ptet*-r)	gatggtcgacggtatatctccttcttaaag
T636 (*dcaA*808-f)	cgacaacaaggcaaacagtg
T659 (NheI-*dcaA*-f)	gatcgctagcggcgaaatcaacagg
T740 (*dcaA*861-r)	cctgacagcacctttggc
T772 (*pceA*644-f)	cgatgttgaaagtgtgcgacaac
T637 (*dcaA*-Y298F-f)	ggaaagtttTctccagtatgg
T638 (*dcaA*-Y298F-r)	ccatactggagAaaactttcc
T821 (*dcaA*-Y298S-f)	ggaaagtttCctccagtatgg
T822 (*dcaA*-Y298S-r)	ccatactggagGaaactttcc
T823 (*dcaA*-Y298T-f)	ggaaagttACctccagtatgg
T824 (*dcaA*-Y298T-r)	ccatactggagGTaactttcc
T825 (*dcaA*-Y298H-f)	ggaaagttCactccagtatgg
T826 (*dcaA*-Y298H-r)	ccatactggagtGaactttcc
T639 (*dcaA*-R357Q-f)	cgagacatcAGatctccaaag
T640 (*dcaA*-R357Q-r)	gactttggagatCTgatgtctc
T748 (*dcaA*-W118F-f)	cggagtctTCgctgtagaat
T749 (*dcaA*-W118F-r)	attctacagcGAagactccg
T750 (*dcaA*-T294V-f)	ccaatgccgcgGTTgggaaag
T751 (*dcaA*-T294V-r)	ctttcccAACcgcggcattgg
T752 (*dcaA*-N324L-f)	gtcaggaTTGaataccggat
T753 (*dcaA*-N324L-r)	atccggtattCAAtcctgac
T756 (*dcaA*-W432F-f)	gctctttctTCgcctataacgg
T757 (*dcaA*-W432F-r)	ccgttataggcGAagaaagagc
T641 (*dcaA*-C387S-f)	gcaaaaaatCtgcggatgcc
T642 (*dcaA*-C387S-r)	ggcatccgcaGatttttgc
T643 (*dcaA*-C439S-f)	ctgcgcaaattCtgtagctg
T644 (*dcaA*-C439S-r)	cagctacaGaatttgcgcag
T768 (*pceA*-Y298F-f)	ggaaaagttTctccaatatggc
T769 (*pceA*-Y298F-r)	ccatattggagAaacttttccc
T827 (*pceA*-Y298S-f)	ggaaaagttCctccaatatggc
T828 (*pceA*-Y298S-r)	ccatattggagGaacttttccc
T829 (*pceA*-Y298T-f)	ggaaaagtACctccaatatggc
T830 (*pceA*-Y298T-r)	ccatattggagGTacttttccc
T831 (*pceA*-Y298H-f)	ggaaaagtCactccaatatggc
T832 (*pceA*-Y298H-r)	ccatattggagtGacttttccc
T833 (*pceA*-R357K-f)	gagacatAAGatcgccaaagtc
T834 (*pceA*-R357K-r)	ctttggcgatCTTatgtctcgg
T770 (*pceA*-R357Q-f)	gagacatcAGatcgccaaagtc
T771 (*pceA*-R357Q-r)	ctttggcgatCTgatgtctcgg
T835 (*pceA*-R357N-f)	gagacatAAcatcgccaaagtc
T836 (*pceA*-R357N-r)	ctttggcgatgTTatgtctcgg
T837 (*pceA*-R357E-f)	gagacatGAGatcgccaaagtc
T838 (*pceA*-R357E-r)	ctttggcgatCTCatgtctcgg

[a] Restriction enzyme recognition sites are underlined; bold: *Strep*-tag II sequence; mutated nucleotides are written in upper case characters.

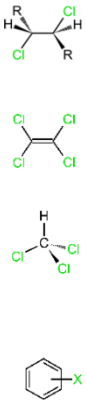

```
                                                                                                F31
                                                                                                 ↓
DcaA_Ddi          ------------------ADIVAPITETSEFPYKVDAKYQRYNCMKNFFEK-------T    34
DcaA_DWL          ------------------ADIMAPITETSEFPYKVDAKYQRYNSLKNFFEK-------A    34
PceA_Smul         ------------AEKEKNAAEIRQQFAMTAGSPIIVNDKLERYAEVRTAFTHPTSFFKPN    48
PceA_DhY51        ------------------ADIVAPITETSEFPYKVDAKYQRYNSLKNFFEK-------T    34
PceA_DhPCES       ------------------ADIVAPITETSEFPYKVDAKYQRYNSLKNFFEK-------T    34
PceA_Dres         ------------------ADIVAPITETSEFPYKVDAKYQRYNSLKNFFEK-------T    34
PceA_Dhc195       -------------PMFHDLDELVASTPSTRNLPWFVKEREHGDPTTPIDWDMIQRRP---    44
PceA_DhPCE1       ------------------------------------------------------------    0
CtrA_DesPR        AAATALGGKSLIDP----KQVYAGTVKELDELPFNIPADYKPFTNQRNIFGQ-------A    49
TmrA_DUNSWDHB     -----LGGKSLIDP----KQVYAGTVKELDELPFNIPADYKPFTNQRNIFGQ-------A    44
CfrA_Deh          -----LGGKSLIDP----KQVYAGTVKELDELPFNIPADYKPFTNQRNIYGQ-------A    44
TcbA_DhcCBDB1     -----------ATPVFHDLDELISSKPEVRESPWWVKEREFEDPTVEIDWSLKTHFD---    46
RdhA3_DhDCB2      --------KETFAPLTAEAAEIIAPIRETAEPFYQVDPKYQRLPAEKLAYLR-------M    45
CprA5_DhPCP1      --------KETFAPLTAEAAEIIAPIRETAEPFYQVDPKYQRLPAEKLAYLR-------M    45
CprA_Ddh          -------------------------AETMNYVPGPTNARSKLRPV---------------    20
CprA_DhDCB2       -------------------------AETLNYVPGSGKIRSKLRPV---------------    20
CprA3_DhPCP1      ------------------------VASTGSSGSVNGARSKLHPK---------------    20
CprA_Dchl         ------------------------ATDTLNYVPGRKSQNSKLHPE---------------    21
NpRdhA_Np         ---------------------------------PGWEDAEEEKRPL---------------    13
BhbA_Com          --------------------------------NASNVVDYTGRNY---------------    13

DcaA_Ddi          FDPEANKTPIKFHNDDVSKITGKKDTGKDLPTLNAERLGIKGRPATHSETGVLFFGQHTG    94
DcaA_DWL          LDPEANKTPIKFHYDDVSKITGKKDTGKDLPILNAERLGIKGRPATNAETGVLFFSQHIG    94
PceA_Smul         YKGEVKPWFLSAYDEKVRQI----ENGENG-------------------------------    74
PceA_DhY51        FDPEANKTPIKFHYDDVSKITGKKDTGKDLPTLNAERLGIKGRPATHTETSILFHTQHLG    94
PceA_DhPCES       FDPEENKTPIKFHYDDVSKITGKKDTGKDLPMLNAERLGIKGRPATHTETSILFHTQHLG    94
PceA_Dres         FDPEANKTPIKFHYDDVSKITGKKDTGKDLPTLNAERLGIKGRPATHTETSILFQTQHLG    94
PceA_Dhc195       -YTWVRMDPTLPVYDNLKSIGAPVSRWLDWEDKKAE-------------DEI--------    82
PceA_DhPCE1       ------------------------------------------------------------    0
CtrA_DesPR        LLGVPEPRALVERFDEVRW-----------------------------------------N-    69
TmrA_DUNSWDHB     VLGVPEPLALVERFDEVRW-----------------------------------------N-    64
CfrA_Deh          VLGVPEPLALVERFDEVRW-----------------------------------------N-    64
TcbA_DhcCBDB1     -YNLVHSWVS-------------KETAQEWQEKQAE---------------L---------    69
RdhA3_DhDCB2      FDPEENKGPIKFHFDDVSKITGKKDTGKDLPLLNAESLGIKGRPATLSETGAIFFSHHDG    105
CprA5_DhPCP1      FDPEENKGPIKFHFDDVSKITGKKDTGKDLPLLNAESLGIKGRPATLSETGAIFFSHHDG    105
CprA_Ddh          H--DFAGAKVRFVENNDEWLGTT---------------KIISKVKKTSEADAGFMQAVRG    63
CprA_DhDCB2       H--DFAGAKVRFVENNDQWLGTT---------------KILTKVKMTSEADAGFMQAVRG    63
CprA3_DhPCP1      V--DYGGASVRFVENNDQWLGTS---------------QIVGTVNRTHEAEQGFNLALRG    63
CprA_Dchl         H--NYGGASVRFVEHNDQWLGTT---------------KIIGTIKNPNEADMGFNLAARG    64
NpRdhA_Np         HMGRYPMETIRRVDEPTTLVVRQ-------------------EIQRVAKRGDFFKRAEAG    54
BhbA_Com          RDSLYPVETLKRVDDTTTFIDED-------------------RIPRVPKSSEFFLRAAFG    54

                                                  W118          F124
                                                   ↓             ↓
DcaA_Ddi          VMPHQRSKETGNTLLDDALQAGVWAV------EFDFHGFNATDNGPGTVITPYPINPMTN    148
DcaA_DWL          AMLTQRHNETGWTGLDAALKAGAFAV------DFDYSGFNCVSGGPGCVITPYPINPMTN    148
PceA_Smul         --PKMKAKNVGEARAGRALEAAGWTL------DINYGNIY-----PNRFFMLWSGETMTN    121
PceA_DhY51        AMLTQRHNETGWTGLDEALNAGAWAV------EFDYSGFNATGGGPGSVIPLYPINPMTN    148
PceA_DhPCES       AMLTQRHNETGWTGLDEALNAGAWAV------EFDYSGFNAAGGGPGSAIPLYPINPMTN    148
PceA_Dres         AMLTQRHNETGWTGLDEALNAGAWAV------EFDYSGFNAAGGGPGSVIPLYPINPMTN    148
PceA_Dhc195       LYAKAREDFPGWEPGLDGFGDIRTTALTHASEMFSFGNFPTRMNLGGNMVDLVAAVRAAG    142
PceA_DhPCE1       ------------------------------------------------------------    0
CtrA_DesPR        --GWLTDGSPGLTVLDGAAARASFAV------DYYFNGENSACRANKGFFEWHPKVP---    118
TmrA_DUNSWDHB     --GWQTDGSPGLTVLDGAAARASFAV------DYYFNGENSACRANKGFFEWHPKVP---    113
CfrA_Deh          --GWQTDGSPGLTVLDGAAARASFAV------DYYFNGENSACRANKGFFEWHPKVA---    113
TcbA_DhcCBDB1     IREAVANNTPGNTLKDMALA--NMGLHYAGSDLFNYSQLSRP-EYSTVILDTF---D-VS    122
RdhA3_DhDCB2      SVLPLREKEMGWRALDMALVVASWSV------EYHYNGFTAPGSGPGGVIAHYPFNPMTN    159
CprA5_DhPCP1      SVLPLREKEMGWRALDMALVVASWSV------EYHYNGFTAPGSGPGGVIAHYPFNPMTN    159
CprA_Ddh          LYG-------------PDPQR---------------------GF--FQFIAKHPFGGTIS    87
CprA_DhDCB2       LYG-------------PEPQK---------------------GF--FQFIAKDPFGGSIS    87
CprA3_DhPCP1      KLS-------------SEAQV---------------------AMYHYNFVMKHPFDGALG    89
CprA_Dchl         ILG-------------DQAKK---------------------GV--NNFIAKHPFGSSIS    88
NpRdhA_Np         DLG-------------EKAKQ---------------------EKKR-FP-MKHPLALGMQ    78
BhbA_Com          DLG-------------KAPQE---------------------ASKDGYSVAKAPLAAALR    80
```

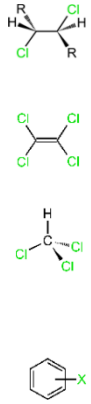

```
DcaA_Ddi      -EIANEPVMVPGLYNWDNIDVESVRQQGKQWKFKSKEEASKMVKKAACFLGADLVGIAPY   207
DcaA_DWL      -EIANEPVVVPGLYNWDNIDVESVRQQGQQWKFKSKEEASKMVKKAACFLGADLAGIAPY   207
PceA_Smul     -TQL-----------WAPVGLD-----RRPPDTTDPVELTNYVKFAARMAGADLVGVARL   164
PceA_DhY51    -EIANEPVMVPGLYNWDNIDVESVRQQGQQWKFESKEEASKIVKKATRLLGADLVGIAPY   207
PceA_DhPCES   -EIANEPVMVPGLYNWDNIDVESVRQQGQQWKFESKEEASKILKKATRLLGADLVGIAPY   207
PceA_Dres     -EIANEPVMVPGLYNWDNIDVESVRQQGQQWKFESKEEASKMVKKATRLLGADLVGIAPY   207
PceA_Dhc195   GYLGSTD-----SY-AGPKMVHTPEEMGGTKYQGTPEDNLRTIKAGIRYFGGEDVGALEL   196
PceA_DhPCE1   ------------MYAWDEEKSR------QKATFTDLKEASLIVKDAARFLGASLVGIAEY   42
CtrA_DesPR    ----------ELNFRWGDPERN-----IHSPGVKSAEEGTMAVKRMARFFGAAKAGIAPF   163
TmrA_DUNSWDHB ----------ELNFKWGDPERN-----IHSPGVKSAEEGTMAVKRMARFFGAAKAGI-PF   157
CfrA_Deh      ----------ELNFKWGDPERN-----IHSPGVKSAEEGTMAVKKIARFFGAAKAGIAPF   158
TcbA_DhcCBDB1 ---GQ----------IDNKYGLTRTQLGIPKWQGTPEENSAMVAAVLHFLGSTRVGYVSI   169
RdhA3_DhDCB2  -ETGTEPVFLAGMYSWDNTKARERREQGRQWKFESVEEASRIVKKAARFLGADMAGIAPY   218
CprA5_DhPCP1  -ETGTEPVFLAGMYSWDNTKARERREQGRQWKFESVEEASRIVKKAARFLGADMAGIAPY   218
CprA_Ddh      -WARNLI-------AA--EDVVDGDAEPTKTPIPDPEQMSQHIRDCCYFLRADEVGIGKM   137
CprA_DhDCB2   -WARNLI-------AP--EDVVDGAPEATKTPIPDPEQMSQHIRDCCYFLRADEVGIGKM   137
CprA3_DhPCP1  -IFSNYV-------SA--ENIVGGTPNQEKLPIPDPEQMSQNIKDTAYFLRADEVGIGKM   139
CprA_Dchl     -SGLMFI-------AG--EEAVTGQPAKEKLPIPDPEQMSQHIKDAAYFLRADEVGIGRM   138
NpRdhA_Np     -PLIQNM-------VPLQGTREKLAPTGKGGDLSDPGRNAEAIKALGYYLGADFVGICRA   130
BhbA_Com      -LALNVY----------SVLQRGEPAPQKVSYLDPVRNAELVKATLHFLGADIAGLSRA   128
                                                       :       .  .*

DcaA_Ddi      DERW---TYSTWGRKIPKPCKMPNGRTKLMPWDLPKVLSGGGVEVFGHEKF-----EPDW   259
DcaA_DWL      DERW---TYSTWGRKILKPCKMPNGRTKLMPWDLPKMLSGGGVEVFGHAKF-----EPDW   259
PceA_Smul     NRNW---VYSEAVT---IPADVPYEQSLHKEIEKPIVFKD------VPLPI-----ETDD   207
PceA_DhY51    DERW---TYSTWGRKIYKPCKMPNGRTKYLPWDLPKMLSGGGVEVFGHAKF-----EPDW   259
PceA_DhPCES   DERW---TYSTWGRKIQKPCKMPNGRTKYLPWDLPKMLSGGGVEVFGHAKF-----EPDW   259
PceA_Dres     DERW---TYSTWGRKILKPCKMPNGRTKYLPWDLPKMLSGGGVEVFGHAKF-----EPDW   259
PceA_Dhc195   DDKLKKLIFTVDQY--------------------GKALEFGDVEECIETPKQ--------   228
PceA_DhPCE1   DQKW---VYSTWYDFSTKES---------IP-----------------------------   61
CtrA_DesPR    DKRW---VFTETAAFVKTPEG---ESLKFIP-----------------------------   188
TmrA_DUNSWDHB DKRW---VFTETAAFVKTPEG---EDLKFIP-----------------------------   182
CfrA_Deh      DKRW---VFTETYAFVKTPEG---ESLKFIP-----------------------------   183
TcbA_DhcCBDB1 NENNKKVWFSPDKA--------------------NRIISWGDVEEPVNTPGILWPGNKLG   209
RdhA3_DhDCB2  DDRW---TFSTWCRPNLKPFKLPNGRTEYFPTDPFKL-MKGEVEVYGSTSV-----EADW   269
CprA5_DhPCP1  DDRW---TFSTWCRPNLKPFKLPNGRTEYFLTDPFKL-MKGEVEVYGSTSV-----EADW   269
CprA_Ddh      PEYG---YYTHHVSDT----------VGLMS-----------------KP------VEEC   161
CprA_DhDCB2   PEYG---YYTHHVADT----------VGLMT-----------------KP------VEEC   161
CprA3_DhPCP1  PEYA---YYSHKAPFS---------HEELIR-----------------DD------I-SH   163
CprA_Dchl     PEFA---YYSHKTTVP---------RTKMAA-----------------AP------VEEW   163
NpRdhA_Np     EPWM---YYASDEVE-------------------------------------------     142
BhbA_Com      PAWV---WYSHK-QD-------------------------------------------     139
                     ::

                                                                Y298
DcaA_Ddi      EKYAGFKPKSVIVFVLEEDYEALRTSP--SVIANAATGKVYSSMGGVSYKIAVFLRKLGY   317
DcaA_DWL      EKYAGFKPKSVIVFVLEEDYEAIRTSP--SIISSTSVGKGHSNMGEVAYKIAVFLRKLGY   317
PceA_Smul     ELIIPNTCENVIVAGIAMNREMMQTAP--NSMACATTAFCYSRMCMFDMWLCQFIRYMGY   265
PceA_DhY51    EKYAGFKPKSVIVFVLEEDYEAIRTSP--SVISSATVGKSYSNMAEVAYKIAVFLRKLGY   317
PceA_DhPCES   EKYAGFKPKSVIVFVLEEDYEAIRTSP--SVISSATVGKSYSNMAEVAYKIAVFLRKLGY   317
PceA_Dres     EKYAGFKPKSVIVFVLEEDYEAIRTSP--SVISSATVGKSYSNMAEVAYKIAVFLRKLGY   317
PceA_Dhc195   -VTIPNKCKYIFLWTMRQPYEWTRRQS--GRFEGAATETSYERAYNTKAHFQDFVRGLGY   285
PceA_DhPCE1   -AEFPFPVKSVIVIXVDTXYRGCLTSP--SLISSAATGLGYSKMAETARKMATFIRMLGY   118
CtrA_DesPR    -PDFGFEPKHVISMIIPQSLEGVKTSP--SFLGSSEYGLGCAQYGYAPFGLSMFIKDLGY   245
TmrA_DUNSWDHB -PDFGFEPKHVISMIIPQSLEGVKCAP--SFLGSAEYGLSFAQIGYAAFGLSMFIKDLGY   239
CfrA_Deh      -PDFGFEPKHVISMIIPQSPEGVKCDP--SFLGSTEYGLSCAQIGYAAFGLSMFIKDLGY   240
TcbA_DhcCBDB1 SLVLPNKCNSLISFVIPQSGI-SKYHH--TALSRAATFLGYAESTIISARLQIFLKTLGY   266
RdhA3_DhDCB2  EKYAGFTPKSVIAMTFEMDYEAYRTAP--SVLQGAAPGKSYSNMGEVAYKVASFLREIGY   327
CprA5_DhPCP1  EKYAGFTPKSVIAMTFEMDYEAYRTAP--SVLQGAAPGKSYSNMGEVAYKVASFLREIGY   327
CprA_Ddh      VTPVTKIYPNVIVVMIDQGIETMWASTGYDGISGAMSMQSYFTSGCIAVIMAKYIRTLGY   221
CprA_DhDCB2   VTPVTKIYPNVIVVMIDQGIETMWASTGYDGISGAMSMKSYFTSGCIAVILAKYIRTLGY   221
CprA3_DhPCP1  STPVTEKLPYVIVVMVDQHLETMLASTGYDGISSAQSMRGYHATAVISVILAQYIRNLGY   223
CprA_Dchl     TVPFEEKHPYVIVVMVDQHLETTLASTGYDGISGAQSFKGYHATGNIAVILAQYIRNLGY   223
NpRdhA_Np     GKPIEAYHDYAVVMLIDQGYETMEGASGDDWISASQSMRAYMRGAEIAGVMAAHCRRMGY   202
BhbA_Com      GTEMPVAHPFAATVMIDQGFETMEGASGDDWISSAQSMRTYMRAGLVCGVLGDHLRGLGY   199
                         .               :  :             .  .  : :**
```

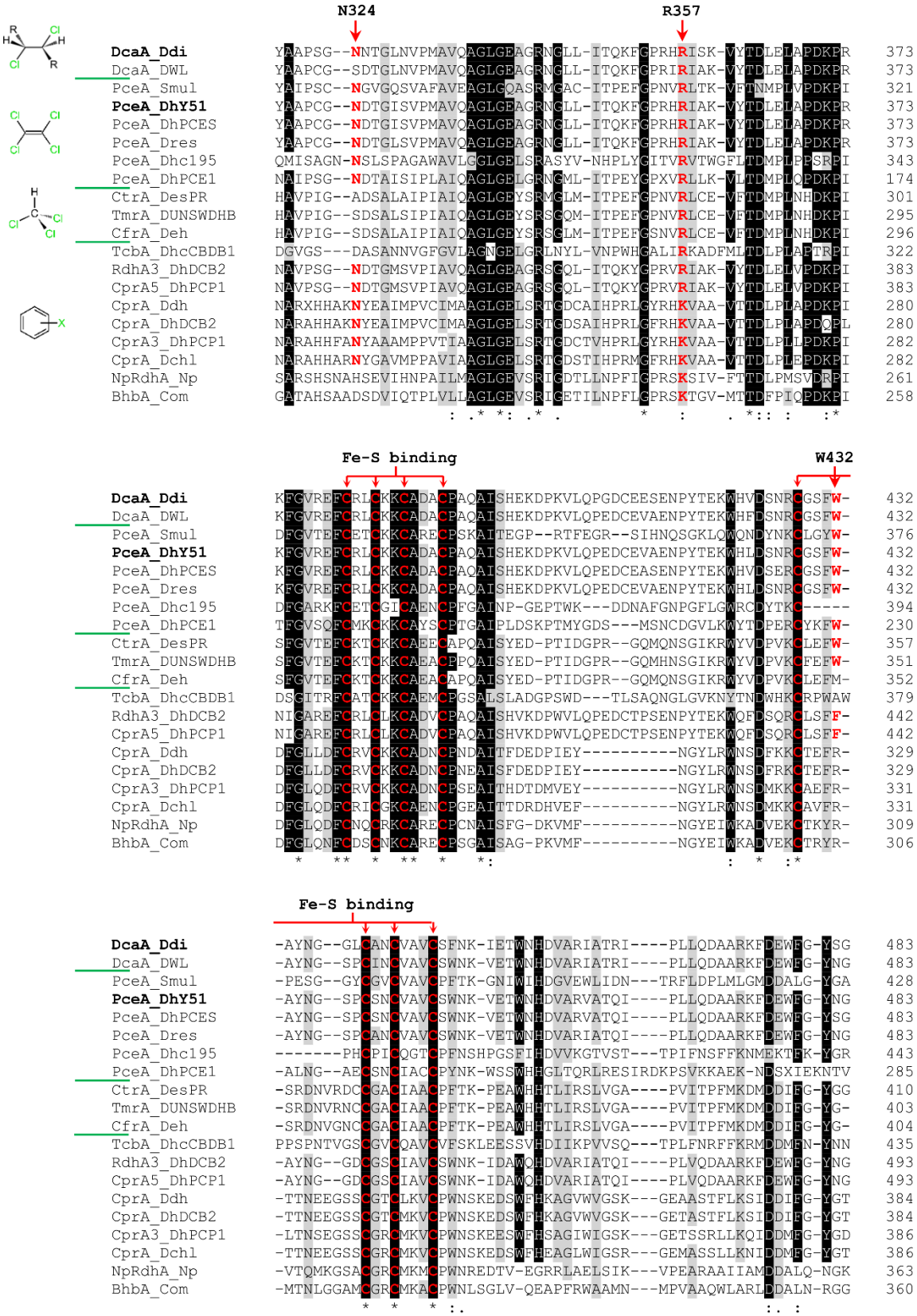
N324
R357
Fe-S binding
W432
Fe-S binding
DcaA_Ddi
DcaA_DWL
PceA_Smul
PceA_DhY51
PceA_DhPCES
PceA_Dres
PceA_Dhc195
PceA_DhPCE1
CtrA_DesPR
TmrA_DUNSWDHB
CfrA_Deh
TcbA_DhcCBDB1
RdhA3_DhDCB2
CprA5_DhPCP1
CprA_Ddh
CprA_DhDCB2
CprA3_DhPCP1
CprA_Dchl
NpRdhA_Np
BhbA_Com

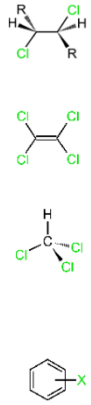

```
DcaA_Ddi        PVNPDERLESGYV----QN-----------MVKDF----------------WNNPESIKQ    512
DcaA_DWL        PVNPDERLESGYV----QN-----------MVTDF----------------WNNPESIKQ    512
PceA_Smul       KRNITEVWDGK-I--NTYGLDADHFRDTVSFRKDRVKKS--------------------    464
PceA_DhY51      PVNPDERLESGYV----QN-----------MVKDF----------------WNNPESIKQ    512
PceA_DhPCES     PVNPDERLESGYV----QN-----------MVKDF----------------WNNPESIKQ    512
PceA_Dres       PVNPDERLESGYV----QN-----------MVKDF----------------WNNPESIKQ    512
PceA_Dhc195     -KNPAT-WWDE-VDDYPYGV-------DTSY-----------------------------    464
PceA_DhPCE1     PSEPGTSMADQSSKKREYNIVDYAICKAAAAISDYXAKDNCFVIHEQDLCEWSSKHNQSK    345
CtrA_DesPR      KPNDKKAIADWWK-------------------------------------------------    423
TmrA_DUNSWDHB   KPN-EKAKADWWK-------------------------------------------------    415
CfrA_Deh        KLNDEKAIADWWK-------------------------------------------------    417
TcbA_DhcCBDB1   PENPEE-WWSRDYKNYPYSR-------AVPGN-----------------------------    459
RdhA3_DhDCB2    PVNPEERIESGYI----AN-----------MVKDF----------------WKDTEPTK-    521
CprA5_DhPCP1    PVNPEERIESGYI----AN-----------MVKDF----------------WKDTEPTK-    521
CprA_Ddh        ETIEKYKWWLEWP--EKYP-LKPM--------------------------------------    405
CprA_DhDCB2     ETIEKYKWWLEWP--EKYV-MK----------------------------------------    403
CprA3_DhPCP1    EIIEKYKWWLEWP--ERYT-LPKHL-------------------------------------    408
CprA_Dchl       ETIDKYKWWLEWP--ELYK-IQ----------------------------------------    405
NpRdhA_Np       RNLIK-RWWFDLE--VIDG-VAGAPRMGTN-ERDLSPDRGDKIGANQKLAMYPPRL--QP    416
BhbA_Com        INPRK-KWWWDIT--NDGT-GKIVVAKEVN-VRGLNKH-IKIKHEDQTLAAYPAPL--AP    412

DcaA_Ddi        ----------------------------------------    512
DcaA_DWL        ----------------------------------------    512
PceA_Smul       ----------------------------------------    464
PceA_DhY51      ----------------------------------------    512
PceA_DhPCES     ----------------------------------------    512
PceA_Dres       ----------------------------------------    512
PceA_Dhc195     ----------------------------------------    464
PceA_DhPCE1     MKFQTLHKL-----------------------------    354
CtrA_DesPR      ----------------------------------------    423
TmrA_DUNSWDHB   ----------------------------------------    415
CfrA_Deh        ----------------------------------------    417
TcbA_DhcCBDB1   ----------------------------------------    459
RdhA3_DhDCB2    ----------------------------------------    521
CprA5_DhPCP1    ----------------------------------------    521
CprA_Ddh        ----------------------------------------    405
CprA_DhDCB2     ----------------------------------------    403
CprA3_DhPCP1    ----------------------------------------    408
CprA_Dchl       ----------------------------------------    405
NpRdhA_Np       PPGTTLDAVLPVDRSGGLAEYAAAETPAAARARLKSSAG    455
BhbA_Com        LP---LPMPSPVDREAGIEAYKNLLTPEQHQQRVRDGET    448
```

Figure S1. Amino acid sequence alignment of selected RDases. Selected RDases with different substrate preferences, including DCA-RDases, PCE-RDases, chloroform RDases and aryl halide RDases were aligned with Clustal Omega [1]. Residues conserved to more than 80% have a black/grey colored background. Residues involved in active site formation and iron-sulfur cluster binding are colored in red. DcaA_Di – *Desulfitobacterium dichloroeliminans* DCA1 1,2-DCA RDase (Q08GR2), DcaA_DWL – *Dehalobacter* sp. WL 1,2-DCA RDase (B5TS67), PceA_Smul – *Sulfurospirillum multivorans* PCE RDase (W6EQP0), PceA_DhY51 – *Desulfitobacterium hafniense* Y51

PCE RDase (Q8L172), PceA_DhPCES *Desulfitobacterium hafniense* PCE-S PCE RDase (Q848J2), PceA_Dres – *Dehalobacter restrictus* PER-K23 PCE RDase (Q8GJ27), PceA_Dhc195 – *Dehalococcoides mccartyi* 195 PCE RDase (Q3Z9N3), PceA_DhPCE1 – *Desulfitobacterium hafniense* PCE1 (AAG46188.1), CtrA_DesPR – *Desulfitobacterium* sp. strain PR chloroform RDase (R9YJY6), TmrA_DUNSWDHB – *Dehalobacter* sp. strain UNSWDHB chloromethane RDase (WP_034377773.1), CfrA_Deh – *Dehalobacter* sp. chloroform RDase (K4LFB7), TcbA_DhcCBDB1 – *Dehalococcoides mccartyi* CBDB1 chlorobenzene RDase (Q3ZWF5), RdhA3_DhDCB2 – *Desulfitobacterium hafniense* DCB-2 chlorophenol RDase (B8FVX4), CprA5_DhPCP1 – *Desulfitobacterium hafniense* PCP1 3,5-dichlorophenol RDase (Q6V7J3), CprA_Ddh – *Desulfitobacterium dehalogenans ortho*-chlorophenol RDase (Q9XD04), CprA_DhDCB2 - *Desulfitobacterium hafniense* DCB-2 3-chloro-4-hydroxy-phenylacetate RDase (P81594), CprA3_DhPCP1 - *Desulfitobacterium hafniense* PCP1 2,4,6-trichlorophenol RDase (Q8RPG3), CprA_Dchl – *Desulfitobacterium chlororespirans* RDase (Q8RQC9), NpRdhA_Np – *Nitratireductor pacificus* pH-3B *ortho*-dibromophenol RDase (K2MB66), BhbA_Com – Comamonas sp. 7D-2 bromoaromatic RDase (K4MLZ9). The latter two sequences were shortened by removal of the duplicated N-terminal cobamide-binding domain and in case of BhbA the C-terminal NAD(P)H-dependent oxidoreductase domain. UniProtKB and NCBI protein accession numbers are given in brackets. X = halogen substituent in the structural formulae of the RDase substrates

[1] Sievers F, Wilm A, Dineen D, Gibson TJ, Karplus K, Li W, Lopez R, McWilliam H, Remmert M, Söding J, Thompson JD, Higgins DG (2011) Fast, scalable generation of high-quality protein multiple sequence alignments using Clustal Omega. *Mol Syst Biol* 7, 539. doi:10.1038/msb.2011.75

Supplementary Information

Selective, light-driven enzymatic dehalogenations of organic compounds

Bhavin Siritanaratkul[†], Shams T. A. Islam[†], Torsten Schubert[‡], Cindy Kunze[‡], Tobias Goris[‡], Gabriele Diekert[‡] and Fraser A. Armstrong*[,†]

[†] Inorganic Chemistry Laboratory, Department of Chemistry, University of Oxford, South Parks Road, Oxford OX1 3QR, Oxfordshire, United Kingdom
[‡] Institut für Mikrobiologie, Friedrich-Schiller-Universität Jena, Lehrstuhl für Angewandte und Ökologische Mikrobiologie, Philosophenweg 12, 07743 Jena, Germany

UV irradiation of TiO_2-PceA with *c*DCE

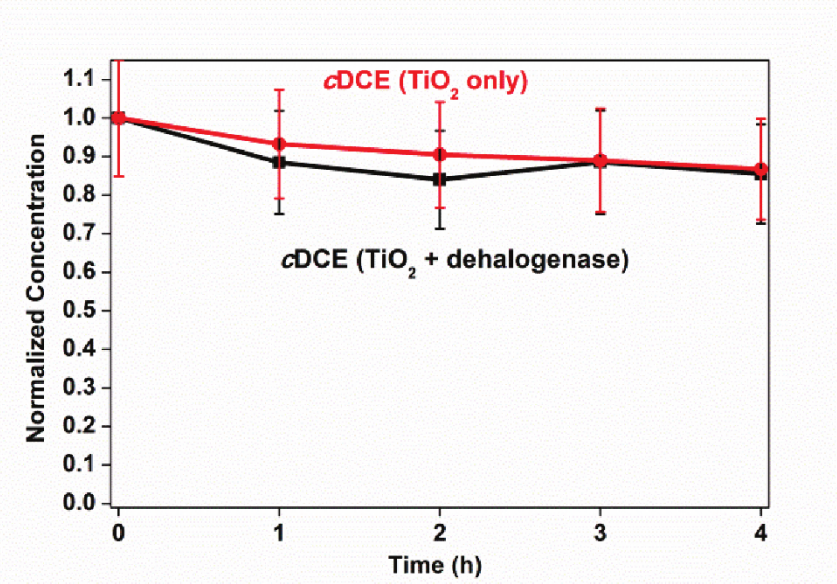

Figure S1. Time course of the *c*DCE concentration for reaction solutions containing both TiO_2 nanoparticles and PceA (black line) or TiO_2 only (red line), irradiated with UV light.

PceA on a PGE electrode after injection of *c*DCE

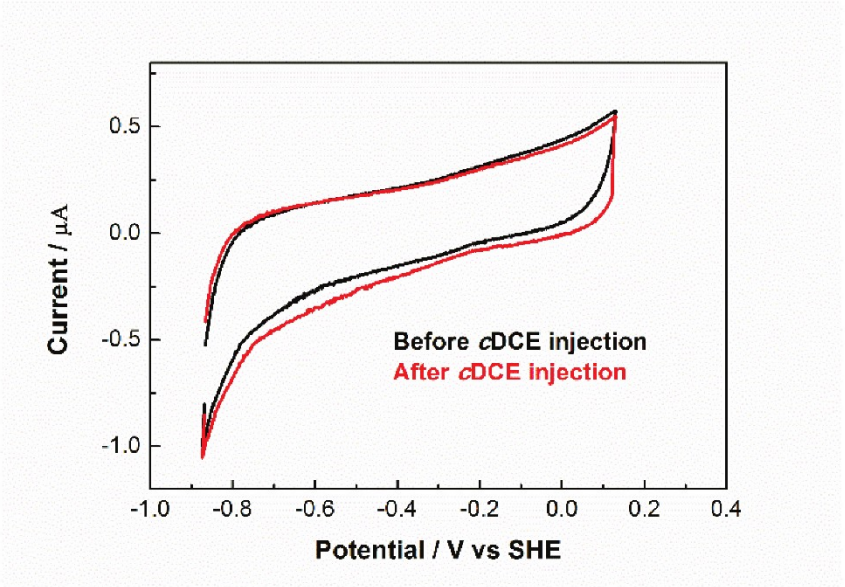

Figure S2. Cyclic voltammograms of PceA on a PGE electrode, before (black) and after (red) injection of *c*DCE 0.8 mM. Reaction conditions: Tris buffer, pH 7.0, 25 °C, scan rate 20 mV/s, electrode is stationary.

Visible light-dye-modified TiO_2

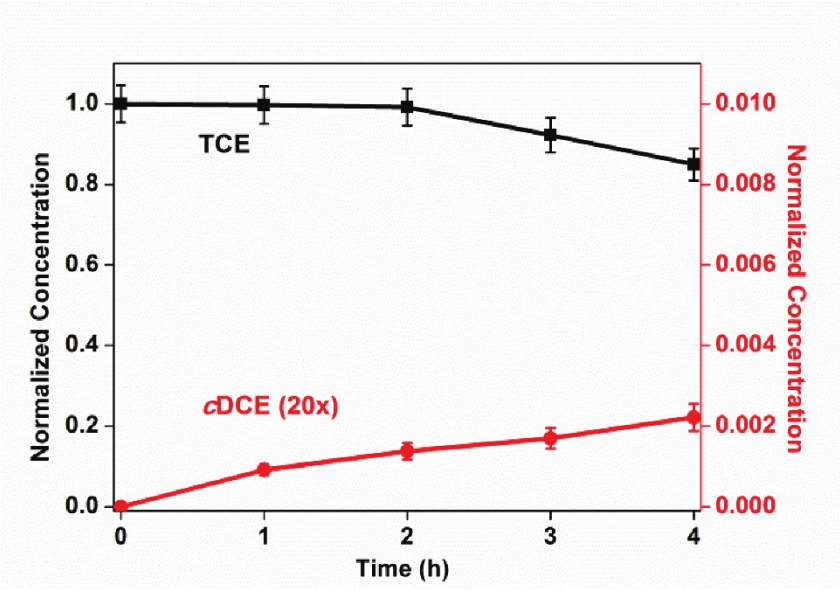

Figure S3. Time course of concentrations of TCE (black line, left axis) and *c*DCE (red line, magnified 20 times, right axis) for a Ru dye-TiO_2-PceA system under visible light irradiation ($\lambda >$ 420 nm). The Ru system has been described previously.[1, 2]

References

1. E. Reisner, D. J. Powell, C. Cavazza, J. C. Fontecilla-Camps and F. A. Armstrong, *Journal of the American Chemical Society*, 2009, **131**, 18457-18466.
2. T. W. Woolerton, S. Sheard, E. Reisner, E. Pierce, S. W. Ragsdale and F. A. Armstrong, *Journal of the American Chemical Society*, 2010, **132**, 2132-2133.

Acknowledgements

On the last pages of my thesis I would like to seize the opportunity and thank all the people who supported me during my PhD studies.

First of all, I would like to address my gratitude to Prof. Dr. Gabriele Diekert for giving me the opportunity to work on this interesting research topic and to complete my PhD thesis at the Department of Applied and Ecological Microbiology of the Friedrich Schiller University Jena.

I wish to express my sincere gratidude to Dr. Torsten Schubert for his excellent and committed support and guidance throughout this project. This thesis wouldn't have turned out this way without his dedicated discussions and helpful advices and suggestions.

Special thanks go to Dr. Martin Bommer, Prof. Dr. Holger Dobbek & Dr. Jochen Fesseler from the Humboldt-Universität zu Berlin for their excellent work in X-ray structure analysis and the rewarding collaboration over the last years.

I am deeply grateful to Prof. Dr. Wilfred Hagen from the Delft University of Technology for his work on EPR studies including protein-substrate interactions and cofactor characterization.

Furthermore, I want to thank Bhavin Siritanaratkul, Shams Tania Islam and Prof. Dr. Fraser Armstrong from the Oxford University for joining our team and establishing an electrochemical reactor for RDase application.

A big thank you goes to all members of the DFG-funded research unit FOR1530 – "Anaerobic Biological Dehalogenation" and all colleagues of the Department of Applied and Ecological Microbiology for always fruitful discussions in numerous meetings and for a pleasant work atmosphere. Here, I would especially like to thank Peggy Brand-Schön for the endless cultivation of cell mass and Sebastian Keller for great cooperative working on the cobamide variability in PceA and *S. multivorans*.

Finally, I would like to express my heartfelt thanks to my family, who always support me and trust in me and my work, encouraging me whenever needed.

This project would not have been possible without you!

Author's declaration of originality

I, Cindy Kunze, born on 17th June, 1989 in Zwickau (Germany), hereby certify that I am aware of the official doctoral regulations of the Faculty of Biology and Pharmacy of the Friedrich Schiller University Jena. I confirm that this dissertation is my original work and that only sources cited in the text and references have been used. Support in the preparation of the manuscripts was only reveived from named coauthors as well as anonymous reviewers within the peer-review processes during manuscript submission. The exact literature references for manuscripts that have been published elsewhere are given in the corresponding chapters. The help of a doctoral advisor was not used. No commercial or monetary activities are related to the contents of this work. This dissertation has only been submitted to the Council of the Faculty of Biology and Pharmacy of the Friedrich Schiller University Jena, and not to any other university for academic examination or dissertation.

…… ……..

Place, date Cindy Kunze

Scientific publications

peer-reviewed Journal Articles:

Keller S, Kunze C, Bommer M, Paetz C, Menezes RC, Svatoš A, Dobbek H, Schubert T (2017) Selective utilization of benzimidazolyl-norcobamides as cofactors by the tetrachloroethene reductive dehalogenase of *Sulfurospirillum multivorans*. planned for submission in *J Bacteriol*

Kunze C, Diekert G, Schubert T (2017) Subtle changes in the active site architecture untangles overlapping substrate ranges and mechanistic differences of two reductive dehalogenases. accepted in *FEBS Journal,* August 30, 2017.

Kunze C[*], Bommer M[*], Hagen WR, Uksa M, Dobbek H, Schubert T, Diekert G (2017) Cobamide-mediated enzymatic reductive dehalogenation via long-range electron transfer. *Nature Communications* 8, 15858.
[*] These authors contributed equally to this work.

Siritanaratkul B, Islam STA, Schubert T, Kunze C, Goris T, Diekert G, Armstrong FA (2016) Selective, light-driven enzymatic dehalogenations of organic compounds. *RSC Advances* 6, 84882-84886.

Bommer M[*], Kunze C[*], Fesseler J, Schubert T, Diekert G, Dobbek H (2014) Structural basis for organohalide respiration. *Science* 346, 455-458.
[*] These authors contributed equally to this work.

Keller S, Ruetz M, Kunze C, Kräutler B, Diekert G, Schubert T (2013) Exogenous 5,6-dimethylbenzimindazole caused production of a non-functional tetrachloroethene reductive dehalogenase in *Sulfurospirillum multivorans*. *Environmental Microbiology* 16, 3361-3369.